Deliverable 7.7: HITEC - technical report on Material characterisation

Work Package 7

The project leading to this application has received funding from the European Union's Horizon 2020 research and innovation programme under grant agreement No 847593.

http://www.ejp-eurad.eu/

Document information

Project Acronym	**EURAD**
Project Title	**European Joint Programme on Radioactive Waste Management**
Project Type	**European Joint Programme (EJP)**
EC grant agreement No.	**847593**
Project starting / end date	**1st June 2019 – 30 May 2024**
Work Package No.	**7**
Work Package Title	**Influence of Temperature on Clay-based Material Behaviour**
Work Package Acronym	**HITEC**
Deliverable No.	**7.7**
Deliverable Title	**HITEC technical report on Material characterisation**
Lead Beneficiary	**SKB**
Contractual Delivery Date	**March 2023**
Actual Delivery Date	**June 2024**
Type	**Final report of WP7 Task 3.1**
Dissemination level	**Public**
Authors	Daniel Svensson, Patrik Sellin (SKB), Stephan Kaufhold (BGR), Roy Chaaya, Stéphane Gaboreau, Joachim Tremosa (BRGM), María Victoria Villar, Ana María Melón, Ana Beatriz Zabala, Rubén Javier Iglesias (CIEMAT), Jan Najser (CU), Jiří Svoboda, Kateřina Černochová (CTU), Sergey Sayenko (KIPT), Zlobenko B., Bugera S., Fedorenko Yu., Rozko A. (SIIEG NASU), Jaime Cuevas, Almudena Ortega, Ana Isabel Ruiz (UAM), Vlastislav Kašpar, Šárka Šachlová (ÚJV), Veli-Matti Pulkkanen, Olli-Pekka Rauhala (VTT).

To be cited as:

Svensson, D., Sellin, P, (SKB), Kaufhold, S., (BGR), Chaaya, R., Gaboreau, S., Tremosa, J.(BRGM), Villar, M-V., Melón, A-M, Zabala, A.B., Iglesias, R. J., (CIEMAT), Najser, J. (CU), Svoboda, J., Černochová, K. (CTU), Sayenko, S. (KIPT), Zlobenko B., Bugera S., Fedorenko Y., Rozko A. (SIIEG NASU), Cuevas, J., Ortega, A., Ruiz, A. I. (UAM), Kašpar, V., Šachlová, S., (ÚJV), Pulkkanen, V-M., Rauhala, O-P. (VTT) (2023): HITEC technical report on Material characterisation. Final version as of 23.11.2023 of deliverable D7.7 of the HORIZON 2020 project EURAD. EC Grant agreement no: 847593.

Disclaimer

Acknowledgement

This document is a deliverable of the European Joint Programme on Radioactive Waste Management (EURAD). EURAD has received funding from the European Union's Horizon 2020 research and innovation programme under grant agreement No 847593.

Status of deliverable		
	By	Date
Delivered (Lead Beneficiary)	[SKB]	22 May 2024
Verified (WP Leader)	Markus Olin [VTT]	15 Feburary 2024
Reviewed (Reviewers)	Liu Jinsong (SSM) Michael Holmboe (University of Umeå)	28 February 2024 10 May 2024
Approved (PMO)	Bharti Reddy	31 May 2024
Submitted to EC	Andra (Coordinator)	03 June 2024

Authors

Organisation	Authors
BGR	Stephan Kaufhold
BRGM	Roy Chaaya, Stéphane Gaboreau, Joachim Tremosa
CIEMAT	María Victoria Villar, Ana María Melón, Ana Beatriz Zabala, Rubén Javier Iglesias
CU	Jan Najser
CTU	Jiří Svoboda, Kateřina Černochová
KIPT	Sergey Sayenko
SKB	Daniel Svensson, Patrik Sellin
SIIEG NASU	Zlobenko B., Bugera S., Fedorenko Yu., Rozko A.
UAM	Jaime Cuevas, Almudena Ortega, Ana Isabel Ruiz
ÚJV	Vlastislav Kašpar, Šárka Šachlová
VTT	Veli-Matti Pulkkanen, Olli-Pekka Rauhala

Executive Summary

A number of different high temperature experiments were performed with bentonite clays. Both field experiments at a hard rock laboratory and laboratory scale experiments have been performed. Some experiments by heating the clay either in an open system while allowing the clay to dry or in a closed system with water available. No general significant transformation of montmorillonite was observed in the experiments. In several cases the CEC of the bentonite was affected by the heating, but with no correlation to any observed mineralogical changes.

There are indications that dry heating of the bentonite had a stronger impact on the clay properties, than heating of water saturated bentonite. Swelling pressure seemed mainly unaffected by thermal treatment, while hydraulic conductivity sometimes increased somewhat. Unconfined compression test showed that a lower maximum deviator stress was seen in all materials compared to the references in the ABM5 field test.

There were examples of (i) redistribution of sulphates, (ii) formation of carbonates, (iii) dissolution of quartz and cristobalite. These are observations that are not new.

There were examples of compacted bentonite blocks that were physically disintegrated in parts of the experiments. The mechanism for this is not fully understood, and it is unclear if this could actually happen in a real repository as well at high temperatures. Possibly it was due to the delayed heating in relation to the water saturation of the bentonite clay.

The liquid limit and swell index of dry treated bentonite are lower than corresponding reference material. The decrease of both parameters is observed as a function of the heating time. None of the analyses performed could detect any specific high temperature reaction. During the test period the experiments did not alter the bentonite in a way that it lost its important properties as a buffer material.

Table of content

List of figures

List of Tables

Glossary

HLW	High-Level Waste
SF	Spent Fuel
WP	Work Package

1. Introduction

The overall objective of Task 3 is to conduct research activities to facilitate the evaluation of whether an increase of temperature is feasible and safe by applying existing and the within the task newly produced knowledge about the behaviour of clay buffer materials at elevated temperatures.

The increase of temperature may result in strong evaporation near the heater and vapour movement towards the external part of the buffer. As a consequence, part of the barrier, or all of it, depending on the particular disposal concept, will remain unsaturated and under high temperatures during periods of time that can be very long. Moreover, the high temperature gradient (and pore pressure) even crossing boiling point of water will lead to several adverse effects as Sauna effects.

The objectives of Task 3 subtask have been defined:

- Assessment of the impact of having clay buffer subjected to high temperatures over long time periods on the clay buffer properties. (Subtask 3.1)
- Determination of bentonite hydro-mechanical properties for temperatures higher than 100°C, which will provide parameters for the modelling work. (Subtask 3.2)
- Identification of key processes at high temperature, particularly those affecting the saturation rate, because this will determine the time the buffer is in dry conditions and under high temperature. (Subtask 3.3)
- Calibration and development of suitable THM models for clay buffer at higher temperatures. (Subtask 3.3)

This document describes carried out work within the subtask 3.1 and focuses on the analysis of bentonite samples (content and properties) from selected high temperature experiments.

2. BGR (KIT)

2.1 Introduction

The ABM-tests were conducted in order to be able to directly compare the performance of different bentonites and clays under repository conditions. The first 3 tests (ABM-1, -2, -3) were installed in 2006 (Eng et al. 2007). In 2012 three additional ones were started (Sandén et al. 2018). The target temperature of the tests was 130°C for all tests except for ABM-5. The temperature of ABM-5 was low at the beginning (50°C) because of slower water saturation. In 2016 the temperature was increased up to 250°C for about 6 months and in 2017 ABM-5 was excavated. Temperature profiles are shown in Fig. 1.

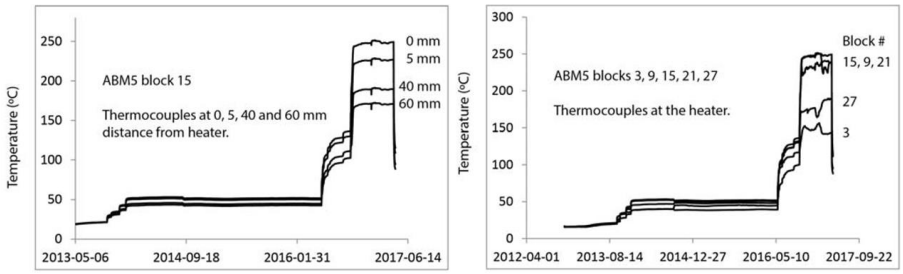

Figure 2.1 Temperature profiles (left: temperature in block 15 at different distances to the heater; right: temperatures at the heater of blocks 3, 9, 15, 21, 27)

The temperature reached 250°C at the contact of the samples which were in the central part of the column (9, 15, 21). At the contact of the upper- and lowermost blocks lower temperatures were observed (about 150°C for blocks 3 and 27). In the hottest blocks (e.g. #15, Figure *2.*1 left) more than 150°C were reached in a distance of 6 cm. This experiment is, therefore, the hottest bentonite large scale deposition test which was conducted so far.

The aim of the study is to investigate the chemical and mineralogical changes and try to find out if there are any specific mineral reactions which can only be explained by the high temperature.

2.1.1 Material

After dismantling of the ABM-5 test in the Äspö URL, samples were collected and sent to BGR. The fotograph shown in Figure 2.2 illustrates the different states of the different blocks after dismantling.

Figure 2.2 Photograph of a part of the ABM-5 experiment after dismantling

Table 2.1 lists all samples sent to BGR including information about the state of the sample. As in the cases of previous analyses of ABM-blocks (Kaufhold et al., 2013; Kaufhold et al., 2017) each block should be sampled at variable distances to the contact face. In some cases only fragments were present which made it impossible to get suitable samples. Sampling of the blocks was done at 4 different distances to the contact face (0.1, 1, 5 and 8 cm). A minimum of 2 g was required for a comprehensive characterization. The actual depths at which the 0.1 cm sample was taken, therefore, depended on the available area of the contact. The material from the contact was scratched off using a sharp knife until 2 g were reached. The actual depths of sampling, therefore, depended on the available surface of the contact and hence on sample size. Sampling of the blocks is shown in Figure 2.3, Figure 2.4, Figure 2.5.

Table 2.1 List and state of samples sent to BGR as well as samples taken at BGR from the blocks (numbers = cm distance from heater; "x" distance to heater could not be determined).

Block no.	Material	Remark	Direction	Comment	0.1	1	5	8	x
30	MX80		30 S		√	√	√	√	
29	MX80		29 N		√	√	√	√	
28	Asha 505		28 S		√	√	√	√	
27	Calcigel	Termoelement		Fragments				√	√
26	Deponit CAN			Fragments	√	√	√	√	
25	Febex		25 W		√	√	√	√	
24	GMZ			Fragments		√	√	√	
23	Ibeco SEAL		23 W		√	√	√	√	
22	Ikosorb		22 W		√	√	√	√	
21	Kunigel V1	Termoelement		Fragments	√	√	√	√	√
20	MX80	Copper	20 W		√	√	√	√	
19	Asha NW BFL-L		19 W		√	√	√	√	
18	Rokle		18 W		√	√	√	√	
17	Saponite		17 W		√	√	√	√	
16	Asha 505	Copper	16 NW		√	√	√	√	
15	MX80	Termoelement+Titanium	15 W		√	√	√	√	
14	Rokle		14NW		√	√	√	√	
13	Febex		13 W		√	√	√	√	
12	Saponite			Fragments	√			√	√
11	Ibeco SEAL		11 S		√	√	√	√	
10	Calcigel			Fragments	√	√	√	√	
9	Asha NW BFL-L	Termoelement	9 N	Partial	√		√		√
8	MX80		8 S		√	√	√	√	
7	Ikosorb		7 S		√	√	√	√	
6	GMZ			Fragments					√
5	Kunigel V1			Fragments	√	√	√	√	
4	Deponit CAN			Fragments	√	√	√		
3	Asha NW BFL-L	Termoelement+Titanium	3 N		√	√	√		
2	MX80		2 SE		√	√	√	√	
1	MX80		1 N		√	√	√	√	

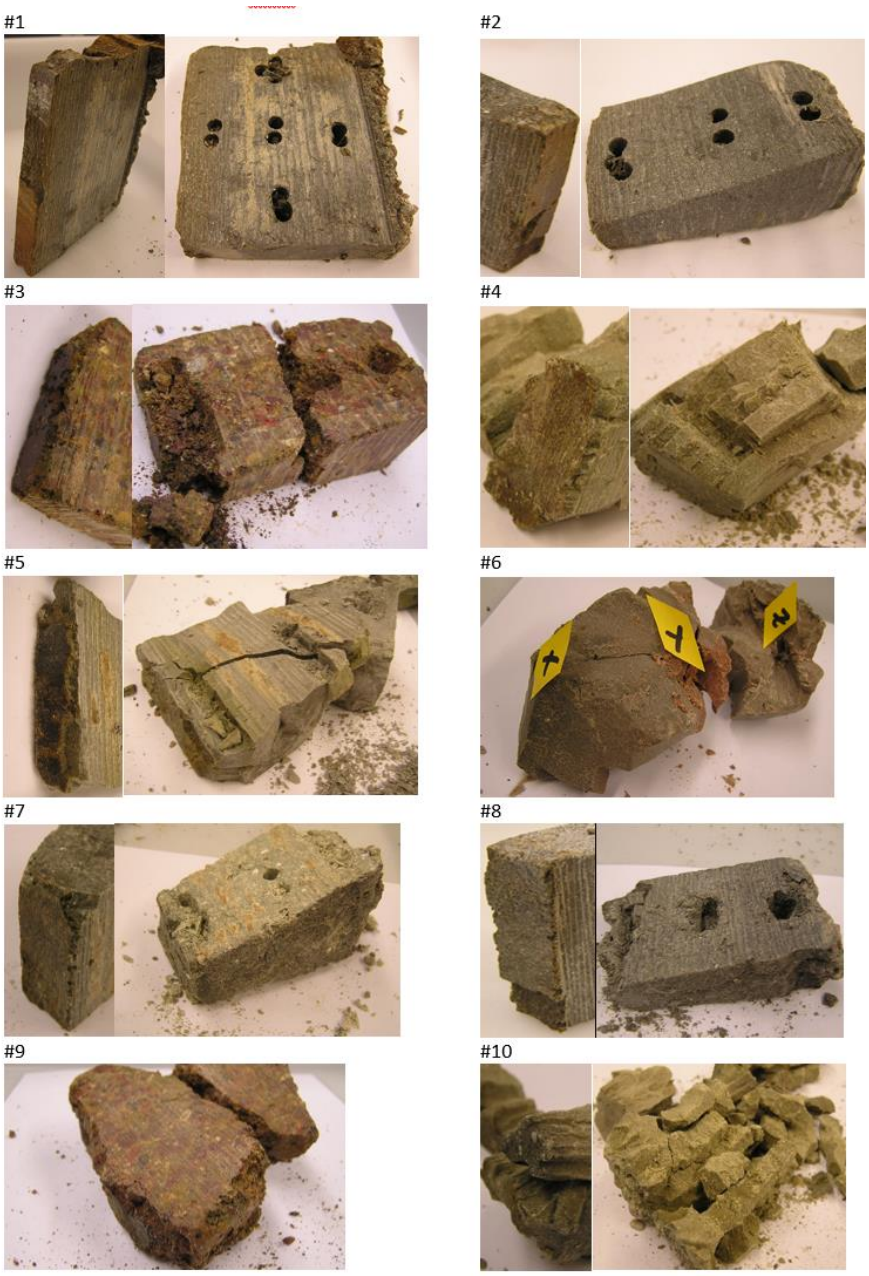

Figure 2.3 Photos of sampling blocks 1 – 10

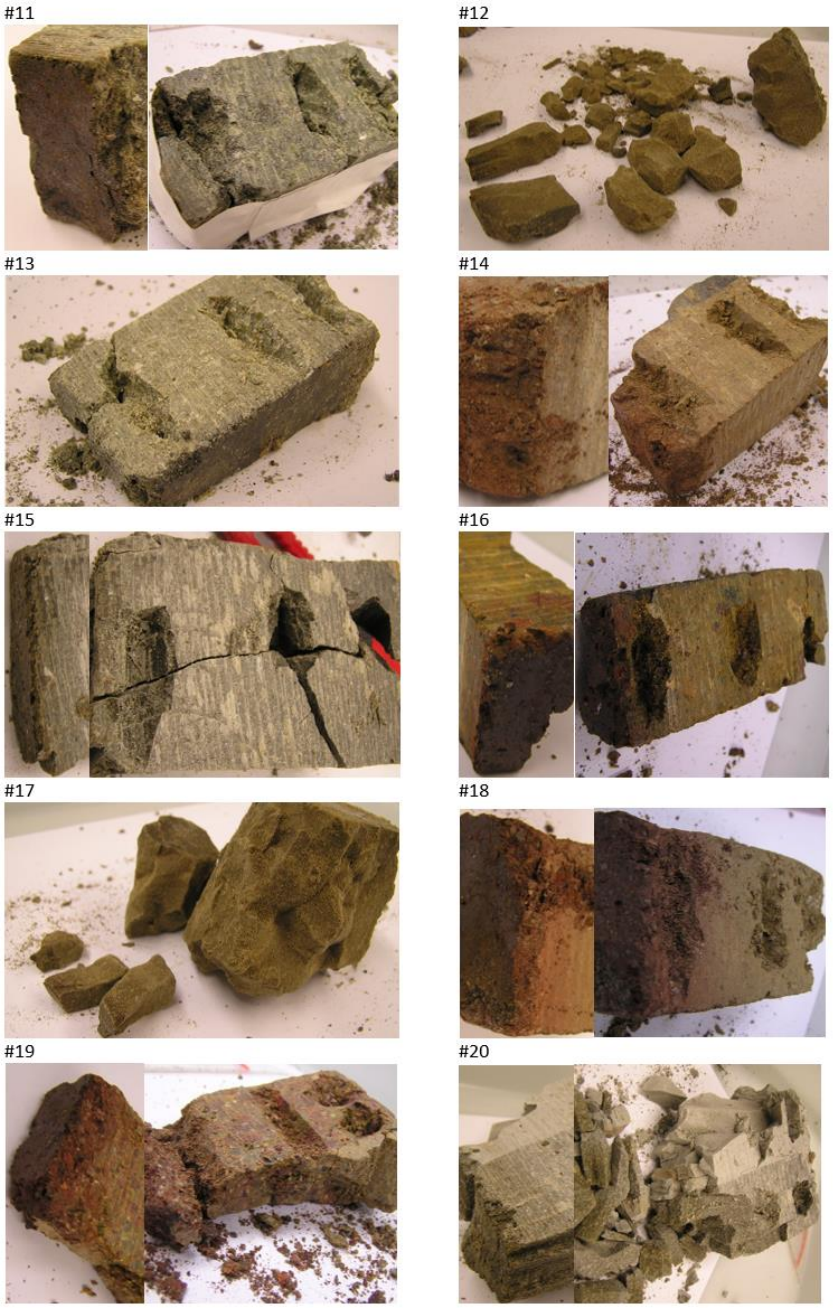

Figure 2.4 Photos of sampling blocks 11 – 20

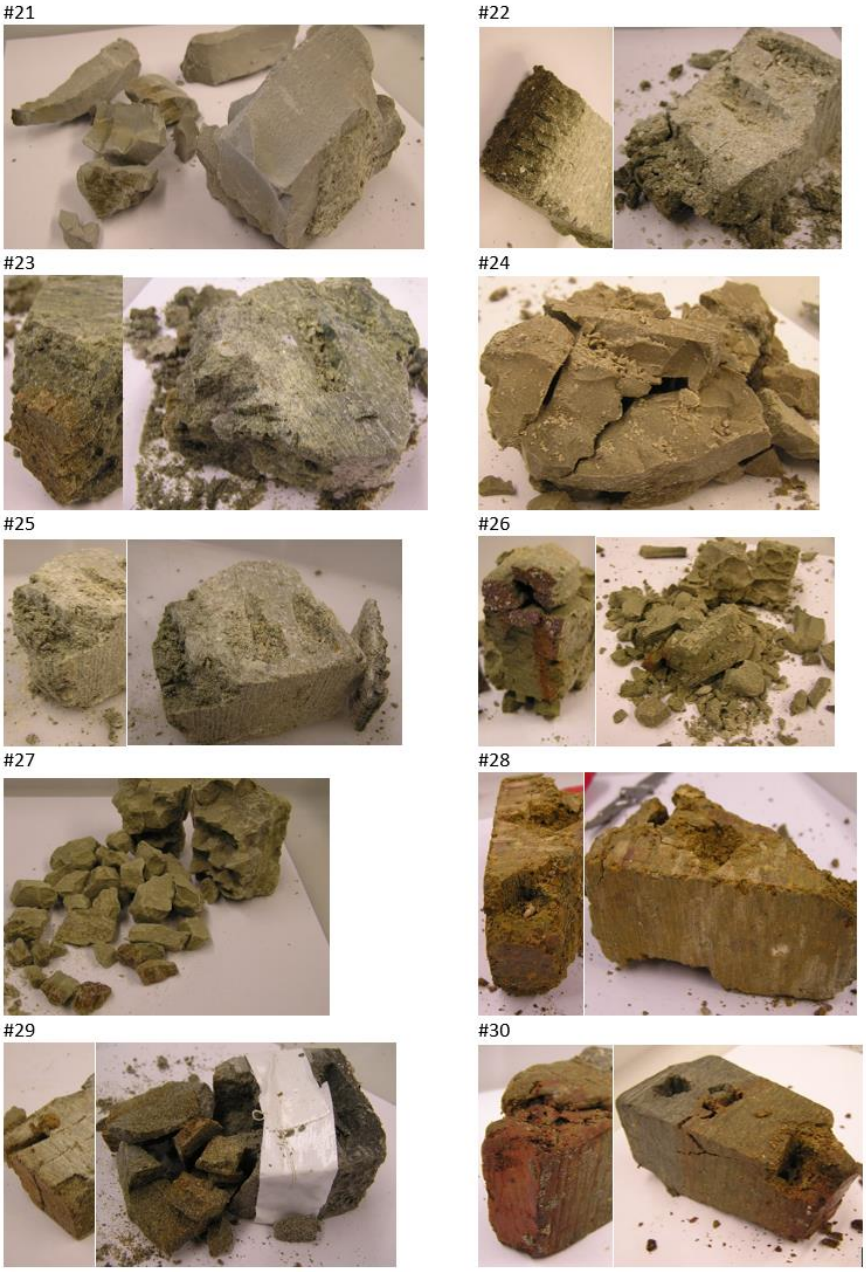

Figure 2.5 Photos of sampling blocks 21 – 30

2.1.2 Research plan

Samples from all ABM-5 blocks taken and sent to BGR.

Sampling of the blocks at different distances to get four samples per block and one piece with contact for SEM.

Drying and grinding (sample preparation)

Chemical and mineralogical analysis

- Elemental analysis (ICP, Actlabs)
- XRD
- LECO
- IR
- STA
- SEM

Table 2.2 BGR - *ABM-5*

2.1.2.1 Material (BoM item): 30 blocks from the ABM-5 test conducted by SKB
2.1.2.2 Material treatment (sample preparation for test and loading procedure): Four samples taken from each block. A reference sample is considered additionally. 2.1.2.2.1 Laboratory treated material Analysis will be based on the samples taken from the blocks and the references. 2.1.2.2.2 Material from T3.3 none
2.1.2.3 Temperature (to which material was/will be exposed to) and exposure time 150 – 250 °C for 6 months (see Fig. 1)
2.1.2.4 Tests carried out (name, description, sample preparation, procedure, results): Chemical and mineralogical analysis as specified in 2.2.1 2.1.2.4.1 Permeability - K [m/s] No permeability measurements 2.1.2.4.2 Swelling pressure - σ_{sw} [MPa] No swelling pressure tests
2.1.2.5 Schedule and expected date(s) of results delivery: Sample preparation started: M6 First analyses available M12 → results M18 CEC results interpreted, reporting / publication M18 → results M24 Reporting / publication M30 → results M36

2.2 Procedures

2.2.1 Laboratory set-ups, procedures and protocols

The chemical analysis was performed by ACTLABs® using the analytical tools 4B1 QOP Total (Total Digestion using different acids, analysis by ICP-OES), 4C QOP XRF Fusion (Whole Rock Analysis-XRF), and 4F-Cl QOP INAA—Short Lived (INAA). The effect of different water contents on the elemental composition was eliminated by normalizing all values not considering the loss on ignition.

The organic carbon (C_{org}) content was measured by combustion with a LECO CS-444-Analysator after dissolution of the carbonates. Carbonates were removed by treating the samples several times at 80 °C with HCl until no further gas evolution could be observed. Samples of 170–180 mg of the dried material were used to measure the total carbon (C_{total}) content. Total inorganic carbon (C_{inorg}) was calculated by the difference of C_{total} and C_{org}. The samples were heated in the device to 1800–2000 °C in an oxygen atmosphere and the CO_2 and SO_2 were detected by an infrared detector. The device was built by LECO (3000 Lake Avenue, St. Joseph, MI, USA).

Thermoanalytical investigations were performed using a Netzsch 449 F3 Jupiter thermobalance equipped with a DSC/TG sample holder linked to a Netzsch QMS 403 C Aeolus mass spectrometer (MS). Then, powdered material (100 mg) previously equilibrated at 53% relative humidity (RH) was heated from 25 to 1150 °C with a heating rate of 10 K/min. The devices were manufactured by Netzsch (Gebrüder-Netzsch-Straße 19, Selb, Germany).

XRD patterns were recorded using a PANalytical X'Pert PRO MPD Θ-Θ diffractometer (Cu-Kα radiation generated at 40 kV and 40 mA), equipped with a variable divergence slit (20 mm irradiated length), primary and secondary sollers, Scientific X'Celerator detector (active length 0.59°), and a sample changer (sample diameter 28 mm). The samples were investigated from 2° to 85° 2Θ with a step size of 0.0167° 2Θ and a measuring time of 20 s per step. For specimen preparation, the back loading technique was used.

For the detailed clay mineralogical investigation, texture slides of the <2 µm fraction were prepared. Oven-dried clay fractions <2 µm of the contact samples (if available) were dispersed using ultrasound. A suspension containing approximately 60 mg solid clay fraction was sucked through porous ceramic tiles of 27 mm diameter using a vacuum-filter in order to orient the clay minerals (aluminosilicates) preferentially parallel to their basal planes. The final solid density was approximately 15 mg/cm^2. These so-called oriented aggregates were x-rayed from 2.5 to 40° 2 theta (air-dried and ethylene glycol solvated) with a step size of 0.03° 2Θ. The measuring time was 6 s per step. The scans were run on a PANalytical X'Pert PRO MPD Θ–Θ diffractometer (Co-Kα radiation generated at 40 kV and 40 mA), equipped with a variable divergence slit (20 mm irradiated length), a primary and secondary soller, a proportional counter, and a secondary monochromator.

A Zeiss Sigma 300 V P FEG scanning electron microscope operating at 15 kV was used to evaluate samples on the micro scale using the high-vacuum mode. The microscope was equipped with the following detectors: Bruker Xflash® 6/60 EDX detector, high-definition backscattered electron detector (HDBSD), secondary electron detector (SE2), variable pressure secondary electron detector (VPSE), and an InLens detector for detection of secondary and backscattered electrons, respectively.

For measuring mid infrared (MIR) spectra, the KBr pellet technique (1 mg sample/200 mg KBr) was applied. Spectra were collected on a Thermo Nicolet Nexus FTIR spectrometer (MIR beam splitter: KBr, detector DTGS TEC; FIR beam splitter: solid substrate, detector DTGS PE). The resolution was adjusted to 2 cm^{-1}. Measurements were conducted before and after drying of the pellets at 150 °C in a vacuum oven for 24 h. The spectrometer was built by Nicolet Instruments, Madison, Verona Road, WI, USA.

2.2.2 Data and other results available

All data are available and were already published open access by Kaufhold et al. (2021). The raw data is available in the supplements of this publication.

2.3 Results

All analyses were completed. The interpretation and reporting, however, of the CEC data is still ongoing. Results obtained so far were published (Kaufhold et al., 2021) and summarized in chapter 2.3.2.

2.3.1 Investigation performed

Work is described in 2.2.1.

2.3.2 Results from investigation

Geochemical profiles

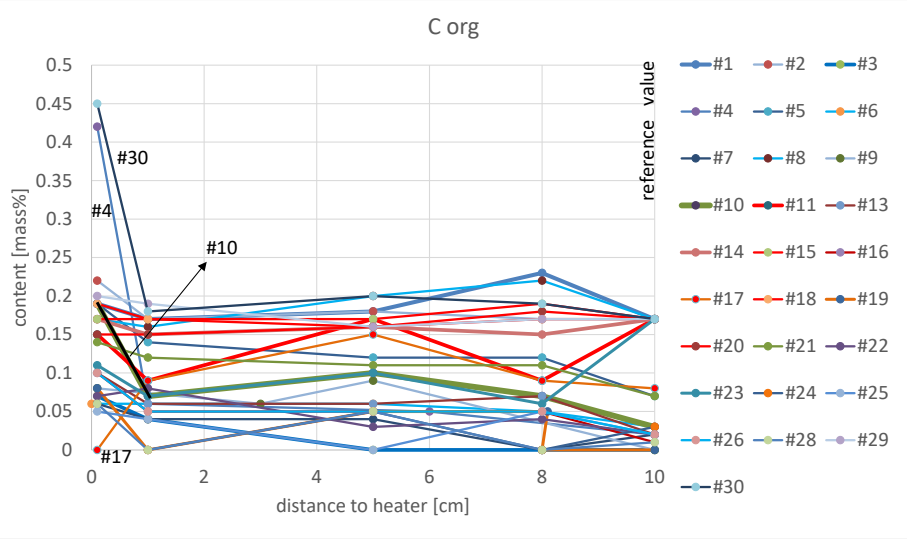

Figure 2.6 Organic C distribution within the blocks. Profiles from the hotter central part are red

In the ABM-2 test high C organic contents (Figure 2.6) were observed at the interface which could be explained by Molykote® which was used for lubrication (between heater and bentonite). The C_{org} contents were partly above 1 mass%. High contents were particularly observed at the lowermost part of the experiment. In the ABM-5 only 2 samples showed increased C_{org} contents. Also no increase of the Zn value was observed which proves that no molykote was used to setup ABM-5. The organic carbon contents measured in ABM-5 rather reflect the formation of siderite which was proved by STA. Organic carbon is distinguished from inorganic carbon by acid digestion and repeated LECO measurements. Siderite is known to be less soluble in hydrochloric acid hence some siderite remains after acid treatment which is counted as organic matter (as acid solubility was used to discriminate between organic and inorganic carbon). The formation of siderite was proven which explains the results and is discussed later. The “hot profiles” (red curves) do not differ from the others.

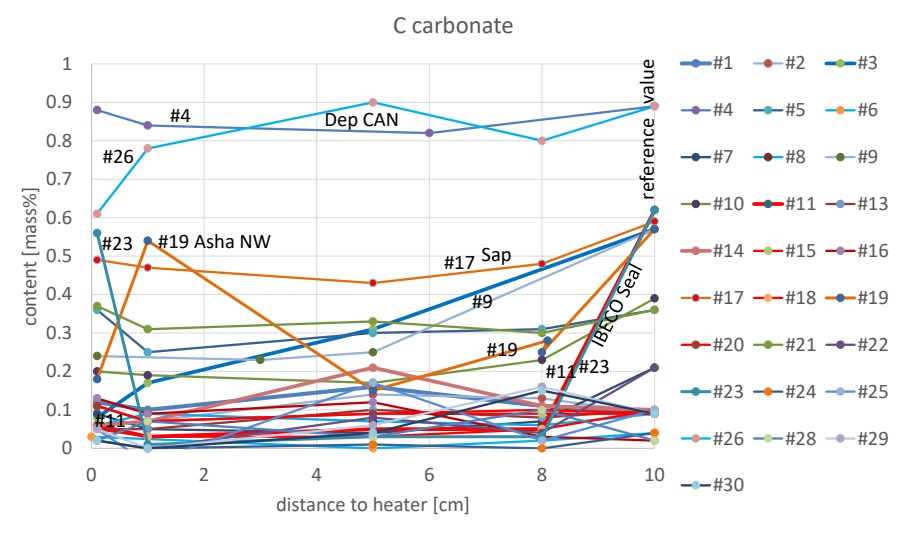

Figure 2.7 *Inorganic (Cinorg) C distribution within the blocks (LECO). Profiles from the hotter central part* are red

Carbonate dissolution and precipitation was found in different medium to large scale deposition tests. LECO analysis of all samples (Figure 2.7) indicates that different carbonate redistribution reactions occurred. Most samples had a C_{inorg} content of < 0.2 mass% and did not show any carbonate redistribution. Some specific reactions could be identified: A few samples showed some carbonate enrichment in the center of the blocks with larger values compared to the reference (e.g. #1, #14). This indicates that carbonate was either transported into the barrier by the saturating fluid or that carbonate was dissolved in other blocks and transported vertically. Significant differences indicating carbonate dissolution was observed for both blocks made out of Ibeco Seal (#11, #23). However, meanwhile it is clear that a difference charge of this material was sent to BGR as reference which explains the differences. The slightly higher carbonate content of these blocks at the heater, therefore, points towards carbonate precipitation. The blocks made out of Asha NW (#9, #19) showed much lower values in the blocks compared with the reference which points towards carbonate dissolution. Only the sample taken in 1 cm distance to the heater showed the same values as the precursor. The largest carbonate content was found in the sample Deponit CAN (about 0.9 mass%). Both blocks were not in the hottest part but showed different reactions. In block 26 carbonate was dissolved near the heater whereas it precipitated near the heater in block 4.

Carbonate dissolution and precipitation (redistribution) showed different patterns which do not allow to derive a general rule. Different profiles were observed for the same material and temperature. Therefore, the differences of the profiles neither can be explained by material properties (type of carbonate present) nor by the different temperatures in the package. Carbonate redistribution is likely more affected by local differences, possibly by porosity and water content. No systematic differences were found between the profiles of the hotter part compared with the others.

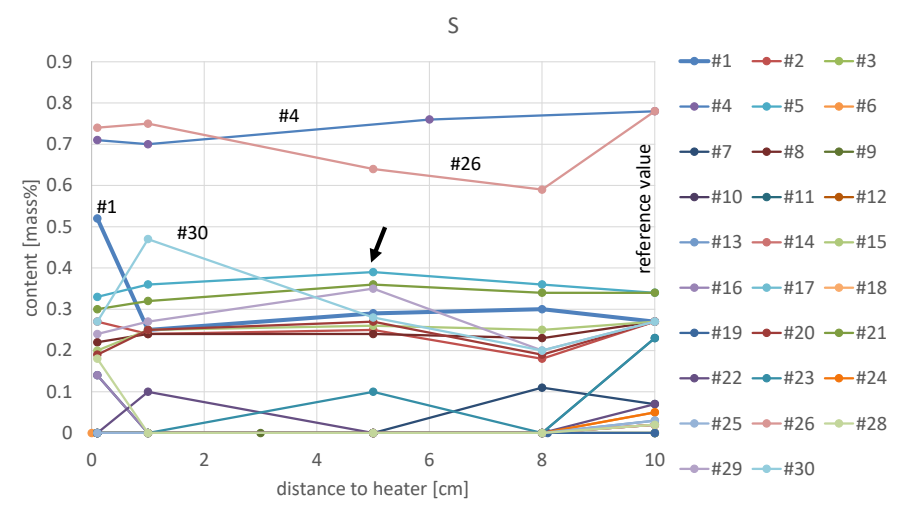

Figure 2.8 S distribution within the blocks

In the LOT-A2 experiment, which was also conducted at temperatures higher than 90°C, a redistribution of gypsum was detected (Kaufhold & Dohrmann, 2009). Gypsum was obviously dissolved both near the granite and near the heater and precipitated in the centre of the block. In the ABM-1 and ABM-2 tests different S-profiles were measured (Kaufhold et al., 2013; 2017). Most of the samples of ABM-5 (Figure 2.8) showed a slight increase of the S-content in the central part (arrow in Fig. 8) and some dissolution at the inner and outer parts. This behavior was similar to the results found in the LOT-A2 experiment but much less pronounced. The amount of S which precipitated in the central part of the LOT-A2 blocks was much larger. S concentrations below 0.1 mass% are close to detection limit and hence not discussed further. Most of the samples, however, showed S-contents ranging from 0.2 – 0.4 mass%. Three samples showed an untypical behavior: in block 1 a significant increase of the S content directly at the heater was observed which may be related to the different hydraulic conditions of this block (direct contact to granite at the bottom). The top block (#30) showed S enrichment at a distance of 1 cm. The extraordinary behavior of these blocks may result from the special hydraulic properties caused by the fact that there were no seals above and below for which water could not only enter from the outside.

Commenté [LJ1]: To be consistent with other spellings of this word.

Blocks 26 and 4, both Deponit CAN, showed the highest S-content but different profiles. For both samples slightly lower values were found in the block after the experiment compared to the reference which proves that gypsum is at least partly soluble and also transported vertically.

Gypsum as the main S-source in bentonites is partly soluble and can be transported through the barrier and no specific profiles of the hotter part were observed.

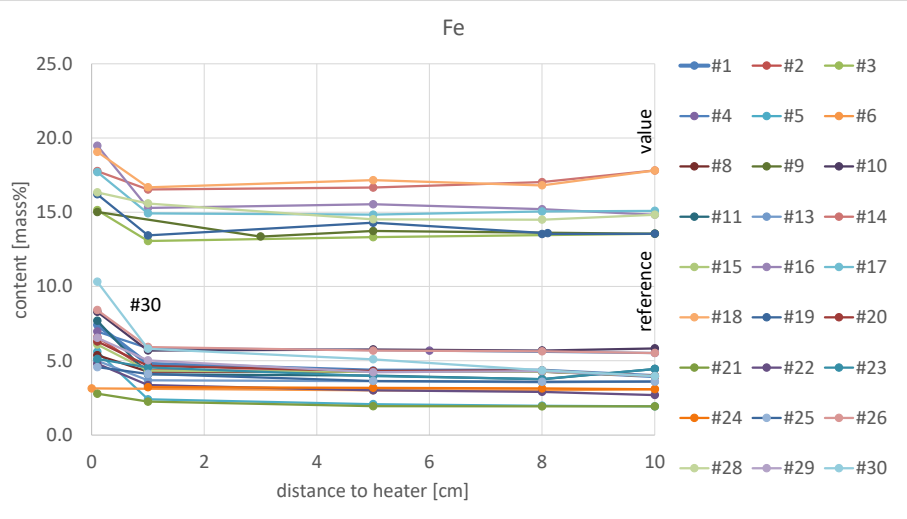

Figure 2.9 Fe distribution in the blocks

Some chemical variations in the block can be caused by heterogeneities in the material (e.g. ASHA) because some of them contain quite coarse grains. Most of the blocks, however, showed an increase of the Fe_2O_3 content at the contact (0.1 mm sample) of more than 1 mass% (Figure 2.9). The largest increase was found for the top block (#30: + 4.5 mass%). These values can hardly be compared with those of the other studies because of different contact areas (as explained above). A couple of samples, however, showed (slightly) increased Fe-contents even at a distance of 1 cm. This increase was small but it indicates that Fe was mobile and could be at least partly transported in the system. No specific reactions in the hot parts were identified.

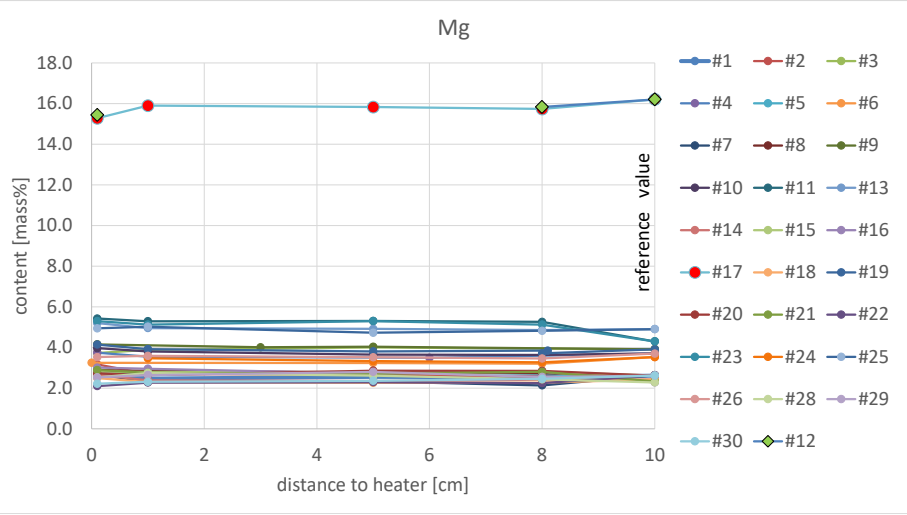

Figure 2.10 Mg distribution in the blocks

Mg enrichment close to the heater was observed in many large scale tests, regardless if Fe or Cu heater was used. This enrichment is of particular interest because it could be correlated with the neoformation of phases as triocthahedral smectite and/or brucite (Kaufhold et al., 2018).

In the ABM-2 test (Kaufhold et al., 2017), MgO enrichments at the contact of 0 – 3 mass% were observed. The most significant MgO increase was observed at the face of the FEBEX experiment (+ 6 mass% MgO) which at least partly can be explained by the fact that a larger sample was available and hence the very top could be sampled. Using IR spectrometry, formation of brucite was found and by XRD formation of trioctahedral domains was observed. In the ABM-2 experiment only formation of trioctahedral domains was observed, commonly associated with significant MgO increase. The MgO increase in the ABM-5 blocks, however, was not typical for a special type of bentonite (Fig. 10). As an example, the two blocks of Deponit CAN and ROK showed either 0 – 0.3 mass% or 1.8 – 2.8 mass% MgO increase. These values, therefore, seem to depend more on the local conditions (temperature, water content, type of solution diffusing through the bentonite) than on the type of bentonite. The significantly larger temperature of ABM-5 could have affected the formation of Mg-rich phases. Kaufhold et al. (2019) showed that the temperature affects the ratio of Mg/Si which can be dissolved from smectites in a way that it decreases with increasing temperature which means that the solubility of Si increases more than that of Mg. Accordingly one could expect Si phases to be precipitated at the heater. Surprisingly only a slight increase of the MgO value was observed. The largest values (+ 1 mass% MgO) were observed for the two IBECO Seal bentonites which, however, is supposed to result from a different charge of the reference material. Notably, a slight decrease or increase of the MgO value compared to the reference value can be explained by cation exchange. For the first time a saponite was tested in a deposition test. Interestingly a slight decease of the MgO value at the heater was observed for both saponite samples. The curve of #12, however, is not complete because it could only be sampled at the contact. The 3 points shown in Figure 2.10, however, are identical to those measured for sample #17 which was also made of saponite. Both saponite blocks, therefore, show Mg decrease at the heater but no specific reactions of the material from the hotter parts was found.

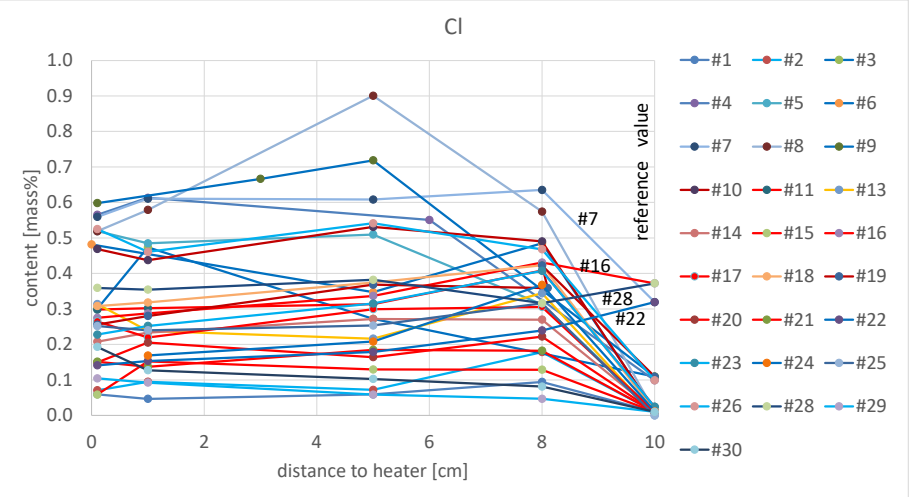

Figure 2.11 Cl profiles in all blocks (without #12, #27). Red lines indicate a central position in the package which was exposed to larger temperature and blue lines indicate colder temperature.

Most samples showed an initial Cl-content of ≤ 0.1 mass% and an increase in the reacted blocks which can only be explained by Cl derived from the rock water which migrated into the blocks. In most blocks Cl even reached the heater because the contents measured there were higher compared to the

reference materials (Figure 2.11). The two samples Asha 505 and Ikosorb (#7, #16, #22, #28) had a larger initial Cl content. However, different behavior was observed. Ikosorb showed Cl increase in block 7 and decrease in block 22. Asha 505 showed increase in block 16 and decrease in block 28. The Cl migration into the blocks apparently did not depend on the material but on local differences. Also no effect of the actual temperature on the Cl profiles was observed.

XRD

XRD is the reference method in mineralogy. The detection limit, however, varies around 1 mass% which means that minor changes cannot be detected.

Almost all samples showed a shift of the d001 peak position which can be explained by cation exchange. This effect is even better observed considering the XRD pattern of oriented mounts (Fig. 16, 17, 18) and will be compared with CEC data in future.

Differences others than d001 shifting such as varying muscovite/feldspar/quartz peak intensities were also observed but these do not necessarily point towards actual mineral reactions. Small differences of these intensities can also be explained by single crystal reflexes. Also the reference samples were recorded with slightly higher intensity which translates into a better signal/noise ratio. Generally XRD is not a method to unambiguously detect minor mineral changes. Varying peak intensities may point to actual mineral reactions but these should be validated based on chemical data.

Significant differences of the peak intensity, however, such as that of the gypsum peak of the 1 cm sample of block 30 point to actual mineralogical differences. LECO data prove a slightly larger S-content of this sample which suggest that gypsum was actually enriched in this sample (at a distance of 1 cm to the heater).

All results derived from XRD were summarized in Tab. 2. All XRD power pattern are shown in Figure 2.12, Figure 2.13, and Figure 2.14.

Table 2.2 Summary of XRD results

distances from heater (cm)			d(060)		sulphate phases				pyrite XRD				inorganic carbon phases																			
					gypsum								calcite				dolomite/ankerite				siderite				cristobalite				goethite				clinoptilolite			
Block	Material/abbreviation	REF	0.1	new (0-1)	REF	0.1	1	5	8	REF	0.1	1	5	8	REF	0.1	1	5	8	REF	0.1	1	5	8	REF	0.1	1	5	8	REF	0.1	1	5	8	REF	0.1	1	5	8
30	MX80	1.498	✓		+	(?)	+	+	?	+															+	+	+	+									
29	MX80	1.498	✓		+	+	(?)			+	(?)	?	(?)	?											+	+	+	+									
28	Asha 505	1.500	✓		(?)	(?)				(?)	(?)	(?)			(?)	+	+	+	+											+	+	+	+					
27	Calcigel (CAL)	1.498		no contact sample											+					++				+														
26	Dep. CAN	1.498	✓		+	+	+	?	(?)	+	(?)	(?)	(?)	(?)	++	+	+	++	++	+	+	+	+	+	(?)	(?)	(?)												
25	Febex	1.499	✓												+	+	+	+	+						+	+	+											
24	GMZ	1.498(5)		no contact sample																					+		++	++										
23	Ibeco Seal (IBE)	1.498	✓												+	+	(?)		?	+																		
22	Ikosorb (IKO)	1.495	✓												+	+	+	+	+																			
21	Kunigel V1 (JNB)	1.498	✓							+	?	?	?	?	+	+	+	+	+						(?)	(?)	(?)	(?)							+	+	+	+	+
20	MX80	1.498	✓		+					+	?	(?)	(?)	?	++	+	+	+	+																			
19	Asha-NW BFL-L	1.500	✓												?										+	?	+	+	+									
18	Rokle (Rawra)	1.505	✓																																			
17	Saponite	1.512	✓												+	+	+	+	+	+	?	+	?															
16	Asha 505	1.500	✓		(?)	(?)				(?)	+	+	+																									
15	MX80	1.498	✓		+					+	(?)	(?)	(?)	(?)											+	+	+	+										
14	Rokle (Rawra)	1.505	✓												?																							
13	Febex	1.499	✓												+	+	+	+	+						+	+	+	+										
12	Saponite	1.512	✓												+	+	(?)		+																			
11	Ibeco Seal (IBE)	1.498	✓												+	(?)				+																		
10	Calcigel (CAL)	1.498	✓												+	(?)	(?)	(?)	(?)	++	+	+	+	+	(?)	+	+	+	+									
9	Asha-NW BFL-L	1.500	✓												++	+	+																				
8	MX80	1.498	✓		+					+	(?)	(?)	(?)												+	+											
7	Ikosorb (IKO)	1.495	✓	1.54(5)											+	+	+	+	+																			
6	GMZ	1.498(5)		no contact sample																					+		++	++										
5	Kunigel V1 (JNB)	1.498	✓							+	?	?	?	?	+	+	+	+	+						(?)	(?)	(?)								+	+	+	+	
4	Dep. CAN	1.498	✓		+	+	(?)	(?)		+	(?)	(?)			++	++	++	++		+	+	+	+		(?)	(?)	(?)											
3	Asha-NW BFL-L	1.500	✓												++	+	+								+	(?)	(?)											
2	MX80	1.498	✓		+	(?)	(?)	(?)		+	(?)	(?)	(?)													+	+	++	+									
1	MX80	1.498	✓		+	+	?	+	+	+	?	?	?	?												+	+	+	+									

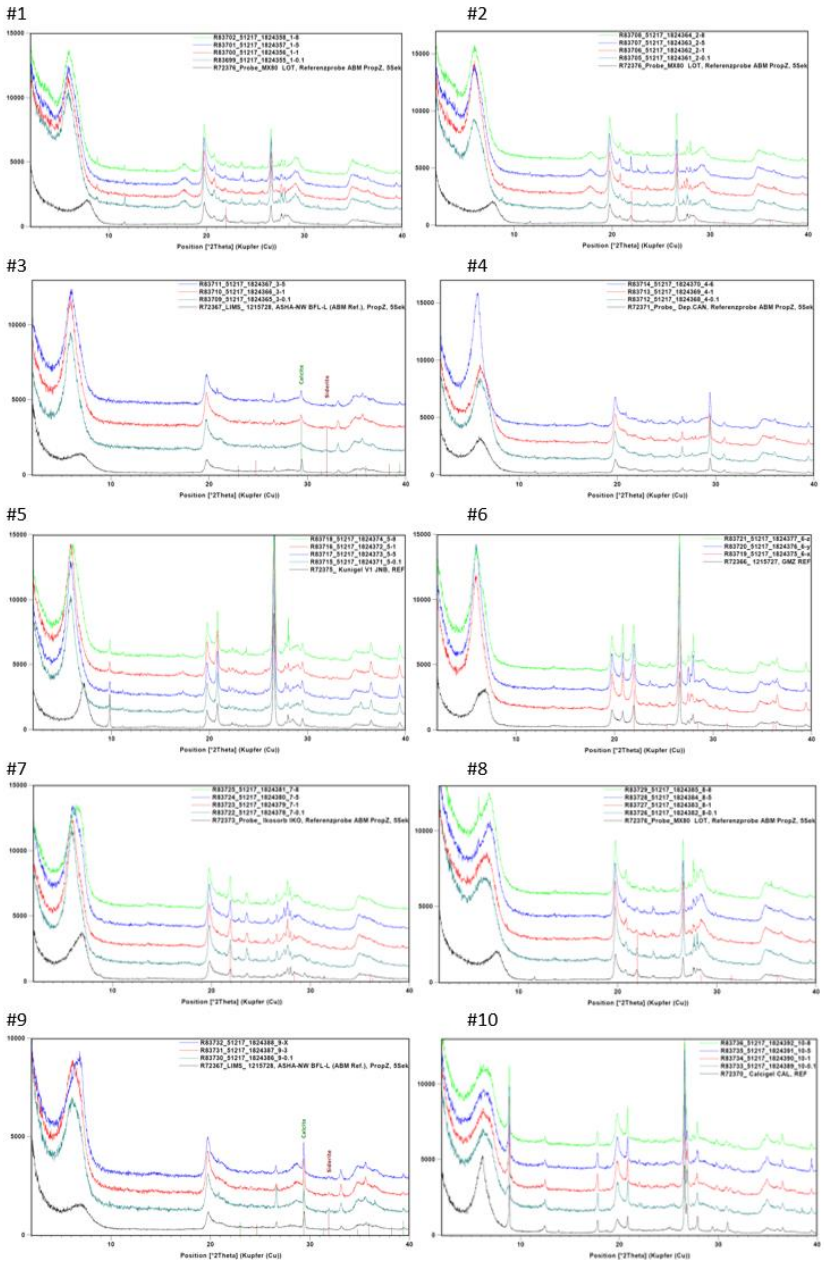

Figure 2.12 Powder XRD results of blocks 1 – 10

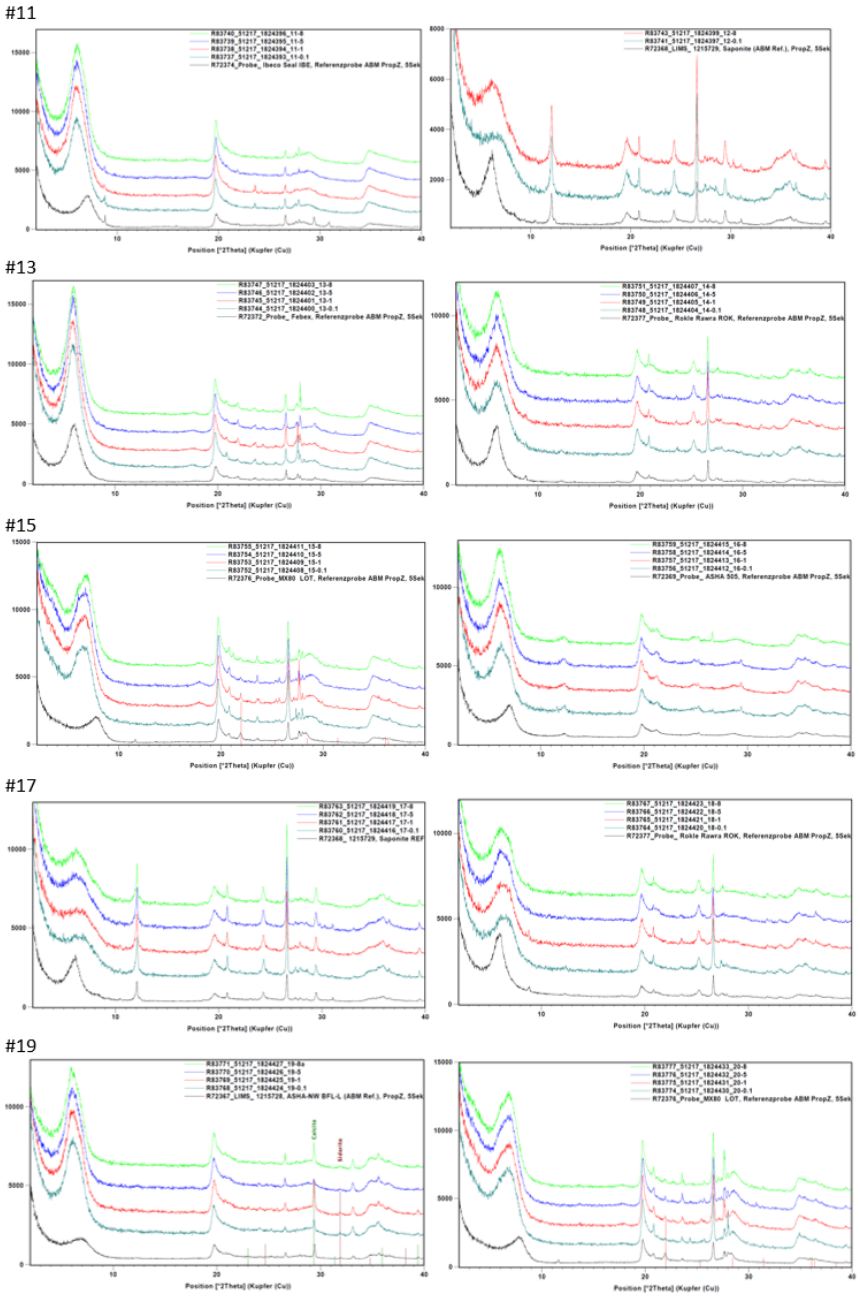

Figure 2.13 Powder XRD results of blocks 10 – 21

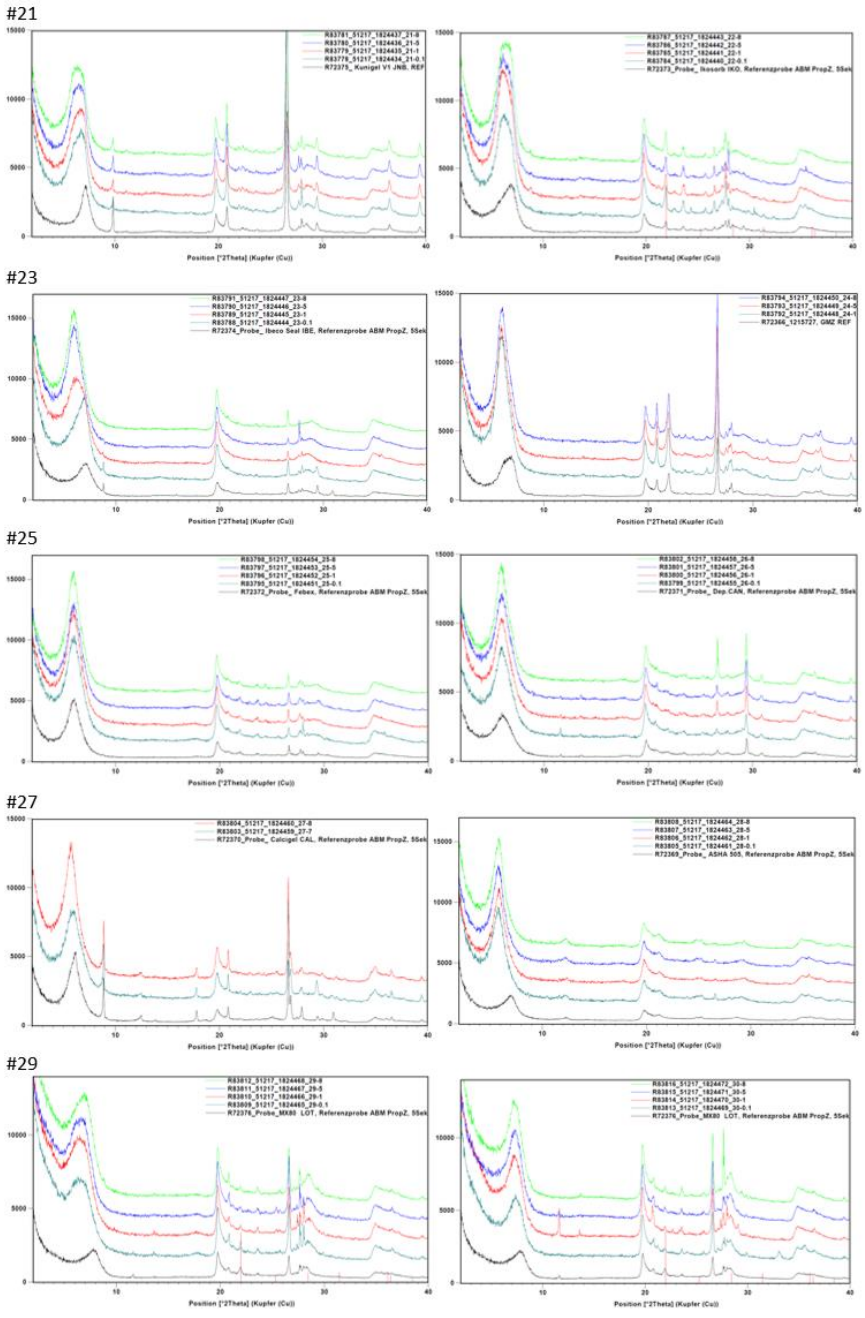

Figure 2.14 Powder XRD results of blocks 21 – 30

Special attention was paid towards changes of the d060 reflexes indicating formation of trioctahedral phases at the heater. Such phases were found before (Kaufhold et al., 2013; Kaufhold et al., 2017, Kaufhold et al., 2018; Svensson et al., 2015) based on XRD and IR. In the ABM-5 samples no changes of the d060 were observed although some Mg-enrichment was observed. The extent of the Mg enrichment at the heater, however, was small comparted with yet published results. The largest MgO increase was found in both Ibeco Seal blocks (#11: +1.1 mass% MgO, #23: +1.0 mass% MgO) but that could be explained by a different reference material. Also some MgO enrichment was found in block 16 (0.7 mass%) and block 21 (0.6 mass%). However, no changes of the d060 reflexion were found (Figure 2.15).

The saponite samples (#12, #17) showed some decrease of the MgO content at the heater but no changes of the d060 reflection could be observed (as in the cases of the others).

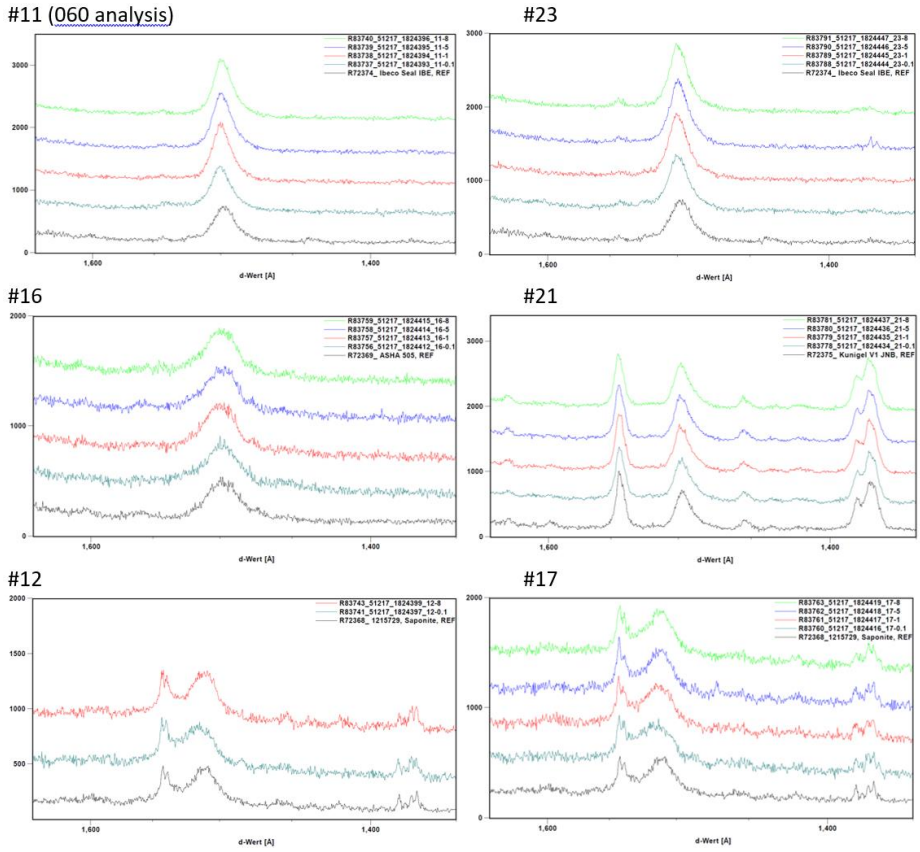

Figure 2.15 Analysis of the possible change of the 060 position (selected samples)

Oriented mounts

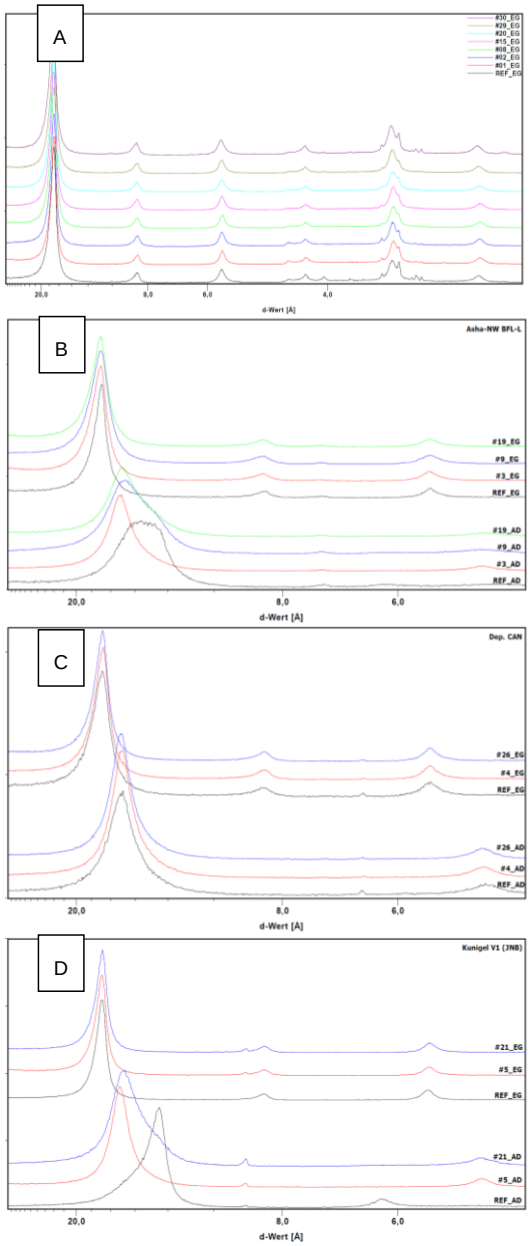

Figure 2.16 XRD of oriented mounts (black: reference sample, bottom: air dried, upper pattern: EG saturated; A: MX80, B: ASHA-NW BF, C: DepCAN, D: Kunigel)

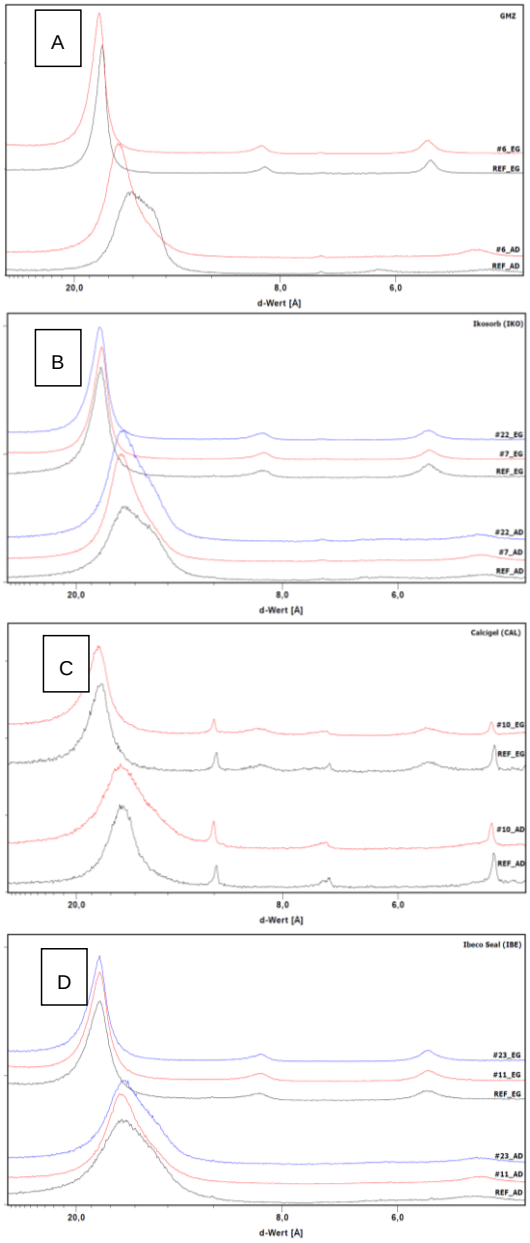

Figure 2.17 XRD of oriented mounts (black: reference sample, bottom: air dried, upper pattern: EG saturated; A: GMZ, B: IKO, C: CAL, D: IBE)

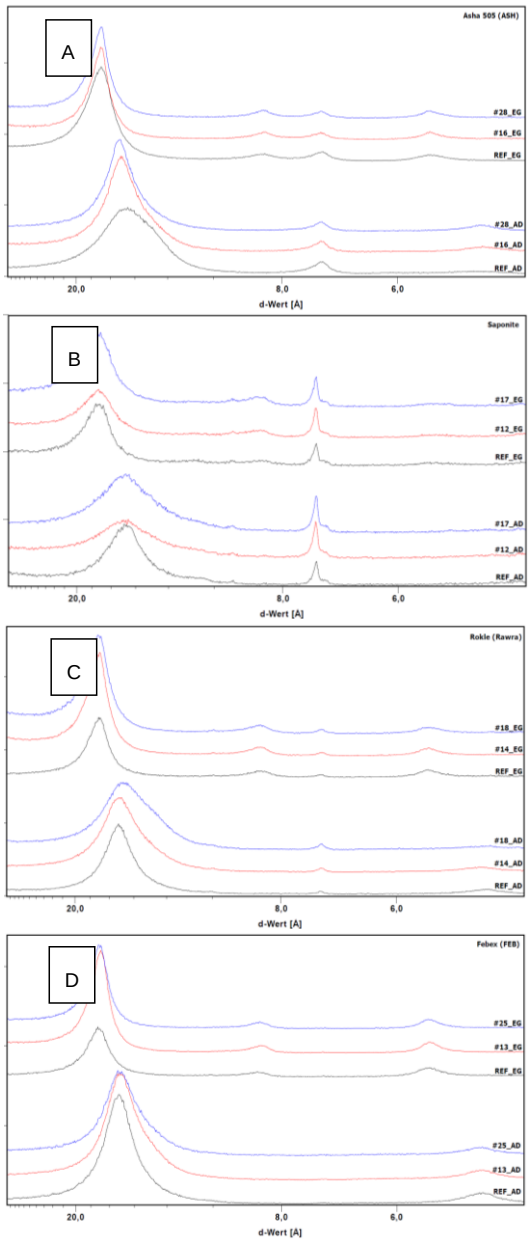

Figure 2.18 XRD of oriented mounts (black: reference sample, bottom: air dried, upper pattern: EG saturated; A: ASHA 505, B: Saponite, C: ROK, D: FEB)

XRD pattern of oriented mounts were recorded to investigate the possible loss of swelling capacity (Figure 2.16, Figure 2.17, Figure 2.18). The samples were measured both in air dried and EG (ethylene glycol) saturated state. Most significant changes were shifts of the d001 reflection of air-dried samples (contact samples against reference). One example for a significant shift caused by cation exchange is shown in Figure 2.16-D. This shift can be explained by exchange of monovalent by divalent cations. Also the peak shape sometimes changed. As an example, the broad peak of ASHA NW (Figure 2.16-B) either changed to a sharper peak (blocks 19 and 3) or to a different shape of a broad peak. This different behaviour can be explained by different cation exchange and the resulting differences of the interlayer hydration state. In none of the samples peaks were observed which point towards the formation of non-swelling minerals out of smectite. From the XRD perspective, therefore, no loss of the swelling capacity was observed.

Commenté [LJ2]: Is it ethylene glycol? Explain when the abbreviation is first used.

Simultaneous thermal analysis

Simultaneous thermal analysis is particularly valuable for the investigation of C- and S-phases because of the sensitivity of the mass spectrometer (detection limit can be as low as 0.01 mass%). Analyses were performed using air which results in oxidation of organic matter and outgassing of CO_2. Carbonates decompose forming CO_2 and pyrite oxidizes at about 500°C which in turn can be detected as SO_2 in the quadrupole mass spectrometer. Dehydration and dehydroxylation are detected using atomic mass 18. Shifts of the dehydration peak can be explained by cation exchange which, however, is better characterized using CEC methods. The type of exchangeable cation also affects the peak position of the dehydroxylation (Wolters & Emmerich, 2007). Small shifts of this peak, therefore, do not necessarily point to structural modifications of the smectite.

STA data is reasonably discussed together with LECO data providing quantitative information about C- and S-contents.

Most samples showed a decrease of the carbonate content at the heater contact except for #16 where carbonate content increased from 0.02 – 0.13 mass% (C-content) which corresponds to about 1.5 mass% carbonate. In the STA curves a slight increase of the CO_2 curve is observed (Figure 2.20). All other samples showed constant or decreased carbonate contents. A couple of samples showed increasing organic C contents, possibly beeing an artefact due to the formation of siderite, as organic carbon is determined based on LECO measurements with and without acid digestion. Siderite is less soluble in hydrochloric acid than Ca-carbonate and hence explains the increased organic C contents. This transformation was validated by STA. The STA curves of some samples show decreasing calcite peaks (between 700 and 800°C) but increasing intensity between 500 and 600°C which corresponds to siderite. The contact sample of block 10 showed complete calcite dissolution and precipitation of siderite. To prove that the 550°C peak corresponds to siderite, parallel measurements were performed under nitrogen, which would prevent the oxidation of real organic matter. No changes of the curves were observed which indicates that this peak can be assigned to siderite. In other blocks (4, 5, 9, 12) siderite formation was observed but calcite was still present. In block 11 complete carbonate dissolution was observed without any signs of siderite formation.

Commenté [LJ3]: The relation between increased organic carbon and formation of siderite (which is an inorganic carbonate mineral) is not so obvious. Explain is needed.siderite

Calcite dissolution in combination with siderite formation could be hardly observed before because of the large amount of lubricant which was used in ABM-1 and ABM-2. The contact sample of block 3 of ABM-2, however, in which the real organic C content was low, indicates a similar reaction. The formation of siderite at the expense of calcite, therefore, is not specific for high temperature reactions but it could only be detected because no lubricant was used in this experiment.

A significant increase of the S-content was found in the contact sample of block 1 (0.27 → 0.52 mass%) which may have resulted from the exposed position of this block. Most of the blocks did not show any change of the S-contents. Interestingly both blocks made of IBE and ASHA 505 showed significant changes. In the contact samples of #11 and #13 (IBE) a decrease of S was found (0.23 → < 0.1 mass%) and in #16 and #28 (ASHA 505) an increase was found from 0.02 → 0.14/0.18 mass%. The different changes of the S-content would indicate locally different conditions (porosity, T-gradient, water content,

etc.) but the fact that different blocks made out of the same bentonite showed similar behavior points to material specific reactions. Hence it cannot be decided if locally different conditions or material properties are relevant. The different reactions of pyrite, however, indicate locally different conditions. As an example, pyrite was preserved in the contact sample of block 4 but it was oxidized in #5 (Figure 2.20).

Infrared spectroscopy

IR spectroscopy is often used as complementary mineralogical analysis. In the present study all contact samples, which were suspected to include the most significant mineralogical changes, were compared with the spectra of the reference materials (Figure 2.23-Figure 2.26). Different shapes of the background can be explained by different particle size and/or different sample mass used to produce the KBr pellet. The different backgrounds sometimes pretend differences in the OH-deformation range which is particularly valuable to characterize smectites. A detailed inspection of these bands, however, did not reveal any change in the octahedral composition of the smectites. The only significant differences of a few spectra were related to the carbonates. The carbonate (around 1440 cm^{-1}) of the contact sample of block 11 was significantly reduced which is in agreement with STA (compare Figure 2.24 and Figure 2.20). Similar results were obtained for block 12 but both, STA and IR prove that only part of the carbonate was dissolved. Moreover, there is a shift of the IR band position and the additional STA-peak point towards recrystallization of the carbonate (compare Figure 2.24 and Figure 2.20). In the contact sample of block 17, in contrast, only a decrease of the STA carbonate peak and lower IR band intensity point to partial carbonate dissolution not accompanied by recrystallization. Overall, STA is more sensitive towards identifying differences of the carbonate abundance compared with XRD and IR.

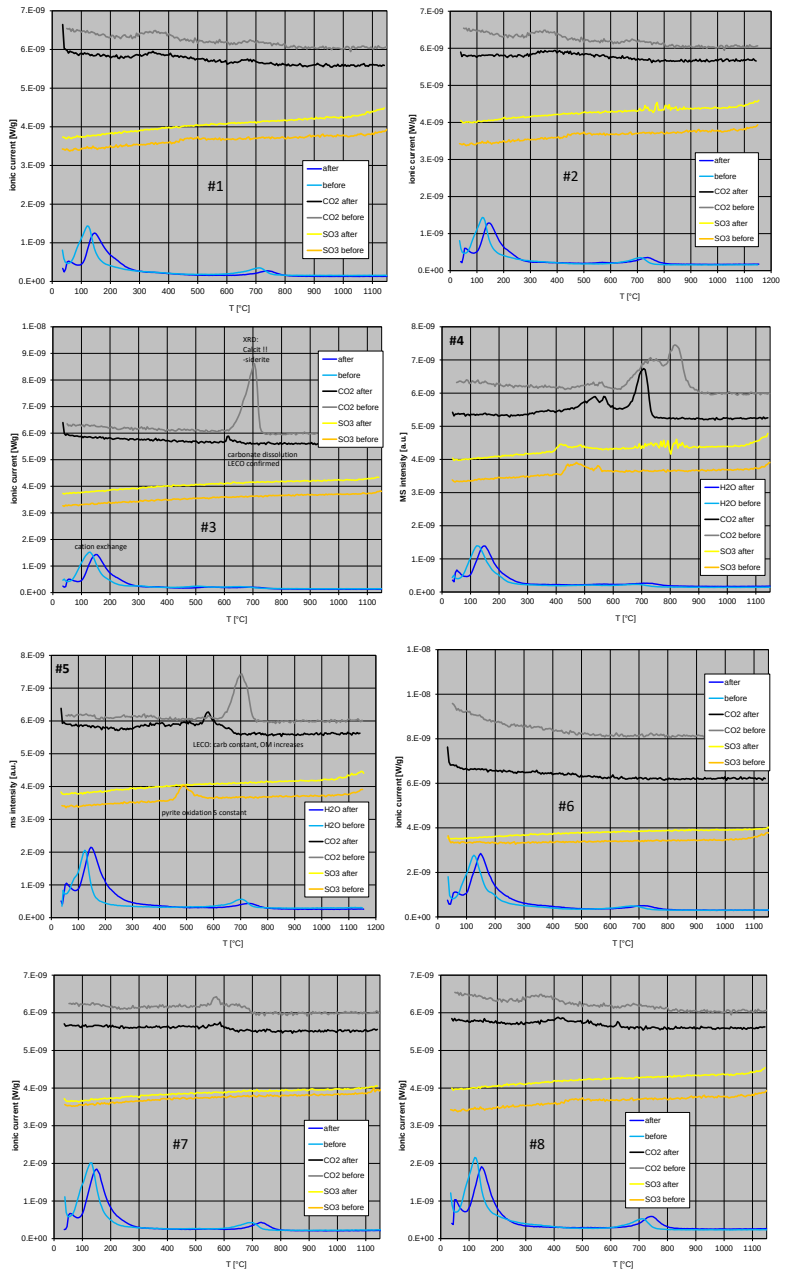

Figure 2.19 MS curves of STA (blocks 1 – 8)

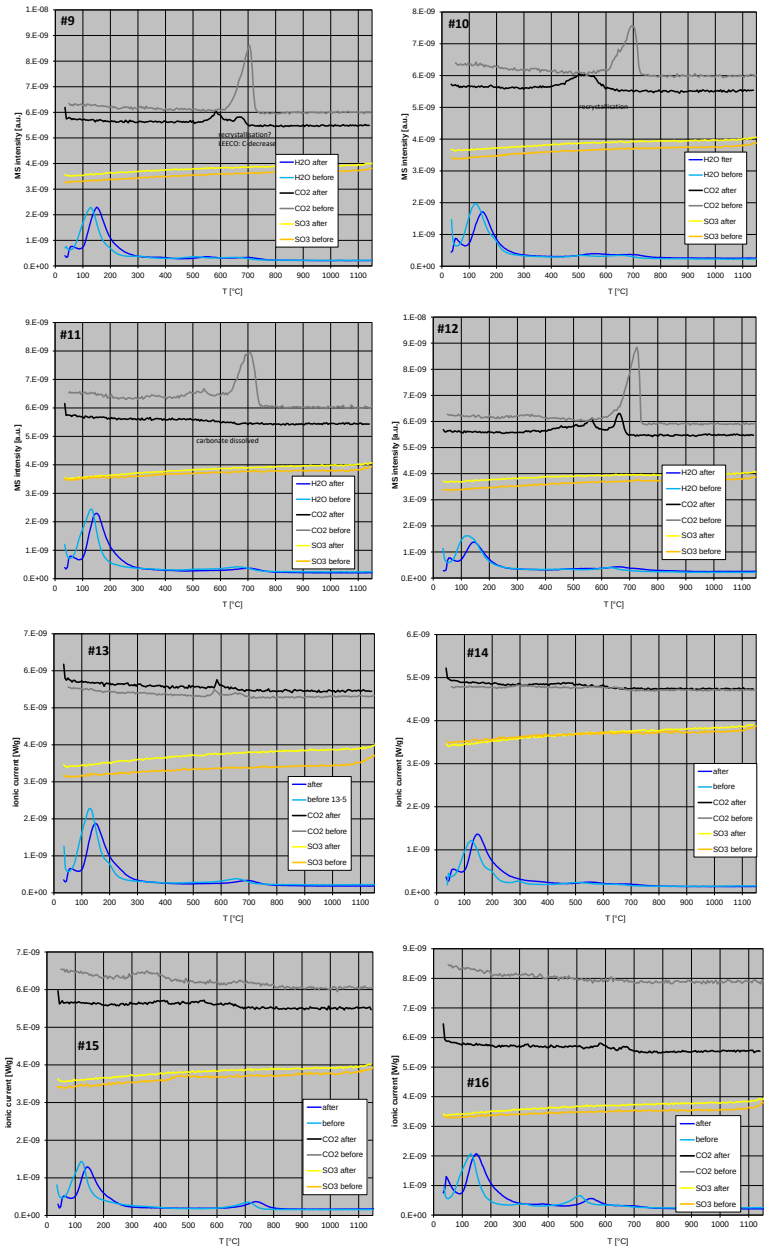

Figure 2.20 MS curves of STA (blocks 9 –16)

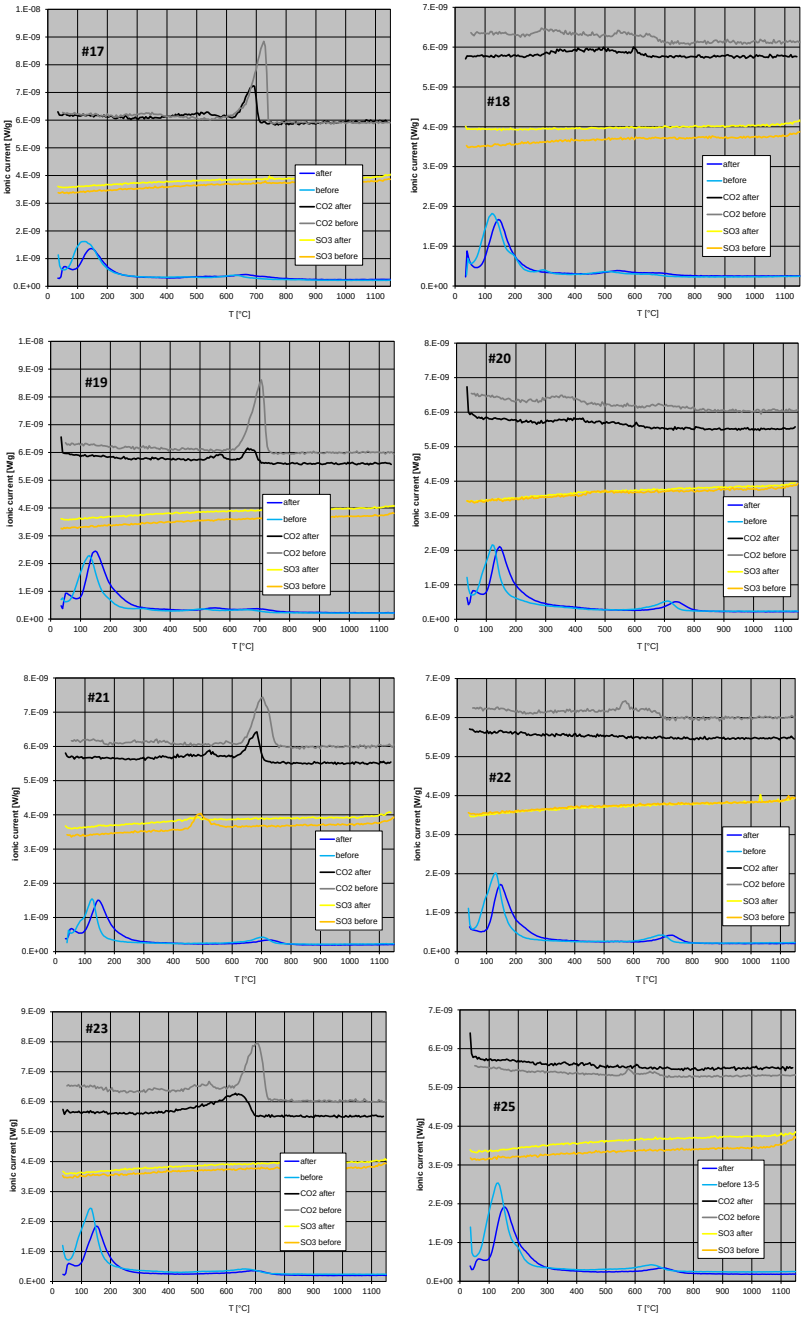

Figure 2.21 MS curves of STA (blocks 17 – 25)

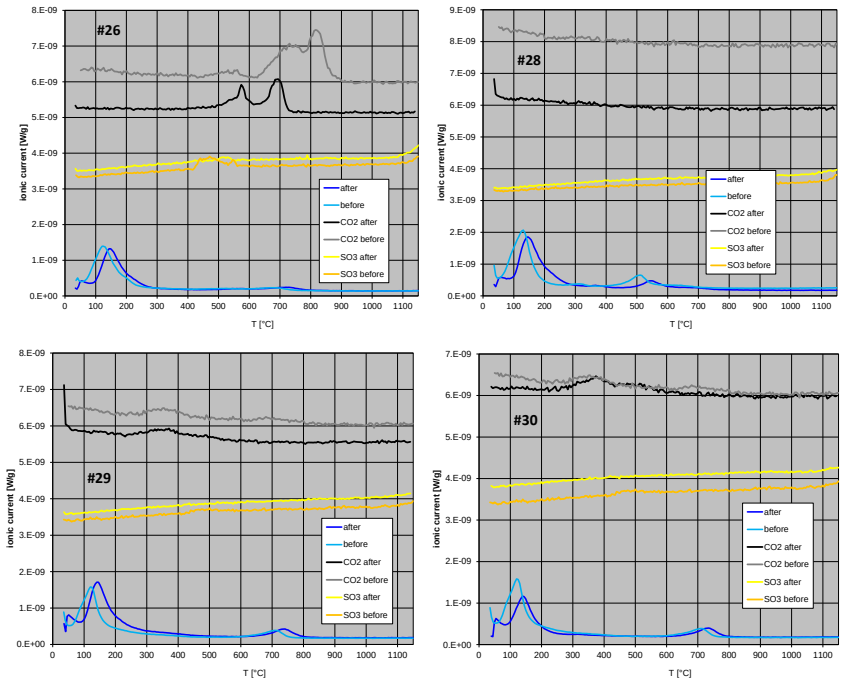

Figure 2.22 MS curves of STA (blocks 26 – 30)

IR spectrometry

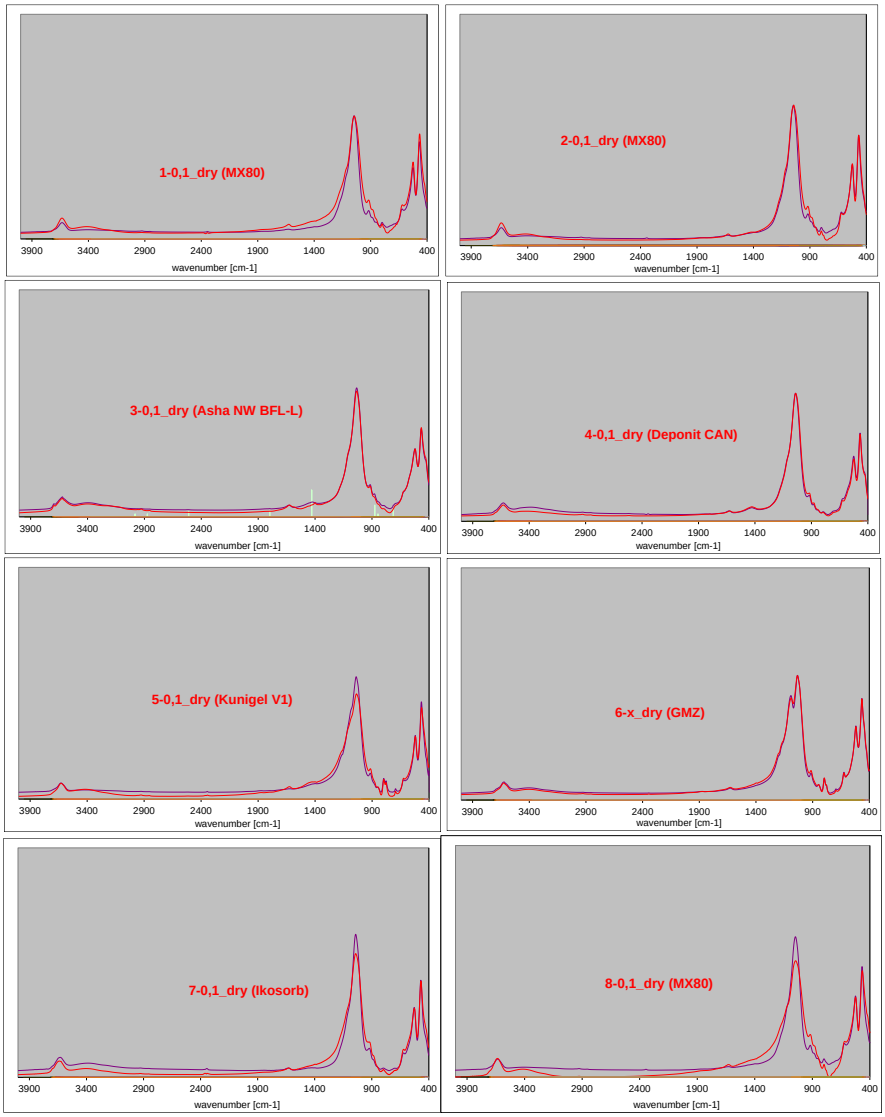

Figure 2.23 IR spectra of blocks 1 – 8 (purple reference, red: 0.1 cm sample)

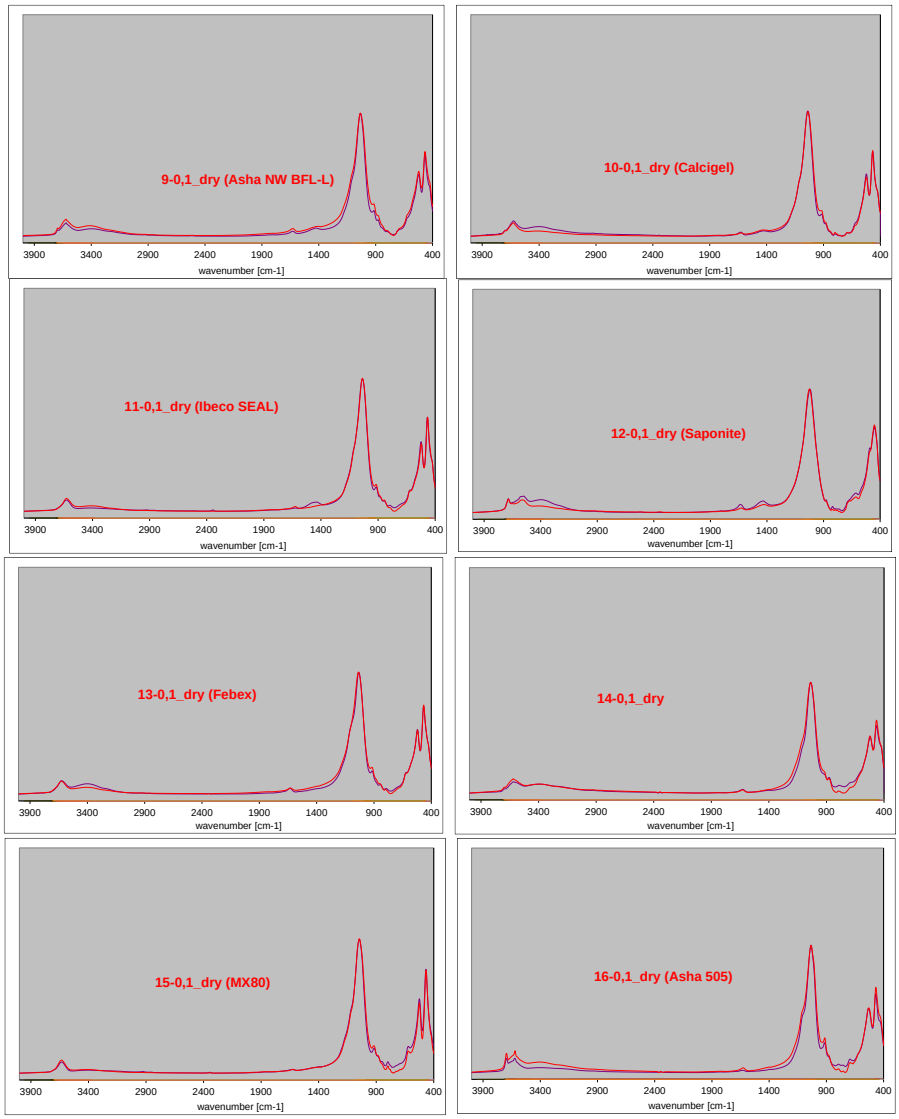

Figure 2.24 IR spectra of blocks 9 – 16 (purple reference, red: 0.1 cm sample)

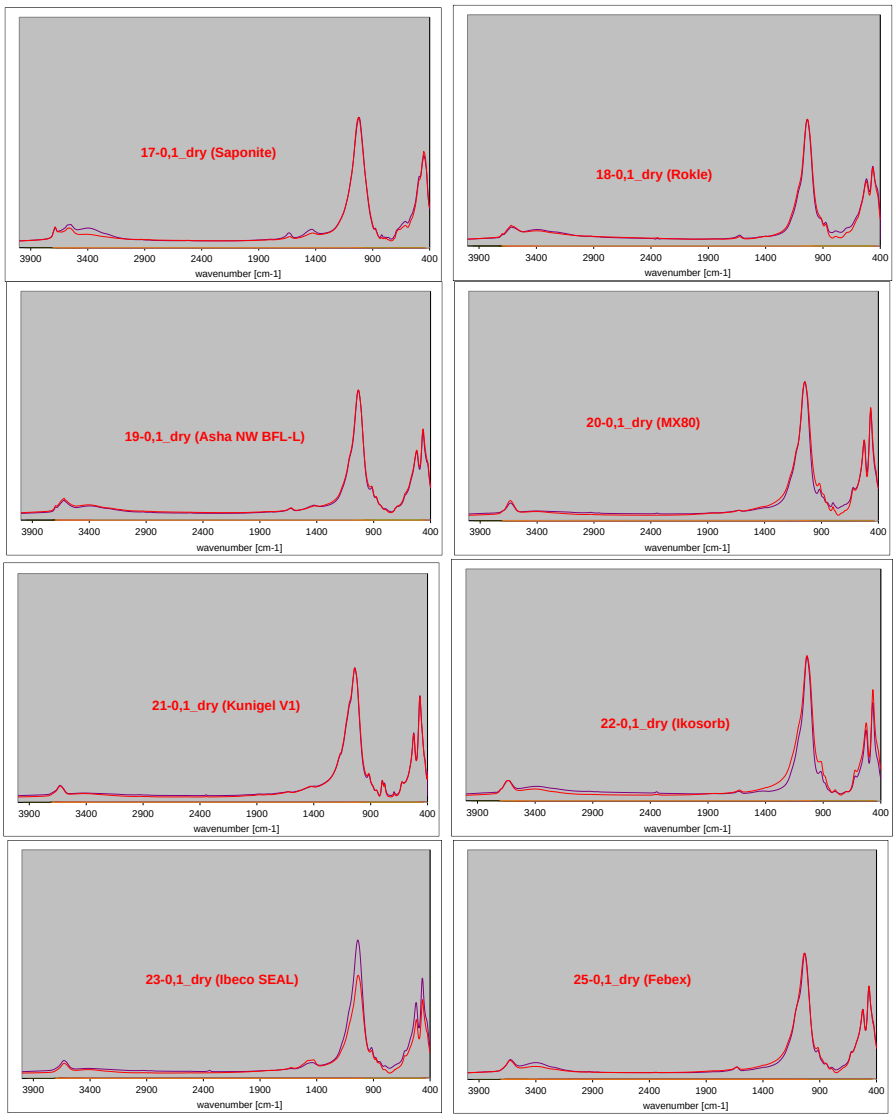

Figure 2.25 IR spectra of blocks 17 – 25 (purple reference, red: 0.1 cm sample)

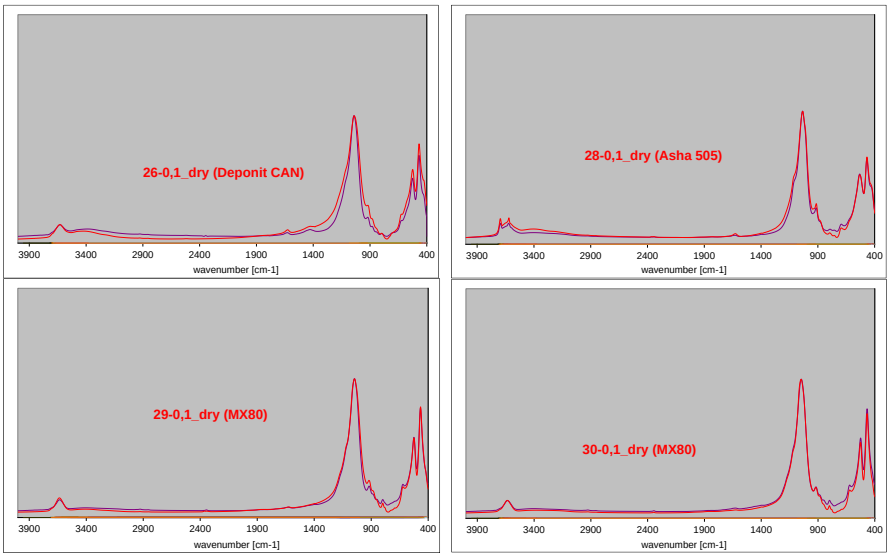

Figure 2.26 IR spectra of blocks 26 – 30 (purple reference, red: 0.1 cm sample)

2.4 Conclusion

The conclusions have been published before (Kaufhold et al., 2021). Results of XRD, XRF, elemental C and S, and STA were not always concise, which results from the fact that many mineralogical changes were close to the detection limit of the methods. Some unambiguous results, however, were found. Cl concentrations did not depend on material properties or temperature. The Cl content was assumed to result from effects such as inflowing water. On average, a higher Cl increase was found in the lower part of the test, but at the very bottom, the highest water content and lowest Cl increase were found. The reason for different Cl increases could, therefore, not be identified and are supposed to be related to the hydraulic conditions outside and inside the blocks. An additional effect of temperature cannot be excluded. In blocks #1 to #19, the Fe_2O_3 increase was restricted to the contact. Blocks #20 to #30 all showed a slight to significant increase of the Fe content, even in the 1 cm sample, which indicated both increased corrosion and migration of Fe into the blocks in the upper parts of the test, which can hardly be explained because of the lower water content and hence lower degree of saturation in this zone.

Mg enrichment at the heater, as observed in most of the previous bentonite field experiments, was comparably low. Interestingly the Mg rich 'Saponite' even lost some of its Mg content, also indicating some mobility of Mg within these compacted clays. Implying that some of the Mg was present as an interlayer cation or similar. Carbonate dissolution and precipitation (redistribution) showed different patterns, which does not allow to derive a general rule. Different profiles were observed for the same material and temperature. Therefore, the differences of the profiles cannot be explained by either material properties (type of carbonate present) or by the different temperatures.

Commenté [LJ4]: Does this imply that the magnesium is not located in the structure of the clay mineral but it is rather in the cation-exchange position?

Carbonate redistribution is likely more affected by local differences, possibly of porosity and water content. Because of the absence of any lubricant, it was possible to observe a recrystallization of carbonate in some contact samples, where siderite formed at the expense of Ca(Mg)-carbonates (proved by STA and LECO and sometimes XRD).

The gypsum redistribution resembled what was found in the LOT test (increase in the center of the blocks), but this effect was much less pronounced in the ABM5 test. The most significant gypsum increase was found in the upper and lowermost blocks. The identified gypsum may possibly have been

anhydrite in the experiment that may have hydrated during storage, as there are indications of moisture in the samples during the storage.

By XRD, no additional interstratification of smectites for any block in comparison with the reference materials was indicated. The neoformation of trioctahedral phases could be indicated only in block #7 (Ikosorb). In the only block with trioctahedral smectites as starting material, #17 ('Saponite'), no evidence for the presence of (additional) dioctahedral phases was observed.

None of the analyses performed could detect any specific high temperature reaction.

3. BRGM (ANDRA)

3.1 Introduction

The optimization of the swelling behaviour of bentonites in a nuclear waste disposal as a function of the physical and chemical conditions and the imposed temperature requires a good description of the mechanisms driving the swelling of the bentonite during the infiltration of a given solution. Indeed, the swelling of a bentonite has its origin at the crystal layer scale. The two main mechanisms driving the swelling of smectite rich materials are the crystalline swelling and the osmotic swelling. Several experiments have been undertaken to understand the effect of temperature on these mechanisms of crystalline and osmotic swelling.

In task 3.1, BRGM is characterizing the water adsorption properties of a smectite, depending on the temperature, the relative humidity, its density and the saturation cation. The X-ray diffraction measurements on bentonite powder at 25°C and 80°C allow studying the effect of temperature on the crystalline pressure. The acquisition of water adsorption isotherms at 25 °C and higher temperature makes possible the evaluating of the effect of temperature on crystalline and osmotic water. The Kunipia-G bentonite was used in these tests.

3.1.1 Material

A smectite provided by Kunimine Industries was used for this study (Table 3.1). This material, available as Kunipia-G grade, is a highly pure montmorillonite (95%) and has among others the advantage of avoiding long purification steps to remove secondary mineral phases. Kunipia-G was also chosen for its particular granulometry, which differs from other materials of the same type. Indeed, its platelet structure generates a rather large inter-aggregate porosity identifiable by µCT at dry state.

Powder XRD patterns indicate traces of quartz and carbonates (Figure 3.1). Examination of the 060 band at 1.49 Å indicates that Kunipia-G is a dioctahedral smectite.

XRD patterns obtained on oriented preparations recorded in air-dried conditions after ethylene glycol solvation or after temperature increase (550 °C) show that (i) the basal spacing recorded in the air-dried state is compatible with a Na interlayer counter-ion, (ii) a rationality of the 001 reflections (Figure 3.1) proving the absence of illite/smectite mixed layered minerals.

The cation exchange capacity (CEC) determined by the chloride cobaltihexamine displacement method (Orsini and Rémy, 1976) is 115 mequiv/100 g with the following distribution of exchangeable cations: Na 91%, Ca 8%, K 1.0%.The dry particle density of Kunipia-G is 2.71 Mg/m^3.

The specific surface area determined from a nitrogen adsorption experiment using the BET equation (Brunauer et al., 1938) is 42 m^2/g, similar to the specific surface area (SSA) founded by Kozaki et al. (1999).

The water sorption isotherms (data not shown) have a typical shape for swelling clays and particularly for Na-exchanged smectites, with two steps on the water adsorption curve (Cases et al., 1992). Considering the desorption branch of the water isotherm, and assuming that in this state all the interlayers are accessible, applying BET formalism gives an estimated total surface area of around 524–660 m^2/g.

In order to avoid the cationic exchange effect on the water retention capacity and swelling pressure of smectite (being complicated to study), a preliminary phase to the planned tests consisted in homoionizing our smectite in sodium and calcium form.

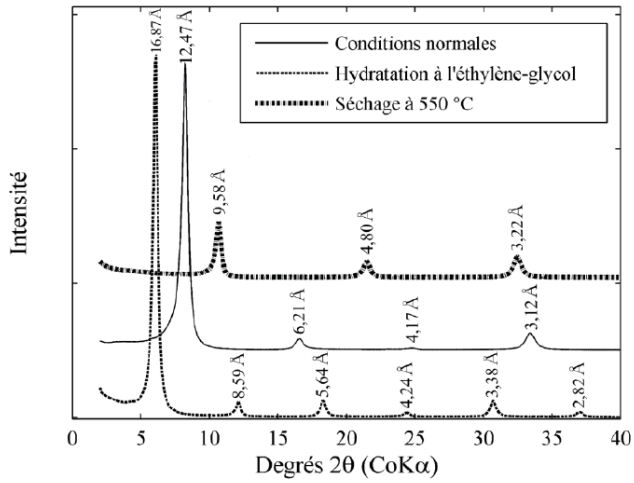

Figure 3.1 XRD pattern on Kunipia-G bentonite on orientated preparations in air-dried conditions, after ethylene glycol solvation and after drying at 550°C (Massat et al., 2016)

Table 3.1 Summary of Kunipia-G mineralogical and chemical properties (Massat et al., 2016)

Type	Sodium smectite
Smectite content	95%
Accessory phases	1–2% carbonates 2–3% quartz
Particle density (Mg/m^3)	2.71
CEC (mequiv/100 g)	115.0
Exchangeable cations	91% Na, 8% Ca, 1% K
Specific surface area, BET H_2O (m^2/g)	524–660
Specific surface area, BET N_2 (m^2/g)	42

3.1.2 Research plan

Table 3.2 BRGM – Synthesis of research plan in task 3.1

3.1.2.0 Material (BoM item): Kunipia-G. Powder as delivered by producer
3.1.2.1 Material treatment (sample preparation for test and loading procedure): studied densities : 1.4; 1.5; 1.6; 1.9.
3.1.2.2 Temperature (to which material was/will be exposed to) and exposure time: XRD (25; 80°C) ; Isotherms (24; 42°C)
3.1.2.3 Tests carried out (name, description, sample preparation, procedure, results): XRD in saturated conditions; Water adsorption isotherms.
3.1.2.4 Schedule and expected date(s) of results delivery: End of 2021

3.2 Procedures

3.2.1 Laboratory set-ups, procedures and protocols

3.2.1.1 XRD

The interlayer spacing of a sodium and a calcium montmorillonite are monitored using X-ray diffraction (XRD) analysis on oriented powders while increasing the relative humidity of the sample at temperatures of 25°C and 80°C. The analysis of the (001) ray of the diffractograms allows us to estimate the average basal distance separating the montmorillonite layers. A preliminary analysis of this ray at different temperatures helps us determining the initial conditions to be imposed in order to reach the driest possible state of the material prior to any hydration experiment. It turns out that the optimum dry state of calcium Kunipia-G is reached by heating it at 200°C for 7h while heating under 100°C for 1h was sufficient for sodium Kunipia-G. A humidification path followed by a drying path was then applied. Note that a 95% RH was required to intercalate 3 layers of water in the interlayer spaces of Na and Ca Kunipia. Also note that the maximum humidity that can be reached at 80°C is 70%.

3.2.1.2 Isotherms

As a complementary approach to define the water retention capacity, sorption isotherms were obtained in a temperature and humidity controlled chamber (Figure 2). Sodium and Calcium Kunipia-G are compacted at different densities in constant volume cells and then placed in an isolated chamber in which water and nitrogen flows are forced to generate a known relative humidity. The temperature is also fixed. Then a measurement of the mass of these cells is made every day until reaching the equilibrium allowing us to follow the evolution of the water content as a function of the humidity. According to these results, we can conclude on the effect of density, confinement conditions and temperature on the water retention capacity of bentonites.

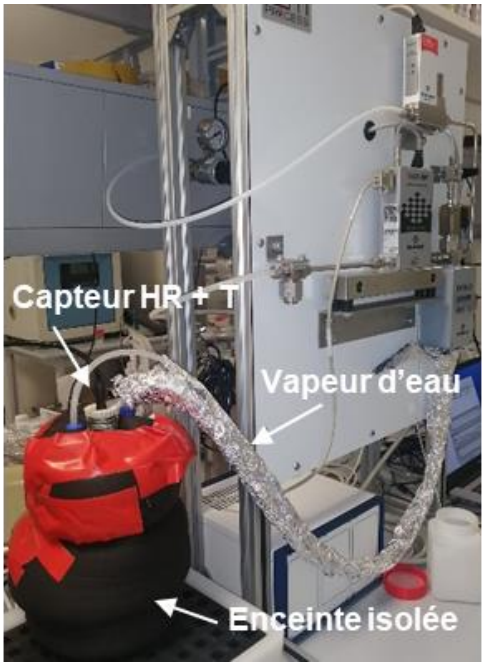

Figure 3.2: Used device for isotherm determination. Capteur is the sensors for humidity and temperature . Vapeur shows the water vapour. Enceinte isolée is an isolated enclosure. Poudre is the clay powder and cellules is reaction cells.

Commenté [LJ5]: Explain the texts in the pictures (French to English) in Figure caption?

3.2.2 Data and other results available

3.3 Results

3.3.1 Investigation performed

XRD measurements on Na-Kunipia and Ca-Kunipia have already been performed at 25°C and 80°C for various relative humidities. The acquisition of water sorption isotherms at room temperature (24°C) on Na-Kunipia is ended. Acquisition of isotherms at 42°C is on-going.

3.3.2 Results from investigation

DRX

An increase of temperature from 25°C to 80°C has a very negligible effect on the dehydration of the interlayer spaces (Figure *3.3)*. Thus, it can be noticed that the basal distance recorded at a temperature of 80°C with whatever relative humidity is slightly lower than that measured at a temperature of 25°C (Figure 3.4). From these results, a preliminary hypothesis can imply that temperature variation impacts very slightly the interlayer water retention capacity. However, the measured difference between T=25°C and 80°C is greater for sodium bentonite than for calcium bentonite. This can be explained by the high binding energy of divalent cations to water molecules. Thus the recommended temperature for dehydrating the interlayer spaces of a divalent smectite is much higher than that for a monovalent smectite. The evolution of the basal distance as a function of relative humidity was reported in the graph of Figure 3.*5* for Kunipia sodium and Kunipia calcium allowing to verify the effect of the interlayer cation on the hydration kinetics of smectites. The basal distances of Kunipia-Na show that no water layer is accommodated in the interlayer space by increasing the relative humidity from 0 to 20%. An increase of humidity up to 50% was required to hydrate everywhere with one water layer unlike Kunipia-Ca which

already accommodates 2 water layers at 50% RH. These results confirm that divalent smectites are more easily hydrated (at a lower RH) than monovalent smectites. This is related to the affinity of the cations to water, i.e. to their ionic potential. The higher the ionic potential, the faster the cation hydrates.

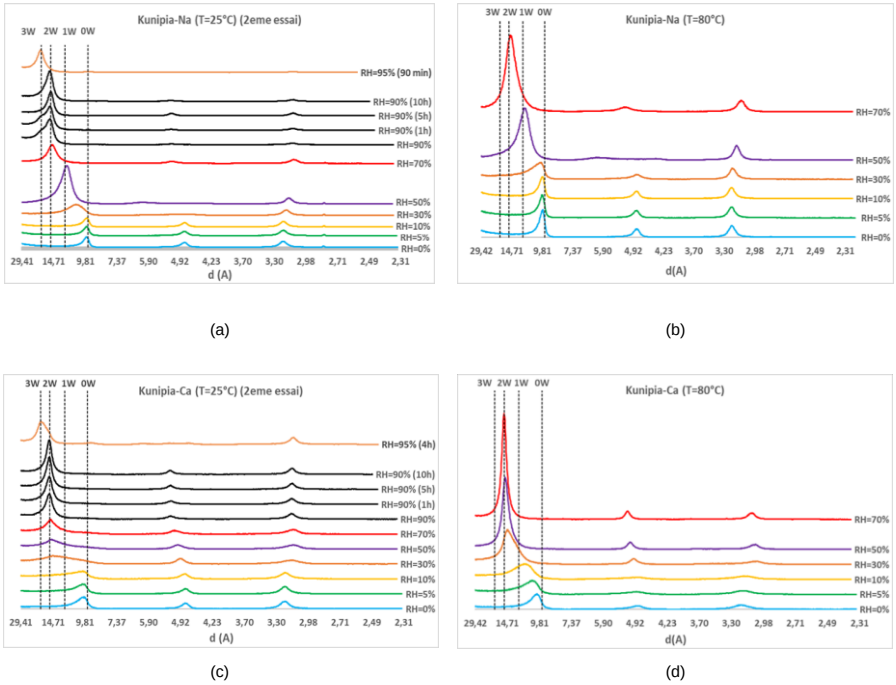

Figure 3.3 X-ray diffractograms acquired upon humidification of a Kunipia-Na at (a) T=25°C; (b) T=80°C and a Kunipia-Ca at (c) T=25°C; (d) T=80°C.

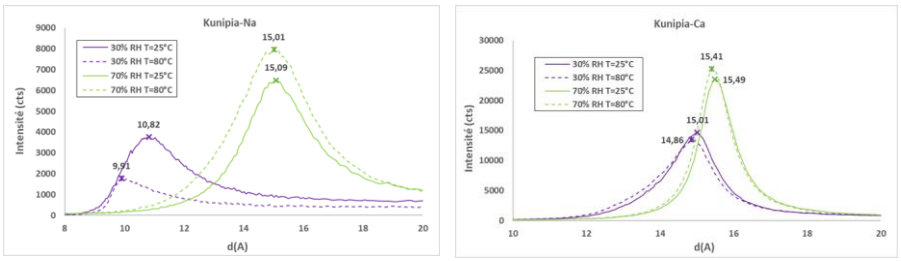

Figure 3.4 Recorded basal distances of a Kunipia-Na (a) and a Kunipia-Ca (b) at temperatures of 25°C and 80°C for relative humidities of 30% and 80%.

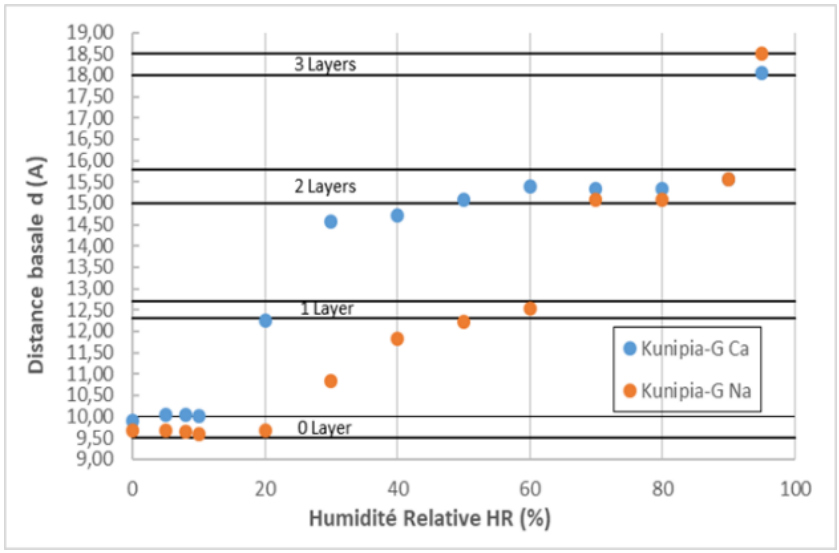

Figure 3.5 Evolution of d(A) of Kunipia-Na and Ca as a function of RH(%) at T=25°C.

Water retention isotherms

Measured water retention isotherms are shown in Figure 3.*6*.

Before studying the influence of various parameters on the water retention capacity, we compared our data to an isotherm that was acquired with a volumetry equipment (blue points), we notice that our results are aligned with this isotherm thus our acquisitions are reliable.

The retention curves of the different samples overlap almost in a first phase but diverge as the capillary condensation phenomenon occurs (inflection point). In fact, for low relative humidities, the suction is governed by the intra-aggregate pores which are not impacted by the densification. The water retention capacity in this humidity range is only related to the specific surface. The larger the specific surface of the material, the higher the retention capacity is. Since we are dealing with the same material (same specific surface), the curves overlap.

While in a state relatively close to saturation, the suction is governed by the inter-aggregate pores. Hence, the water retention capacity depends on the compaction state of the sample. The values of water content and humidity for which saturation is reached depend, therefore, on the density/index of the voids. In particular, the looser the sample, the higher the water content at saturation and the lower the suction (saturation is reached at a higher relative humidity). In fact, it takes many more layers of water to form a capillary meniscus in a relatively loose sample (larger macropores).

In conclusion, the lower the density of the sample, the higher its retention capacity.

Moreover, it has been found that hydrated bentonite at free volume continues to accommodate water even when the suction is nullified (RH=100%) while this possibility is hindered at constant volume where the sample continues to accommodate water until filling all its porosity.

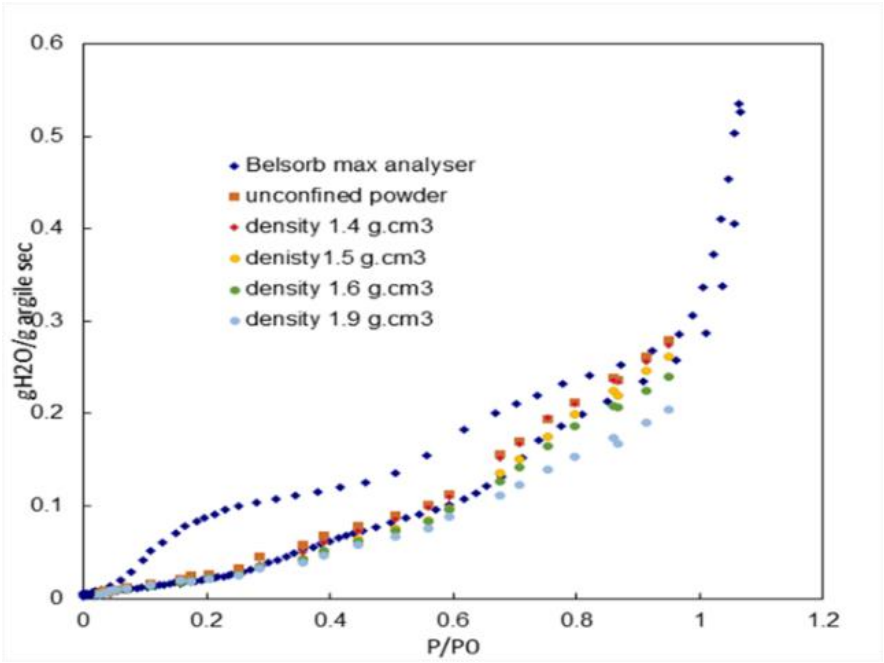

Figure 3.6 Water retention isotherms of a Kunipia-Na compacted at densities of 1.4; 1.5; 1.6 and 1.9 at T=24°C. Absorbed mass of water (g) as a function of the relative humidity (RH).

Commenté [LJ6]: Is the horizontal axis relative humidity or another parameter

3.4 Conclusion

XRD measurements on Na-Kunipia and Ca-Kunipia have been performed at 25°C and 80°C for various relative humidity. Our results suggest that the temperature has a little effect on the interlayer water retention capacity. The results also show that, at low relative humidity, Ca-Kunipia is more easily hydrated than Na-Kunipia.

Water retention isotherms have been measured on Na-Kunipia compacted at densities of 1.4, 1.5, 1.6 and 1.6 g/cm^3 at a temperature of 24°C. It has been shown that, depending on the vicinity to sample saturation, water hydrates different types of porosity, namely the intra-aggregate porosity at low relative humidity and the macroporosity at higher relative humidity. A temperature of 42°C is now applied on the same cells. A comparison between the isotherms at 42°C and 24°C will allow us to conclude on the temperature effect on the water retention capacity of bentonites.

4. CIEMAT + UAM (CIEMAT)

4.1 Introduction

Mineralogical alteration of the bentonite buffer due to thermal, hydraulic, and chemical gradients may impair the safety functions of the engineered barrier. These alteration processes may include loss of montmorillonite mass, cementation due to the precipitation of secondary minerals, alteration of cation exchange capacity (CEC), and dissolution of accessory minerals. There is a need to reduce conceptual and modelling uncertainties to a lower level, and to this end, research is being conducted to assess the long-term mineralogical and geochemical alteration of the buffer under thermal gradients at various water saturation conditions. Bentonite material coming from laboratory thermo-hydraulic tests simulating the conditions of the barrier during operation has been characterised. The temperature of the heater in these TH tests, which were performed in Task 3.3, was 140 and 150°C. Additionally, the post-mortem results of a set of TH tests performed in the context of another project were made available partly in-kind by Posiva. The TH tests were performed at CIEMAT and the post-mortem results have been obtained by UAM and CIEMAT. The temperature of the heater in these tests was 110°C, and the results will serve as a baseline for the new tests mentioned above performed at higher temperature. Different bentonites, groundwater compositions, boundary conditions and durations have been thus explored.

4.1.1 Material

Several materials are being considered. MX-80 and Ibeco powders have been used in tests performed outside the framework of HITEC, but whose post-mortem characterisation results are presented inside Task 3.1. MX-80 pellets were used in a thermo-hydraulic test that was dismantled in November 2021 (Task 3.3, see Deliverable 7.9). Finally, the Barakade bentonite was used in the new tests started in Task 3.3. One of these test was dismantled in September 25th 2023 and the other one will be dismantled in December 2023. Hence no post-mortem results are available yet.

4.1.1.1 MX-80 bentonite

It comes from Wyoming (USA), produced by American Colloid Co. It is a bentonite of volcanic origin, powdered and Na-homogenised. It has been used in the form of powder and pellets. The powder used was received from Posiva (supplier Sibelco Nordic AB).The pellets used were received from Mont Terri and are the same as those used in the HE-E in situ experiment (Gaus, Garitte et al. 2014). They are irregular pellets of size <10 mm, dry density 2.75 g/cm^3 and water content 6%.

The content of smectite is 76%, with illite (8%), kaolin (3%), feldspars (9%), and minor quantities of cristobalite, tridymite, magnetite, pyrite, quartz, biotite, calcite, anatase. The characterisation performed by UAM in the batch used gives a montmorillonite content of 77%, dolomite 9%, calcite 5%, quartz 4% and smaller contents of cristobalite, K-feldspars and plagioclase. Ca^{2+} is the main exchangeable cation (36 meq/100 g), with also Na^{+} (22 meq/100 g) and Mg^{2+} (19 meq/100 g). CEC: 77 meq/100 g. The main soluble ions are sulphate, chloride and sodium ((Kiviranta, Kumpulainen et al. 2018)).

4.1.1.2 IBECO

It comes from Milos (Greece) and it is a granulate (maximum grain size: 8 mm) received from Posiva and supplied by Minelco/LKAB.

The content of smectite is 76%, with illite (8%), kaolin (3%), feldspars (9%), and minor quantities of cristobalite, tridymite, magnetite, pyrite, quartz, biotite, calcite, anatase. The characterisation performed by UAM in the batch used gives a montmorillonite content of 77%, dolomite 9%, calcite 5%, quartz 4% and smaller contents of cristobalite, K-feldspars and plagioclase. Ca^{+} is the main exchangeable cation (36 meq/100 g), with also Na^{2+} (22 meq/100 g) and Mg^{2+} (19 meq/100 g). CEC: 77 meq/100 g. The main soluble ions are sulphate, chloride and sodium ((Kiviranta, Kumpulainen et al. 2018)).

4.1.1.3 Bara-Kade bentonite

The material with commercial name 'Bara-Kade' is Wyoming sodium bentonite similar to MX-80. Its use was proposed by Posiva in June 2020, although it had not been initially foreseen. The as-received water content was 8.2%.

4.1.2 Research plan

Table 4.1 CIEMAT - Characterisation of material from TH cells

4.1.2.1 Material (BoM item): Pelletised bentonite with low water content (MX-80) MX-80 and Ibeco powder Barakade bentonite
4.1.2.2 Material treatment (sample preparation for test and loading procedure): All the material comes from thermo-hydraulic (TH) tests: – MX-80 pellets and Barakade bentonite come from tests described in Task 3.3 – MX-80 powder and Ibeco granulate come from TH tests performed outside the framework of HITEC
4.1.2.3 Temperature (to which material was/will be exposed to) and exposure time – Heater T=140°C for 10 years (MX-80 pellets) – Compacted MX-80 and Ibeco powder in TH cell for 2.5 years with heater T=110°C (as a baseline for tests at higher T). These TH tests were performed outside the framework of HITEC – Barakade bentonite. In TH cells with heater T=150°C for ~3 years
4.1.2.4 Tests carried out (name, description, sample preparation, procedure, results): Determination of specific surface area, pore size distribution, soluble salts, cation exchange capacity, exchangeable cations, FTIR, swelling pressure, hydraulic conductivity (CIEMAT), elemental analysis, mineralogical characterisation by XRD, SEM, TEM, thermogravimetry, etc. (UAM).
4.1.2.5 Schedule and expected date(s) of results delivery: MX-80 and Ibeco powder with heater T=110°C: May 2021 MX-80 pellets with heater T=140°C: 2022 Barakade with heater T=150°C: at the end of the project

4.2 Procedures

Two TH cells were dismantled and subsampled in May 2020 and another one in October. MX-80 and IBECO bentonites were subjected in them to thermo-hydraulic gradients for 2.5 years, with a heater temperature of 110°C (Cells C3, C4 and C5). Once the bentonite blocks were extracted from the cells, they were cut into five 2-cm thick sections with a saw. Each of these sections, numbered from 1 (uppermost) to 5 (closest to the heater), was subsampled for the different measurements. Each section was separated in internal (in the middle of the sections) and external (close to the steel wall) zones, to check any potential "wall effect".

For the TH test with MX-80 pellets (cell HEE-B), the column was dismantled after more than 9 years of hydration (10 years of heating), since its length was 50 cm, it was sliced in 26 slices 2-cm thick (two of them were 1-cm thick).

In both kinds of cells subsamples were taken for the physical, mineralogical and geochemical characterisation of bentonite, which was performed by the Universidad Autónoma de Madrid (UAM) and CIEMAT. The procedures for post-mortem analyses were the same for all the cells and are described below.

The pore size distribution of each subsample was determined by mercury intrusion porosimetry (MIP). The specific surface area of the bentonite samples was determined using the BET method to analyse the adsorption isotherms of nitrogen gas.

XRD randomly oriented powder patterns were obtained in samples equilibrated at 55% relative humidity. The mineralogical composition of these samples was determined by means of the Reference Intensity Ratio (RIR) method, which can be taken as semi-quantitative. Oriented aggregates were also prepared from suspensions of the <0.5 μm size fraction. The structural formulae of the smectite was calculated using analyses on the Ca^{2+} homoionised <0.5-μm fraction.

Fourier Transform Infrared Spectroscopy (FTIR) was used as an additional method for the analysis of the mineral composition. Thermogravimetric analysis (TGA) was used to characterise materials that exhibit loss or gain of weight due to decomposition, oxidation or dehydration. Magic Angle Spinning Nuclear Magnetic Resonance was applied to study the local structure of silicates. High Resolution Transmission Electron Microscopy (HRTEM) allowed the direct observation of visual images of structural details of mineral samples, providing information on defects, transformations, and physical and chemical characteristics at a nanometre scale. Complementary to TEM, SEM-EDX studies were performed to detect singular surface characteristics of clay near the hydration surface or materials adhered to the heater.

Simultaneous determination of the percentage of carbon, hydrogen, nitrogen and sulphur was also performed with an elementary chemical analyser.

The total content of soluble salts (dissolved inorganic solutes) was analysed in 1:8 solid:liquid aqueous extract solutions. After phase separation by centrifugation, the supernatants were filtered and the concentration of major cations analysed by Inductively Coupled Plasma-Atomic Emission Spectrometry, sodium and potassium by flame atomic emission spectrometry (FAES), anions by ion chromatography and alkalinity by potentiometric titration.

The CEC was measured with a 0.01 M copper triethylenetetramine (Cu-trien) solution. The determination of the exchangeable cation population was performed by using caesium as index cation.

A custom-built high-pressure oedometer that keeps the samples at constant volume while measuring the water intake and the swelling pressure developed on saturation was used to measure swelling pressure and hydraulic conductivity of two samples from each cell, one of them prepared from section 2 and the other one from section 5, i.e. the closest to the heater. The specimens used for these determinations were not remoulded, and they were obtained by trimming to fit the oedometer ring. Deionised water was used in the oedometer tests.

4.3 Results

Two TH cells were dismantled and subsampled in May 2020 and another one in October. MX-80 and IBECO bentonites were subjected in them to thermo-hydraulic gradients for 2.5 years, with a heater temperature of 110°C. The post-mortem analysis of these samples, partly financed by Posiva, who allows in-kind their use in HITEC, will serve as a baseline for future similar tests performed at higher temperatures. A report was prepared for Posiva on the mineralogical, geochemical and hydro-mechanical post-mortem analyses of the bentonite coming from the 2.5-year cells (Villar, Cuevas et al. 2021) and a summary of it is given in the first subsection below.

Cell HEE-B with MX-80 pellets was dismantled in November 2021 and the post-mortem results were detailed in a public report (Villar, 2023), which is summarised in the second subsection below.

Apart from the different duration of the two set of tests (2.5 and ~9 years of hydration under TH gradient), the heater temperature and the height of the bentonite columns were different (110 *vs*. 140°C and 10 *vs*. 50 cm, respectively), which gave place to different thermal gradients during hydration (Figure 4.1).

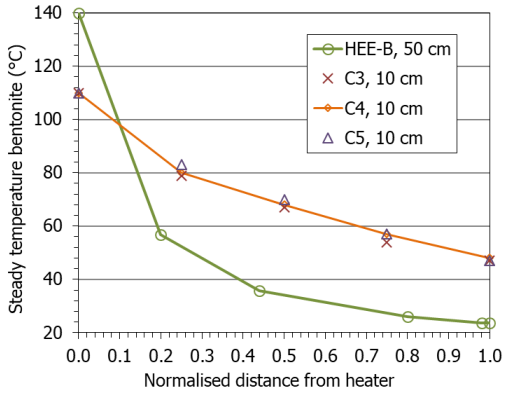

Figure 4.1. Steady temperatures in the thermo-hydraulic tests analysed with normalised distances to the heater (the height of the columns is indicated in the legend)

4.3.1 Cells with MX-80 and Ibeco powder

Two THC tests were performed in stainless steel cylindrical cells using MX-80 bentonite compacted to a dry density of 1.57 g/cm^3 with a water content of ~17% (C4 and C5) and another one using Ibeco bentonite compacted with the same characteristics (C3). At the bottom of the cells a heater was placed and set initially at 90°C. Once the relative humidity inside the bentonite reached equilibrium –which took about two months in cells C3 and C4 and 4.5 months in cell C5– hydration of the bentonite through a porous filter placed on the surface of the block opposite to the heater started with water coming from a flask hanged 1 m above the cells. The composition of the water in cells C3 and C4 reproduced that of a saline groundwater, mainly containing chloride, sodium and calcium (ionic strength 0.5 mol/L), whereas in cell C5 quite dilute glacial water was used. The temperature of the heater was increased to 110°C after hydration had been going on for 490 days in cells C3 and C4 and 329 days in cell C5.

After 2.5 years of hydration the heaters were switched-off and after a short cooling period the cells were dismantled. The bentonite blocks were extracted and cut into five sections to obtain samples for the different post-mortem determinations. The blocks had a consistent state, with no cracks, except for cell C3, where the bottom half was very dry and disaggregated easily (Figure 4.2). The water intake and final water content distribution were influenced by the salinity of the hydration water, with lower overall water intake and steeper water content gradients in the two cells saturated with saline water. Evaporation occurred at least through the bottom part of cell C3, which might have affected some of the results.

Figure 4.2. Final appearance of samples from tests C3, C4 and C5 (from left to right)

The post-mortem analyses described in section 4.2 were carried out in subsamples of the three bentonite blocks and the results obtained are summarised below.

The BET specific surface area (SSA), which is higher for Ibeco bentonite (45 *vs*. 26 m^2/g), decreased towards the heater in cells C3 and C4 and was similar and above the initial value in all the samples for cell C5. This parameter is usually related to the water content.

No significant montmorillonite structural modifications took place during operation. The structural formulae and the layer charge of the samples analysed are shown in Table 4.2. Octahedral Mg relatively increased near the heater, although globally the octahedral Mg content was lower in the treated MX-80 samples compared to the reference one and higher in the Ibeco treated samples (cell C3) than in the reference one. In all the samples from the cells the layer charge decreased with respect to the values of the reference samples. The divalent character of the smectites (more calcic) tended to increase towards the heater.

Table 4.2: Montmorillonite structural formulae ($O_{10}(OH)_2$ basis) and layer charge ($mol/O_{10}(OH)_2$)

Sample	Distance to heater (cm)	Structural formula	Layer charge
Ibeco		$(K_{0.055}Ca_{0.228})(Al_{1.366}Mg_{0.308}Fe_{0.233}Ti_{0.052})(Si_{3.866}Al_{0.134}O_{10})(OH)_2$	0.512
C3-1e	9	$(K_{0.044}Ca_{0.232})(Al_{1.331}Mg_{0.326}Fe_{0.265}Ti_{0.048})(Si_{3.863}Al_{0.137}O_{10})(OH)_2$	0.509
C3-5e	1	$(K_{0.039}Ca_{0.229})(Al_{1.358}Mg_{0.346}Fe_{0.242}Ti_{0.038})(Si_{3.858}Al_{0.142}O_{10})(OH)_2$	0.497
MX-80 (*)		$(K_{0.006}Ca_{0.224})(Al_{1.521}Mg_{0.242}Fe_{0.182}Ti_{0.006})(Si_{3.929}Al_{0.071}O_{10})(OH)_2$	0.454
C4-1e	9	$(K_{0.012}Ca_{0.177})(Al_{1.552}Mg_{0.212}Fe_{0.186}Ti_{0.008})(Si_{3.965}Al_{0.035}O_{10})(OH)_2$	0.365
C4-5e	1	$(K_{0.010}Ca_{0.179})(Al_{1.517}Mg_{0.221}Fe_{0.221}Ti_{0.008})(Si_{3.946}Al_{0.054}O_{10})(OH)_2$	0.368
C5-1i	9	$(K_{0.005}Ca_{0.197})(Al_{1.543}Mg_{0.218}Fe_{0.184}Ti_{0.012})(Si_{3.936}Al_{0.064}O_{10})(OH)_2$	0.398
C5-5e	1	$(K_{0.005}Ca_{0.187})(Al_{1.531}Mg_{0.239}Fe_{0.189}Ti_{0.006})(Si_{3.956}Al_{0.044}O_{10})(OH)_2$	0.380

In cell C3, chlorite (2:1:1 sheet silicate) was detected at less than 1-2 mm from the heater. Abundant halite precipitation was observed in large pores (triggered by heating) at distances of less than 5 mm from the heater. The overall content of carbonates increased in the area at less than 4 cm from the heater. In the area at less than 2 cm from the heater calcite predominated over dolomite, in contrast with the rest of the cell, where dolomite was the predominant carbonate. This would match with the dissolution of dolomite in the contact with the heater and the incorporation of magnesium to the newly formed chlorite. The exchangeable magnesium content also increased above the initial value close to the heater.

In the MX-80 samples from tests C4 and C5, calcium sulphate (probably anhydrite) was detected by FTIR and SEM in areas at less than 4 cm from the heater. Total consumption of oxygen seems to have occurred in both experiments, explaining the presence close to the heater of pyrite (Figure 4.3) and of oxides in different oxidation states in the case of C4. As a result of the hydration with saline water in cell C4, carbonates and sulphates precipitated at various locations, NaCl-spotted areas were observed close to the heater and corrosion occurred in the contact with the steel elements. None of these features were observed in cell C5, hydrated with glacial water. In this cell, close to the hydration surface calcium carbonates precipitated.

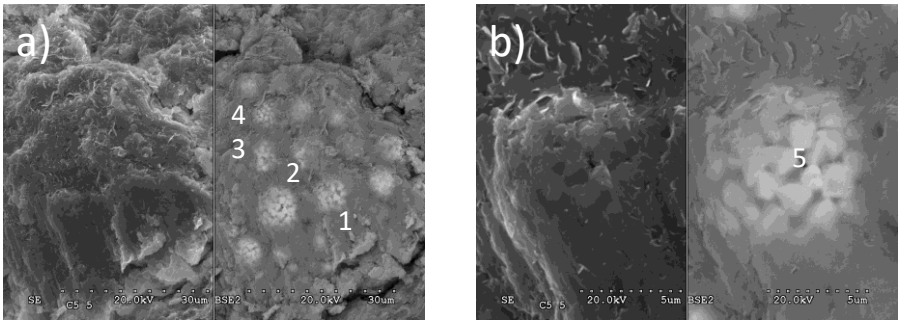

Figure 4.3 Cell C5 SEM photographs of clay in contact with the steel heater (sample C5-5). a) double image under secondary electrons (SE) and backscattering mode (BSE) revealing framboidal pyrite precipitation; b) detail of a)

The changes in the pore water composition inferred from the aqueous extracts were affected by 1) the composition of the incoming water, 2) the dissolution of mineral species present in the initial bentonite as a result of the water content increase, 3) cation exchange processes.

The ions coming with the hydration water and those coming from the dissolution of minerals were transported by advection and accumulated in the lower half of the columns at the bottom, precipitating closer to the heater (Figure 4.4). The overall concentration of the ions in the samples increased significantly with respect to the initial one. The maxima in sulphate concentration were in all cells accompanied by increases in the soluble sodium and calcium contents, possibly indicating the precipitation of anhydrite at less than 4 cm from the heater in cells C4 and C5 and at 3 cm from the heater in cell C3 (in the latter case it was not possible to ascertain if the sulphate was gypsum or anhydrite). The precipitation of carbonates close to the heater in all cells was reflected in the decrease in bicarbonate content from the hydration surface towards the heater.

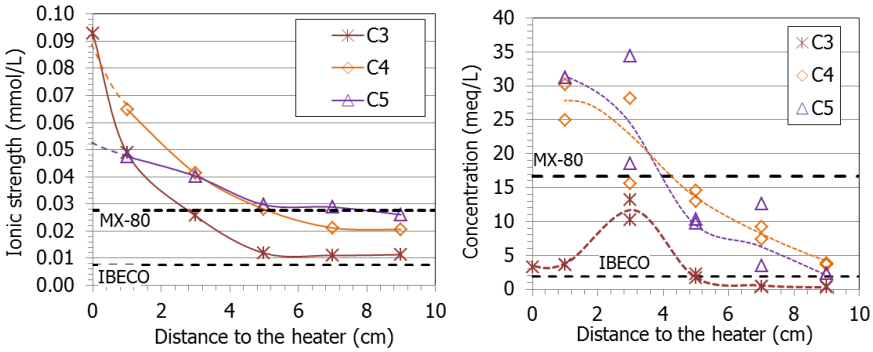

Figure 4.4: Ionic strength (left) and concentration of sulphate (right) in 1:8 aqueous extracts of samples from tests C3, C4 and C5 (the curves on the right show approximate trends)

Cation exchange processes could also supply new soluble cations. This would be the case in cells C3 and C4, where the content of soluble magnesium increased while the exchangeable one decreased (except close to the heater, where both increased). In the more saturated areas of the MX-80 cells C4 and C5 the exchangeable calcium content decreased.

4.3.1 Cell HEE-B with MX-80 pellets

A 50-cm long column of Wyoming-type bentonite pellets was heated at its base at 140°C while Pearson water was supplied through its upper surface at a very low pressure for nine years. During the test the temperatures remained constant and relatively low in most of the column: only in the 10 cm closest to the heater the temperatures were higher than 60°C, and higher than 100°C in the 5 cm closest to the heater. At the end of the experiment the upper half of the column was virtually saturated, but in the lower half the water content decreased sharply towards the heater, where it was close to 0%. There was also a dry density gradient along the column: it increased from the hydration surface towards the heater. The online results and dismantling and sampling activities are described in (Villar, 2022).

During the dismantling and sampling operations, the column was divided into twenty-six sampling sections, numbered from S0 close to the hydration surface to S25 close to the heater (Figure 4.5). The thickness of the sampling sections was 2 cm, except for sections S24 and S25, which were 1-cm thick to allow for a better discrimination in the hottest area. Each of these sections was subsampled for the different measurements. The subsampling of the sections was performed by sawing or cutting with knives. The subsamples were taken for the physical, mineralogical and geochemical characterisation of the bentonite summarised in the sections below. The combination of online measurements of water intake and some of the post-mortem results allowed to conclude that, at some moment during the test, vapour started to leak through the sensor inlet located at 10 cm from the heater, and this artefact affected some of the results.

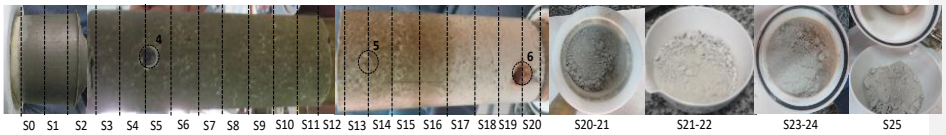

Figure 4.5: Appearance of the 25 sampling sections (hydration zone on the left, the photographs may show deformed diameters along the column which are not real)

~~4.3.1.0~~4.3.1.1 Mineralogy

XRD and FTIR showed that all the samples were composed predominantly of di-octahedral smectite. This was confirmed by the chemical composition obtained by XRF of the <0.5-µm fraction and by numerous localised analyses performed in clay-prevailing areas by SEM-EDX. Smectite showed a remarkable structural stability supported by the constancy of de-hydroxylation temperatures recorded by TGA, in agreement with the constancy of layer charge magnitude and distribution and NMR measurements for all samples. The smectite is actually a montmorillonite, maintaining its composition along the column independently of the temperature during operation, hydration degree reached or salt concentration in specific zones.

Cristobalite and quartz were also present as accessory minerals in the <0.5-µm fraction, correlated with the presence of small amounts of a micaceous illite-like accessory mineral phase. This illite could not be coupled to mixed-layer formation, as the smectite expanded regularly upon EG solvation without signs of alteration. Then, its detection is not considered an indication of alteration and is attributed to the decrease in the size of the illite-like aggregates contained in the original pellets.

Although pyrite was observed by SEM in several locations along the bentonite column (but not close to the heater), it cannot be related to precipitation under reducing conditions because it is an accessory mineral of the untreated bentonite.

~~4.3.1.1~~4.3.1.2 Cation exchange complex

As for the exchangeable cation complex, its population could be assessed using results obtained with different techniques: XRD, TGA, the localised structural formula calculations by SEM-EDX and the direct chemical analysis after displacement with Cs:

- The XRD of the bulk samples showed basal spacings corresponding to predominantly monovalent exchangeable complexes, with values <1.3 nm, tending to decrease towards the heater. The deconvolution of the random powder XRD patterns showed a contribution of divalent cations in the areas at more than 10 cm from the heater, where the value of the main basal spacing was clearly greater (Figure 4.6).

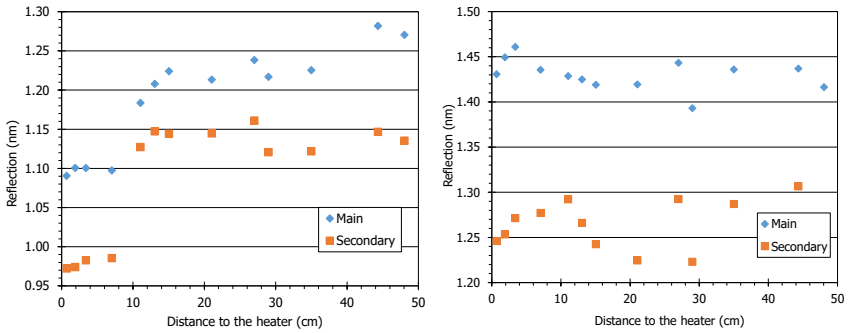

Figure 4.6: Main and secondary peaks obtained by deconvolution of the basal reflection of the of bulk powder samples stabilised at 50% RH (left) and of air-dried oriented aggregates (right)

- The TGA results, with dehydration temperatures at 54°C, also pointed to sodium as the main exchangeable cation, particularly nearer the heater. In the middle part of the column the dehydration temperatures were higher, indicating a more divalent cation occupancy in the exchange complex (Caglar, 2009).
- Consistently, the structural formulae calculated from SEM-EDX showed a predominance of Na as the exchangeable cation.

These observations could be related to the replacement of cations in the original exchange complex (in which Na predominates, but also Ca and Mg were included) by the sodium coming with the hydrating saline water.

However, it is remarkable that the basal reflections of the smectite in the oriented aggregates pointed to the significant presence of divalent cations in the interlayer space (d_{001} ~1.4 nm). It is generally acknowledged that during the preparation of suspensions some soluble species are expected to be dissolved and the released cations may replace others in the interlayer according to the differences in adsorption selectivity influenced by the cation distribution itself. Hence, it is considered that during the preparation of the oriented aggregates some species could be dissolved (gypsum and/or anhydrite) and the calcium released could substitute for sodium in the interlayer. Even though the random powders showed basal spacings corresponding to predominantly monovalent exchangeable complexes, dissolution during sample preparation could be the reason why the oriented aggregates presented larger spacings corresponding to predominantly divalent smectites (although with a bimodal reflection that evinced the presence of both types of cations). However, this explanation is not obvious for the samples near the hydration source, where gypsum was scarce. In the area at 2 cm from the heater calcite was clearly detected (as well as anhydrite), and this would be a potential calcium source during the preparation of the oriented aggregates of samples from the hottest area.

The exchange of Na by Ca during suspension would also have occurred in the samples prepared for the determination of the exchangeable complex by Cs displacement, and could explain the smaller amount of extractable sodium measured in the drier samples, where calcium sulphates (and carbonates) dissolved during sample preparation were present (as shown by SEM observations). Hence, this distribution pattern would not reflect the actual distribution during the test. Nevertheless, the exchangeable cation complex determined showed the predominance at the end of the test of sodium in the interlayer, in agreement with the population in the initial bentonite and the large sodium concentration of the hydration solution. At 10 cm from the heater, the exchangeable magnesium (and potassium) content peaked, but the increase did not progress towards the heater, so maybe it was more related to the accidental evaporation at this level than to temperature. The fact that this cell was hydrated with a highly saline water may also have affected the kind and magnitude of interlayer changes.

The CEC decreased slightly towards the heater. This was not reflected in the evolution of the montmorillonite structural formula and its calcium content along the column (Figure 4.7, left), with the exception of the perturbation at 11 cm, with the increase in calcium and magnesium (S19, Figure 4.7, right). Hence, the decrease in CEC has no obvious explanation, although this phenomenon has been observed systematically in other bentonite heating experiments. In contrast to the generalised reduction of CEC normally observed in other tests, in the present column the CEC decreased only in the warmer areas. Dehydration and the decrease in surface area as a result of aggregation and formation of dense aggregates have been argued as possible explanations. In turn these processes could lead to a decrease in some surface positions for cation exchange. Considering that full rehydration of these samples was achieved during the continuous batch steps for calcium saturation of the montmorillonite (Figure 4.8), it is possible that CEC could also be recovered, which should be tested in the future. Another explanation for the CEC decrease would be the smectite alteration, but the results of this research point to no significant changes in its crystal-chemistry.

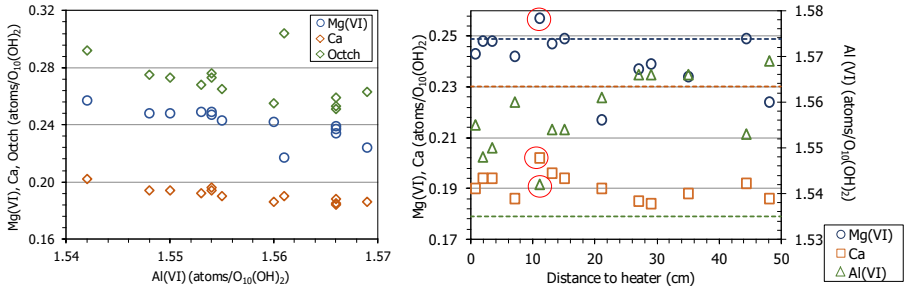

Figure 4.7: Ca, Mg and octahedral charge in the corrected structural formulae as a function of octahedral Al (left) and of the distance to the heater (right). The horizontal dotted lines indicate the values for the reference sample (the circled symbols correspond to sample S19, at 11 cm from the heater)

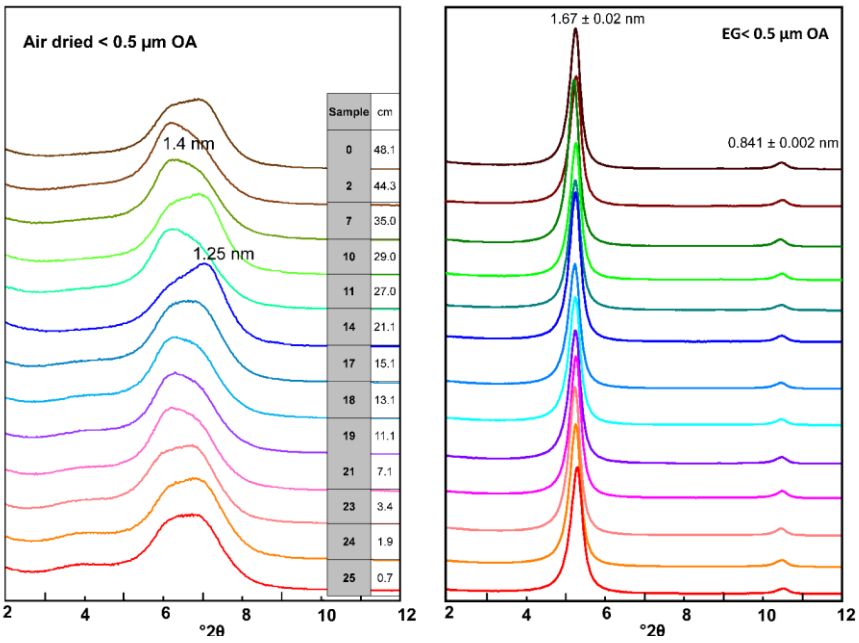

Figure 4.8: XRD patterns of the air dried (OA) and ethylene-glycol solvated (EG) oriented aggregates of samples taken along the bentonite column (the distance to the heater of each sample is indicated)

~~4.3.1.2~~4.3.1.3 Movement of soluble species

Other similar heating-hydration tests showed that hydration caused the dissolution of some species and that the solubilised ions were transported towards the heater and precipitated farther away along the bentonite column as the test lasted more. Those tests also showed that, for a given duration, the chloride concentration in the aqueous extracts peaked closer to the heater than the sulphate one, given their different size and the implication of sulphate in other dissolution/precipitation processes. Indeed sulphate peaked in this test at ~18 cm from the heater, where the temperature during the test was 40°C, whereas the chloride maximum was at 9 cm from it (*T*~60°C), approximately at the location of sensor RH3 (Figure 4.9). Interestingly, the calcium and sodium concentrations had maxima at these two

Commenté [LJ7]: Was the test sample geometrically longer in space or the test lasted longer in time? Please clarifty.

distances (Figure 4.10), so they must be related both to sulphate and chloride. In fact, gypsum solubility increases in the presence of dissolved NaCl and has its maximum at approximately 40°C (0.05 mol/kg at 1-5 M NaCl, (Marshall, 1966)), which was the temperature at ~18 cm from the heater, where maxima of the two anions were recorded. The high salinity in these areas likely triggered the corrosion of the sensors, particularly the bottom one (Villar, 2022).

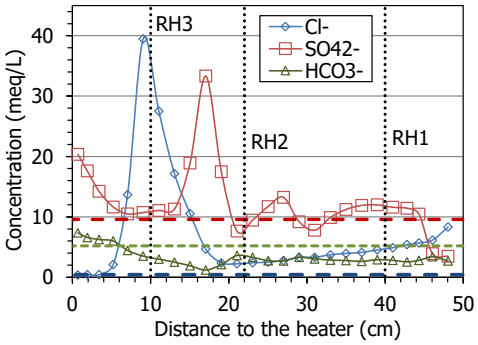

Figure 4.9: Main anions measured in aqueous extracts of samples of cell HEE-B (the horizontal lines indicate the concentrations in the untreated pellets and the vertical dotted lines the positions of the sensors)

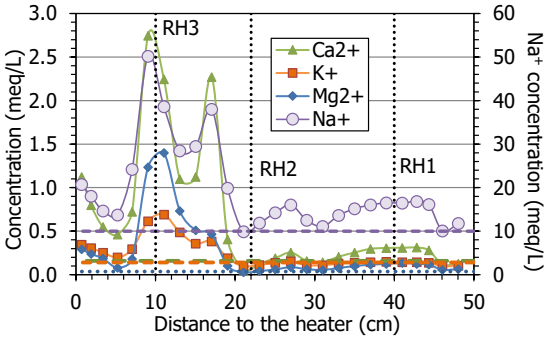

Figure 4.10. Main cations measured in aqueous extracts of samples of cell HEE-B (the horizontal lines indicate the concentrations in the untreated pellets and the vertical dotted lines the positions of the sensors)

The pattern of gypsum distribution as observed by XRD would indicate that sulphate leaching took place. In the more hydrated bentonite, gypsum could not be detected, which could indicate its dissolution and transport. In fact, gypsum appeared in the region between 10 and 30 cm from the heater, where its solubility would tend to decrease because of the progressively higher temperature: between 40°C, close to its maximum solubility, and 60°C, close to an anhydrite-predominant environment. Hence, it would precipitate or be replaced by the less soluble anhydrite. In fact, SEM observations allowed to spot occasional calcium sulphates close to the heater (presumably anhydrite traces that were not possible to detect by XRD), as also the FTIR results showed. In the 10 cm closest to the heater (temperatures higher than 60°C) gypsum was again absent. However, the sulphate concentration in the aqueous extracts was greater than the initial one in this area, tending to increase towards the heater.

The increase of bicarbonate in the aqueous extracts near the heater zone may relate to the observed presence of calcite and its dissolution during the preparation of the aqueous extracts. The observation

of carbon-rich fill in the cavities could indicate the evolution of a gas phase either with carbon coming from the steel heater or CO_2 appearing as a co-product of the evaporation of the salty solutions produced at ~10 cm from the heater. CO_2 degassing was invoked to explain calcite precipitation in similar TH tests (Fernández, 2010). Calcite was not detected close to the hydration surface and the bicarbonate content was small in this area. In contrast, the analysis of the water left in the hydration vessel after the test showed a significant decrease in calcium and an increase in bicarbonate content relative to the initial value. Both observations could be related to the dissolution of calcite in the more hydrated area, the diffusion of bicarbonate towards the hydration source and the incorporation of the calcium released to the exchangeable complex substituting for sodium.

The high temperature in the 5 cm closest to the heater could have also caused the dissolution of quartz and cristobalite inferred from the results in Figure 4.11, although presumably the extremely dry conditions in this zone may have limited the dissolution reactions. The relatively high extractable silica in this zone could be related to the presence of amorphous silica, more soluble than quartz and not easily detected by XRD due to its small amount. It must be pointed out that, although it seems evident that vapour leaked through the bottom sensor inlet, this did not happen from the beginning of the test, and during an undetermined period of time (which may have been long) liquid water was probably able to reach areas closer to the heater than the level of the sensor location. In fact, the distribution pattern of soluble ions (Figure 4.9, Figure 4.10) shows minimum values at 5 cm from the heater followed by a progressive increase towards it, with overall values in the area higher than the initial ones. This would indicate that water loaded with soluble species was able to reach the area at less than 10 cm from the heater and when this water supply stopped as a consequence of the vapour leak, the accumulated salts redistributed by convection-concentration processes.

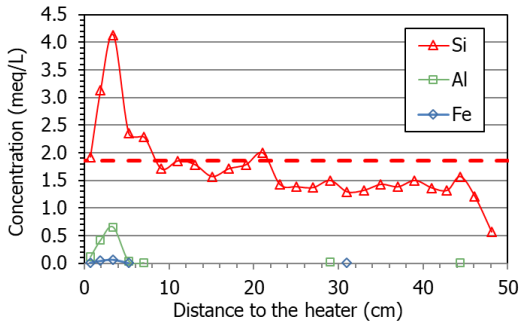

Figure 4.11. Cations measured in aqueous extracts of samples of cell HEE-B (the horizontal line indicates the Si^{4+} concentration in the untreated pellets, the other ions were not detected)

~~4.3.1.3~~4.3.1.4 Specific surface area

A microstructural effect observed was the decrease in specific surface area for those samples at less than 15 cm from the heater (*T*>42°C), which were also those with dry density higher than the initial one (*Figure 4.12*). The lowest values of a_s were measured in the column samples located at 10 cm from the heater (minimum value was 17 m^2/g, around the sensor RH3 leaking inlet), where the temperature was lower than 60°C. For this reason it is considered that the decrease in a_s was more related to sustained evaporation than to temperature. Evaporation through the sensor inlet would cause shrinkage, densification and aggregation of particles in an area where the water content had been previously higher. Nevertheless, in the 5 cm closest to the heater (where presumably the water content was never higher than the initial one), a_s decreased towards the heater, reaching at the contact a value of 25 m^2/g. Conversely, the specific surface area of all the samples at more than 15 cm from the heater increased with respect to the initial value.

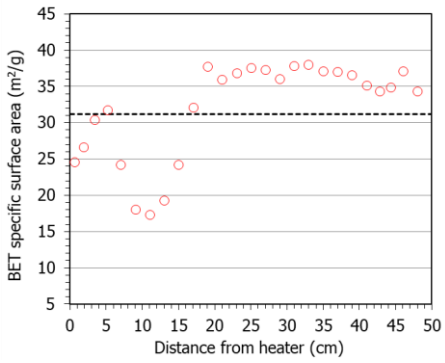

Figure 4.12. BET specific surface area of samples from cell HEE-B and of the initial pellets (dotted horizontal line)

4.4 Conclusion

Two sets of thermo-hydraulic tests were analysed by CIEMAT and UAM. The tests consisted in heating a bentonite column through the base while water was injected on top for 2.5 and ~9 years. In one set of tests (C3, C4, C5) the columns were 10 cm high and the heater was set at 110°C. Two of these tests were performed using MX-80 powder (saturated with saline and dilute water, C4 and C5 respectively) and the other one using Ibeco bentonite (C3). In the other set of TH tests (consisting just of test HEE-B) the height of the column was 50 cm and the heater was set at 140°C. It was saturated with saline water and MX-80 pellets were used.

In tests C3-C5 no significant montmorillonite structural modifications took place during operation. Octahedral Mg relatively increased near the heater, although globally the octahedral Mg content was lower in the treated MX-80 samples compared to the reference one and higher in the Ibeco treated samples than in the reference one. In all the samples from the cells the layer charge decreased with respect to the values of the reference samples.

In cell C3, chlorite (2:1:1 sheet silicate) was detected at less than 1-2 mm from the heater. Abundant halite precipitation was observed in large pores (triggered by heating) at distances of less than 5 mm from the heater. The overall content of carbonates increased in the area at less than 4 cm from the heater. In the area at less than 2 cm from the heater calcite predominated over dolomite, in contrast with the rest of the cell, where dolomite was the predominant carbonate. This would match with the dissolution of dolomite in the contact with the heater and the incorporation of magnesium to the newly formed chlorite. The exchangeable magnesium content also increased above the initial value close to the heater.

In the MX-80 samples from tests C4 and C5, calcium sulphate (probably anhydrite) was detected in areas at less than 4 cm from the heater. Total consumption of oxygen seems to have occurred in both experiments, explaining the presence close to the heater of pyrite and oxides in different oxidation states in the case of C4. As a result of the hydration with saline water in cell C4, carbonates and sulphates precipitated at various locations, NaCl-spotted areas were observed close to the heater and corrosion occurred in the contact with the steel elements. None of these features were observed in cell C5, hydrated with glacial water. In this cell, close to the hydration surface calcium carbonates precipitated.

The changes in the pore water composition inferred from the aqueous extracts were affected by 1) the composition of the incoming water, 2) the dissolution of mineral species present in the initial bentonite as a result of the water content increase, 3) cation exchange processes.

The ions coming with the hydration water and those coming from the dissolution of minerals were transported by advection and accumulated in the lower half of the columns at the bottom, precipitating

closer to the heater. The overall concentration of the ions in the samples increased significantly with respect to the initial one. The maxima in sulphate concentration were in all cells accompanied by increases in the soluble sodium and calcium contents, possibly indicating the precipitation of anhydrite at less than 4 cm from the heater in cells C4 and C5 and at 3 cm from the heater in cell C3 (in the latter case it was not possible to ascertain if the sulphate was gypsum or anhydrite). The precipitation of carbonates close to the heater in all cells was reflected in the decrease in bicarbonate content from the hydration surface towards the heater.

At the end of the HEE-B test all the samples continued to consist predominantly of a dioctahedral smectite, with no significant differences from the original with respect to the distribution of structural cations and layer charge. No evidence of mixed-layer formation was detected. Sodium continued to predominate in the exchangeable cation complex (according to the measurement of the basal spacing, thermogravimetry, and Cs displacement results), probably as a consequence of the hydration with a predominantly sodic solution. However, some contribution of divalent cations toward the hydration surface could be detected.

Despite the lack of montmorillonite alteration at the structural level, the drier samples, those that were subjected to temperatures >60°C, remarkably had a significant resistance to rehydration under room relative humidity conditions. However, this was not an irreversible process, as the samples hydrated normally when the relative humidity was high (97%) and expanded as expected when suspended in water.

Although hydration took place with a highly saline water – which seems to have inhibited the formation of colloids – the overall increase in water content allowed the dissolution of some species and the solubilised ions were transported toward the heater and precipitated at two distinct areas: sulphate, sodium, and calcium peaked at ~18 cm from the heater whereas chloride moved closer to the heater (accompanied by sodium and calcium), concentrating at 9 cm from it, coinciding with a vapour leak area. This leak started at some undetermined moment during the test through a sensor inlet. This experimental artefact seems to have conditioned the processes around it, such as the movement of solubilised ions. The liquid-water availability was probably affected also in the areas of temperatures higher than 60°C, which would limit the reactivity there. Nevertheless, evidence of precipitation of calcite and calcium sulphates and dissolution of cristobalite and quartz were observed in the areas where the temperature was higher than 100°C.

Around this sensor inlet the specific surface area of the bentonite was lowest, indicating aggregation of particles likely caused by shrinkage when water evaporated from bentonite whose water content was higher prior to the start of the leak. From this point towards the heater the bentonite was disaggregated, with specific surface areas smaller than the initial one.

It can be concluded that in any of the tests structural modifications of the bentonite were not observed, but that dissolution and precipitation of species occurred and were conditioned by the kind of bentonite and hydration water. These processes were accompanied by modification of the exchangeable cation complexes. The use of pellets instead of compacted blocks does not seem to have been an additional source of uncertainty.

Commenté [LJ8]: "were observed" or "were not observed"?

Commenté [VGMV9R8]: In any…. were observed

5. CU (SÚRAO)

5.1 Introduction

The research activities focused on determining the hydromechanical properties of thermally treated BCV bentonite. The bentonite was heated to 150°C for 1 year. After the heat treatment, the water content was equilibrated to match the suction conditions of the original BCV bentonite. The research plan included the determination of swelling pressures, hydraulic conductivity and constant load swelling carried out on homogeneous samples compacted from treated bentonite powder. The samples were compacted to different initial dry densities. The tests were carried out using a new set of in-house developed constant volume "MPC" cells (to determine swelling pressures and hydraulic conductivity) and oedometers (for constant load swelling tests). The main objective was to define the hydromechanical behaviour of thermally treated bentonite and to identify differences in comparison to the properties of thermally untreated BCV bentonite.

5.1.1 Material

The original material used in the experimental programme was Czech Ca-Mg bentonite from the Černý vrch deposit (BCV). The material is produced industrially by Keramost Ltd in the form of powder with an original water content of approximately 11%. References to research reports describing the basic properties of the material are given in section 6.1.1.

5.1.2 Research plan

The planned laboratory experiments involved the determination of the hydromechanical properties of thermally loaded BCV bentonite. Bentonite powder was subjected to 1 year of thermal treatment followed by equilibration of the water content. The whole preparation process took 17 months.

The evaluation of the hydromechanical properties included the determination of swelling pressure and hydraulic conductivity in constant volume cells. Both parameters were measured on samples compacted to different initial dry densities (1.4, 1.6 and 1.8 g/cm^3) in order to identify the material behaviour in the wide range of initial states. As the new set of constant volume cells with an improved design was manufactured for the EURAD project, a new set of experiments was carried out on thermally untreated BCV bentonite for direct comparison. The results were compared with existing data on untreated BCV bentonite to assess the performance of the new cells.

A set of constant load swelling tests was carried out on thermally treated samples in oedometers. The samples were compacted to initial dry density of 1.6 g/cm^3 and subjected to vertical loads of 0.025, 0.75, 1.55 and 4.1 MPa. The samples were then flooded and fully saturated. After reaching constant swelling strain, the final void ratios were calculated. The results were compared with untreated BCV samples tested in the same way in the past.

Table 5.1 CU – hydromechanical characterisation in constant volume cell and oedometer

5.1.2.1 Material (BoM item): BCV bentonite (Ca-Mg type), powder as delivered by producer
5.1.2.2 Material treatment (sample preparation for test and loading procedure): Bentonite was heated in its original state (powder) at 150°C for 1 year. After thermal treatment, the water content of the bentonite powder was equilibrated by the vapour equilibrium method at the same suction as the original BCV bentonite.
5.1.2.3 Temperature (to which material was/will be exposed to) and exposure time 150 °C for 12 months
5.1.2.4 Tests carried out (name, description, sample preparation, procedure, results): Swelling pressure, hydraulic conductivity and swelling pressure tests under controlled suction were performed in constant volume MPC cells. Samples were prepared from 36 grams of treated powder by uniaxial compression with controlled force directly into the test cells. The diameter of the samples was 50 mm and the initial height varied depending on the required initial dry density. 5.1.2.4.1 Swelling pressure Compacted samples installed in constant volume MPC cells were saturated with distilled water through the bottom base. Only a low external water pressure of 10 kPa was applied during saturation. The swelling pressure acting on the opposite side of the samples was measured by a loadcell. Test continued until swelling pressure reached a constant value. 5.1.2.4.2 Hydraulic conductivity Hydraulic conductivity was determined after measurement of swelling pressures on the identical samples. Both sides of the samples were connected to pressure and volume controllers and a constant pressure gradient was applied. After reaching the constant flow rate, hydraulic conductivity was determined. 5.1.2.4.3 Swelling pressure at controlled suction Swelling pressure at controlled suction was measured in the same constant volume MPC cells and test samples were prepared in the same way. Constant suction was controlled by the vapour equilibrium method. The air with constant relative humidity circulated through both bottom and top porous stones and the water content of the samples gradually equilibrated. When constant swelling pressure was reached, the relative humidity of the circulating air was increased and a new suction was applied. 5.1.2.4.4 Constant load swelling Samples were compacted to oedometric rings, installed in oedometer cells and uniaxially loaded to the required vertical stress. The samples were flooded with distilled water and vertical swelling was monitored until full saturation was reached.

5.2 Procedures

5.2.1 Material treatment and equilibration

BCV bentonite powder in its original form and with a water content of approximately 11% was placed in the oven and heated at 150°C for 12 months (Figure 5.1(a)). After 12 months, the bentonite powder was removed from the oven and cooled to laboratory temperature in a closed desiccator to prevent air humidity from entering the soil.

The water content of the bentonite powder was then equilibrated in a controlled environment using the vapour equilibrium method. The powder was placed in desiccators with air humidity of 43.2% controlled by a saturated solution of K_2CO_3 (Figure 5.1(b)). This value was chosen based on the available retention curve of BCV bentonite (Laufek, 2021). It imposes a suction of 113 MPa in bentonite and a corresponding water content of 10.7%, which is close to the initial state of BCV bentonite. The aim of this process was to equilibrate the thermally treated bentonite under the same conditions as the original BCV bentonite before the preparation of the test samples.

(a) (b)

Figure 5.1 Thermal loading of BCV bentonite (a) followed by equilibration in desiccator with controlled relative humidity of 43.2%.

The process of bentonite equilibration is relatively time consuming, especially when a large amount of bentonite is placed in the desiccator. To speed up the equilibration process, a small portion of bentonite powder was placed in a separate desiccator and the water content of the bentonite was checked regularly. The powder reached a constant water content after approximately three months (Plate 1 in Figure 5.2). The remaining material, which was divided into two other desiccators, reached equilibrium after approximately five months. The final water content of the thermally treated powder reached 7.4-7.8 % with an average of 7.5%. This confirmed the previous observation (Laufek, 2021) that the retention capacity of thermally treated BCV bentonite is lower compared to the original material.

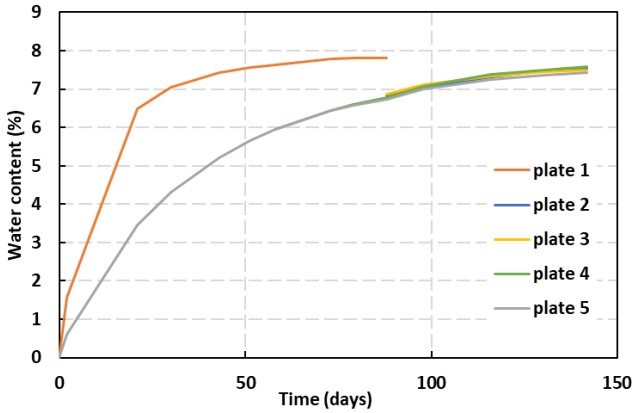

Figure 5.2 Equilibration of water content of thermally treated bentonite in time.

5.2.2 Samples preparation

All bentonite samples prepared for hydromechanical tests were compacted directly into test cells in a uniaxial frame with controlled compaction force. Each sample was prepared from 36 g of thermally treated powder equilibrated to water content of 7.5%. The diameter of all samples tested was 50 mm. The aim of a well defined preparation procedure was to ensure repeatability and identical initial states of the samples.

The test programme included samples with target initial dry densities of 1.4, 1.6 and 1.8 g/cm^3, achieved by applying vertical loads of 2 090, 5 070 and 12 280 kg, resulting in typical initial sample heights of 11.8, 10.3 and 9.2 mm respectively.

The samples for constant volume tests were prepared directly in MPC cells, which were used in slightly modified configurations for the swelling pressure, hydraulic conductivity and suction controlled swelling pressure tests. The samples for constant load swelling tests were compacted in oedometric rings with lubricated inner walls to minimise wall friction during swelling.

5.2.3 Test procedures

Constant load swelling

A conventional oedometer apparatus was used for the constant load swelling tests. Samples compacted to the initial dry density of 1.6 g/cm^3 were tested in the rigid stainless steel rings of 50 mm diameter and 20 mm height. The rings with the samples were installed in oedometer devices and loaded to the required vertical stresses (0.025, 0.75, 1.55 and 4.1 MPa).

When the initial deformation reached a constant value, the samples were flooded with distilled water. Vertical deformations of the samples were recorded until constant values were reached. Due to the high applied loads and relatively small deformations of the samples, the apparatus compliance correction was determined and included in the evaluation of the tests.

Swelling pressure

The swelling pressure tests were carried out in stainless steel constant volume MPC cells consisting of a confining ring, a bottom base and a piston held in a fixed position by a rigid frame. A small loadcell was placed between the piston and the frame.

The metal porous plates connected to drainage lines were integrated into the bottom base and piston to allow saturation of the sample. The sample was saturated with distilled water through the bottom base. A low water pressure of 10 kPa was applied during saturation (Figure 5.3). The increase in swelling pressure was monitored until a constant value was reached.

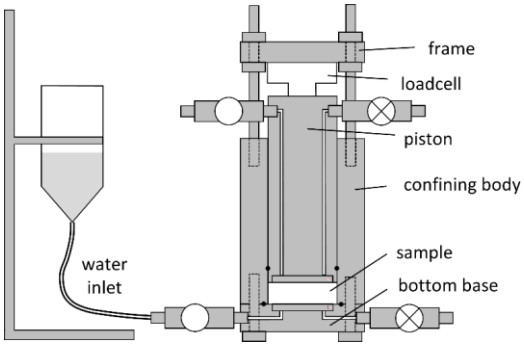

Figure 5.3 Configuration of MPC cell for swelling pressure measurement.

Hydraulic conductivity

Hydraulic conductivity was determined after measurement of swelling pressures on the identical samples. Prior to the measurement, pressure and volume controllers were connected to both sides of the sample (Figure 5.4) and a constant pressure gradient of 300 kPa was applied. A higher water pressure was applied to the bottom base, generating an upward flow of water. After reaching a constant flow rate, hydraulic conductivity was measured.

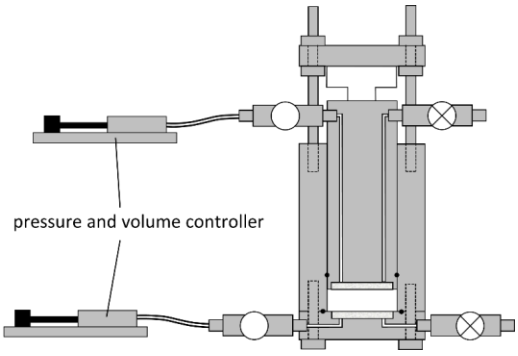

Figure 5.4 Configuration of MPC cell for measurement of hydraulic conductivity.

Swelling pressure at controlled suction

The samples for the suction controlled swelling pressure tests were prepared in the same way as the samples for the fully saturated swelling pressure tests. Three samples compacted to initial target densities of 1.4, 1.6 and 1.8 g/cm^3 were exposed to the air of constant relative humidity, which was controlled by different saturated salt solutions. Total suction has a unique relationship with relative humidity described by Kelvin's law. A forced air circulation was used to accelerate the equilibration of the samples (Figure 5.5).

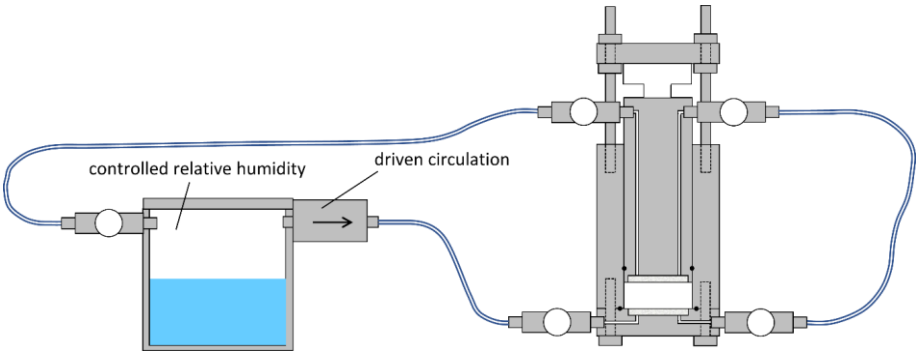

Figure 5.5 Configuration of MPC cell for suction controlled swelling pressure test.

The samples were compacted after equilibration of the treated bentonite powder at a relative humidity of 43.2%, and during the tests they were gradually wetted by applying the relative humidities and total suctions listed in Table 5.1. After equilibration of the suction, the salt solution was replaced by a new one, imposing a higher relative humidity. The equilibration of swelling pressures took approximately two months for each suction level, which resulted in a long duration of the whole test. After the set of tests performed on thermally treated samples, a similar set of tests was carried out on original BCV bentonite to provide reference values.

Table 5.1 Salt solutions used for vapour equilibrium method, corresponding relative humidities and total suctions.

solution	relative humidity	total suction
NaBr	59,1	71,1
NaCl	75,5	38,0
KCl	85,1	21,82
K_2SO_4	97,6	3,29
H_2O	100	0

5.3 Results

5.3.1 Constant load swelling

The final dry densities and void ratios were calculated from the final dimensions, dry mass and specific gravity of 2.76 g/cm^3. The results are presented in Table 5.2 and Figure 5.6 in direct comparison with identical tests previously carried out on untreated BCV bentonite. The final void ratios decrease with increasing vertical load with a linear trend in the presented semilogarithmic scale. The regression lines of thermally treated and original material exhibit the same trend. Minor differences between individual results are within the range of experimental error.

Table 5.2 Comparison of final dry densities and void ratios of samples before and after thermal treatment

Vertical load [MPa]	original BCV bentonite		thermally treated bentonite	
	$\rho_{d\text{-final}}$ [g/cm^3]	e_{final} [-]	$\rho_{d\text{-final}}$ [g/cm^3]	e_{final} [-]
0.025	1.04	1.67	1.05	1.62
0.75	1.42	0.94	1.36	1.02
1.55	1.47	0.88	1.45	0.90
4.1	1.63	0.69	1.64	0.68

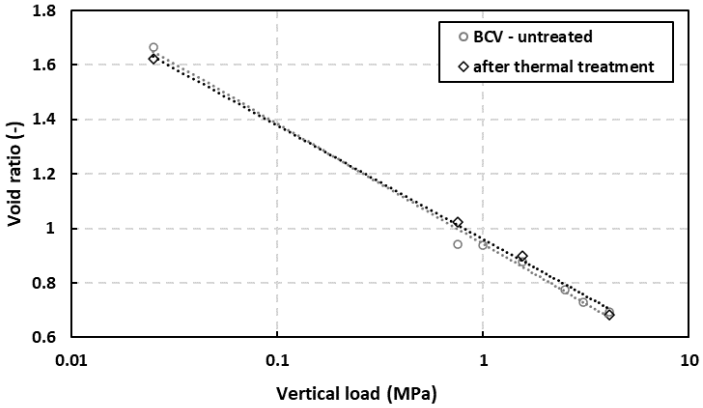

Figure 5.6 Results of constant load swelling tests of bentonite samples compacted to initial dry density 1.6 g/cm^3.

5.3.2 Swelling pressure

Swelling pressure was measured on thermally treated samples compacted to 1.4, 1.6 and 1.8 g/cm^3 and on four samples of the original BCV bentonite. The time evolution of the swelling pressure is shown in Figure 5.7. Equilibration of swelling pressure in the thermally treated samples took approximately 200-500 hours depending on the initial dry density. Comparison of the thermally treated and untreated samples compacted to 1.6 g/cm^3 shows that the swelling pressure evolution of the thermally treated sample took significantly longer compared to the original BCV bentonite.

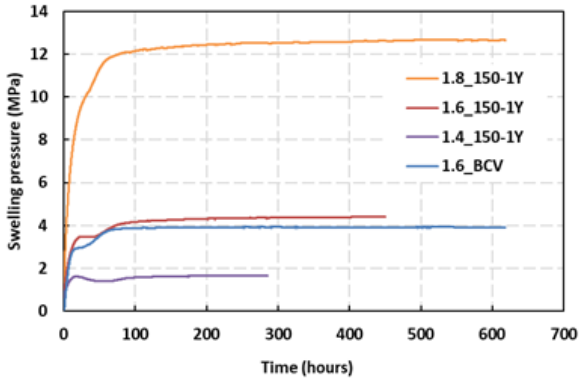

Figure 5.7 Evolution of swelling pressure in time.

The final swelling pressures are presented in Figure 5.8. It confirms a typical trend of linear increase in swelling pressure with dry density on a semilogarithmic scale. Three sets of data are shown in the graph. The test results represented by full symbols were measured in a new set of MPC constant volume cells with an improved design. The results show similar swelling pressures of thermally treated bentonite compared to original BCV, although slightly lower swelling pressures were obtained for thermally treated samples compacted at higher dry densities. Comparison of the untreated BCV swelling pressures determined in the original MPC cells, represented by empty symbols, with the results obtained from the new cells shows a good agreement.

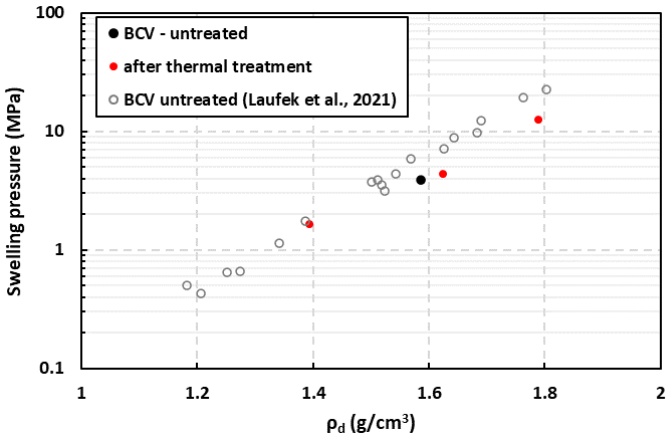

Figure 5.8 Dependency of swelling pressure on dry density.

5.3.3 Hydraulic conductivity

Hydraulic conductivity of thermally treated bentonite is presented in Figure 5.9. No direct measurement in the same cell was performed on untreated BCV bentonite. The thermally treated samples are therefore compared with previous results obtained in the original set of MPC cells. The comparison indicates that the thermal treatment resulted in slightly higher hydraulic conductivity. The resulting

difference is not expected to be related to differences in the design of the cells used for the two sets of experiments.

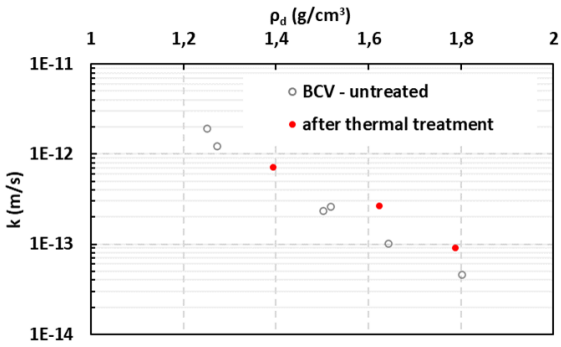

Figure 5.9 Dependency of hydraulic conductivity on dry density

5.3.4 Swelling pressures at controlled suction

The evolution of swelling pressures of the thermally treated samples in the suction-controlled test is presented in Figure 5.10. The total duration of the test reached 400 days with variable length of the individual stages. The initial stage with a suction of 71 MPa was partially influenced by the failures of air conditioning in the laboratory during the summer months. The resulting temperature variations influenced the swelling pressure development in the time interval 30-70 days. Each stage was terminated after full swelling pressure equalisation. The only exception was the stage with 3 MPa suction, where the measured swelling pressures varied significantly and no equilibrium was reached. For this reason, this stage was not included in the final evaluation.

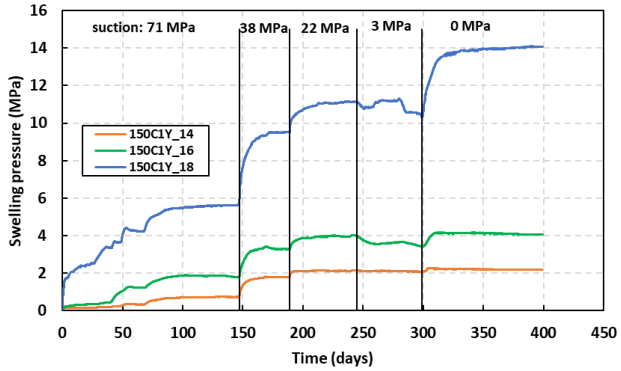

Figure 5.10 Evolution of swelling pressures in suction-controlled test with thermally treated samples.

The final swelling pressures obtained for each stage are shown in Figure 5.11. The samples with different dry densities showed a qualitatively similar behaviour, represented by the parallel regression lines in the graph. The slope of the regression lines is similar to the line representing the water saturated samples (see Figure 5.8), which is also shown for the comparison.

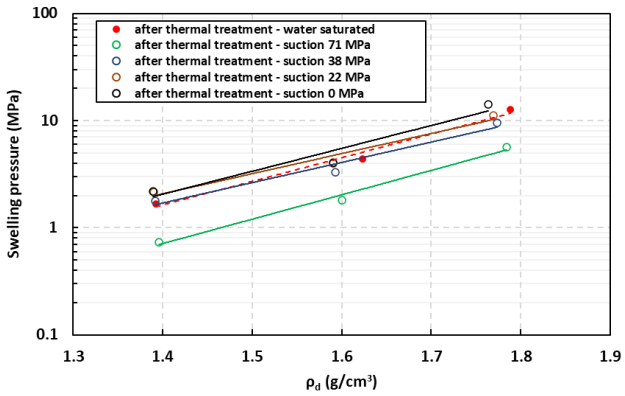

Figure 5.11 Results of suction-controlled swelling pressure tests on thermally treated samples.

The results obtained for the untreated BCV bentonite are presented in Figure 5.12 and indicate similar behaviour to the thermally treated samples. Both sets of the samples show that the swelling pressures measured in the final stage of the suction-controlled tests (relative humidity 100%) are in good agreement with water saturated samples. In the case of the thermally treated samples, the maximum swelling pressures measured in the final stage of the test are even slightly higher compared to water saturated samples. This could indicate that the slightly lower swelling pressures of the two thermally treated samples shown in Figure 5.8 could be due to experimental error rather than a reduced swelling capacity of the thermally treated samples.

A direct comparison of the swelling pressures determined in the two suction controlled sets is presented in Figure 5.13. It shows slightly higher swelling pressures for the thermally treated samples compacted to target densities 1.4 and 1.8 g/cm³ and slightly lower values for the 1.6 g/cm³ sample. In general, no clear difference was found between the two data sets and small differences measured can be attributed to scatter caused by experimental error.

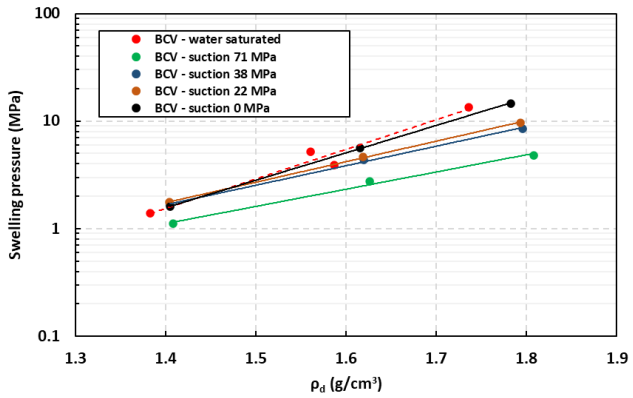

Figure 5.12 Results of suction-controlled swelling pressure tests on BCV samples.

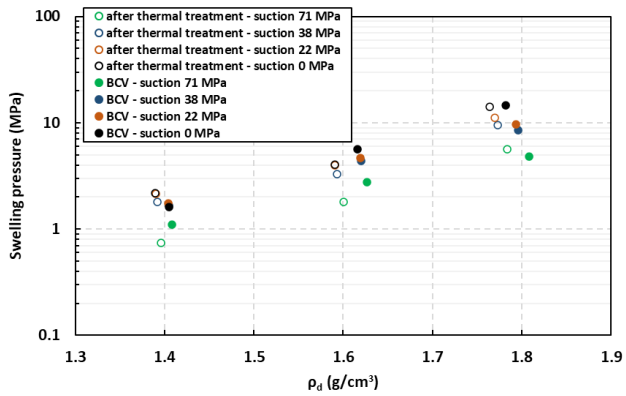

Figure 5.13 Comparison of suction controlled tests on thermally treated and original BCV samples.

5.4 Conclusion

The aim of the presented research was to evaluate the effect of long-term thermal exposure (1 year at 150°C) on the hydromechanical properties of BCV bentonite. The differences between the original BCV and the thermally treated bentonite were investigated by swelling pressure tests, constant load swelling tests, suction controlled swelling pressure tests and hydraulic conductivity measurements.

Hydraulic conductivity measurements showed slightly higher values for the thermally treated samples. Despite the higher hydraulic conductivity, the thermally loaded material exhibited a slower equilibration of swelling pressure. Different retention properties were also indicated from equilibration of the bentonite powder after thermal treatment, which resulted in water content of 7.5% at 43.2 % relative humidity compared to 10.7 % for the original BCV bentonite.

Constant load swelling tests showed no difference between the two materials. Swelling pressure tests also showed similar values for both materials. Thermally loaded samples compacted to higher dry densities showed slightly lower swelling pressures compared to untreated samples. However, suction controlled swelling pressure tests gave very similar results for both materials at all suction levels, with thermally treated samples even giving slightly higher maximum swelling pressures compared to water saturated tests. Overall, the experiments investigating swelling properties provided no clear evidence of a reduction in the swelling capacity of BCV bentonite as a result of thermal treatment.

6. CTU (SÚRAO)

6.1 Introduction

The source term for the increased temperature of the buffer, which consists of bentonite clay, is the decay heat generated by the radiation from the spent fuel. The radiation can have long-term effects on the material properties of the clay. Bentonites of Czech origin are expected to be used as buffer and backfill material in the Czech geological repository, therefore the research was based on testing this type of high swelling clay after long-term heating at 150 °C. The aim of the research was to determine the possible temperature effect on the hydraulic-mechanical properties after high temperature exposure. As it is assumed that the material of the buffer, or its part, can be saturated and exposed to elevated temperatures at the same time, the material was tested in two moisture conditions - saturated (as a water suspension) and dry. The research aimed to evaluate the trends and changes of hydraulic-mechanical properties of bentonite in the two moisture conditions after different time steps of temperature exposure. The objectives included laboratory experiments leading to determine the hydraulic conductivity, swelling pressure, liquid limit and swell index of dry and wet treated bentonite after 6, 12 and 24 months of thermal loading at 150 °C. The above parameters were also determined on samples taken from a small-scale experiment carried out as part of subtask T3.3, described in D7.9.

6.1.1 Material

Bentonites of Czech origin are considered to be used as buffer and backfill material in the Czech geological repository, therefore the research in the HITEC project was focused on Czech bentonite of calcium/magnesium (Ca/Mg) type extracted from the Černý Vrch deposit. The material was extracted and processed (dried and ground) by the producer, and the texture of the final original material ready for testing was a very fine powder. The material was tested for the first time in 2017 and its designation is BCV_2017. The basic characteristics of the tested bentonite are summarised in (Hausmannová, et al., 2018). The data concerning the original material are acquired from another projects (Hausmannová, et al., 2018), (Červinka R., 2018), (Svoboda J., 2019). The same bentonite was used in HITEC T3.2 and T3.3

6.1.2 Research plan

The aim of the project was the determination of the hydraulic and mechanical properties of Ca/Mg bentonite after exposure to high temperatures (wet and dry). Three sampling campaigns were carried out for each bentonite in each moisture condition. Sampling was carried out after 6, 12 and 24 months of thermal loading. After sampling, hydraulic conductivity, swelling pressure, liquid limit, and swell index were tested. Hydraulic conductivity and swelling pressure depend on dry density. Therefore, laboratory tests for these properties were carried out on sets of samples with different dry densities.

A summary of the material, procedures and measurement method used is given in the Table 6.1

The material that originated from the medium-scale experiment (T3.3) was also tested within subtask T3.1. The experiment was based on heating from below and simultaneous saturation of bentonite from above in the presence of a temperature gradient. Once the medium-scale experiment was dismantled, the material was tested in the laboratory. The water content, dry density, hydraulic conductivity, swelling pressure, and liquid limit were investigated. Small scale experiment and its results and conclusions are described in detail in D7.9.

Table 6.1 CTU – Summary of material, procedure and methods used

6.1.2.1 Material (BoM item): BCV bentonite (Ca-Mg type), powder as delivered by producer
6.1.2.2 Material treatment (sample preparation for test and loading procedure): Two sources of material were used: laboratory treated and samples form T3.3 6.1.2.2.1 Laboratory treated bentonite Two types of treatment were used: • ”Dry“ - powder material will be placed into 150 °C (drying allowed) • “Wet“ - bentonite water suspension will be placed into 150 °C (drying prevented) Loading lasted 6, 12 and 24 months (e.g. 3 campaigns were done). Wet samples were dried and milled after treatment as part of the test preparation. 6.1.2.2.2 Material from T3.3 Samples obtained from medium scale experiments in Task 3.3
6.1.2.3 Temperature (to which material was exposed to) and exposure time 150 °C for 6, 12 and 24 months
6.1.2.4 Tests carried out (name, description, sample preparation, procedure, results): Permeability and swelling pressure were measured in constant volume cells (D=30mm, H=20mm). First the hydraulic conductivity was measured then the swelling pressure was determined. Liquid limits were determined by fall cone method. 6.1.2.4.1 Permeability - K [m/s] Permeability was measured using a constant pressure gradient permeameter. Samples were compacted directly into constant volume cells, then a water gradient was applied, and water inflow and total pressure development were measured. Once stable flow (total pressure) had been obtained, permeability was calculated. The pressure gradient was then released, and swelling pressure measurement began. 6.1.2.4.2 Swelling pressure - σ_{sw} [MPa] Swelling pressure was determined on a fully saturated sample from the permeability test. The pressure gradient was no longer applied, and once the total pressure stabilized, it equaled the swelling pressure (there was no pore pressure in the sample).

6.2 Procedures

Laboratory treated bentonite

The experimental procedure consisted of two consecutive parts – long-term exposure to high temperature followed by sampling and laboratory testing.

Two vessels containing dry bentonite (dry treated bentonite) were placed in the laboratory oven at 150°C. One vessel of 10 liters contained dry bentonite with a water content originally provided by the producer, which was 7-10%. This vessel was placed into the oven without any lid, thus allowing for drying.

The second type of vessel contained wet bentonite (bentonite suspension). In this case, drying was not allowed. It was necessary to design a special pressure vessel (with a volume of 14 liters) that prevented

water from escaping and could withstand the pressure of water vapors forming inside. The vessel and suspension were designed in a way to prevent the boiling of the suspension.

Sampling was carried out from each of the vessels after 6, 12, and 24 months of thermal treatment. The analysis of dry bentonite samples usually took place immediately after natural cooling down to laboratory temperature (the water content was not equilibrated to laboratory humidity). If immediate testing was not possible, the samples were hermetically sealed in plastic bags once the suitable temperature was reached.

The material was dried of extra water in a laboratory oven at 60°C for two weeks in order to process the sampled wet material more effectively. Water content of the samples after drying was 5-6% water.

Material from the sampling (from both vessels) was then used for the investigation of permeability, swelling pressure, and liquid limit. Part of the material was compacted and analyzed in a specially designed apparatus for the measurement of saturated hydraulic conductivity and swelling pressure. Powdered material was further prepared for liquid limit determination, which was performed using the fall cone test.

Bentonite from small scale experiment

In T3.3, two experiments were carried out, each time with a different BCV bentonite form. The first experiment was carried out with powdered bentonite (LMC1) with a low dry density (900 kg/m^3) and the second experiment was carried out with pelletized BCV bentonite (LMC2) with a higher dry density (1400 kg/m^3). The bentonite was placed in a vessel with a diameter of 30 cm and a depth of 25 cm. A heater was located at the bottom of the vessel and a laboratory temperature was applied to the top of the vessel; thus a temperature gradient was applied to the bentonite. The vessel was hermetically sealed, and the saturation was carried out through the lid at the top of the vessel. The bentonite was therefore heated and hydrated simultaneously. The medium scale model and the experiment are described in detail in D7.9, which describes the results from the water content distribution and dry density analysis. In D7.7, the results of the hydromechanical properties are presented and compared with the results obtained from laboratory treated bentonite.

During the dismantling of both experiments, samples were taken to analyse hydraulic conductivity, swelling pressure and liquid limit. Samples were taken at various distances from the heater.

6.2.1 Laboratory set-ups, procedures and protocols

The main objectives of the research were to determine hydro-mechanical properties as saturated hydraulic conductivity, swelling pressure and liquid limit of bentonite after thermal treatment in dry state and as a suspension. The testing of hydraulic conductivity and swelling pressure were performed in special permeameter cells. The measurement in the permeameter is based on forced saturation of the sample, while the constant hydraulic gradient is maintained, and the volume change of the sample is prevented. The experimental determination of hydraulic conductivity is based on Darcy´s law.

Liquid limit is determined using fall cone method performed according to standard ČSN EN ISO 17892-12 (2018)

Material preparation and the facility for the laboratory thermal loading

Bentonite for treatment in dry moisture condition had not undergone any special treatment before it was put into vessel. Two vessels with dry treated bentonite were prepared. Each vessel contained 8,5 kg of bentonite. The vessels had no lid and drying of bentonite was allowed and desired. The open vessels with bentonite were placed into the laboratory oven and heated at 150°C.

Unlike dry treated bentonite, wet treated bentonite required specially designed pressure vessel (Figure 6.1). There were two requirements – the drying of the bentonite was not allowed and the pressure inside the vessel had to ensure no boiling of the bentonite suspension. The material was split into two identical

vessels of 14 litres. Into the each of the vessel was poured mixed suspension consisting of 5.6 kg of bentonite and 11.36 kg of distilled water. The bentonite suspension and sampling of the wet bentonite after treatment are shown in Figure 6.2.

Commenté [LJ10]: Is it litres? Write explicitly. A small "el" looks very much like the figure 1 (one).

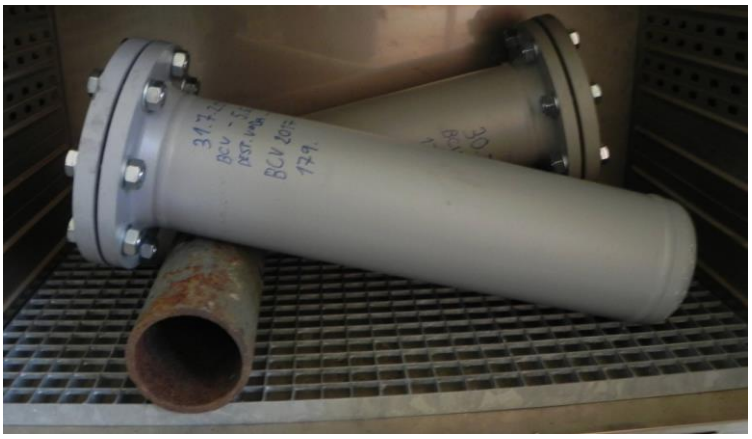

Figure 6.1 Pressure vessel for thermal treatment of wet bentonite

Figure 6.2 Wet bentonite before treatment poured into the vessel (left). Sampling of wet bentonite after 6 months of thermal treatment (right)

Material preparation and the facility for the medium-scale experiment

The experiment and its set-up are described in detail in D7.9. Only a brief description will be given here. The bentonite was placed in a vessel in a natural water content (10-12%) and then manually compacted. Two tests were carried out each time with a different form of bentonite. In the first test powdered bentonite was used, in the second test pelletized bentonite was used. The vessel is fitted with a heater at the bottom and a lid, with an inlet at the top for saturating the bentonite. After assembly, the bentonite was heated at 150°C from below and saturated with distilled water at 3-8 bar from above. The first test

lasted 14 months and the second test lasted 8 months. The Figure 6.*3* shows the set-up of the experiment and the state of the bentonite inside the experiment after its finish, during sampling.

Figure 6.3 Medium-scale experiment (left) and bentonite inside the experiment during dismantling (right)

Laboratory set-up for hydraulic conductivity and swelling pressure measurement

Specially designed constant volume permeameter cells are used for testing under standard conditions (constant volume, constant hydraulic gradient). The cell includes a cylindrical steel chamber (ring) for the housing of the samples (diameter: 30 mm, height: 20 mm). The constant volume of the sample is ensured by the rigid structure of the experimental cells while allowing for the monitoring of total pressure. The top and bottom of the samples have been fitted with sintered steel permeable plates to prevent the leaching ("mobilisation") of the material. The sample is constrained in vertical direction by piston which is positioned between the upper flange and the upper surface of the steel plates. The miniature load cell, which provide the measurement of the force induced by swelling of the bentonite, is placed between the top of the piston and the upper flange. A load cell is connected to a central data logger and the signal is consequently recalculated to pressure expressed the total pressure and swelling pressure. The pore pressure is monitored by electronic pressure transmitter and it is connected to the data logger. The hydraulic gradient is provided by pressure vessel with gas (argon) which actuates over pressure vessel with the saturation medium, which is distilled water. The saturation water is pushed to the sample from the bottom and over the top of the sample atmospheric pressure is applied [Figure 6.4]

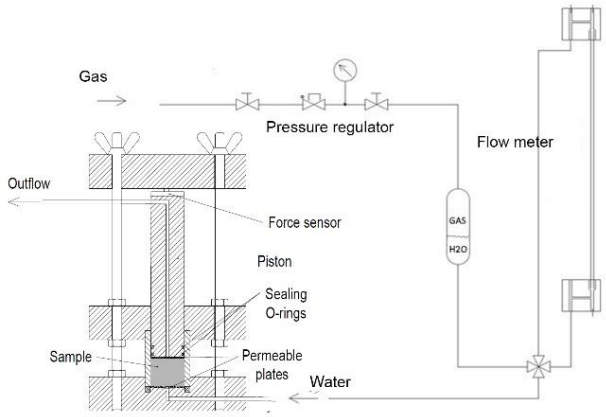

Figure 6.4 Constant volume permeameter cell

Sample preparation for the testing in the permeameter cell:

- Thermal treatment in the laboratory oven at 150°C for 6, 12, 24 months
- Sampling
- Natural cooling down (dry material), drying in the laboratory oven at 60°C (wet material)
- Compaction to the target dry density
- Assembling the permeameter cell with the sample and instrumentation
- Connecting to the saturation system

Sampled material for testing is compacted by uniaxial way in the chamber up to the target dry density, then the chamber is placed to the permeameter cell followed by positioning of the piston and load cell and ensuring the rigidity of the whole system. Then the permeameter cell is connected to the system of saturation via steel tube and fittings.

One testing batch consists of five samples. The range of the dry densities in the batch is 1300 kg/m^3 – 1600 kg/m^3. Initial water content of dry treated bentonite is 0% and of wet treated bentonite is 6%.

Procedure of the measurement in the permeameter cell

The samples are firstly saturated, and their permeability and swelling pressure are measured once the water flow through the sample is steady.

Water is pushed from the bottom part of the cell under a pressure of 1 MPa. The hydraulic gradient corresponds to the difference between the input injection pressure and the output pressure, which is the atmospheric pressure. Once the flow has stabilised, the permeability is determined, and the water pressure is switched off to allow for the equalisation of the pore pressure in the sample. The swelling pressure is then measured.

Liquid limit measurement

Liquid limits are determined after each sampling of dry and wet material after given time steps of thermal treatment. This analysis is performed by fall cone test according to Czech standard ČSN EN ISO 17892-12 (2018). The preparation of dry material consists of natural cooling down of the sample. The sample of wet material is freed of excess of water in the oven at 60°C and then milled to acquire fine powder and then in both cases the preparation follows the standard (2018). Distilled water was used for the wetting of the material before and during the test.

6.3 Results

6.3.1 Investigation performed

The testing was focused on determination of hydraulic and mechanical properties of thermally treated bentonite subjected to the elevated temperature in wet and dry state. While the laboratory-heated bentonite was exposed to the same temperature throughout its volume, the bentonite from the small scale experiment was exposed to a temperature gradient.

Laboratory heated bentonite

Determination of hydraulic conductivity, swelling pressure and liquid limit of dry treated and wet treated bentonites was done for 6, 12 and 24 months of thermal treatment. Swell index was performed with wet treated and dry treated bentonite after 12 and 24 months of thermal treatment. The samples after each test of hydraulic conductivity and swelling were analysed for final water content, density, and dry density. The set of hydraulic conductivity and swelling pressure measurement at each time-step contained 6 samples with different dry density.

The overview of measurements done is shown in the Table 6.2

Table 6.2 Summary of tests performed on dry treated and wet treated bentonite after 6, 12 and 24 months of thermal treatment

Treatment	DRY TREATED			WET TREATED		
months of treatment	6	12	24	6	12	24
hydraulic conductivity	✓	✓	✓	✓	✓	✓
swelling pressure	✓	✓	✓	✓	✓	✓
liquid limit	✓	✓	✓	✓	✓	✓
Swell index	-	✓	✓	-	✓	✓

Bentonite from small scale experiment

In the dismantling experiment using powdered bentonite, 4 samples were taken at different distances from the heater. From these samples hydraulic conductivity and swelling pressure were determined. Two additional samples were taken to determine the liquid limit. These samples were taken from the lower part of the experiment, near the heater, and another sample was taken from the upper part of the experiment, where the bentonite was almost unaffected by temperature. All six samples were saturated and the degree of saturation was around 1. Bentonite was exposed to the elevated temperature in a saturated state.

In the dismantling experiment using pelletized bentonite, 2 samples for hydraulic conductivity and swelling pressure were taken. one sample was taken near the bottom, in the immediate vicinity of the heater and the second sample was taken 50 mm above the heater where the temperature was 120°C. The assumption was that the bentonite would be most affected where it was exposed to the highest temperature and in a dry state. The degree of saturation of both samples was <0.3. One sample was taken from the bottom of the vessel, where the bentonite is most affected by the elevated temperature for the liquid limit analysis.

6.3.2 Results from investigation

Saturated hydraulic conductivity and swelling pressure

A summary of the results of hydraulic conductivity and swelling pressure is given in Table 6.3

Table 6.3 Summary of the results of saturated hydraulic conductivity, saturated hydraulic conductivity converted to 10 °C (k10) and swelling pressure of wet treated and dry treated bentonite after 6, 12 and 24 months of thermal exposure.

wet/dry treated	months of treatment	ρd [kg/m3]	k [m.s-1]	k10 [m.s-1]	σw [MPa]
DRY TREATED	**6**	1299	1.51E-12	1.03E-12	1.10
		1361	1.23E-12	8.38E-13	2.32
		1432	6.77E-13	4.61E-13	1.94
		1463	3.28E-13	2.45E-13	2.84
		1541	1.94E-13	1.45E-13	5.06
		1535	2.94E-13	2.21E-13	3.76
	12	1319	8.25E-13	6.19E-13	1.14
		1621	1.83E-13	1.41E-13	7.48
		1440	4.92E-13	3.78E-13	1.92
		1382	1.32E-12	9.57E-13	1.26
		1476	5.13E-13	3.70E-13	2.45
		1521	3.09E-13	2.24E-13	3.64
	24	1433	7.75E-13	5.55E-13	
		1514	3.65E-13	2.61E-13	3.77
		1788	1.01E-13	7.18E-14	15.81
		1409	4.16E-13	3.61E-13	1.80
		1448	4.85E-13	4.22E-13	2.15
		1589	1.88E-13	1.64E-13	3.39
WET TREATED	**6**	1259	1.23E-12	1.05E-12	1.32
		1340	4.20E-13	3.55E-13	1.38
		1362	3.02E-13	2.57E-13	2.34
		1382	3.86E-13	2.86E-13	2.33
		1456	3.22E-13	2.37E-13	2.94

		1584	1.30E-13	9.03E-14	7.39
	12	1399	4.83E-13	3.54E-13	1.46
		1448	3.40E-13	2.46E-13	2.33
		1504	2.84E-13	2.09E-13	2.91
		1559	2.02E-13	1.56E-13	4.66
		1543	1.24E-13	9.20E-14	6.54
		1541	1.55E-13	1.15E-13	5.85
	24	1438	2.64E-13	2.03E-13	4.02
		1518	1.92E-13	1.48E-13	5.55
		1613	1.43E-13	1.10E-13	5.92
		1389	4.14E-13	3.15E-13	2.02
		1288	1.74E-13		1.44
		1764	6.85E-14	5.00E-14	18.61

The results of hydraulic conductivity and swelling pressure measurement are visualized in Figure 6.5 - Figure 6.8.

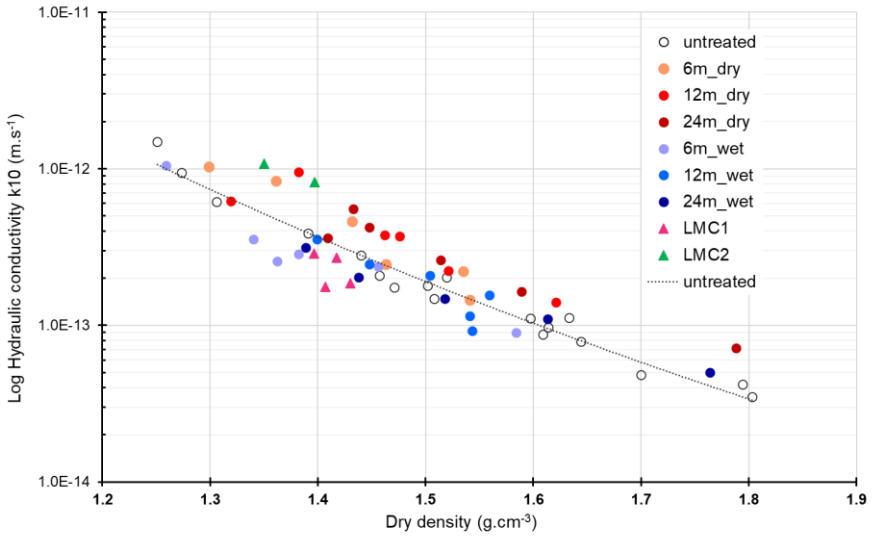

Figure 6.5 Hydraulic conductivity of dry and wet treated bentonite BCV_2017 after 6, 12 and 24 months at 150°C and of the samples from medium scale experiment: test 1 with powdered bentonite(LMC1) and test 2 (LMC2) using pelletized bentonite, all compared with untreated bentonite and its trend line.

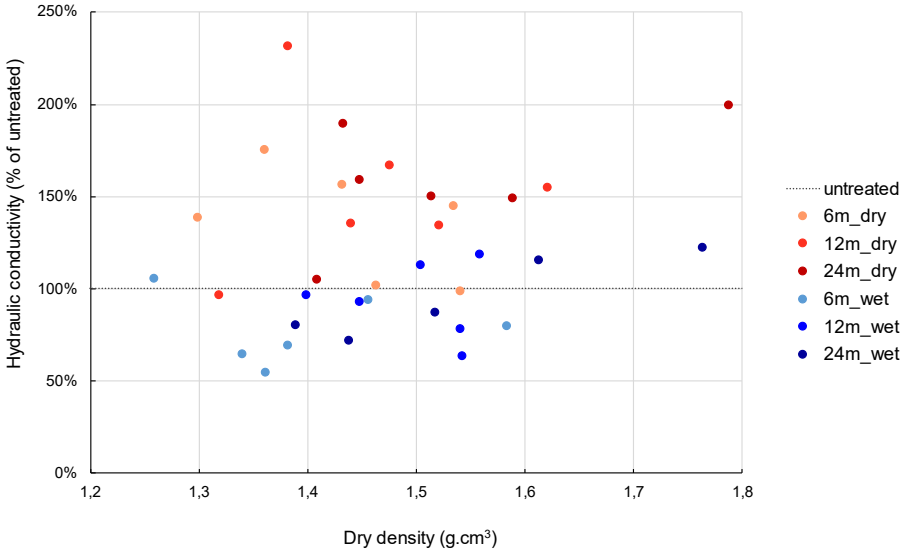

Figure 6.6 Hydraulic conductivity of dry and wet treated bentonite BCV_2017 after 6, 12 and 24 months at 150°C compared with untreated bentonite expressed as a percentage of untreated bentonite.

Hydraulic conductivity - dry bentonite

Figure 6.5 shows that the hydraulic conductivity of the dry treated bentonite is slightly higher than that of the untreated material. However, no change in this characteristic is observed with the duration of treatment. The change in hydraulic behaviour due to thermal exposure occurred after the first 6 months of heating, no deteriorating trend with loading time is observed. Figure 6.6 shows that 90 % of values measured of dry treated bentonite exceed hydraulic conductivity of untreated bentonite.

Hydraulic conductivity – wet bentonite

Hydraulic conductivity of wet treated bentonite is in some cases lower than hydraulic conductivity of untreated bentonite and there is noticeable difference between dry and wet material. The batches of dry and wet bentonite are divided by the curve of trend of untreated material, while the values of hydraulic conductivity of dry material are situated above the curve and the values of wet treated bentonite are under the curve. Thermal exposure does not affect the hydraulic behaviour of wet treated bentonite in negative way, hydraulic conductivity of such bentonite is even slightly lower, which is shown in Figure 6.6

Hydraulic conductivity – medium scale experiment

The hydraulic conductivity of the samples from the experiment where powdered bentonite was used is comparable to the hydraulic conductivity of the unaffected samples. Bentonite was exposed to elevated temperature in the saturated state in this test (LMC1). The hydraulic conductivity does not depend on the position of the sample and is comparable for samples taken close to the heater with samples taken further away from the heater.

The hydraulic conductivity of bentonite taken from the second test (LMC2) where pelletized bentonite was used is higher than the hydraulic conductivity of unaffected bentonite. The bentonite in the second test was saturated only at the surface and the degree of saturation decreased towards the heater. Near the heater, at the point from which the samples were taken, the degree of saturation was <0.2. The bentonite was therefore exposed to elevated temperature in the dry state. The hydraulic conductivity of the samples taken from the vicinity of the heater corresponds to the hydraulic conductivity of the laboratory heated bentonite in the dry state.

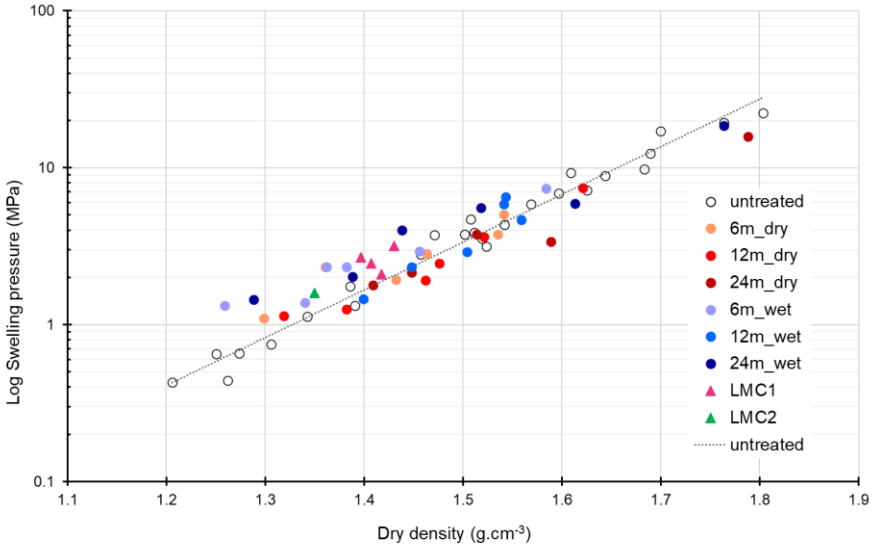

Figure 6.7 Swelling pressure of dry treated and wet treated bentonite after 6, 12 and 24 months at 150°C and of the samples from medium scale experiment: test 1 with powdered bentonite (LMC1) and test 2 (LMC2) using pelletized bentonite, all compared with untreated bentonite

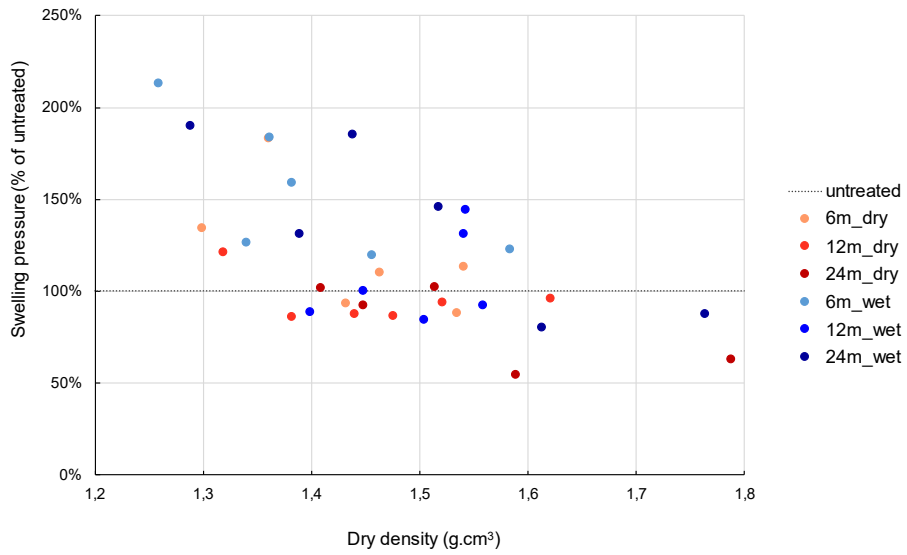

Figure 6.8 Swelling pressure of dry and wet treated bentonite BCV_2017 after 6, 12 and 24 months at 150°C compared with untreated bentonite expressed as a percentage of untreated bentonite.

Swelling pressure – dry treated bentonite

Figure 6.7 shows that the swelling pressure of dry treated bentonite is not affected by elevated temperature. Lower values in two samples may indicate heterogeneity of dry treated bentonite to which higher bulk density samples could be more sensitive. No trend is observed related to the duration of thermal loading.

Swelling pressure – wet treated bentonite

Swelling pressure of wet treated bentonite is slightly higher compared to both, untreated and dry treated material, especially in the range of low dry densities up to 1500 kg.m^{-3}. No trend is observed related to the duration of heating.

Swelling pressure – medium scale experiment

The swelling pressure of the samples taken from the first test (LMC1) where powdered bentonite was used is slightly higher than the swelling pressure of the unaffected bentonite, as could be seen in Figure 6.7. The bentonite in the first test was subjected to elevated temperature at a fully saturated state.

The swelling pressure of the samples taken from the second test (LMC2) where pelletized bentonite was used is not influenced by temperature and is comparable to the swelling pressure of unaffected bentonite.

Liquid limit

A summary of the results of liquid limits is given in the Table 6.4. Which is visualized in Figure 6.9. Liquid limit of untreated material is taken from another projects (Červinka R., 2018), (Červinka R., 2018), (Svoboda J., 2019)

Table 6.4 *Summary of the results of BCV_2017 liquid limit measurements*

Treatment	months of treatment	wL
DRY TREATED	6	130 %
	12	125 %
	24	120 %
WET TREATED	6	143 %
	12	134 %
	24	127 %
UNTREATED	0	141 %

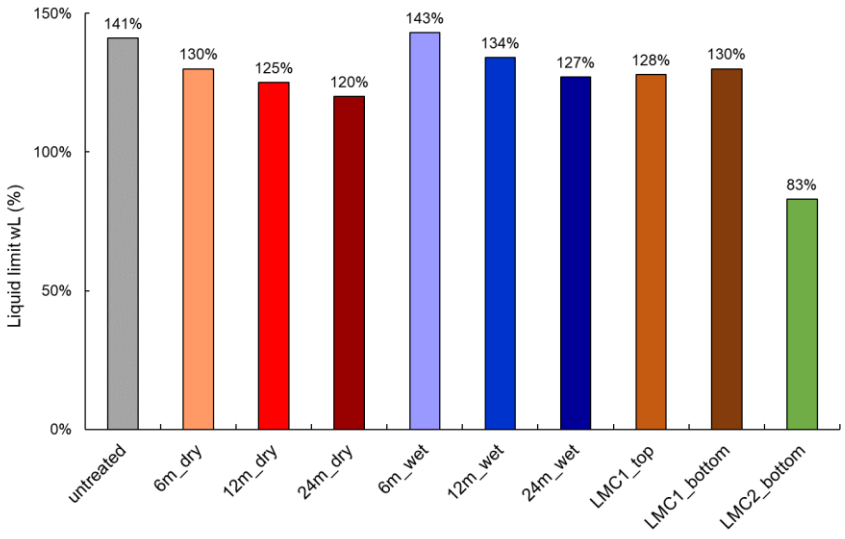

Figure 6.9 Liquid limits of dry treated bentonite after 6, 12 and 24 months at 150°C, wet treated bentonite after 6, 12 and 24 months at 150°C and untreated bentonite

Figure 6.9 shows the difference in liquid limit between dry and wet treated bentonite compared to untreated bentonite. Liquid limit of dry treated bentonite is noticeably lower than the liquid limit of untreated and wet treated bentonite. This means that the bentonite, once heated, is unable to take up enough water to maintain the liquid limit it had before heating. This is consistent with the results of the hydraulic conductivity and swell index of dry treated bentonite, which also show changes in these parameters in the negative way.

The same behaviour can be observed on samples taken from the experiment. The liquid limit of the bentonite taken from the first test (LMC1 – powdered bentonite) is the same as the liquid limit of the unaffected bentonite. The powdered bentonite in this test was subjected to thermal action in a fully saturated state. The liquid limit from the second test (LMC2) is significantly lower than the liquid limit of both the affected and unaffected bentonite. The pelletized bentonite used in this test has a significantly lower liquid limit even in the unaffected state. This phenomenon was observed in tests performed on pelletized bentonite in the Engineered Barrier 200 project (Laufek et al., 2021). Previously unpublished results showed a significantly lower liquid limit for pelletized bentonite compared to powdered bentonite. A value of 103 was measured for the pelletized bentonite in the unaffected state. The liquid limit of this bentonite even decreases after exposure to elevated temperature in dry state.

Swell index

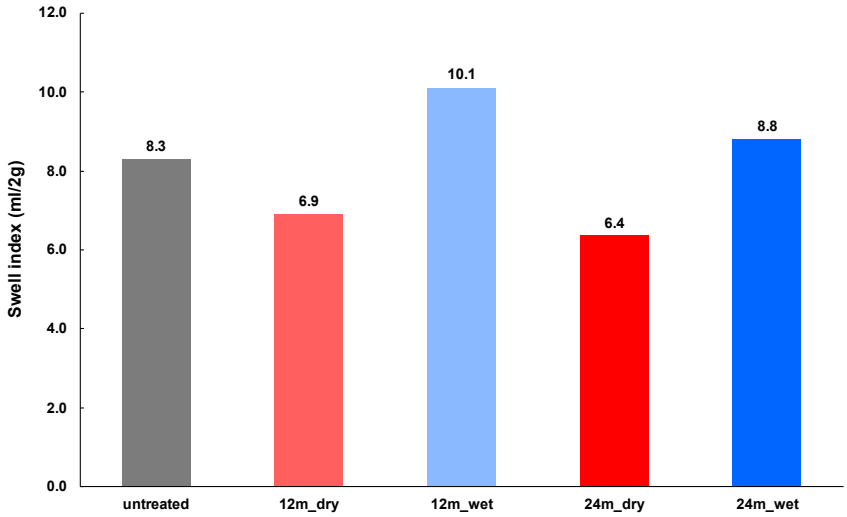

Figure 6.10 Swell index of dry and wet treated bentonite after 12 and 24 months at 150° compared to untreated bentonite.

On Figure 6.10 is shown the differences between dry treated, wet treated and untreated bentonite. The results are consistent with the liquid limit measurement. For both parameters a decrease was observed for dry treated bentonite after heating.

6.4 Conclusion

The main objectives of the research were to determine possible changes in the hydro-mechanical properties of bentonite after exposure to elevated temperatures and the potential evolution of these properties depending on the duration of the treatment.

Hydraulic conductivity, swelling pressure, liquid limit and swell index of dry treated and wet treated bentonite were tested. Based on the research carried out, the following conclusion can be drawn:

- Exposure to elevated temperatures had the most significant effect on the bentonite treated in the dry state.
- Behaviour of dry treated bentonite is consistent with respect to measured parameters.
- Hydraulic conductivity of dry treated bentonite is slightly higher, and it does not depend on the duration of heating. The change of hydraulic conductivity occurred in the first heating time step and remained stable thereafter.

- Swelling pressure of dry treated bentonite is less affected by heating than hydraulic conductivity. The swelling pressure is lower, but not significantly. No trend depending on duration of heating observed.
- The liquid limit and swell index of dry treated bentonite are lower. The decrease of both parameters is observed as a function of the heating time.
- In contrast to dry treated bentonite, wet treated bentonite shows slight improvement of hydro-mechanical characteristics compared to untreated bentonite. Although the change is not significant, this finding is valuable with respect to behaviour of dry treated bentonite.

The results from the medium-scale experiment confirm, on a medium scale, the conclusions drawn from the testing of laboratory heated bentonite. Since both powder and pellets were used in the medium scale experiment, it can be stated that it does not matter whether it is pellets or powder, the more important influence is the moisture state in which the bentonite is exposed to the elevated temperature. While the swelling pressure and hydraulic conductivity are the same for both pellets and powder, the liquid limit is generally lower for pellets, and after exposure to elevated temperatures in the dry state, the liquid limit is further reduced.

7. KIPT (ChRDI)

7.1 Introduction

7.1.1 Material

The largest deposits of bentonite in Ukraine are located in the Cherkasy region in the place of Dashukovka. This bentonite is considered as a buffer and backfill material in the system of geological disposal of spent nuclear fuel and high-level waste. Consequently the bentonite of the Dashukovka's deposit (Cherkasy region), this bentonite is used in research carried out by the KIPT team within the framework of the HITEC project, and the material was named as PBC (**P**owder **B**entonite from **C**herkasy region of Ukraine). PBC contains Na-montmorillonite up to 60% and Ca, Mg - montmorillonite up to 20%. Natural bentonite of the Dashukovskoye deposit is polyphase minerals - along with the main phase of montmorillonite, there are α-quartz and calcite $CaCO_3$. Studies of the behaviour of PBC bentonite at temperatures > 100°C are carried out for the first time in Ukraine.

7.1.2 Research plan

The main aim of research was to study the properties of PBC bentonite, subjected to thermal treatment at 150°C for 3, 6, 12 months.

Planned experimental procedure:

- Conducting thermal treatment of PBC bentonite at 150°C for 3, 6, 12 months.

Planned investigation:

- analytical studies (XRD and DTA) to identify structural changes in PBC as a result of thermal treatment;
- determining the characteristics of permeability and swelling pressure at room temperature.

Table 7.1 KIPT - Permeability and swelling pressure in constant volume cell

7.1.2.1 Material (BoM item): PBC bentonite (Ca-Mg type and sodium-fortified), powder as delivered by producer Joint stock company “Dashukovskiy bentonites” (Dashukovka, Cherkasy region of Ukraine).
7.1.2.2 Material treatment (sample preparation for test and loading procedure): BPC powder bentonite was used. BPC powder bentonite with natural moisture 10% was compacted directly in the stainless steel container that is not tightly closed with a lid. Then the container is placed into the laboratory oven for 150°C thermos-treatment. Loading lasted 3, 6 and 12 months.
7.1.2.3 Temperature (to which material was/will be exposed to) and exposure time 150 °C for 3, 6 and 12 months.
7.1.2.4 Tests carried out (name, description, sample preparation, procedure, results): XRD and DTA/GA analytical methods were carried out to identify structural changes in PBC as a result of thermal treatment. Permeability and swelling pressure were measured in constant volume cell (D = 30 mm, H = 10 mm). At first permeability was measured followed by swelling pressure determination. 7.1.2.4.1 Permeability - K [m/s] Permeability was measured using a laboratory facility (*Figure 7.2*) with constant pressure gradient. Samples will be compacted directly into constant volume cell then water gradient is applied, water inflow and total pressure development measured. Once a stable flow (and total pressure) is obtained, the permeability is calculated. The pressure gradient is then released and the swelling pressure is measured. 7.1.2.4.2 Swelling pressure - σ_{sw} [MPa] Swelling pressure is determined on fully saturated sample from permeability test. The pressure gradient is no longer applied and once the total pressure stabilises it equals to swelling pressure (no pore pressure in sample).
7.1.2.5 Schedule and expected date(s) of results delivery: Treatment start: M6 First results → M12 Results for reporting → M24

7.2 Procedures

7.2.1 Laboratory set-ups, procedures and protocols

150°C thermal treatment of PBC bentonite was carried out in a laboratory oven. Samples were loaded in the stainless steel container, diameter 50 mm and height 90 mm (*Figure 7.1*).

Figure 7.1 Stainless steel container

The laboratory facility (*Figure 7.2*) for permeability measurement at room temperature consists of a measuring cell, a frame, a dynamometer with a dial gauge, a pressure screw, and a tubing system for supplying a constant hydraulic head to the sample and for measuring the amount of passed water. The measuring cell is a stainless steel cylinder with a piston, upper and lower porous plugs (porous alumina).

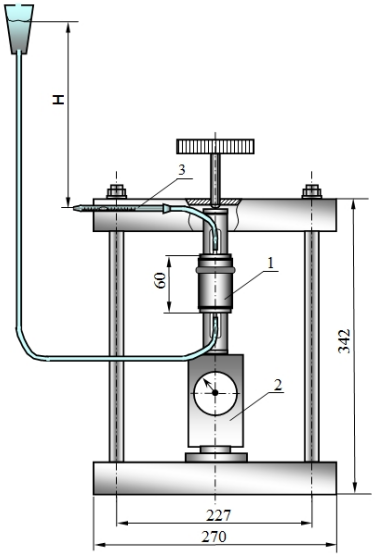

1 - measuring cell; 2 – dynamometer; 3 - flow meter; H - hydraulic head

Figure 7.2 KIPT laboratory facility to measure the permeability and swelling pressure of PBC bentonite at room temperature

The bentonite powder is compacted directly in the measuring cell. The measuring cell is mounted on a dynamometer and the clamping screw creates a preliminary axial stress in the sample. Distilled water is fed into the sample through the lower porous plug. The hydraulic head is created by a column of water in a supply tube with a height (H) of up to 2.4 m. The volume of the passed water is measured at the

exit from the sample by the movement of water in a glass measuring capillary with a graduation value of 0.002 cm^3.

When water is supplied to the sample, during swelling of bentonite the stress on the dynamometer changes, and the swelling pressure is calculated from the dial gauge.

7.2.2 Data and other results available

These studies are being carried out for the first time at the KIPT. The analysis of works on determining the permeability and swelling pressure of various bentonites from various foreign literary sources is carried out. These data were used for comparison with the results of tests and measurements carried out at the KIPT.

7.3 Results

7.3.1 Investigation performed

Thermal treatment of PBC bentonite was carried out at 150°C for 3, 6 and 12 months.

The thermo-treated samples were used for the following studies:

- analytical studies (XRD and DTA) to identify structural changes in PBC bentonite as a result of thermal treatment;

- measurement of permeability and swelling pressure of thermo-treated PBC bentonite at room temperature.

7.3.2 Results from investigation

The treatment period of 3 months practically did not lead to changes in the state of PBC bentonite. Therefore, attention was paid to samples thermo-treated for 6 and 12 months.

Comparison of XRD data for the initial PBC bentonite and after thermal treatment at a temperature of 150°C for 12 months showed that no phase transformations occurred during thermal treatment, the weight ratios of the phases remained (*Figure 7.3*, *Figure 7.4*).

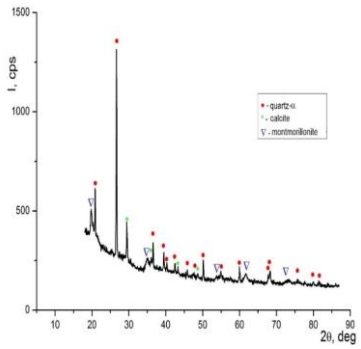

Figure 7.3 XRD pattern of the initial PBC

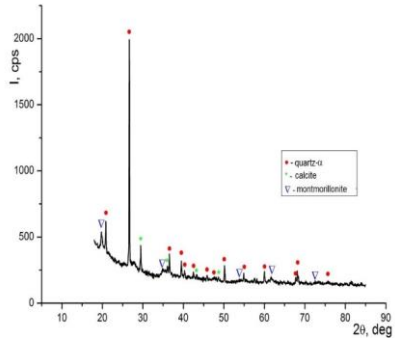

Figure 7.4 XRD pattern of the PBC after 150°C treatment, 12 months

Results of **DTA/GA** investigation of treated PBC is presented below in *Figure 7.5* and *Figure 7.6*.

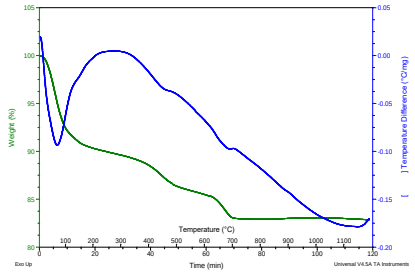

Figure 7.5 DTA/TG curves of the initial PBC

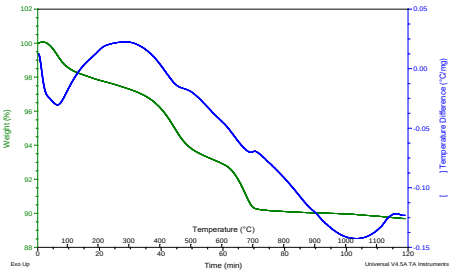

Figure 7.6 DTA/TG curves of the PBC after 150°C treatment, 12 months

The following judgments can be made:

- weight loss in both bentonite powders occurs up to temperatures around 700°C;
- the total weight loss of the initial powder is 16.9%, and that of the thermo-treated powder is 9.8%;
- the difference in weight loss is associated with the release of adsorbed and interlayer water from bentonite when held at a temperature of 150°C for a long time (12 months).

Permeability

Permeability measurements were carried out for PBC bentonite thermo-treated at 150°C for various periods of time. It is shown that at a density of bentonite in the measuring cell equal to 1.73 g/cm^3, the permeability K=(3,3 ... 3,6)·10^{-11} m/s at hydraulic gradient (95 ... 160 °C) after 6 months of treatment and K=(1,8… 2,1)·10^{-10} m/s at 1.65 g/cm^3 and hydraulic gradient (90… 130 °C) after 12 months treatment.

Commenté [LJ11]: Unit?

Commenté [LJ12]: Unit?

Swelling pressure

The swelling pressure at room temperature was measured for PBC bentonite thermo-treated at 150°C for 6 and 12 months and the results are shown in *Figure 7.7*. For comparison, the data for the MX-80 are taken from CIEMAT report (M.V. Villar, 2004).

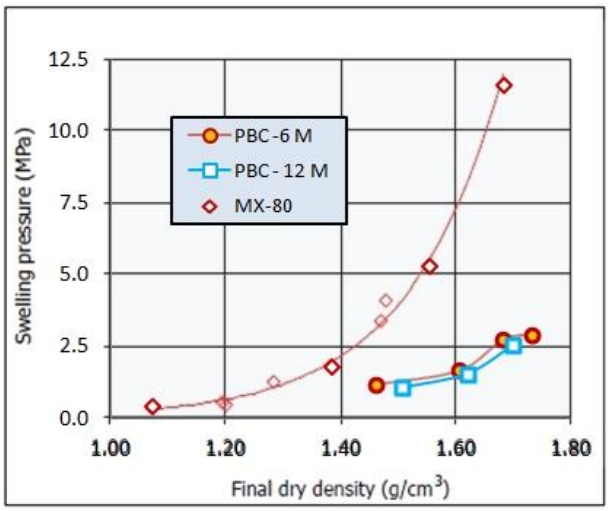

Figure 7.7 Swelling pressure of compacted PBC bentonite compared to MX-80

It should be noted that the value of swelling pressure is lower than for MX 80 bentonite, which is apparently due to the lower Na-montmorillonite content in the Ukrainian PBC bentonite.

7.4 Conclusion

Thermal treatment of bentonite was carried out at 150°C for 3, 6, 12 months.

Analytical studies of thermo-treated PBC bentonite were performed using XRD and DTA/GA.

Results of XRD investigation of PBC bentonite before and after 150°C heating for period up to 12 months showed that no phase transformations occurred during thermo-treatment, the weight ratios of the phases remained.

Permeability and swelling pressure were measured at room temperature for bentonite thermo-treated at 150°C for 6 and 12 months.

8. SIIEG NASU (ChRDI)

8.1 Introduction

The Ukrainian DGR concept considers crystalline rock environments. The design is based on the multiple barrier principle. The most common buffer material for engineered barrier systems (EBS) is compacted bentonite, which features low permeability and high retardation of radionuclide transport (IAEA-TECDOC-1718, 2013); (Zlobenko B.,1995). Establishing the thermal limit for bentonite in a nuclear waste repository is potentially important, as the thermal limit plays a major financial challenge requiring long-term strategic planning for used fuel management. Characterisation of long-term mineralogical changes for EBS concerning the long-term geological evolution is needed for safety assessment purposes.

The Cherkassy deposit is one of the largest in Ukraine. The area of the layer is 195 km^2, the total reserve is 825 million tons, and in the Dashukovsky site, it is 5.3 million tons. The clays are commercially available in crushed and dried form from the Dashukovsky plant, which produces bentonite powder on the market. In some cases, additives such as soda ash are added to bentonite to induce desired changes in the swelling or rheological properties of the bentonite. Bentonite PBA-22 «Extra» is industrially milled powder. This material was forwarded as a candidate material for studying in HITEC.

Commercial calcium bentonite (PBA-22 «Extra») was chosen as the clay component of the buffer materials as it is less sensitive to saline rock water. The expected porosity enhancement and reduction due to mineral dissolution and precipitation, respectively, have been evaluated in experiments with elevated temperatures in the autoclave. The study of the effect of temperature on bentonite properties by analysing the change of properties of preheated material. The properties of these preheated materials are usually tested at laboratory temperature and compared with those obtained in non-heated material to assess the changes during operation. Montmorillonite mineralogical stability at high temperatures has been studied in (Leupin O.X. 2014). The tests by Valter [5] with MX-80 bentonite with different degrees of saturation stored at different temperatures in a closed system showed high mineralogical stability but considerable changes in physicochemical properties, particularly above the critical temperature of 120°C. The cation exchange capacity decreased during heating at 150°C by approximately 10%. Specific surface area dropped by more than 50%. Water vapour adsorption ability dropped by 25% within three months at 120°C. These changes were mostly related to the variations in the interlayer cation composition (a slight conversion from sodium to an earth alkali form of bentonite) and the smectite aggregation processes. Keeping the swelling properties stable at these elevated temperatures is important. However, there remain uncertainties regarding the long-term stability of bentonite EBS. To predict how well the barrier will function over time at repository-relevant temperatures, it is important to understand the thermal alteration effects on montmorillonite, a main constituent of bentonite.

The study aimed to investigate the thermal load on Ca-bentonite at 150°C in “dry” and “wet” conditions. Multiple analysis techniques have been used to characterise the bentonite clay, such as XRD, cation exchange capacity, surface area, morphology changes by SEM, swelling pressure and permeability.

8.1.1 Material

The object of study was bentonite of the Cherkassy deposit. The clay is sage-green, homogeneous, and solid, with wax glitter on the fracture. It intakes water and swells well. Bentonite PBA-22 «Extra» is industrially milled powder. The basic characteristics of tested bentonite PBA-22 «Extra» have been summarised in (B. Zlobenko, 2023).

The mineralogical composition of the bentonite has been PBA-22 «Extra» analysed by X-ray diffraction (XRD) using DRON-4-07 diffractometers with a Cu anticathode.

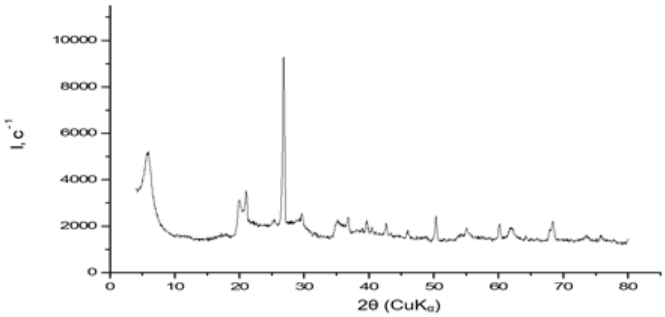

Fig. 8.1.1. The X-ray diffractogram of bentonite PBA-22 «Extra» used in this study

According to the mineral composition, natural bentonite clay is represented mainly by Ca montmorillonite and highly dispersed quartz. The content of montmorillonite is 70 - 85%. Besides, bentonite contains variable quantities of quartz (5-20 %) and calcite -"carbonate" (2-5 %). Other accessories (zircon, rutile, apatite) and trace minerals amount to 0.8 %.

The studied bentonite is classified as Al, Fe montmorillonite. The differential thermal analysis (DTA) of bentonite samples shows the total weight loss is about 17.8%.

Because the analysis of the chemical and mineral composition of the bentonite clays was performed in different laboratories and on different samples, the chemical composition of bentonite is unstable and depends on the water content. The following variations in chemical composition (in mass %) are observed: SiO_2 – 50 - 60; Al_2O_3 – 14 - 19.5; Fe_2O_3 + FeO – 2.4 - 7 and more; MgO – 1.7 - 2.6; CaO – 1.3 - 3.0; H_2O – 10 - 14. In addition, there are K_2O and Na_2O, sometimes sulfur (SO_3^{2-}) and carbon (mainly CO_3^{2-}). Results of the chemical analysis of the bentonite PBA-22 «Extra» sample received by the wet chemical method are given in Table 8.1.1.

TABLE 8.1.1. CHEMICAL COMPOSITION OF BENTONITE PBA-22 «Extra»

Properties	Method	Elements	Bentonite
Chemical analysis	Wet chemical analysis (values, %)	SiO_2	54.7
		Al_2O_3	16.3
		Fe_2O_3	5.7
		FeO	0.3
		MgO	3.2
		CaO	2.1
		Na_2O	0.1
		K_2O	0.7
		H_2O^+	5.7
		H_2O^-	11.4
Cation Exchange Capacity	Ammonium Acetate Extraction (meq/100 g)		92.6

The ammonium acetate method measured the cation exchange capacity (CEC) of bentonite samples at pH 8, which is 92,6 meq/100 g of dry clay that dissolved calcite.

The calculated crystal chemical formula of bentonite PBA-22 «Extra» based on the averaged data of chemical analyses is $(Al_{1,21}Fe^{3+}_{0,49}Mg_{0,30})$ $[Al_{0,18}Si_{3,82}]$ $O_{10}(OH)_2$ + $(Ca_{0,17}Na_{0,03})$,

TABLE 8.1.2. PHYSICAL-CHEMICAL PROPERTIES OF BENTONITE PBA-22 «Extra»

Bentonite PBA-22 «Extra»	Sand fraction,	Colloidal properties	Water absorption*	Specific surface, m^2/g**
Content, %	up to 10.0	25-40	up to 160	90-120

*The liquid water absorption was determined using the Enslin-Neff device.

**The methods applied for determining specific surfaces are gas adsorption methods by nitrogen adsorption.

Table 8.1.3. Specific surface of bentonite, according to adsorption, S, m/g

H_2O*	Hexane*	N_2**
375-400	69-75	90-120

*The specific bentonite surface was evaluated by polar adsorption liquid (vapors of water and hexane), according to the method: (Tarasevich, Yu.I.,1988).

**The method for determining specific surfaces is gas adsorption (nitrogen adsorption).

The methods used to determine grain size distribution and amount of clay and silt fraction were dry/wet sieve analysis and sedimentograph for particle analysis (Mastersaizer-2000).

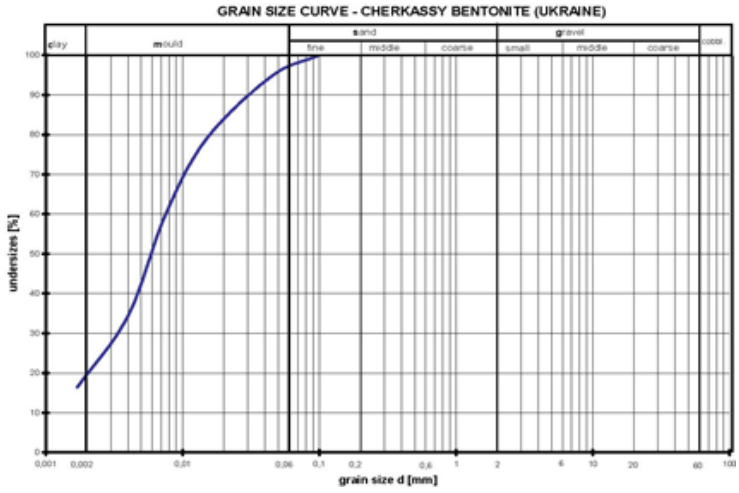

Fig. 8.1.2. Bentonite PBA-22 «Extra» grain size curve.

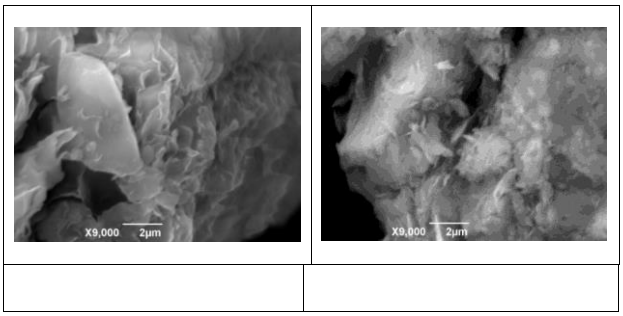

Fig. 8.1.3. SEM image initial sample bentonite PBA-22

TABLE 8.1.4 THERMOPHYSICAL PROPERTIES (NATURAL, POWDER)

Samples	ρ_d (kg/m^3)	Ks (ms^{-1})
Initial PBA-22	1480	2.6 E-13
	1535	4.7 E-13
	1680	3.4 E-14

8.1.2 Research plan

Three campaigns of bentonite investigation of each moisture condition were planned, e.g. sampling and investigation after 3, 6 and 12 months of thermal loading. The geochemical analyses performed on solid samples have two main objectives: (a) to analyse the physical, chemical and mineralogical alterations occurred in the clay by effect of heat and hydration, and (b) in order to analyse the chemical evolution of the bentonite as a function of the temperature. SI IEG has performed analyses in bentonite from dry and wet samples to know the chemical, mineralogical and microstructural alterations in the clay. A general analysis of the clay phases was performed to characterize its chemical, mineralogical and microstructural transformations. The main analyses carried out have been: XRD, IR, thermal analyses (DTA, DTG, TG) and the exchangeable cations (EC).

The plan was to provide laboratory experiments and determination if the hydro-mechanical properties are dependent on dry density of bentonite for samples of various dry densities.

The first two samplings of dry treated bentonite and the first sampling of wet treated bentonite have been done. The laboratory investigations have performed, and some of the hydro-mechanical properties have been determined. The treatment of wet treated material started with 6 months of delay and after lockdown in April we must start anew compared to the plan for 12 months loading. The results of wet treated material will be delayed. The treatment of dry treated material started according to the plan.

8.2. Experimental Procedures

For the experimental procedure, two types of treatment have been applied:

- ”Dry“- powder material was placed in the box in a laboratory oven at 150 °C and drying allowed.
- “Wet “- bentonite with water was placed into an autoclave vessel at 150 °C (drying prevented - the long-term exposure to high temperature followed by sampling and laboratory testing.

The vessel with bentonite PBA-22 «Extra» was placed on the laboratory surface oven at 150°C. Bentonite PBA-22 “Extra” for thermal treatment in a dry state was placed in a metal box made of stainless steel. The manufacturer supplied bentonite with an initial 8-10% water content. Further drying is desirable, so the box is not covered with a lid. The filled vessel was placed in a laboratory drying cabinet in which drying was carried out at a temperature of 150°C.

Wet test bentonite with water, was placed into a special pressure vessel at 150 °C for long-term high-temperature exposure followed by 6-18 months sampling and laboratory testing. The vessel with bentonite PBA-22 «Extra» was placed on the laboratory surface oven at 150°C. This vessel contains wet bentonite, and drying must not be allowed. It was necessary to have a special pressure vessel (autoclave of 5 litres of volume) which prevents water from escaping and withstands the pressure of water vapours forming inside. The PT parameter of the vessel was calculated in a way that prevents the boiling of the suspension. The samples were taken from the vessel after 3, 6, 12 and 18 months of thermal treatment. For better processing of the sampled wet material, the material was dried out of excess water in a laboratory oven at 60°C to a water content of 4-8 % after drying. The material from sampling would be used for further investigation.

8.2.1. Material preparation and the laboratory test for dry and wet thermal loading.

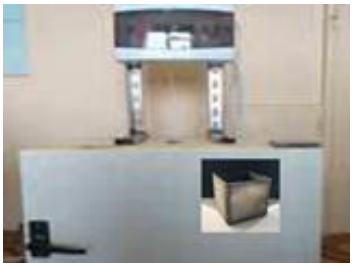

Fig. 8.2.1. Dry program heat cell treatment at 150 °C

Bentonite for treatment in dry condition had not undergone any special treatment before it was poured into box. There was 1.5 kg of bentonite of initial water content 8-10 % as delivered from producer. Further drying is allowed and desired thus the box is not equipped with any lid. Filled box is placed into the laboratory oven at 150°C.

The box with powder samples was heated in a furnace oven at 150°C and kept at temperature from 3 to 18 months. The tests were carried out on bentonite specimens in the box. After test completion, the bentonite specimens were taken out from the box to conduct analysis. After heat treatment, the samples were analysed under laboratory conditions.

8.2.2 The procedure of the wet treatment

Bentonite for treatment in wet conditions requires a specially designed pressure vessel. The material was put in vessels of 5 l. The vessels were poured of 1.3 kg of bentonite and 0.64 kg of distilled water.

	 8.2.3 Teflon gasket (B)	

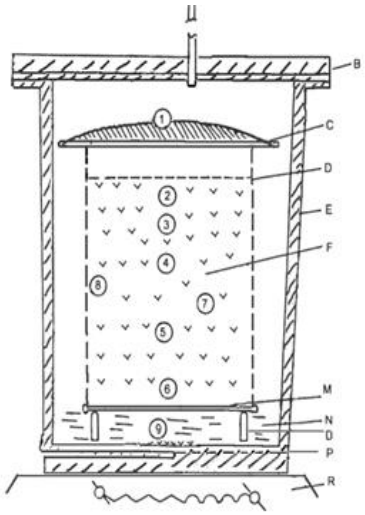

Fig. 8.2.2 The autoclave (A) scheme of sampling pointe.

Fig.8.2.4 Stainless mesh box (D) with bentonite (F)

Fig. 8.2.5 Wet bentonite treatment autoclave placed at 150 °C

The autoclave in Fig. 8.2.2 (A) had a Teflon gasket (B), a bentonite screen (C), and a stainless mesh box with a mesh size of 0.5 mm (D). Bentonite powder (F) weighing 1300 g with a particle size <100 µm was slightly compacted in it. The bottom of the box had a tray (M) placed on a stand (O). Distilled water (N) in 600 ml was preliminarily poured onto the bottom of the autoclave. The temperature of the bottom of the autoclave was in the range of 150°C-156°C, while the pressure in the autoclave was 0.6 MPa - 0.7 MPa. A thermal cover was put on top of the autoclave. The temperature of the upper lid was 145°C, and during the experiment, it did not change, that is, there was a temperature gradient inside the autoclave.

8.3 Results

The main objectives of the investigation were to study in detail the influence of high temperature on the thermal and hydraulic behaviour of compacted bentonites. Laboratory treated material was used (initial and after treatment) for characterization (mineralogy, chemical composition, chemical and mechanical properties). Bentonite clay minerals can adsorb/desorb water from their interlayer, which is connected with changes in d_{00l} spacing.

A general analysis of the clay phases was performed to characterize its chemical, mineralogical and microstructural transformations. The main analyses carried out have been: XRD, IR, thermal analyses (DTA, DTG, TG) and the exchangeable cations (EC). The testing is determination of hydraulic and mechanical properties of thermally treated material.

The powder from each sample was subjected to x-ray diffractometer analysis to determine any possible mineralogical changes that have occurred in tests. The basal spacings of Ca-montmorillonite changed at times of 3 -12 months. The $d_{(001)}$ value of Ca-montmorillonite decreased with increasing time of treatment.

The profile intensity decreased together with a shift of the maximum. Based on XRD spectra of the first basal diffraction (001) of Ca montmorillonite, significant changes induced by dehydration were observed (see Fig. 8.3.1) and showed the evolution of the position, shape and intensity of the 001 reflection as a function of time for 150º C heating temperature. The profile intensity decreased together with a shift of the maximum from 15.36 Å to 12.5 Å during the 6-month exposure.

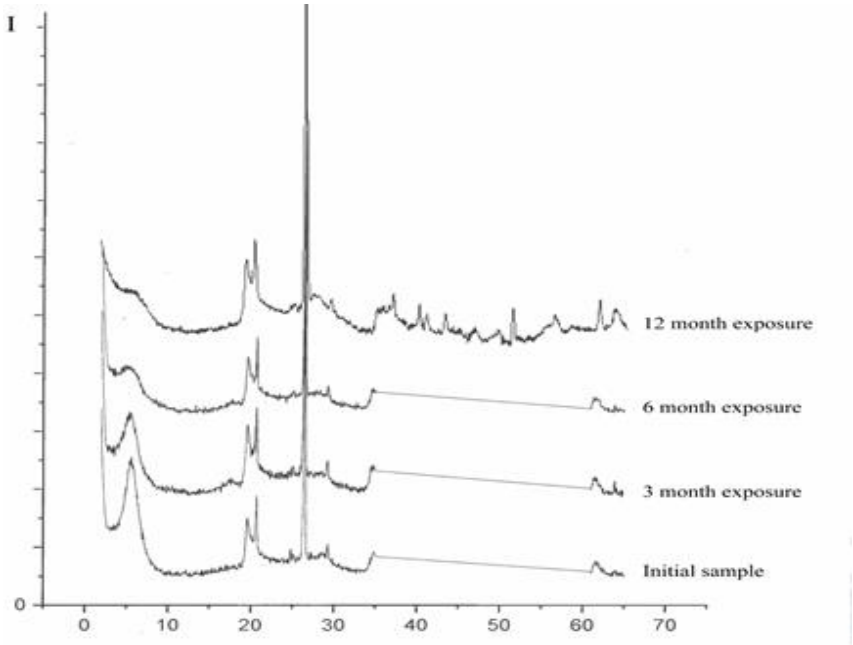

Fig. 8.3.1. XRD patterns of samples after dry thermal tests conducted at 150^{0}C

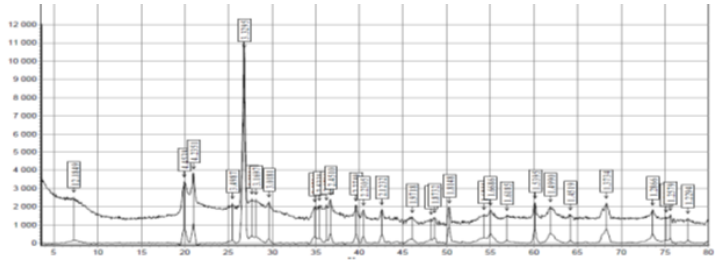

Fig. 8.3.2. XRD of the PBA-22 after 150°C treatment, 12 months

With increasing time of treatment, evolution is observed in peak shape although there is a slight shift to 14.9 Å. The 001 peak decreases in intensity, shifts and broadens, developing a tail toward the high-angle side. After 6 months heating, the 001 peak near 12.5 Å decreases in intensity, broadens and becomes asymmetric and diffuses.

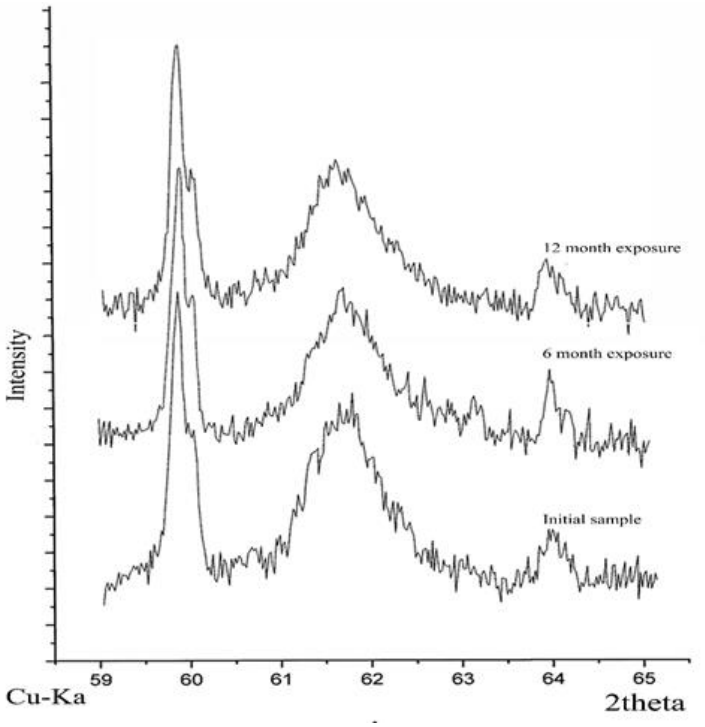

Fig. 8.3.3. The XRD patterns of the powder samples.

The *d* spacing of the (060) reflections increased with time of exposure. This effect was more significant in the longer test.

Table 8.3.1. The (*d)* spacing of the (060) reflections of Ca-bentonite PBA-22 «Extra»

	2 thetas [°]	D [A]	Time
1	61.68	1.5039	Initial
2	61.64	1.5048	6 months
3	61.58	1.5061	12 months

TABLE 8.3.2. PHYSICAL-CHEMICAL PROPERTIES AFTER DRY-TREATMENT BENTONITE PBA-22.

Thermal load time	**CEC_{sum} (meq/100 g) of dry clay**	**CEC_{sum} (meq/100g) of wet clay**
Initial	92.6	92.6
6 month	79.6	87.2

12month	82.1	87.5
18 month	79.4	89.2

The ion exchange capacity of the heated material was lower compared to the initial bentonite material. The specific surface area S_{BET} was determined according to the BET method from the N_2 adsorption isotherm at 77 K.

Commenté [LJ13]: This sentence is incomplete.

An overlap of bands produced by the O−H stretching oscillations of H_2O (O–H_w) and structural OH (O−H_s) in bentonite hampers the study by infrared spectroscopy (IR) of both their layer and interlayer structure (Kuligiewicz, A.,2015).

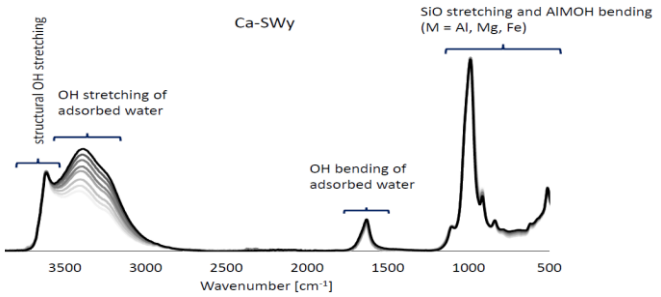

Fig. 8.3.4. IR spectra of water sorption on bentonite –IR experiments [6]

Analysis of the IR spectra of the samples in the region of stretching and bending oscillations of OH groups associated with octahedral cations, as well as in associated water molecules, indicates a clearly defined band for Al-Al-OH at 3622 cm^{-1}. At the same time, the band at 913-915 cm^{-1} is most pronounced in the form of a bend. The band at 875 cm^{-1} corresponds to the bending oscillations of the OH-group in the structural fragment Al-Fe-OH and is most pronounced for bentonite treated for 6 months.

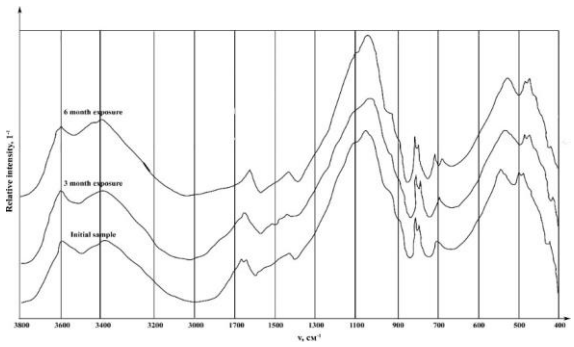

Fig. 8.3.5. IR spectra of the samples for untreated and after dry thermal tests conducted at 150^{0}C

TABLE 8.3.3. WAVENUMBERS (v, cm^{-1}) OF ABSORPTION MAXIMA IN IR SPECTRA OF BENTONITE

Structural groups	M-OH	Al-Al-OH	Al-Fe-OH	H_2O	Si-O-Si
Stretching oscillations	3692	3622	-	3426	1164, 1095, 1039
Deformation oscillations	-	913	875	1634	798; 779; 694; 519; 467

The stretching oscillations bands of OH groups of water molecules for three samples have the same shape but differ in values of the wave numbers at the maximum point. This band is the most intense, and the maximum, in comparison with the other two samples, is shifted to the low-frequency region: (3426 cm^{-1}) < (3430 cm^{-1}) < (3435 cm^{-1}). Obviously, one can speak of a weakening of the energy of hydrogen bonds in the indicated series. At the same time, in the region of deformation oscillations of water molecules, an intense band with symmetrical shape appears at 1632-1634 cm^{-1}.

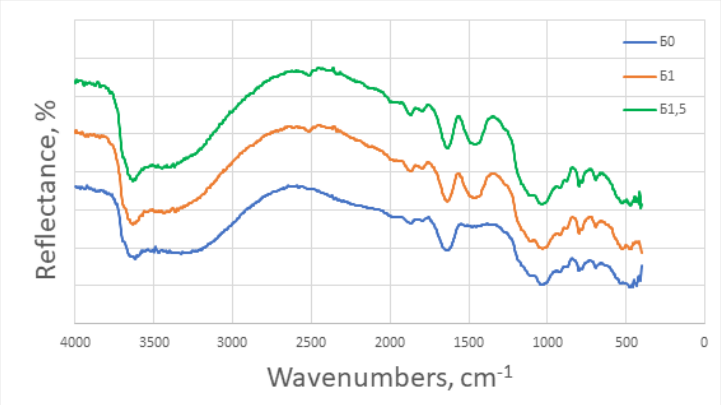

Fig. 8.3.6. FTIR spectres of the bentonite after 150°C treatment for 0-12-18 months

Most studies relating to the influence of temperature on bentonite dehydration have been performed using thermogravimetric or differential thermal analysis. Thermogravimetric analyses (TGA) were performed using a Thermal instrument Q-1500, curves were recorded simultaneously in a static air atmosphere at a heating rate of 5°C/min. For Ca-bentonite there is a first dehydration start near 60–90 °C, usually attributed to water loosely bonded, and another part at 110–150 °C, attributed to strongly held water (see Fig 8.3.7.).

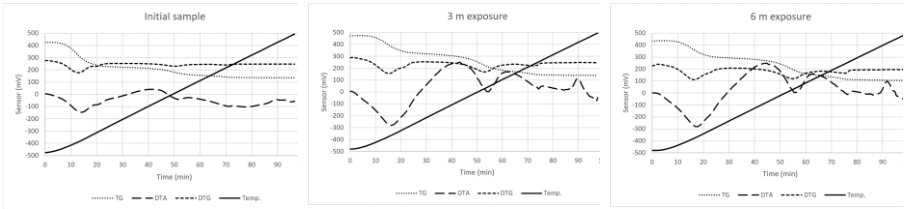

Initial 3 months thermal load 6 months thermal load

Fig. 8.3.7. TGA analysis of Cherkasy bentonite PBA-22 after dry thermal tests conducted at 150°C

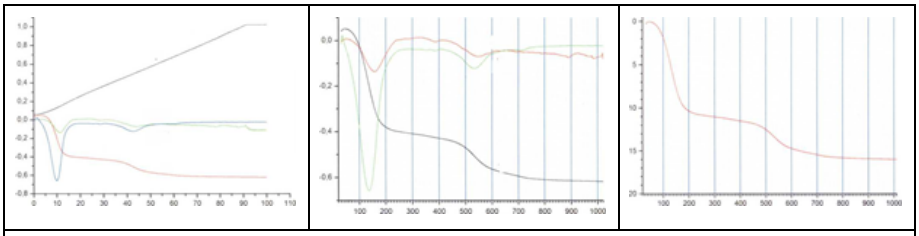

Fig.8.3.8 DTA/TG curves of the PBA-22 after 150°C dry-treatment, 12 months

8.3.1. Swelling pressure and hydraulic conductivity

The specimens were prepared by statically compacting bentonite powder (water content = 12.0 %) to a targeted dry density. Compaction of bentonite powder was carried out using a compression testing machine. The typical water flow characteristic through the compacted bentonite is presented in Fig.8.3.9 for the values of hydraulic conductivity at different dry density after treated. The test results showed that with thermal treatment the hydraulic conductivities for all compacted bentonites are very low, with K_s around E-13 (m s^{-1}). The hydraulic conductivities decrease with increasing dry density of bentonite. The change of hydraulic conductivities in the bentonites at elevated temperatures is attributable to the change of the permeability factor and the density factor.

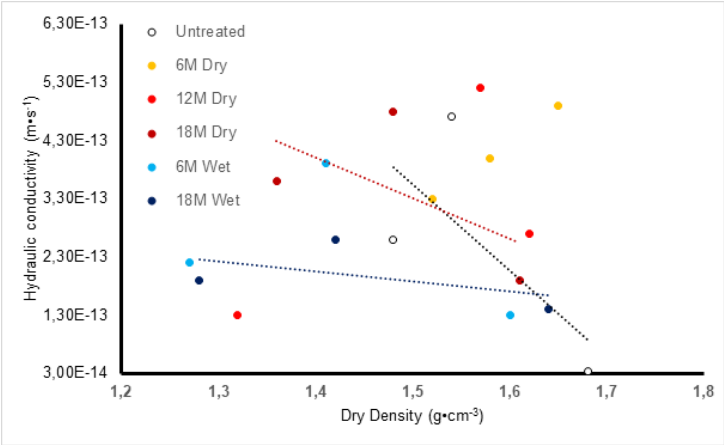

Fig.8.3.9 Hydraulic conductivity of dry and wet treated bentonite after 6, 12 and 18 months at 150°C

Experiments with bentonite exposed to hot water vapor showed that the swelling pressure and hydraulic conductivity were not significantly changed for the investigated temperature of 150ºC. A slight increase in conductivity was recorded.

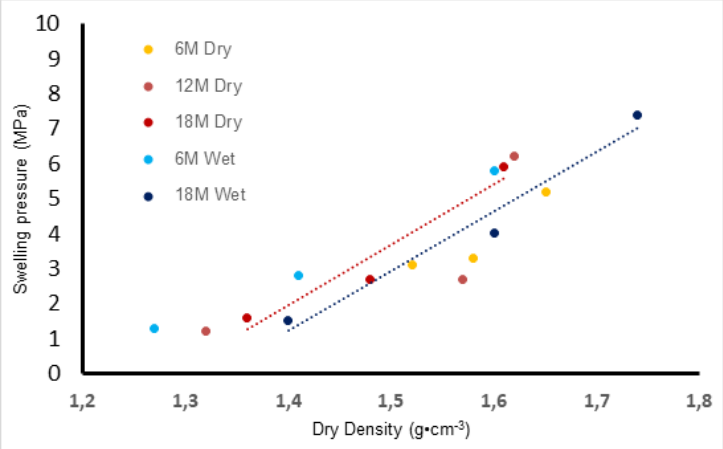

Fig. 8.3.10 Swelling pressure of dry treated and wet treated bentonite after 6, 12 and 18 months at 150°C

8.3.2. Characterizations of bentonite wet treated by 150^{O}C, 18m months

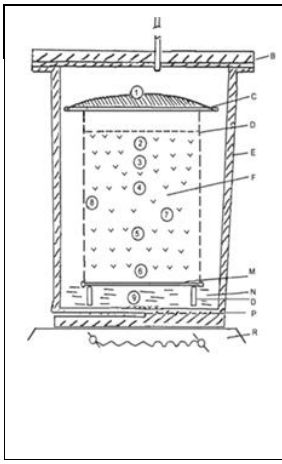

№	Sampling point of bentonite	Humidity, %
1-A	Layer 0 cm	-
2-A	Layer 0-1 cm	66
3-A	Layer 1-2 cm	64
4-A	Layer 6-7 cm	51.5
5-A	Layer 10-11 cm	41.1
6-A	Layer 19-20 cm	43.2
7-A	Average of the 7-11 cm	47

Fig. 8.3.11 Scheme of sampling point of bentonite in autoclave

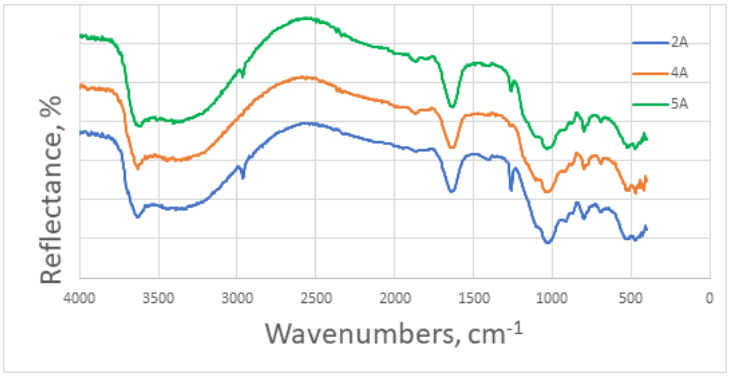

Fig 8.3.12 FTIR spectres of 18 months treated bentonite from the sampling point (2A, 4A, 5A)

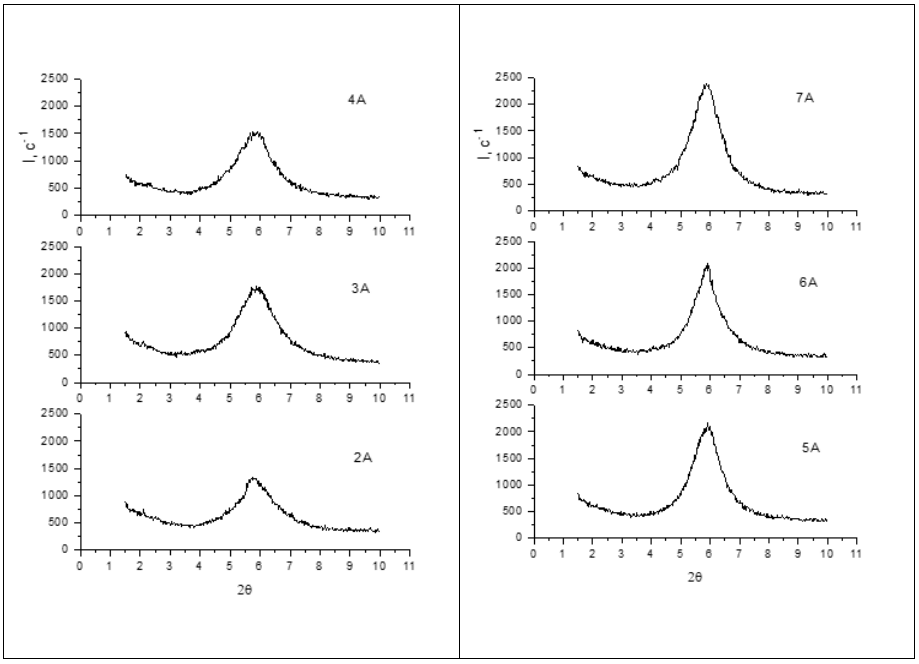

Fig. 8.3.13 XRD patterns of the air-dried samples taken along the bentonite column (the sample point of each sample is indicated)

.

8.4 Conclusion

Heat treatment has changed the structure of clays and their physico-chemical properties. According to presented results it is possible to say that in order to confirm the presumption of effect of thermal loading on bentonite further results of tests are needed.

9. SKB (SKB)

9.1 Introduction

The Wyoming bentonite MX80 from American Colloid Co has long been the reference for buffer material in the Swedish KBS-3 concept. Extending the knowledge base of alternative buffer materials will make it possible to optimise regarding safety, availability and cost. For this reason, the field experiment Alternative Buffer Material was started at Äspö Hard Rock Laboratory during 2006 (Eng et al. 2007), and three additional ones were installed within the ABM45 project in 2012 (Sandén et al. 2018). For the experiments in general the target temperature was 130°C (the only exception was ABM5), the heater was made of steel and different compacted bentonites were installed in direct contact with each other surrounding the central heater. A water saturation system together with a sand filter allowed rapid water saturation. ABM1 was excavated in 2009 (e.g. Svensson et al. 2011; Svensson and Hansen, 2013; Kaufhold et al, 2013) and ABM2 was excavated in 2013 (e.g. Svensson, 2015). The scale of the ABM experiments is significantly smaller (3 dm diameter clay blocks; 1 dm heater; 3 m high) compared to a full scale KBS-3 experiment (Figure 9-1). The different bentonite types are stacked on top of each other (Figure 9-1).

The temperature evolution in ABM5 was different compared to the other ABM experiments. Initially kept low at around 50°C, because it was impossible to get the water pressure to the target level due to leakage as the rock most likely was highly fractured. In 2016 the temperature was increased stepwise to very high temperatures of up to 250°C at the heater interface, making it the hottest bentonite experiment in the history of the Äspö hard rock laboratory (Figure 9-2). ABM5 was excavated in 2017, and is the focus in this chapter. The ABM3, ABM4 and ABM6 experiments are still running and are expected to be excavated in late 2024.

The main purposes of the ABM project are to characterise the mineralogical content of the clays and to identify any differences in behaviour or long-term stability. It is important to notice that the temperatures in the ABM experiments are higher compared to the SKB KBS-3 concept target temperature, and that the heater is made of steel in the ABM-experiments, while the canister is made of copper in the KBS-3 repository.

The ABM5 experiment is especially suitable for the HITEC Task 3.1 to study samples that have been treated at high temperatures under repository like conditions. The focus in this study is on chemical (XRF, CEC) and mineralogical (XRD) impact, physical impact (photo documentation), and impact on important safety functions for the repository (swelling pressure, hydraulic conductivity and uniaxial compression test).

Four bentonites in the ABM5 experiment were selected: MX80 (Wyoming/USA), Calcigel (Bavaria/Germany), Deponit Can (Milos/Greece) and Asha 505 (Kutch/India). The SKB work has been documented in more detail in Svensson et al. (2023). Further data and details regarding the ABM5 experiment is also seen in the BGR (KIT) chapter of this report. More details can be found in Svensson et al. (2023).

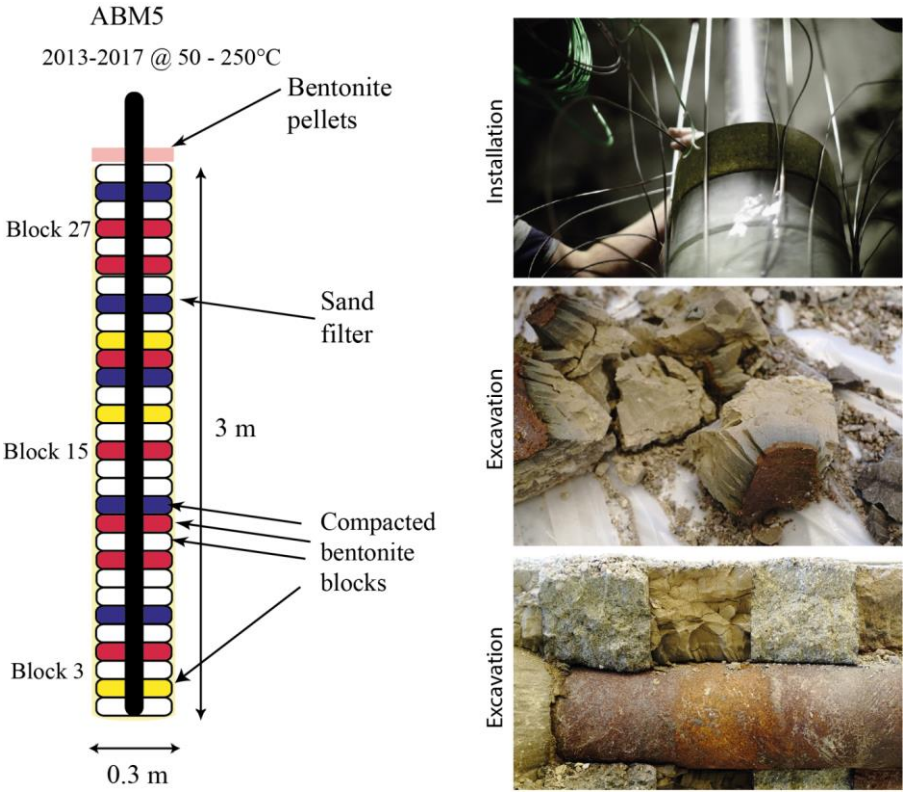

Figure 9.1 Left: Schematic illustration of the ABM5 experiment. Right: pictures from installation and excavation of the ABM5 experiment.

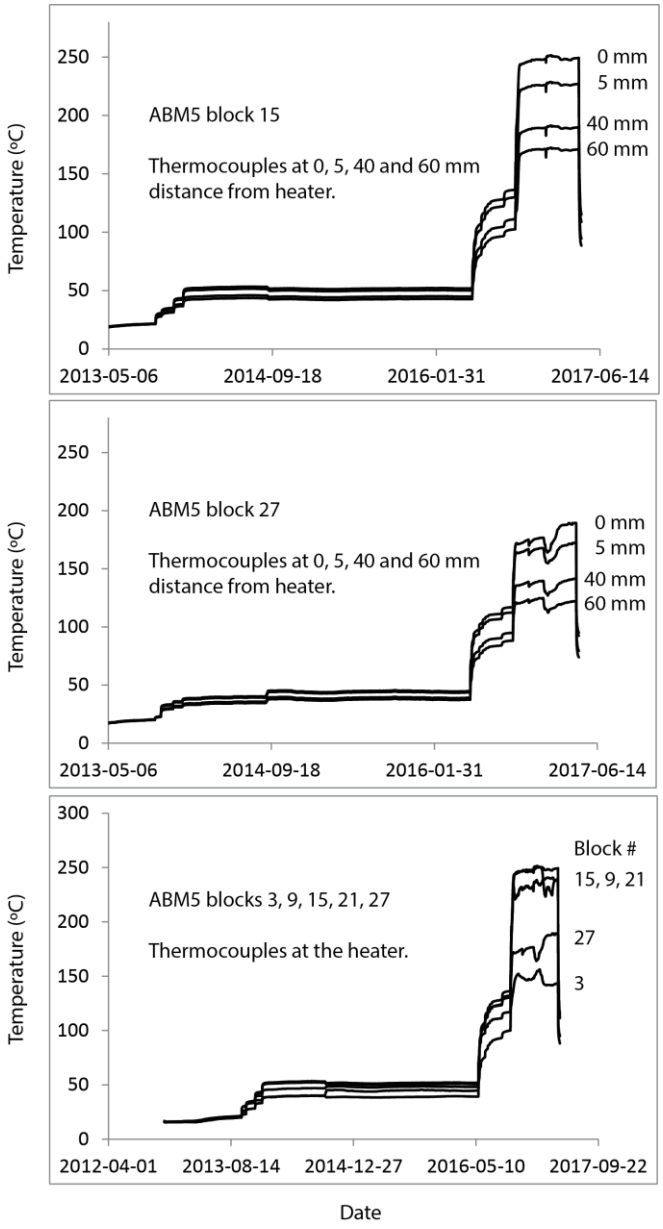

Figure 9.2 Overview of the thermal evolution of the ABM5 experiment.

9.2 Procedures

9.2.1 X-ray fluorescence (XRF) spectroscopy

The equipment used was a Panalytical Epsilon 3 XL spectrometer using a Rh X-ray tube. Helium gas was flowed over the sample during the measurement to reduce the absorption by the air, and the samples were analyzed as compacted discs of pure clay or as a milled sample placed on a mylar foil depending on the amount of sample available. The measurement setup and evaluation was the standard provided from the manufacturer (called Omnian). The XRF does not measure elements with atomic number lower than sodium. The reported elements are reported as e.g. oxides and the sum is normalized to 100%.

9.2.2 Powder X-ray diffraction (XRD)

The XRD data was collected in reflection mode (theta-theta configuration) using a Panalytical X´Pert Pro system with a Co X-ray source (broad focus; λ = 1.789 Å), a PIXcel1D linear detector and programmable divergence- and anti-scatter slits. In order to maximize the intensity no monochromator was used, however a thin Fe filter was used for suppression of white- and Co K-beta radiation, making the K-beta intensity <1% of the K-alpha. The samples were either back-loaded or prepared on a zero-background Si substrate, depending on the amount of sample available. Data collection was done for typically 1-3 hours per sample at 40 kV and 40 mA.

9.2.3 Specific cation exchange capacity (CEC) and extractable cations (EC)

Exchangeable cations (EC) were extracted with an NH_4Cl (or NH_4OAc) solution in 76 % ethanol solution instead of water to minimize dissolution of gypsum.

Exchangeable cations are extracted by shaking milled bentonite (1000 mg ± 10 mg) in ammonium chloride solution in 76 % ethanol (saturated 1 M NH_4Cl; 12.5 ml) on a vibrating table for 30 minutes. After 5 minutes centrifugation at 2700 RCF (relative centrifugal force) the supernatant is separated from the bentonite by decanting the extract to a sample tube. The extraction is repeated totally three times (i.e. same sample is extracted three times with a total volume of approximately 38 ml). After evaporation of the alcohol, the extract is filtrated (0.45 µm filter) and volume corrected with deionised water to 50 ml. The cations are analysed by inductively coupled plasma (ICP) at external laboratory. As EC are reported in relation to the dry weight of a bentonite sample water content of the material is determined by weighing a separate bentonite sample before and after drying at 105 °C for 24 h.

The specific cation capacity (CEC) was measured using a Cu^{2+}-triethylenetetramine complex (Meier and Kahr 1999, Ammann et al. 2005). As the Cu-tri complex has a very strong blue colour this exchange was quantified using spectrophotometry. The measured CEC on pure montmorillonite (or other smectite) correspond very well to the calculated layer charge on Wyoming montmorillonite based on chemical composition (Karnland et al. 2006) hence it is very well established that the Cu^{2+}-complex is absorbed as a divalent cation in amounts corresponding to the permanent charge of the smectite. Milled bentonite (400 mg ± 10 mg) is dispersed in deionised water (33 ml) on a vibrating table for 30 minutes followed by ultrasonic treatment (15 minutes). The bentonite is then equilibrating with Cu (II)-triethylenetetramine solution (7 ml; 45 mM) and left on a vibrating table for 30 minutes. After 5 minutes of centrifugation at 3000 RCF (relative centrifugal force) spectrophotometer measurement at 583 nm of the supernatant is performed against a calibration curve. The CEC is calculated by the difference in the copper concentration before and after ion exchange with the clay and is expressed as cmol(+)/kg dry weight. As the CEC is reported in relation to the dry weight of a bentonite sample the water content of the material is determined by weighing a separate bentonite sample before and after drying at 105 °C for 24 h.

9.2.4 Swelling pressure and hydraulic conductivity

The tests are performed according to the following, for details see also Karnland et al. (2006) and Svensson et al. (2019), the total time for all steps is approximately six weeks:

1. A compacted clay disc is emplaced into the swelling pressure cell or alternatively the clay is compacted in situ in the cell. The compacted clay disc has a diameter of 35 mm and an approximate height of 5 mm, and a specific target density of choice.

2. The clay is saturated with deionised water and the swelling pressure is continuously measured with an external force cell. This is done over a time period of about one week. The swelling pressure is determined as the force divided with the cross-sectional area of the specimen and interpreted when the pressure (force) is considered to be stable.

3. The hydraulic conductivity of the specimen is determined with deionised water. The determination is made by applying a constant pore pressure gradient over the specimen while the amount of water per time unit is measured continuously. The gradient is defined as the applied pressure in meters of water column divided by the height of the sample. The evaluation is made according to Darcy's law. The measurement of the hydraulic conductivity continues for about one week and interpreted when the outflow is considered to be stable.

4. Step 2 is repeated but with a 1 M $CaCl_2$ solution instead of deionised water, this will exchange the bentonite to Ca-form.

5. Step 3 is repeated with the 1 M $CaCl_2$ solution.

6. Step 2 is repeated using deionised water (this removes the salt from the bentonite).

7. The specimen is taken out of the swelling pressure cell, and its bulk density and water content are determined. The bulk density is determined by weighing a sample both in air and submerged in paraffin oil with known density. The water content is determined by drying a sample in an oven at a temperature of 105 ºC for 24 hours. With the known density and water content the dry density is calculated.

9.2.5 Unconfined compression tests

Unconfined compressive strength was determined on crushed and re-compacted specimens from the field experiment and on compacted specimens from the reference material. The water used for the saturation before the unconfined compression tests was either (1) formation water (i.e. from borehole KA2598A at Äspö. Approximately 0.1M Na and 0.06M Ca) or (2) 1 M Ca-chloride solution followed by DI-water. During the measurement a cylindrical specimen is compressed axially with a constant rate of displacement with no radial confinement or external radial stress. With the test the unconfined compressive strength or the maximum deviator stress of the specimen is determined. The strength is commonly determined on specimens having the height equal to double the size of the diameter to allow the failure surface to fully develop. In this study the height was equal to the diameter to keep the time to saturation as low as possible. To minimize the end effect on these short specimens, lubrication of the end surfaces was made. The specimens saturated with ABM-water were exposed to circulating ABM-water, above and under the specimens, over a short period of time but as stagnant water during the main part of the time. The time used for the saturation was 27-34 days. The specimens, ion-exchanged with 1M $CaCl_2$. were prepared for 77-93 days according to the following steps:

1. Saturation by stagnant ABM-water and circulation during shorter time periods, to remove air trapped in the filters, for approximately 5 days.
2. Ion-exchange to be calcium-dominated by continuous circulation of 1M $CaCl_2$ for approximately 40 days.
3. Removing excess salt by continuous circulation of de-ionized water (DI-water) for 30-50 days until low electrical conductivity.

4. End of test and dismantling for the unconfined compression test.

The time used for the ion-exchange was calculated to correspond approximately to get 80% ion-exchange in the central part of the specimens. The time used for the circulation of DI-water, to remove excess salt, was chosen to get low electrical conductivity, less than 0.1 mS/cm. After the preparation, all specimens were removed from the saturation device at least 12 h before the shearing to homogenize while protected from evaporation. For more details see Svensson et al. (2023).

9.3 Chemical and mineralogical evolution in ABM5

The data collection of this part is completed. Further evaluation and comparison with other groups is to be done.

Powder XRD (Figure 9.3 – Figure 9.6) generally show few or no significant changes to the clays, the most obvious change is the change of the smectite 001 reflection, indicating changes in the basal spacing. This is an effect from different water contents of the samples, and this can be due to sample storage or due to increased Ca/Na interlayer cation ratio which is expected after contact with the Äspö ground water. No significant changes could be seen around the 060 smectite reflection (at around 72 deg two theta), so no clear signs of formation of any trioctahedral phases.

CEC in most cases (except MX80) decreased somewhat in the heated samples, especially towards the central heater (Figure 9.7 – Figure 9.10) in the bulk samples. However, in the clay fractions, the opposite was seen, where the CEC actually increased somewhat. The exact reason for this behaviour is not certain. But it is well known that heating and drying of bentonites typically decreases the CEC, this is why samples are not oven dried before the measurement, and instead separate samples are taken for water content determinations. Possibly this can be due to aggregate formation or dehydroxylation reactions. The increase of the clay fractions after the experiment could possibly be connected to the ultra-sonic treatment used during the preparation of the clay fractions, alternatively the smectite layer charge could have increased.

The chemical composition (XRF; Table 9.2) showed that Na decreased in Asha505 and MX80 in the field samples, while Calcigel and DepCAN were unchanged. A general increase in Mg was observed in many field samples (Asha505, MX80, Calcigel), somewhat different from the more typical maxima towards the heater that has been observed in several previous field experiments. Some moderate increases in S towards the heater was observed in Asha505, and a general increase in MX80, while Calcigel actually lost some S, and DepCAN was unaffected. Ca showed a complex behaviour in Asha505 where increases were seen both at the rock contact, and also at some distance from the heater in the 2-10 mm sample. Also MX80 gained a lot of Ca during the test, while Calcigel lost Ca, and DepCAN was unaffected. Significant increase of Fe due to the corrosion was seen on most cases, but not in Calcigel. The amount of corrosion and dissolution/reprecipitation of water-soluble phases such as anhydrite/gypsum typically depends on local factors such as water availability, fractures in the rock and temperature, which is why Fe, S, and Ca show complex variations.

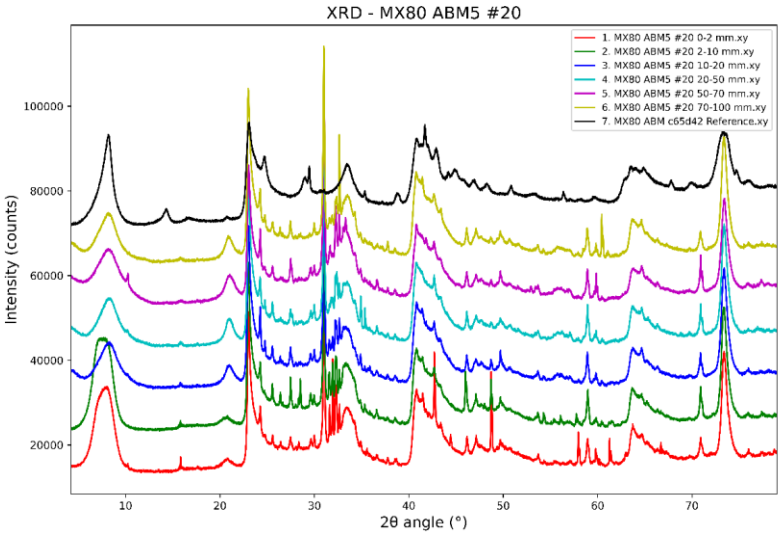

Figure 9.3 XRD patterns of the ABM5 MX80 block 20 profile of samples. Co Kα radiation.

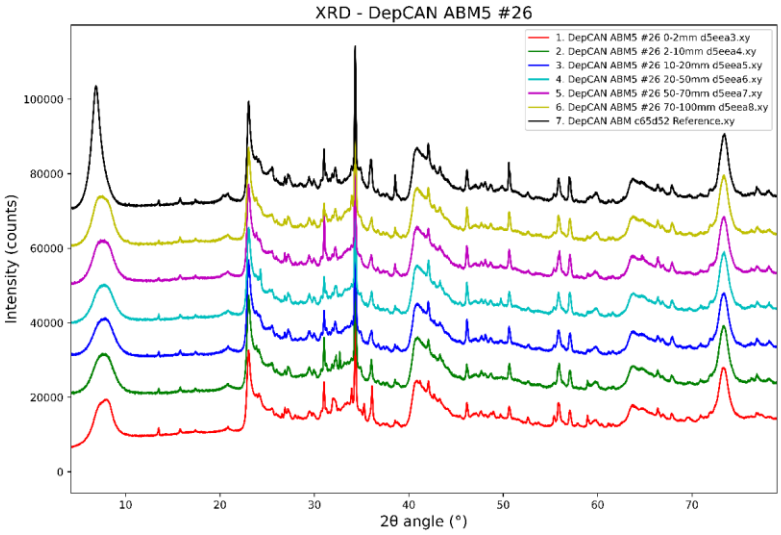

Figure 9.4 XRD patterns of the ABM5 DepCAN block 26 profile of samples. Co Kα radiation.

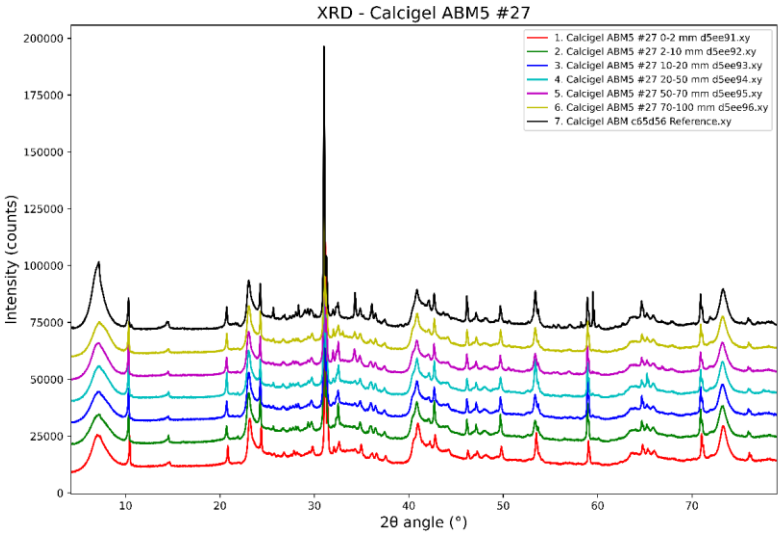

Figure 9.5 XRD patterns of the ABM5 Calcigel block 27 profile of samples. Co Kα radiation.

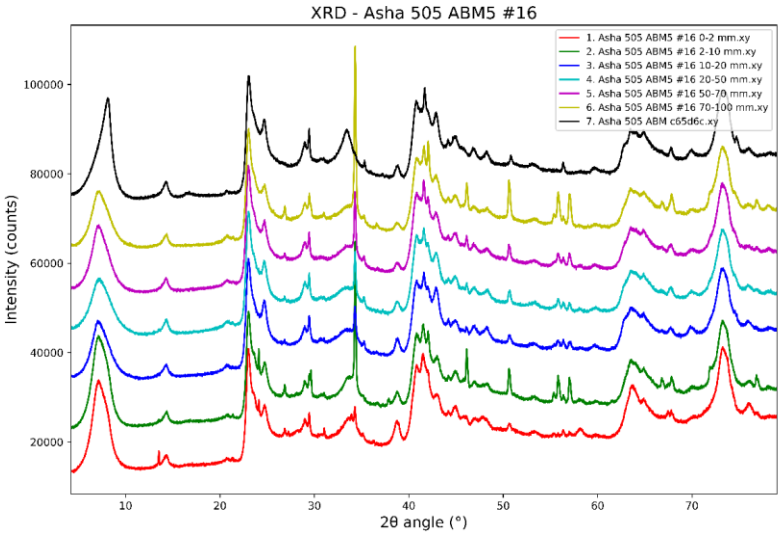

Figure 9.6. XRD patterns of the ABM5 Asha505 block 16 profile of samples. Co Kα radiation.

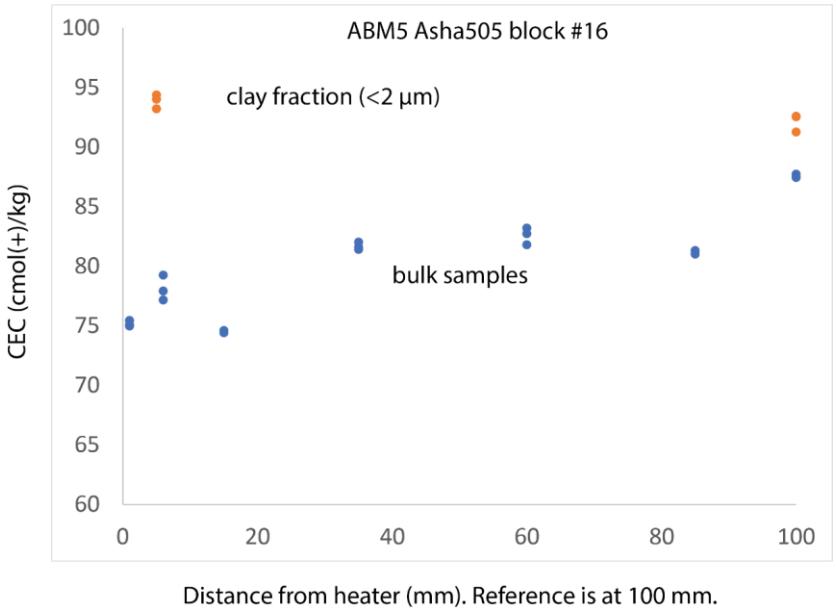

Figure 9.7. CEC of Asha 505 block 16 profile of samples.

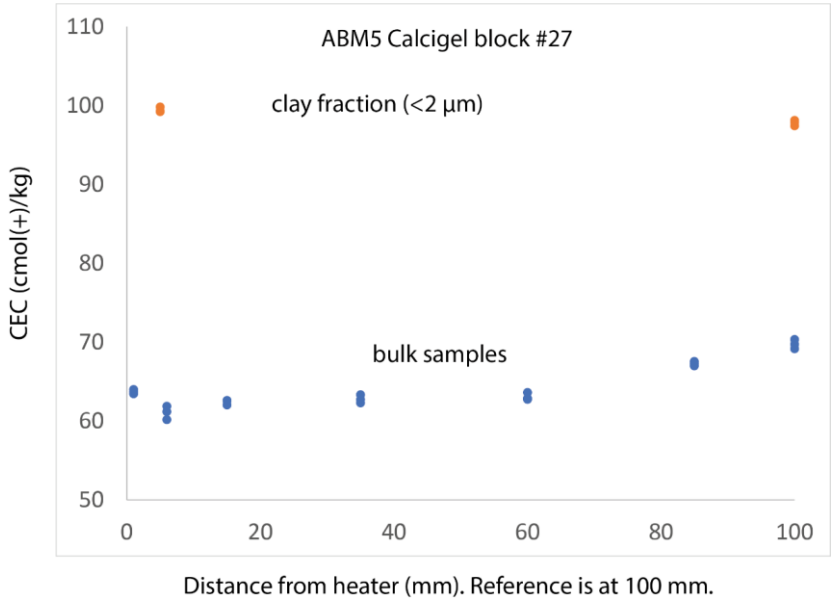

Figure 9.8. CEC of Calcigel block 27 profile of samples.

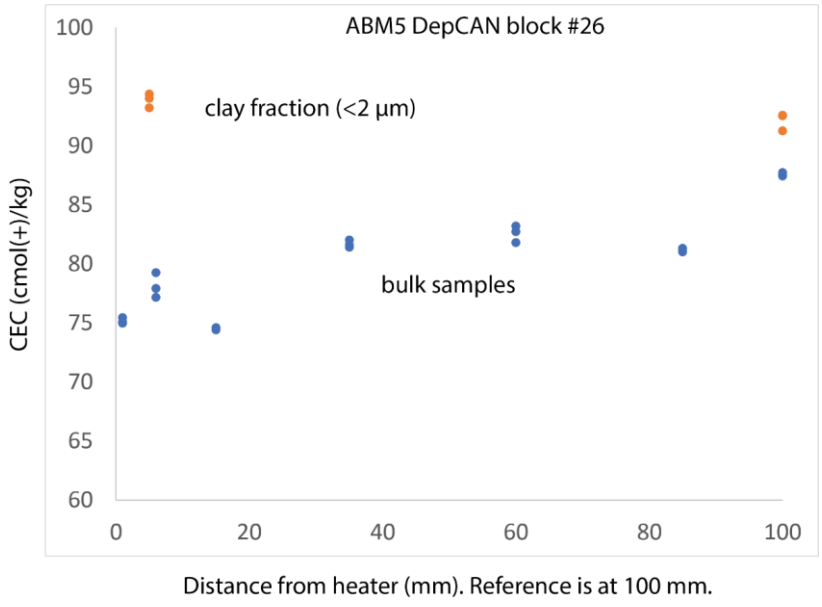

Figure 9.9. CEC of DepCAN block 26 profile of samples.

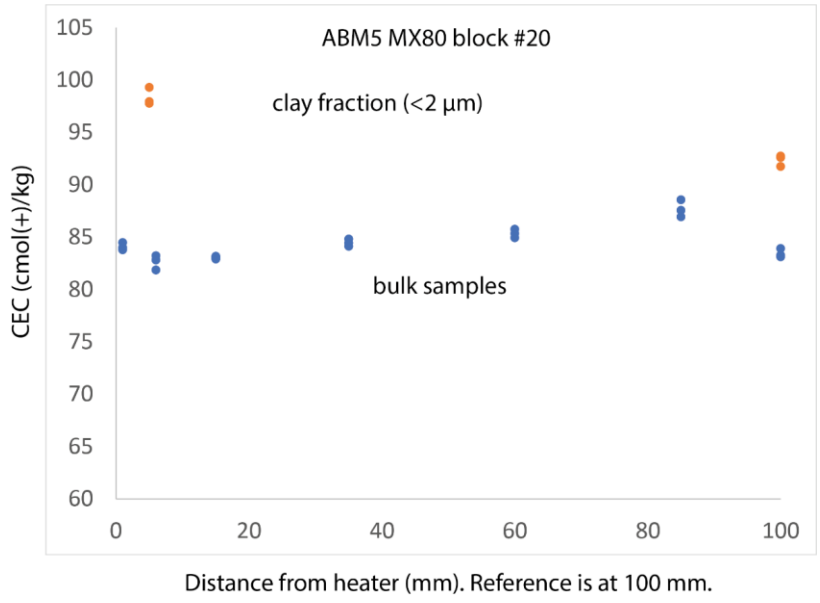

Figure 9.10. CEC of MX80 block 20 profile of samples.

Table 9.1 Exchangeable cations (EC) and cation exchange capacity (CEC) of ABM5 samples. Unit is cmol(+)/kg.

Sample	Sample id	Ca	K	Mg	Na	$\sum_{EC}$	CEC Cu-tri (n=3; SD)
Asha 505 ABM5 #16 0-2 mm	d5ee9d	45.01	1.27	12.68	32.30	91.26	75.2 (0.2)
Asha 505 ABM5 #16 2-10 mm	d5ee9e	46.39	1.18	12.55	32.54	92.66	78.1 (1.1)
Asha 505 ABM5 #16 10-20 mm	d5ee87	47.31	1.25	15.07	29.15	92.78	74.5 (0.1)
Asha 505 ABM5 #16 20-50 mm	d5ee88	49.54	1.45	15.13	31.73	97.84	81.7 (0.3)
Asha 505 ABM5 #16 50-70 mm	d5ee89	50.80	1.35	15.18	32.08	99.41	82.6 (0.7)
Asha 505 ABM5 #16 70-100 mm	d5ee8a	53.54	1.39	15.19	32.62	102.74	81.2 (0.2)
Asha 505 reference	c65d6c	17.02	0.71	16.25	56.02	90.00	87.6 (0.2)
MX80 ABM5 #20 0-2 mm	d5ee97	32.09	1.76	8.46	31.56	73.88	84.1 (0.35)
MX80 ABM5 #20 2-10 mm	d5ee98	36.16	2.42	11.03	34.39	84.00	82.6 (0.7)
MX80 ABM5 #20 10-20 mm	d5ee99	38.00	2.43	11.50	36.01	87.94	83.0 (0.1)
MX80 ABM5 #20 20-50 mm	d5ee9a	38.43	2.62	10.63	37.60	89.28	84.4 (0.3)
MX80 ABM5 #20 50-70 mm	d5ee9b	36.74	2.18	9.85	36.12	84.88	85.3 (0.4)
MX80 ABM5 #20 70-100 mm	d5ee9c	40.31	2.15	10.37	37.32	90.16	87.7 (0.8)
MX80 ABM reference	c65d42	16.72	2.34	7.00	51.95	78.01	83.4 (0.4)
Deponit Can ABM5 #26 0-2 mm	d5eea3	65.35	2.84	3.31	26.07	97.58	77.5 (0.7)
Deponit Can ABM5 #26 2-10 mm	d5eea4	64.81	3.55	5.10	27.41	100.87	79.1 (0.8)
Deponit Can ABM5 #26 10-20 mm	d5eea5	64.99	3.36	5.68	26.89	100.91	78.2 (1.3)
Deponit Can ABM5 #26 20-50 mm	d5eea6	66.75	3.25	5.19	27.65	102.85	78.6 (0.6)
Deponit Can ABM5 #26 50-70 mm	d5eea7	71.27	3.01	3.07	27.59	104.93	80.3 (0.3)

Deponit Can ABM5 #26 70-100 mm	d5eea8	69.87	2.92	2.85	28.41	104.05	83.7 (0.7)
Deponit Can reference	c65d52	39.93	2.40	29.22	22.16	93.72	78.9 (1.4)
Calcigel ABM5 #27 0-2 mm	d5ee91	52.15	3.47	1.59	22.19	79.41	63.7 (0.3)
Calcigel ABM5 #27 2-10 mm	d5ee92	44.33	4.38	3.47	21.57	73.74	61.1 (0.8)
Calcigel ABM5 #27 10-20 mm	d5ee93	44.88	4.27	3.28	22.02	74.46	62.4 (0.3)
Calcigel ABM5 #27 20-50 mm	d5ee94	45.26	3.51	1.42	19.77	69.96	62.8 (0.5)
Calcigel ABM5 #27 50-70 mm	d5ee95	57.89	3.29	1.34	20.47	82.98	63.1 (0.5)
Calcigel ABM5 #27 70-100 mm	d5ee96	56.88	3.08	1.33	19.74	81.02	63.7 (0.3)
Calcigel reference	c65d56	53.95	1.92	16.76	2.64	75.28	69.8 (0.6)

Table 9.2 Chemical composition (XRF) of the ABM5 samples and references

Ident	Na_2O	MgO	Al_2O_3	SiO_2	P_2O_5	SO_3	Cl	K_2O	CaO	TiO_2	MnO	Fe_2O_3
ABM5 Asha #16 0-2mm d5ee85	0.8	2.7	20.7	47.8	0.00	0.4	0.5	0.1	2.7	1.1	0.1	23.0
ABM5 Asha #16 2-10mm d5ee86	0.9	2.8	20.8	48.8	0.00	0.2	1.0	0.1	5.7	1.1	0.1	18.5
ABM5 Asha #16 1-2cm d5ee87	0.9	2.5	22.9	50.3	0.00	0.2	0.3	0.1	2.5	1.1	0.1	19.0
ABM5 Asha #16 2-5cm d5ee88	0.9	2.6	23.1	51.5	0.00	0.1	0.4	0.1	2.7	1.1	0.1	17.4
ABM5 Asha #16 5-7cm d5ee89	1.0	2.5	23.3	51.7	0.00	0.1	0.4	0.1	3.2	1.2	0.1	16.4
ABM5 Asha #16 7-10cm d5ee82	0.9	2.6	22.1	49.6	0.00	0.2	0.4	0.1	6.2	1.2	0.1	16.5
Asha 505 ABM c65d6c	1.8	2.0	24.6	52.1	0.02	0.1	0.5	0.1	0.8	1.3	0.1	16.7
ABM5 MX80 #20 0-2mm d5ee7f	1.0	2.7	21.9	62.9	0.00	0.5	0.7	0.6	2.2	0.2	0.0	7.2
ABM5 MX80 #20 2-10mm d5ee80	1.0	2.7	22.3	63.9	0.00	0.5	0.8	0.6	2.2	0.2	0.0	5.8
ABM5 MX80 #20 1-2cm d5ee81	1.2	2.6	22.6	64.8	0.01	0.6	0.2	0.7	2.0	0.2	0.0	5.1
ABM5 MX80 #20 2-5cm d5ee82	1.2	2.7	22.6	64.9	0.00	0.6	0.2	0.6	2.2	0.2	0.0	4.9
ABM5 MX80 #20 5-7cm d5ee83	1.2	2.6	22.7	64.9	0.01	0.5	0.2	0.6	2.2	0.2	0.0	4.8
ABM5 MX80 #20 7-10cm d5ee84	1.2	2.6	22.6	65.1	0.00	0.3	0.3	0.6	2.1	0.2	0.0	4.8
MX80 ABM c65d44	2.2	2.3	21.9	67.2	0.09	0.2	0.0	0.5	0.5	0.2	0.2	5.0
ABM5 Calcigel #27 0-2mm d5ee91	0.9	3.8	19.9	60.9	0.01	0.2	0.3	2.6	2.9	0.5	0.6	7.9

ABM5 Calcigel #27 2-10mm d5ee92	0.8	3.7	19.6	61.4	0.05	0.2	0.2	2.1	3.3	0.4	0.5	8.3
ABM5 Calcigel #27 1-2cm d5ee93	0.9	3.9	20.0	62.0	0.06	0.2	0.3	2.5	2.9	0.5	0.5	6.8
ABM5 Calcigel #27 2-5cm d5ee94	0.9	3.9	20.0	61.8	0.00	0.4	0.2	2.6	3.2	0.5	0.6	6.9
ABM5 Calcigel #27 5-7cm d5ee95	0.8	3.6	19.2	61.6	0.00	0.3	0.2	2.6	4.8	0.5	0.6	6.7
ABM5 Calcigel #27 7-10cm d5ee96	0.7	3.7	19.8	61.6	0.00	0.3	0.2	2.6	3.9	0.5	0.6	6.9
Calcigel ABM reference c65d56	0.9	3.5	20.9	61.4	0.10	0.4	0.1	1.8	4.1	0.5	0.5	7.5
ABM5 DepCAN #26 0-2mm d5eea3	0.7	3.0	18.9	55.9	0.38	1.7	0.7	1.2	6.9	1.0	0.1	9.7
ABM5 DepCAN #26 2-10mm d5eea4	0.7	3.1	19.9	58.4	0.38	1.1	0.5	1.2	6.6	1.1	1.0	7.3
ABM5 DepCAN #26 1-2cm d5eea5	0.7	3.1	19.9	58.4	0.34	1.3	0.5	1.2	6.8	1.1	1.0	6.8
ABM5 DepCAN #26 2-5cm d5eea6	0.7	3.1	19.9	58.4	0.34	1.3	0.5	1.2	7.0	1.1	1.0	6.5
ABM5 DepCAN #26 5-7cm d5eea7	0.8	3.0	19.9	58.2	0.31	1.1	0.5	1.3	7.5	1.1	0.1	6.5
ABM5 DepCAN #26 7-10cm 5eea8	0.7	3.0	19.8	58.4	0.34	1.0	0.5	1.3	7.3	1.1	0.1	6.5
DepCAN ABM reference c65d52	0.6	3.1	20.3	59.5	0.37	1.3	0.1	1.3	6.2	1.1	0.9	6.3

9.4 Swelling pressure and hydraulic conductivity in ABM5

During the swelling pressure and hydraulic conductivity measurement a lot of data is collected and saved:

(1) Swelling pressure of the original material with DI water
(2) Hydraulic conductivity with DI water
(3) Swelling pressure with 1 M $CaCl_2$
(4) Hydraulic conductivity with 1 M $CaCl_2$
(5) Swelling pressure with DI water.

In order to avoid differences due to salt or changes in the interlayer cation composition, only data from steps (4) and (5) are presented below. No significant change can be seen on the swelling pressure on the samples from ABM5 experiment (Figure 9.11 - Figure 9.14). At low densities possibly some increases in hydraulic conductivity can be observed (Calcigel and Asha505) but is most likely due to scattering in the data that is higher at low densities (Figure 9.11 - Figure 9.14).

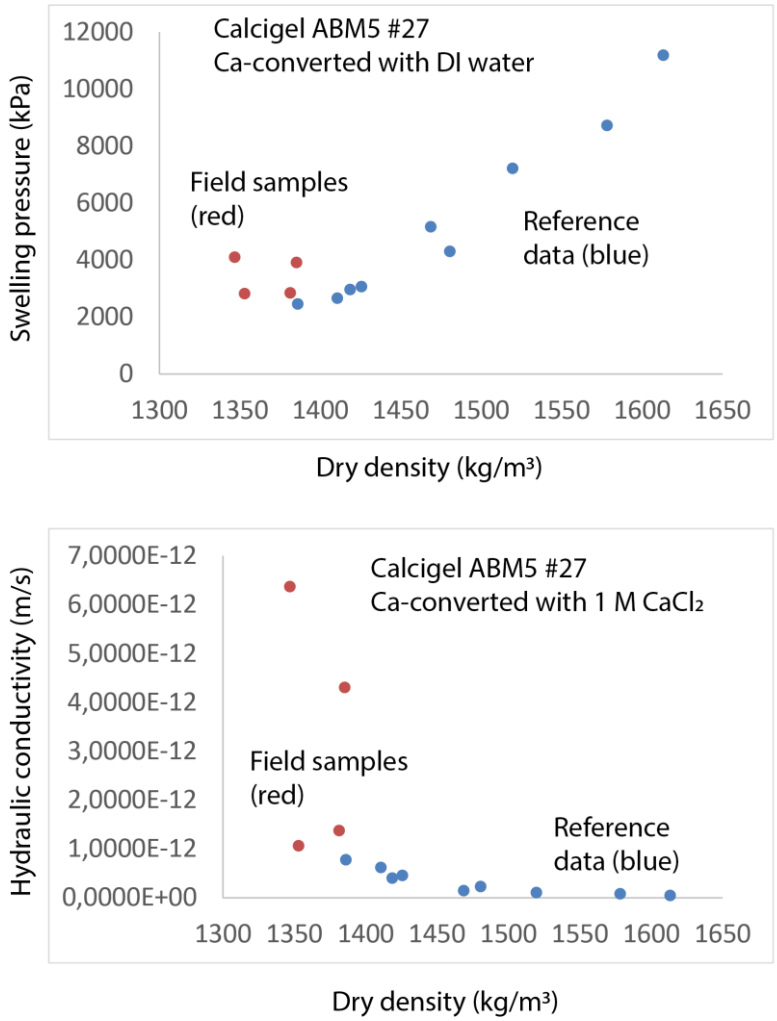

Figure 9.11. ABM5 Calcigel #27 samples compared to reference samples. (a) Swelling pressure after Ca-conversion in DI water. (b) Hydraulic conductivity after Ca-conversion in 1 M CaCl2 solution.

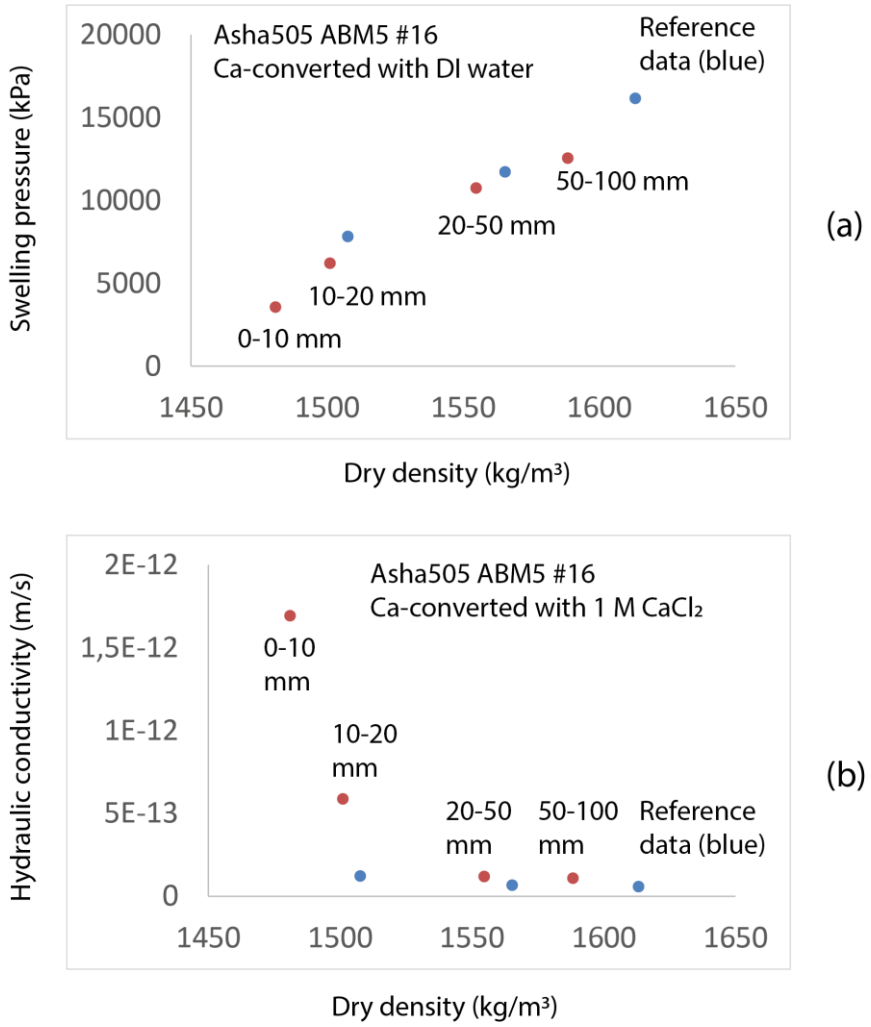

Figure 9.12. ABM5 Asha505 #16 samples compared to reference samples. (a) Swelling pressure after Ca-conversion in DI water. (b) Hydraulic conductivity after Ca-conversion in 1 M CaCl2 solution.

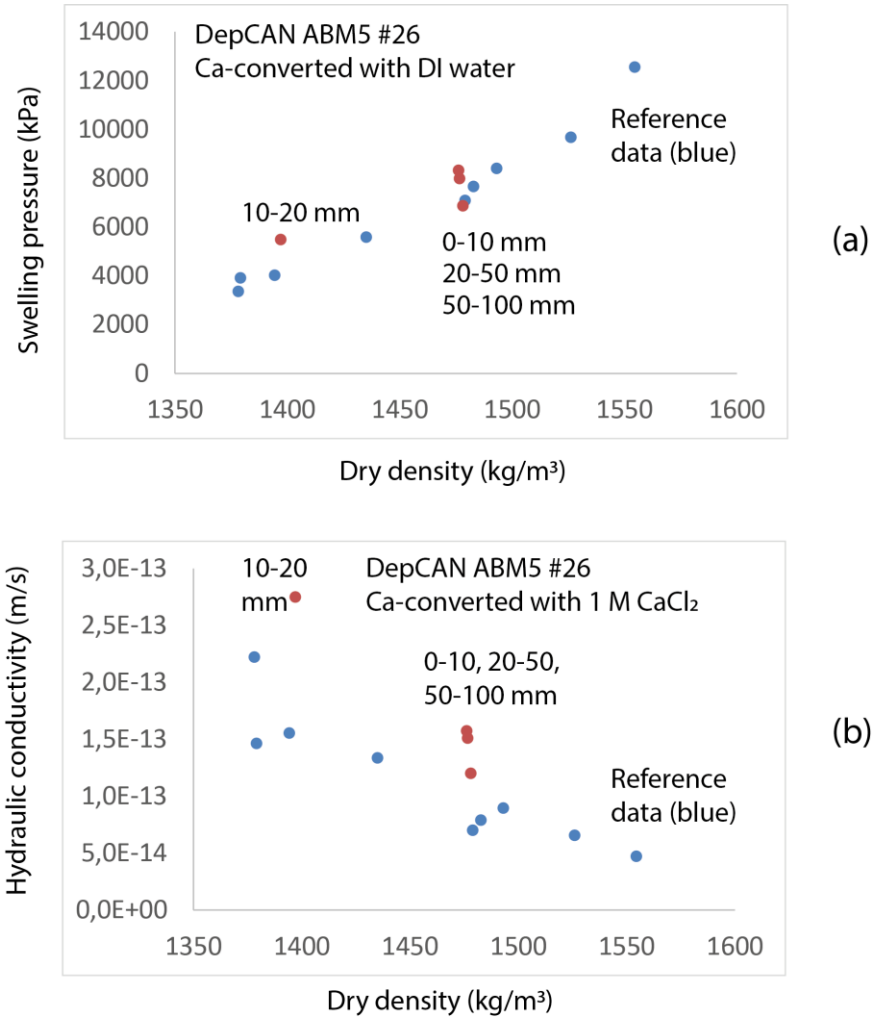

Figure 9.13. ABM5 DepCAN #26 samples compared to reference samples. (a) Swelling pressure after Ca-conversion in DI water. (b) Hydraulic conductivity after Ca-conversion in 1 M CaCl2 solution.

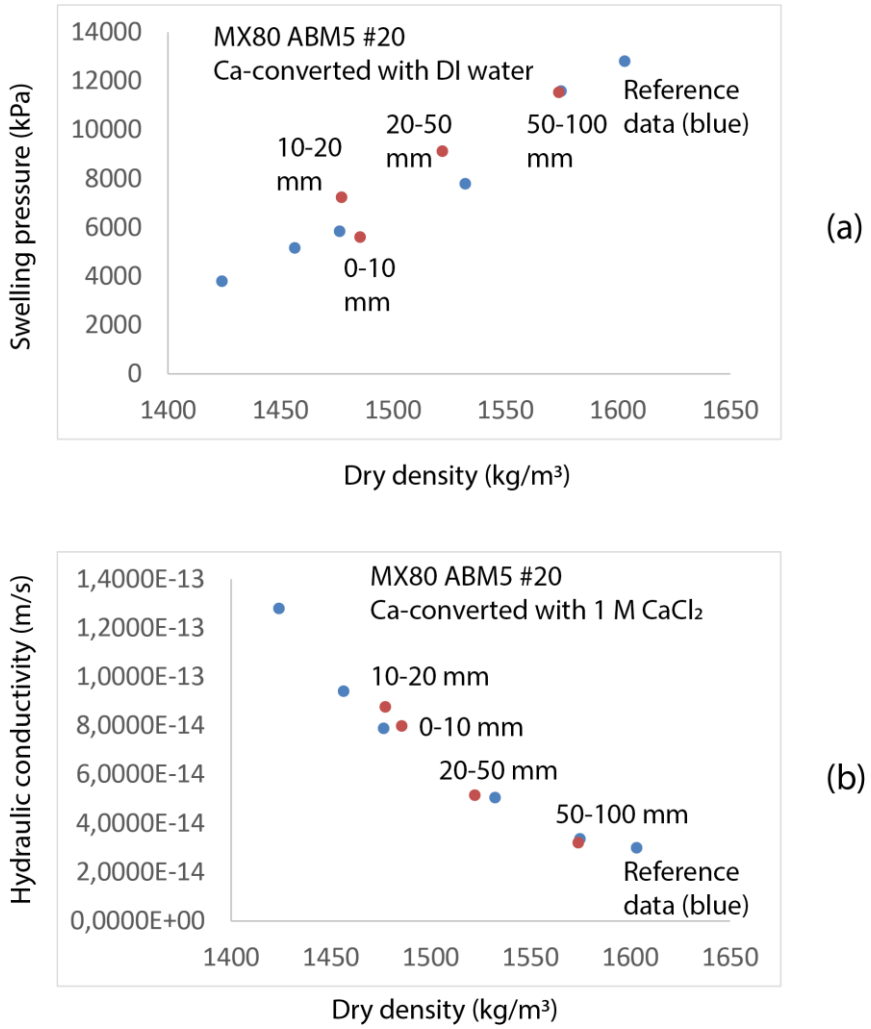

Figure 9.14. ABM5 MX80 #20 samples compared to reference samples. (a) Swelling pressure after Ca-conversion in DI water. (b) Hydraulic conductivity after Ca-conversion in 1 M CaCl2 solution.

Table 9.3 Hydraulic conductivity (HC) and swelling pressure (SP) of ABM5 bentonite samples as a function of the dry density. 1. With DI water, 2. With 1 M $CaCl_2$, and 3. With DI water (Ca-exchanged).

Commenté [LJ14]: Table title is separated from the table contents. Need to redo the layout format.

Sample	Dry density (kg/m3)	HC DI (m/s)	SP DI (kPa)	HC 1M CaCl2 (m/s)	SP 1M CaCl2 (kPa)	SP DI Ca-exch. (kPa)
MX80 ABM Reference	1456	1.27E-13	4765	9.41E-14	2990	5160
MX80 ABM Reference	1476	1.19E-13	5345	7.89E-14	3475	5838
MX80 ABM Reference	1603	7.23E-14	11056	3.00E-14	10432	12809
MX80 ABM Reference	1424	1.39E-13	3701	1.28E-13	2129	3795
MX80 ABM Reference	1532	8.30E-14	7141	5.06E-14	5649	7789
MX80 ABM Reference	1574	4.48E-14	10461	3.37E-14	9154	11581
MX80 ABM5 #20 0-10mm	1485	1.29E-13	5181	7.99E-14	3708	5601
MX80 ABM5 #20 10-20 mm	1477	1.47E-13	6799	8.78E-14	5210	7234
MX80 ABM5 #20 20-50 mm	1522	1.03E-13	8405	5.16E-14	6873	9122
MX80 ABM5 #20 50-100 mm	1573	8.54E-14	10483	3.21E-14	9334	11540
Deponit CAN Reference	1379	2.19E-13	4105	1.46E-13	2669	3911
Deponit CAN Reference	1435	1.72E-13	5760	1.34E-13	4196	5578
Deponit CAN Reference	1479	1.12E-13	7202	7.03E-14	5423	7085
Deponit CAN Reference	1394	2.10E-13	4277	1.56E-13	2849	4021
Deponit CAN Reference	1493	9.01E-14	8536	8.97E-14	6638	8402
Deponit CAN Reference	1526	5.62E-14	9695	6.57E-14	7819	9670
Deponit CAN Reference	1378	2.30E-13	3623	2.22E-13	2246	3356
Deponit CAN Reference	1482	8.07E-14	7852	7.92E-14	5891	7654
Deponit CAN Reference	1554	6.61E-14	12459	4.73E-14	10670	12548
Deponit CAN ABM5 #26 0-10mm	1478	1.82E-13	6580	1.20E-13	5713	6866

Deponit CAN ABM5 #26 10-20mm	1397	3.70E-13	5294	2.75E-13	4524	5487
Deponit CAN ABM5 #26 20-50mm	1476	2.12E-13	7626	1.51E-13	6834	7985
Deponit CAN ABM5 #26 50-100mm	1476	2.26E-13	7865	1.58E-13	7269	8318
Calcigel ABM Reference	1418	4.36E-13	3174	4.07E-13	2356	2967
Calcigel ABM Reference	1468	1.74E-13	5359	1.52E-13	4053	5170
Calcigel ABM Reference	1519	2.09E-14	7463	1.10E-13	5885	7215
Calcigel ABM Reference	1410	6.37E-13	2840	6.19E-13	1997	2659
Calcigel ABM Reference	1386	8.72E-13	2711	7.80E-13	1818	2494
Calcigel ABM Reference	1425	4.72E-13	3264	4.58E-13	2297	3064
Calcigel ABM Reference	1480	2.55E-13	4493	2.31E-13	3414	4304
Calcigel ABM Reference	1578	9.81E-14	8954	8.21E-14	7467	8722
Calcigel ABM Reference	1613	7.17E-14	11393	4.61E-14	9772	11188
Calcigel ABM5 #27 0-10 mm	1381	5.90E-12	2649	1.47E-12	2278	2844
Calcigel ABM5 #27 10-20 mm	1353	4.57E-12	2638	1.14E-12	2321	2819
Calcigel ABM5 #27 20-50 mm	1385	1.90E-11	3649	4.69E-12	3372	3915
Calcigel ABM5 #27 50-100 mm	1346	2.89E-11	4140	6.92E-12	3740	4272
Calcigel ABM5 #27 10-20 mm	1506	9.62E-13	7640	5.86E-13	7581	8328
Calcigel ABM5 #27 20-50 mm	1477	3.49E-12	7743	2.69E-12	7640	8228
Calcigel ABM5 #27 50-100 mm	1503	2.67E-12	9797	1.93E-12	9673	10404
Asha505 ABM Reference	1507	1.65E-13	7554	1.23E-13	7020	7834

Asha505 ABM Reference	1565	1.04E-13	10989	6.70E-14	10883	11728
Asha505 ABM Reference	1613	8.02E-14	14816	5.87E-14	15443	16158
Asha505 ABM5 #16 0-10mm	1481	1.37E-12	3644	1.69E-12	2587	3565
Asha505 ABM5 #16 10-20 mm	1501	7.43E-13	5552	5.87E-13	5361	6221
Asha505 ABM5 #16 20-50 mm	1554	1.90E-13	9892	1.19E-13	9897	10756
Asha505 ABM5 #16 50-100 mm	1588	1.87E-13	11571	1.09E-13	11624	12555

9.5 Unconfined compression tests

9.5.1 Samples saturated with Äspö water

Compared to the references equal or lower maximum deviator stress was seen in all materials (Figure 9.15 – 9.18). The corresponding strain was approximately the same as the references with the exception of Deponit CA-N where the corresponding strain was clearly lower than the references.

Compared to the references the maximum deviator stress and the corresponding strain differed in the following ways for the different materials:

- In Asha505 specimens the deviator stress was lower, and the corresponding strain approximately the same.
- In MX-80 specimens the deviator stress was somewhat lower, and the corresponding strain was the same or higher.
- In Deponit CA-N specimens the deviator stress was somewhat lower, and the corresponding strain clearly lower.
- In Calcigel specimens the deviator stress was clearly lower, but the corresponding strain was approximately the same.

In specimens of Asha505 and MX-80 the influence of position could be evaluated and while no influence was seen on the deviator stress the corresponding strain was higher at the outermost position (at 80 mm) of these two materials. For more details see Svensson et al. (2023).

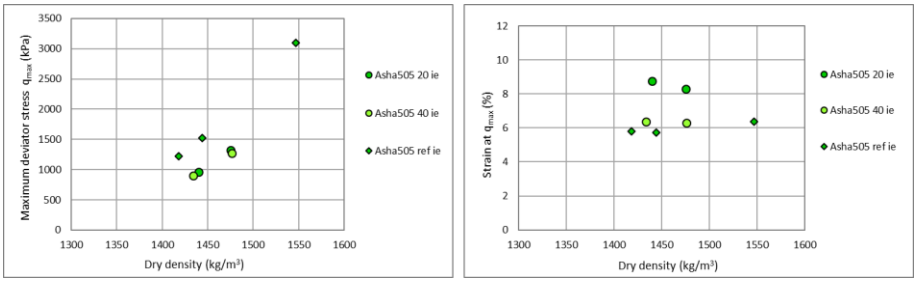

Figure 9.15. Maximum deviator stress and corresponding strain from unconfined compression tests on specimens of Asha505 from block 16 and from the reference material. In the labels the distance from the heater is given in mm and ie denotes that the specimens were ion-exchanged to be calcium dominated.

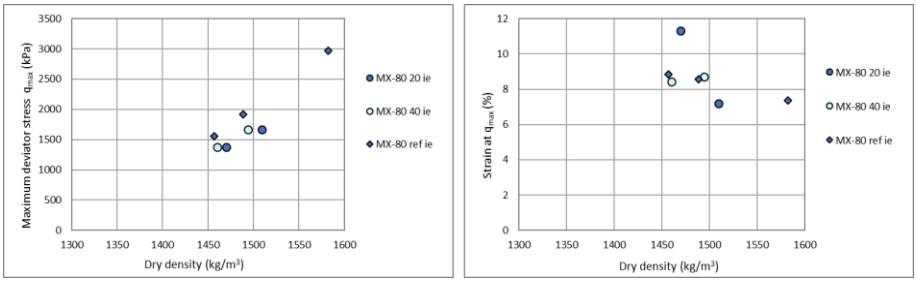

Figure 9.16. Maximum deviator stress and corresponding strain from unconfined compression tests on specimens of MX-80 from block 20 and from the reference material. In the labels the distance from the heater is given in mm and ie denotes that the specimens were ion-exchanged to be calcium dominated.

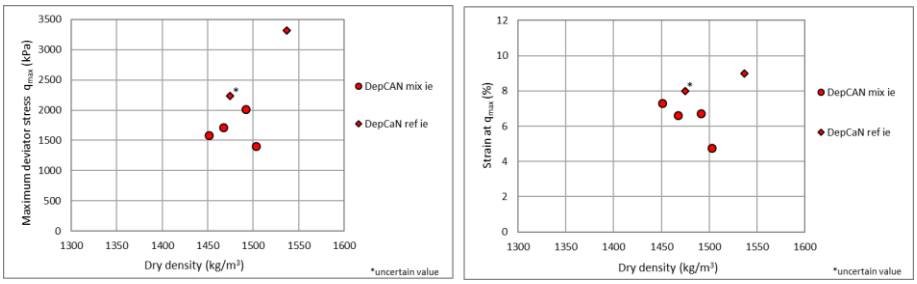

Figure 9.17. Maximum deviator stress and corresponding strain from unconfined compression tests on specimens of Deponit CA-N from block 26 and from the reference material. The specimens were ion-exchanged to be calcium dominated (ie).

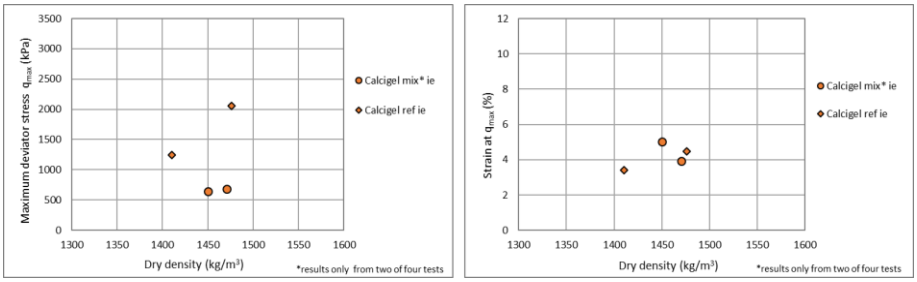

Figure 9.18. Maximum deviator stress and corresponding strain from unconfined compression tests on specimens of Calcigel from block 27 and from the reference material. The specimens were ion-exchanged to be calcium dominated (ie).

9.5.2 Samples ion exchanged to Ca-form

Compared to the references lower maximum deviator stress was seen in all materials (Figure 9.19-Figure 9-22). No large differences in the corresponding strain compared to the references, however with a large scatter for examples of higher strain (Asha505) and lower strain (Deponit CA-N). For more details see Svensson et al. (2023).

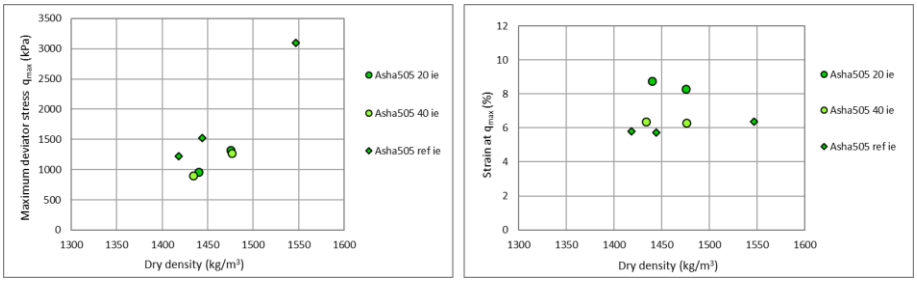

Figure 9.19. Maximum deviator stress and corresponding strain from unconfined compression tests on specimens of Asha505 from block 16 and from the reference material. In the labels the distance from the the heater is given in mm and ie denotes that the specimens were ion-exchanged to be calcium dominated.

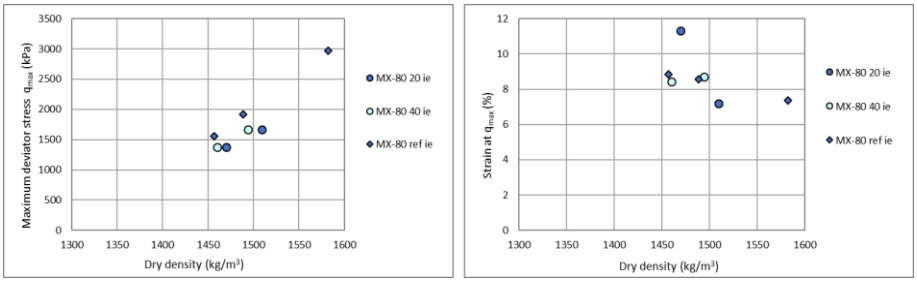

Figure 9.20. Maximum deviator stress and corresponding strain from unconfined compression tests on specimens of MX-80 from block 20 and from the reference material. In the labels the distance from the heater is given in mm and ie denotes that the specimens were ion-exchanged to be calcium dominated.

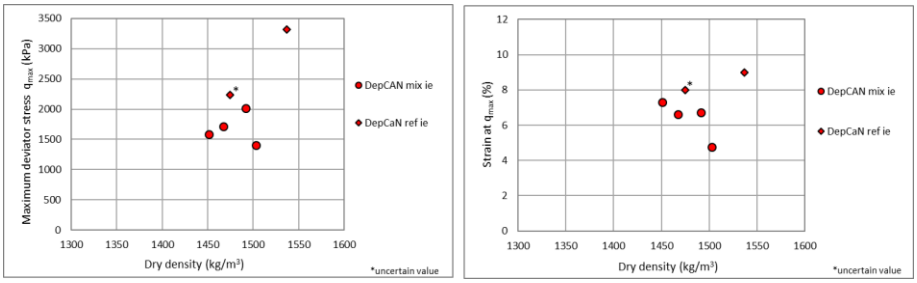

Figure 9.21. Maximum deviator stress and corresponding strain from unconfined compression tests on specimens of Deponit CA-N from block 26 and from the reference material. The specimens were ion-exchanged to be calcium dominated (ie).

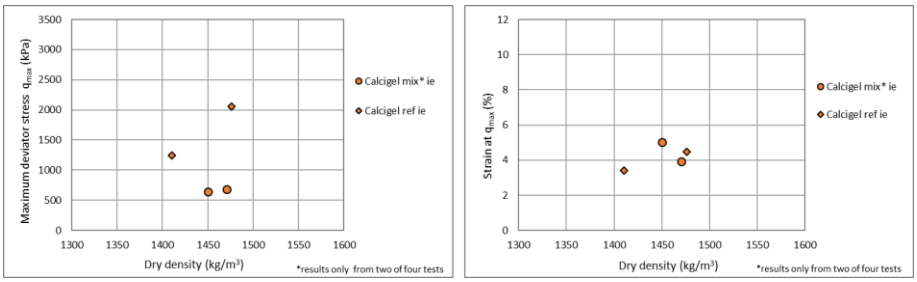

Figure 9.22. Maximum deviator stress and corresponding strain from unconfined compression tests on specimens of Calcigel from block 27 and from the reference material. The specimens were ion-exchanged to be calcium dominated (ie).

9.6 Conclusion

Regarding the chemical and mineralogical investigations, only minor changes could be observed in ABM5 experiment, with the exception of the general moderate drop in CEC in bulk samples from the field, and on the contrary, moderate increase in CEC of the clay fractions (< 2 µm). This is possibly due to aggregate formation in the bulk samples upon the high temperature drying, and the clay fractions were possibly activated by the ultra-sonic treatment during the sample preparation.

No significant changes could be seen on the important safety functions swelling pressure and hydraulic conductivity after the ABM5 experiment.

Compared to the references lower maximum deviator stress was seen in all materials during unconfined compression tests. A lower maximum deviator stress means that the shear strength of the material will be lower. Heating under these conditions seems to make the material softer.

Commenté [LJ15]: In which way will the shear strength be influenced due to this observation and does it have any safety relation? Need a bit more explanation.

The most dramatic impact from the high temperature so far was on the bentonites physical state as many blocks fractured and some even disintegrated during the experiment. This is perhaps the most alarming observation at this point, but further evaluation of the chemical and mineralogical data may show further details that can be of importance.

When ABM5 field samples were compared to the references (after Ca-exchange and washing with DI - water to remove excess salt) a lower maximum deviator stress was seen in all materials. The exchange

to Ca and washing process removed any effects due to cation exchange and/or salt accumulation. For more details see Svensson et al. (2023).

10. ÚJV (SÚRAO)

10.1 Introduction

The aim of the research is to determine a possible temperature impact on mineralogical, geochemical and hydraulic-mechanical properties of bentonite after thermal loading at the temperature of 150 °C. Within the research, several experiments have been performed: X-ray diffraction (XRD), thermal analysis with evolved gas analysis, expandable structures, aqueous leachates, Cs sorption, cation exchange capacity (CEC) and exchangeable cations, specific surface area (SSA), free swelling, saturated hydraulic conductivity (K_s) and water retention curves (WRC). Moreover, two microbiological experiments have been conducted for describing microbiological activity: quantitative polymerase chain reaction and next-generation sequencing. Two types of specimens - bentonite thermally loaded in a dry state and bentonite thermally loaded in a form of a suspension in water - were sampled after 6, 12 and 24 months of thermal loading to capture the time evolution of the observed characteristics. Only input sample, 6-month and 12-month dry samples were subjected to all experiments mentioned above; the rest were subjected to XRD, expandable structures, CEC and exchangeable cations, SSA, K_s, and WRC as originally planned.

10.1.1 Material

The bentonite used in the research is Czech Mg/Ca bentonite from Černý vrch deposit (for more details see (Červinka R., 2018). The bentonite is provided to ÚJV by CTU.

10.1.2 Research plan

Research on two types of specimens was planned: bentonite thermally loaded in a dry state (powder) and bentonite thermally loaded in a form of a suspension in water, both at the temperature of 150 °C. Three time-steps had been chosen: 6, 12 and 24 months. The results were compared to unloaded bentonite (designated as BCV_IN).

All samplings of thermally loaded bentonites have been done by CTU and the samples were shipped to ÚJV. All experiments have been finished now.

Table 10.1 ÚJV – geochemical *and geotechnical characterisation*

10.1.2.1 Material (BoM item): BCV bentonite (Ca-Mg type), powder as delivered by producer
10.1.2.2 Material treatment (sample preparation for test and loading procedure): Two sources of material were used: laboratory treated and samples from T3.3 10.1.2.2.1 Laboratory treated material Two types of treatment were used: • ”Dry“ - powder material was placed into 150 °C (drying allowed) • “Wet“ - bentonite water suspension was placed into 150 °C (drying prevented) Loading lasted 6, 12 and 24 months (e. g. 3 campaigns were planned). Wet samples were dried and milled after treatment as part of test preparation. 10.1.2.2.2 Material from T3.3 Samples obtained from experiments in Task 3.3
10.1.2.3 Temperature (to which material was/will be exposed to) and exposure time 150 °C for 6, 12 and 24 months
10.1.2.4 Tests carried out (name, description, sample preparation, procedure, results): X-ray diffraction, expandable structures, thermal analysis with evolved gas analysis, aqueous leachates, Cs sorption, cation exchange capacity and exchangeable cations, specific surface area, free swelling, saturated hydraulic conductivity, water retention curves, quantitative polymerase chain reaction and next-generation sequencing. The tests are described in 10.2.
10.1.2.5 Schedule and expected date(s) of results delivery: Treatment start: M6/M14 First batch ready for tests M12/M20 → results M15/M23 Second batch ready for tests M18/M26 → results M24/M30 Third batch ready for tests M30/M38 → results M36/M42

10.2 Procedures

Sampling

During the sampling in CTU, a thin layer of bentonite with visibly different colour was observed on the surface of the bentonite powder (see Figure 10.1). It was taken as a separate sample, nevertheless, most of the experiments could not be performed due to very limited amount of the sample.

Figure 10.1 Bentonite sampling

Mineralogical and geochemical characterisation

Bentonite powder samples have been subjected to various determinations, which have provided insight into geochemical properties such as the composition of major minerals, the identification of gaseous products evolved upon heating or soluble phases released on contact with water. Cation exchange capacity (CEC), specific surface area (SSA), and caesium sorption determination were selected to characterise the clay component in bentonite.

Powder X-ray diffractometry (XRD) was conducted on an Empyrean 3rd generation diffractometer (Malvern-PANalytical, NLD) with the following measurement conditions: Co-K_α radiation, a PIXcel3D detector, a range 3.5-105° 2θ, a step of 0.026° 2θ, and a total counting time of 5.25 h. Randomly oriented powder mounts and clay fraction (oriented and glycolated specimens) were analysed. The glycolated specimens were analysed immediately after glycolation in a range of 3.5-65° 2θ and a step of 0.026° 2θ. Minerals were identified employing High.Score Plus 4.8 (PANalytical, NLD) software and PDF-4+ 2020 database. Quantitative analysis was performed using a graphical user interface Profex v.4.2.1.

Analysis of expandable structures was conducted via PXRD on a Bruker D8 Advance diffractometer with the following measurement conditions: Cu-K_α radiation, LynxEye XE detector, automatic divergence slits, Goebel mirror. Air-dry and glycolated specimens were analysed, minerals were identified using Sybilla (McCarty et al., 2009) software.

Thermal analysis with evolved gas analysis (TA-EGA) was performed on SetSys Evolution's apparatus (Setaram, FRA). The weight of the as-received samples was approximately 10 mg. Bentonites were studied under an argon atmosphere (flow of 60 mL/min) in α-Al_2O_3 crucible. The heating rate was set to 10 °C/min in the temperature range of 30-1000 °C. Gases that evolved during heating were analysed with quadrupole mass spectrometer QMG 700 (Pfeiffer Vacuum, DEU) connected to a thermal analyser through SuperSonic System (Setaram, FRA). Specific fragments corresponding to water, carbon dioxide, and sulphur oxides were recorded.

The soluble salts were identified based on aqueous leachates. The dried (105 °C) samples were contacted with deionised water (40 mL) at three solid-to-liquid ratios for seven days. The suspensions were centrifuged, and supernatants were filtered using a 0.2 μm syringe filter. The main cations and bicarbonates in the filtrates were analysed using atomic absorption spectrometer SavantAA (GBC Scientific Equipment, AUS) and titrator Titralab TIM800 (Radiometer Analytical, USA), respectively. The concentration of sulphates, chlorides and fluorides was determined by ion chromatography (ALS Global, CZE).

The highest solid-to-liquid ratio was also tested for caesium sorption. After seven days of shaking the bentonite suspension of 200 g/L, aliquots of CsCl spiked with ^{134}Cs were added and let interact for another seven days. Two initial caesium concentrations of spiking aliquots (0.001 mol/L and 6.4 mol/L) were chosen. Aliquots from supernatants, separated by centrifugation, were determined for ^{134}Cs activity on gamma counter 1480 Wizard 3 (Perkin Elmer, USA). Blank samples (without solid phase) were

prepared and processed in the same way to evaluate the distribution coefficient of Cs. Each sorption experiment under the given conditions was performed in duplicate.

The CEC and exchangeable cations were determined by the Cu(II)-triethylenetetramine (Cu-trien) method. Cu-trien (0.01 mol/L) was mixed with dried (105 °C) samples in the solid-to-liquid ratio of 25 g/L. After interaction for 30 minutes, the suspensions were centrifuged, and supernatants were analysed. The Cu^{2+} concentration was determined by UV/Vis spectrophotometer Specord 205 (Analytik Jena, DEU). The concentration of displaced cations (Na^{+}, K^{+}, Ca^{2+}, and Mg^{2+}) was determined by atomic absorption spectrometer SavantAA (GBC Scientific Equipment, AUS). Two values of cation exchange capacity were derived: CEC_{Vis} from copper depletion and CEC_{SUM} by summing equivalent concentrations of displaced cations.

The specific surface area (SSA) was determined based on the sorption of ethylene glycol monoethyl ether (EGME). 1 g of bentonite powder (dried at 105 °C) was mixed with 2 mL of EGME and equilibrated in a desiccator with $CaCl_2$-EGME solvate. The applied procedure consisted of regular desiccator evacuation and monitoring of the samples until a constant weight was reached. The SSA was derived from the mass ratio of adsorbed EGME and dried bentonite sample.

Geotechnical characterisation

Free swelling tests, determination of water retention curves (WRC) and saturated hydraulic conductivity were selected for geotechnical characterisation. Free swelling tests were performed with 10 mL deionised water and 0.6 g powders (previously dried at 105 °C). This solid-to-liquid ratio allows a better determination of the swell index in graduated cylinders for low swelling materials (such as Ca- and Mg-bentonites) than the standard ratio of 0.02 g/L.

Bentonite dry densities of 1400, 1600 and 1800 kg/m^3 were chosen for determining saturated hydraulic conductivity and WRC. Bentonite powder was compacted in the cylindrical space of a cell body (diameter of 30 mm, thickness of 15 mm) using a hydraulic press MEGA 11-300 DM1S (FORM+TEST Seidner+Co., DEU). In the WRC experiments, a hole was drilled for placing a wireless sensor (diameter of 17 mm, depth of 6 mm). The compacted sample was closed with end-plates composed of stainless steel fabrics placed on the carbon composite percolator. Three-quarter section views of the experimental cells are shown in Figure 10.2.

(**a**) (**b**)

Figure 10.2 Experimental cell set-up for measuring (a) saturated hydraulic conductivity and (b) water retention curves

Saturated hydraulic conductivity of compacted bentonite was determined according to ISO 17892-11:2019. The cells were placed into a desiccator filled with deionised water. The desiccator was regularly vacuumed for at least two weeks. After water saturation, the cell was connected via pressure hoses to the assembly for measuring saturated hydraulic conductivity consisted of an input and output pressure controller (HPDPC and ELDPC, GDS Instruments, GBR). Hydraulic heads of 5, 8, and 10 MPa were

applied for the dry density of 1400, 1600, and 1800 kg/m^3, respectively. The experiment was terminated when a steady-state water flow was reached. The cell was dismantled, and the actual dry density was determined. The hydraulic conductivity was calculated according to Darcy's law and converted to a referential temperature of 10 °C according to the ISO standard.

The block/sensor method was used to determine WRC. A wireless sensor with its internal memory, Hygrochron iButton (Maxim Integrated, USA), was applied for measuring relative humidity and temperature inside the compacted sample exposed to saturated air with water vapour inside a desiccator filled with water. The cell was regularly weighed until a constant mass was reached. When constant mass was achieved, the cells were dismantled, and the sensors were removed. The measured data of relative humidity and temperature were used to calculate the suction pressure according to the Kelvin equation for each time interval. WRC were then constructed as a dependence between suction pressure and gravimetric water content.

Microbiological characterisation

Cultivation of bentonite suspensions in an anaerobic atmosphere rich in H_2 with subsequent molecular genetic analysis was used for studying microbial survivability in bentonite samples exposed to thermal loading. The bentonite suspensions were prepared from 2 g of naturally wet bentonite powders mixed with 10 mL sterile MilliQ water. Samples were incubated in an anaerobic workstation (Don Whitley Scientific, GBR) under an atmosphere containing 94 % Ar and 6 % H_2 at room temperature. Suspensions were sampled at three different cultivation times, immediately after phases mixing (0 d), after 14 and 28 days, and kept in a freezer until DNA isolation. Zero-point (0 d) samples and BCV_IN samples were prepared in duplicate, whereas the heat-loaded samples in triplicate.

The DNA from the bentonite samples was extracted by DNeasy® PowerMax® Soil Kit (QIAGEN, USA) according to the manufacturer's protocol. The extracted DNA was concentrated and purified by the DNA Clean & Concentrator Kit (Zymo Research, USA) and quantified by a Qubit 2.0 fluorometer (Invitrogen, Life Technologies, USA). One back-ground kit control without the sample was coextracted together with samples in each DNA extraction batch to see the laboratory background and possible contaminations resulting from the kit or the laboratory. The extracted DNA was used to describe the microbial composition in the samples (16S rDNA amplicon sequencing, NGS) and for the relative quantification of microbial biomass in the samples (16S rDNA quantitative PCR).

10.3 Results

XRD

The bulk mineralogical composition of the bentonites is shown in Table 10.2. Bentonite samples are dominated by smectite (montmorillonite, d_{060} ~ 1.50 Å), accompanied by quartz and kaolinite. Of all crystalline phases, illite, goethite, anatase, calcite, aragonite, ankerite, siderite and sanidine were quantified in amount < 5 wt. %. Analcime and augite were detected in very small amounts (< 1 wt. %) in the BCV_0.5_y sample. Smectite content decreased slightly or remained almost unchanged in thermally loaded samples. No significant bentonite alteration in terms of mineral transformation can be established considering the uncertainties of the XRD method, especially when dealing with clay minerals and trace minerals.

After the thermal loading, the diffractograms of the samples (Figure 10.3) show a shifting of some of diffraction lines, of course the most visible change is in the basal reflection (001), for example reflection (002) shifts to higher angles, and reflection (113) shifts to lower angles after heating under dry conditions. On the other hand, negligible shifting has been observed on these 2 reflections for samples heated under wet conditions. During the heating experiments elsewhere, a discrete decreasing of the water layers of the smectite from two water layers (2W), one (1W) to totally dehydrated (0W) [d], has been observed. The same is valid for our experiments, where a fully rehydration of smectite is observed during heating under wet conditions (Figure 10.3, Table 10.2), where basal spacing d_{001} changed from 14.63 to 15.19 Å. As expected, on samples heated under dry conditions a discrete loss of water was

observed (Figure 10.3), for example in sample BCV_0.5y_dry after half year of thermal loading we observe all stages of dehydration, i.e. basal distances corresponding to 2W, 1W and 0W; however in the sample subject to one year of thermal loading only full dehydration is observed; the same is expected for sample after two years of heating, but in this case besides the basal distance of 9.73 Å, an almost negligible reflection with basal distance of 14.28 Å is observed, this one is most probably rehydration of smectite during specimen preparation.

Table 10.2 Semiquantitative XRD analysis of randomly oriented powder mounts (wt. %) and parameter of smectite basal peak; bql – below quantification limit, nd – not detected

phases	BCV_IN	BCV_0.5_y_dry	BCV_1.0_y_dry	BCV_2.0_y_dry	BCV_0.5_y_wet	BCV_1.0_y_wet	BCV_2.0_y_wet
Smectite	72	68	71	72	76	74	76
Quartz	10	10	10	10	9	10	11
Kaolinite-1A	6	8	6	2	4	3	1
Illite-2M1	2	3	3	2	2	3	1
Sanidine	2	3	3	3	1	1	1
Goethite [1]	3	3	3	3	4	4	4
Anatase	2	2	2	2	2	2	2
Calcite	1	1	1	2	1	1	1
Aragonite	1	1	1	1	nd	nd	nd
Siderite	1	1	bql	bql	bql	bql	bql
Ankerite	bql	bql	bql	bql	bql	bql	bql
Augite	nd	bql	nd	bql	bql	bql	bql
Analcime	nd	bql	bql	bql	bql	bql	bql
Total	100	100	100	bql	bql	bql	bql
Basal diffraction d(001) (Å)	14.63	14.60 / 12.01 / 9.76	9.76	14.28 / 9.73	15.19	14.85	15.16

[1] Amount of goethite may be underestimated due to the small size of crystallites.

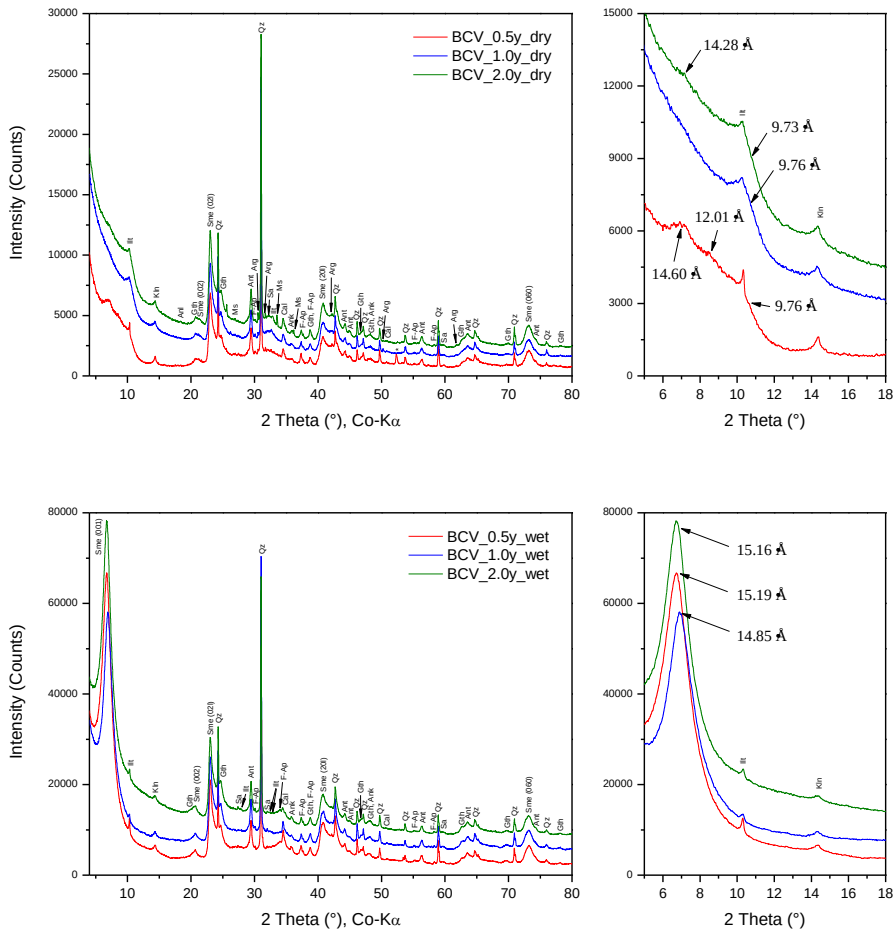

Figure 10.3 XRD patterns of BCV_dry and BCV_wet samples

Expandable structures

No illitization has been proved; percentage of smectite in mixed illite/smectite structures remains the same (80±5 %) in all samples.

TA-EGA

The results of simultaneously performed thermogravimetry (TG) and differential thermal analysis (DTA) supplemented with mass spectrometry identification of evolved gases can be seen in Figure 10.4. Variability of endothermic and exothermic processes in DTA curves suggests a complex composition of BVC bentonite. Four major mass losses were identified from the derivative thermogravimetric (dTG) curves: at approximately 30-200; 200-300; 300-600 and 600-800 °C. Water-related mass losses were found for the first three processes. A shift of 240 °C peak of BCV_IN to higher temperatures was observed for thermally loaded samples. The same shift was also observed in the EGA curves of evolved water. Another difference in the EGA curve for CO_2 can be seen at 105 °C and in the region of 350-550

°C. Very low signal for SO_2 was registered around 800 °C, decreasing in order: BCV_IN > BCV_0.5_y_dry > BCV_1.0_y_dry.

(**a**)

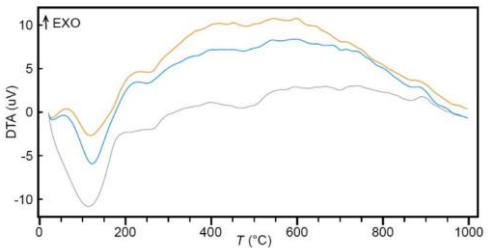

(**b**)

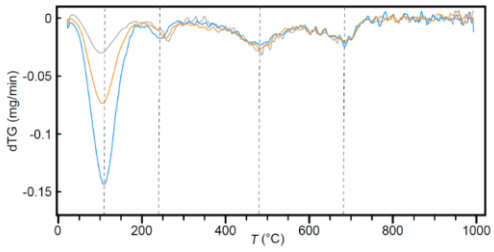

(**c**)

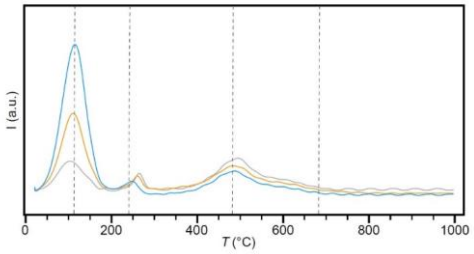

(**d**)

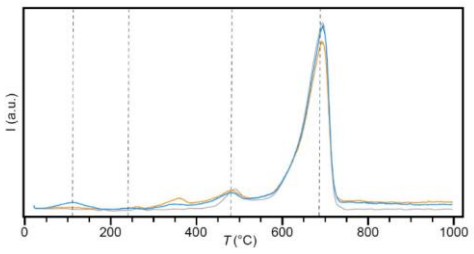

Figure 10.4 TA-EGA. Differential thermal analysis (a), derivative thermogravimetry curves (b) and EGA curves for water (c) and CO2 (d) of the powder samples (BCV_IN blue, BCV_0.5_y_dry orange, BCV_1.0_y_dry grey)

Aqueous leachates

Interaction of bentonite samples with deionised water at three solid-to-liquid ratios resulted in the leachate composition of studied ions presented in Table 10.3. The dominant aqueous species were Na^+ and HCO_3^-. The HCO_3^- source is a dissolution of carbonate phases which are abundant in BCV bentonite. Dissolution of carbonate phases is followed by cation exchange reactions releasing cations, particularly Na^+, into the leachate. The concentrations of all ions increase with increasing bentonite content. Except for chloride and sulphate, all ion concentrations also increase with the heating period of bentonite powder. It follows that the reactivity of soluble phases has changed. The thermal loading somehow affected the bentonite, possibly in terms of mineral transformation or recrystallisation. More considerable changes in bentonite/water reactivity were detected in the first heating period.

Differences in leachable cation concentrations between the heated and input samples were found mostly for calcium, then potassium and magnesium. The released Na^+ concentration is comparable for all materials corresponding to the lowest capability of sodium to compete at smectite exchange sites. Powder heating at 150 °C resulted in the most pronounced increase in leachable fluoride concentrations, up to 2.2 times. The bicarbonate concentration in leachates from the heated samples was a maximum of 1.6 times higher than from the BCV_IN sample. The concentration of leachable SO_4^{2-} decreased with the thermal loading of bentonite powders, indicating a decrease in the solubility of sulphate phases. The concentration of leachable Cl^- increased with the thermal loading of BCV_wet bentonite indicating an increase in the solubility of the chloride under wet conditions. Variation in the total inorganic carbon (TIC, Figure 10.5) indicates possible decay of carbonates well correlating with Ca^{2+} water soluble leachate.

Table 10.3 Aqueous leachates data for the studied BCV samples at three different solid to liquid ratio

Commenté [LJ16]: Table title is separated from the table contents. Redo the format.

Sample no.	s:l (g/L)	c (mM/L)									
		Na^+	K^+	Ca^{2+}	Mg^{2+}	Fe^{x+}	Cl^-	SO_4^{2-}	NO_3^-	F^-	HCO_3^-
BCV_IN	25	1.41	0.13	0.06	0.11	0.00	0.01	0.06	0.00	0.03	1.67
BCV_IN	114	3.80	0.26	0.10	0.23	0.00	0.03	0.25	0.00	0.09	3.75
BCV_IN	202	4.95	0.33	0.13	0.29	0.00	0.05	0.44	0.00	0.10	4.75
BCV_0.5_y_dry	25	1.48	0.26	0.19	0.23	1.26	0.01	0.06	0.00	0.06	2.41
BCV_0.5_y_dry	111	4.06	0.51	0.22	0.36	1.35	0.02	0.23	0.00	0.14	5.06
BCV_0.5_y_dry	197	5.47	0.62	0.27	0.49	1.32	0.04	0.36	0.00	0.16	6.56
BCV_1.0_y_dry	25	1.48	0.32	0.24	0.22	1.25	0.01	0.06	0.00	0.06	2.62
BCV_1.0_y_dry	112	4.06	0.60	0.26	0.33	1.58	0.02	0.21	0.00	0.12	5.18
BCV_1.0_y_dry	202	5.86	0.81	0.33	0.49	1.34	0.04	0.35	0.00	0.14	7.27
BCV_2.0_y_dry	25	1.48	0.31	0.14	0.14	0.00	0.03	0.08	0.00	0.00	2.05
BCV_2.0_y_dry	114	4.14	0.64	0.25	0.32	0.00	0.04	0.24	0.02	0.14	5.07
BCV_2.0_y_dry	194	5.71	0.80	0.33	0.43	0.00	0.06	0.43	0.04	0.20	6.81
BCV_0.5_y_wet	25	1.41	0.22	0.16	0.08	0.00	0.01	0.07	0.00	0.02	1.93
BCV_0.5_y_wet	112	3.36	0.36	0.18	0.10	0.00	0.06	0.28	0.00	0.06	3.56
BCV_0.5_y_wet	200	4.37	0.42	0.21	0.12	0.00	0.11	0.43	0.00	0.04	4.11
BCV_1.0_y_wet	25	1.11	0.17	0.09	0.03	0.00	0.04	0.09	0.00	0.00	1.25
BCV_1.0_y_wet	113	2.62	0.28	0.14	0.06	0.00	0.07	0.26	0.00	0.08	2.39
BCV_1.0_y_wet	195	3.42	0.34	0.18	0.08	0.00	0.12	0.45	0.00	0.13	2.92
BCV_2.0_y_wet	25	1.20	0.19	0.14	0.02	0.00	0.00	0.06	0.00	0.00	2.19
BCV_2.0_y_wet	114	2.89	0.31	0.25	0.03	0.00	0.00	0.18	0.00	0.00	3.68
BCV_2.0_y_wet	210	3.68	0.37	0.28	0.04	0.00	0.00	0.31	0.00	0.00	3.89

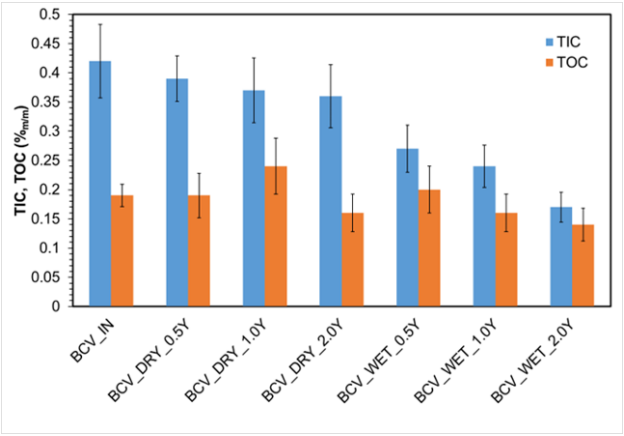

Figure 10.5 Variation in the total inorganic carbon (TIC) and total organic carbon (TOC) in thermally loaded BCV bentonite

Caesium sorption

The used methodology of sorption experiments covered two extremes of the Cs concentration range: 0.0008 and 62 mmol/L of the initial carrier concentration, resulting in the distribution coefficients presented in Table 10.4. In both cases, the lowest decrease in Cs concentration was observed in the supernatant of the BCV_1.0_y_dry sample. This sample contained the largest amount of leachable ions

that may compete in the sorption process. The lowest K_d for BCV_1.0_y_dry could be caused by cation competition or reflects a change of the sorption sites. Cs sorption experiments at a wide concentration range of carrier and competing cations on bentonites, smectite-rich clays, and illite-rich clay identified K^+ as the major competitive cation, followed by Ca^{2+} and finally by Na^+ at low Cs concentration. In our experiments, the main competing cation was Na^+; the concentrations of other competing cations were much lower than those affecting the Cs sorption process. Competition of Cs^+ with leachable cations for sorption sites can also be ruled out in experiments with the applied high concentration, where caesium represents the dominant cation. Decreasing K_d values thus indicate a reduction in the sorption sites for Cs when bentonite powder was thermally loaded.

Table 10.4 Caesium distribution coefficients at two different carrier concentration (low ~ 0.0008 mmol/L Cs, high ~ 62 mmol/L Cs)

bentonite sample	K_d_low (mL/g)	K_d_high
BCV_IN	5322 ± 533	29.28 ± 0.66
BCV_0.5_y_dry	4478 ± 379	28.66 ± 0.65
BCV_1.0_y_dry	2621 ± 164	27.73 ± 0.62

Cation exchange capacity, exchangeable cations, specific surface area

The results of the CEC, exchangeable cations, and SSA measurements are shown in Table 10.5. Both CEC_{vis} and SSA decrease upon heating bentonite at 150 °C in a dry state. The SSA changed substantially after the first heating phase and then lowered less rapidly, the CEC_{vis} steadily declined. Concerning the wet samples, SSA increased compared to the input sample. The sum of exchangeable cations (CEC_{sum}) increase with the heating period of bentonite powder is consistent with the results of the aqueous leachates. Thus, the cation exchange experiment provides summary information about the cation replacements in the smectite interlayers and the interaction of Cu-trien with the sample. The exchangeable cations are summarized in

. Most of the exchangeable sites in BCV bentonite were occupied by magnesium and calcium. The exchangeable cations in thermally loaded samples varied with heating time; magnesium proportion decreased at the expense of calcium. The decrease in Mg^{2+} proportion is more evident in the BCV_wet samples. Sodium remained unaffected upon heating. No measurable amount of displaced iron in supernatants, neither in the CEC determination nor in aqueous leachates, was detected.

Commenté [LJ17]: The figure above repeats itself in the next page. Need to be deleted.

Table 10.5 Cation exchange capacity, exchangeable cations, and specific surface area data

bentonite sample	CEC_{VIS} (meq/100 g)	CEC_{SUM} (meq/100 g)	Ca^{2+} (%)	Mg^{2+} (%)	Na^+ (%)	K^+ (%)	SSA (m^2/g)
BCV_IN	59.9 ± 2.6	62.0 ± 3.9	26.0	57.7	13.5	2.8	478 ± 4
BCV_0.5_y_dry	55.0 ± 2.4	59.1 ± 2.1	36.5	47.2	11.8	4.4	437 ± 4
BCV_1.0_y_dry	50.9 ± 1.3	58.5 ± 1.9	38.5	45.0	11.7	4.9	423 ± 3
BCV_2.0_y_dry	53.7 ± 0.1	57.9 ± 0.9	40.3	43.8	10.5	5.4	416 ± 2
BCV_0.5_y_wet	60.4 ± 1.3	65.0 ± 0.9	53.4	31.1	11.8	3.7	487 ± 8
BCV_1.0_y_wet	64.8 ± 0.5	64.8 ± 6.3	58.9	27.6	9.6	3.9	500 ± 7
BCV_2.0_y_wet	69.8 ± 0.1	63.0 ± 0.1	74.0	11.3	10.8	3.9	500 ± 5

Geotechnical parameters

Free swelling of dried powders in water resulted in different volumes of swollen material. Steady-state volumes of BCV_IN, BCV_0.5_y and BCV_1.0_y were 4.8, 2.1 and 1.8 mL, respectively.

Table 10.6 and Figure 10.6 present the results of saturated hydraulic conductivity measurements. The samples thermally loaded in a dry state showed higher saturated hydraulic conductivities; the wet samples, on the contrary, showed lower saturated hydraulic conductivity.

Table 10.6 Saturated hydraulic conductivity Ks data for studied samples at actual bentonite dry density

bentonite sample	ρ_d (kg/m^3)	K_s (m/s)
BCV_IN	1420	$2.8 \cdot 10^{-13}$
	1581	$1.0 \cdot 10^{-13}$
	1784	$4.2 \cdot 10^{-14}$
BCV_0.5_y_dry	1427	$3.7 \cdot 10^{-13}$
	1605	$1.2 \cdot 10^{-13}$
	1730	$6.0 \cdot 10^{-14}$
BCV_1.0_y_dry	1434	$4.1 \cdot 10^{-13}$
	1587	$1.6 \cdot 10^{-13}$
	1711	$6.1 \cdot 10^{-14}$
BCV_2.0_y_dry	1429	$3.9 \cdot 10^{-13}$
	1611	$1.4 \cdot 10^{-13}$
	1742	$4.7 \cdot 10^{-14}$
BCV_0.5_y_wet	1393	$3.4 \cdot 10^{-13}$
	1598	$8.6 \cdot 10^{-14}$
	1744	$4.8 \cdot 10^{-14}$
BCV_1.0_y_wet	1397	$2.6 \cdot 10^{-13}$
	1624	$8.7 \cdot 10^{-14}$
	1751	$3.5 \cdot 10^{-14}$
BCV_2.0_y_wet	1388	$4.7 \cdot 10^{-13}$
	1602	$1.2 \cdot 10^{-13}$
	1767	$6.7 \cdot 10^{-14}$

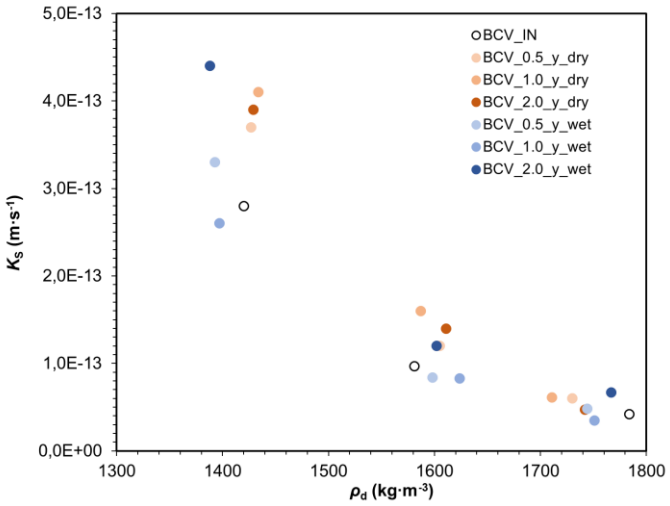

Figure 10.6 Saturated hydraulic conductivity

Water retention curves are displayed in Figure 10.7; wetting paths are depicted with full symbols, drying paths with empty symbols. Drying paths of the retention curves of all samples were similar to each other. Wetting paths, which were measured at first, however differed depending on the way of the thermal loading: whereas the wetting paths of the unloaded samples and wet samples were similar to the drying paths, the wetting paths of the dry samples were significantly shifted towards lower suction pressures. This trend was more significant for lower water content. Thermal loading time seems to have only a minor impact, as the difference between individual thermally loaded samples are not significant.

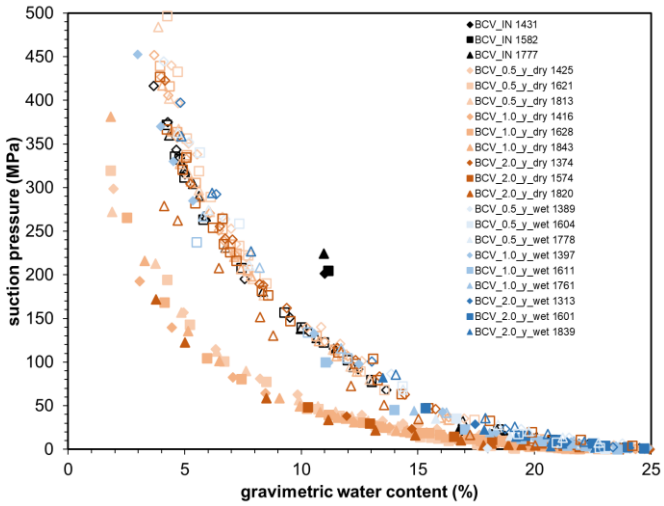

Figure 10.7 Water retention curves of bentonite samples (wetting paths are depicted with full symbols, drying paths with empty symbols, the number correspond to the samples' actual dry densities)

Microbiological characterisation

Generally, the DNA extraction resulted in very low DNA yields, as revealed by Qubit measurement. Therefore, the qPCR method by 16S rDNA marker was used to better distinguish between the samples and estimate the changes in gene copy number in the studied samples. The quantification cycle (Cq) values were related to the Cq values of freshly mixed suspensions (0 d) for each bentonite powder to quantify the magnitude of relative change in gene copy numbers. The PCR efficiency for the 16S rDNA marker was estimated beforehand by measuring the slope of curves constructed from a serial dilution of template DNA from several environmental samples. Relative quantification, displayed in Figure 10.8, showed an increase in the relative abundance of 16S rDNA copies in all samples after 28 days of cultivation in anaerobic conditions. The relative increase varied among samples. The highest relative increase was detected in BCV_0.5_y samples after 28 days of cultivation. A slightly lower relative increase was found for BCV_IN. The lowest relative increase in the gene copies was determined for BCV_1.0_y. Our data also show that the 14 days recovery time for restoring microbial activity from dormant stages is insufficient for most samples.

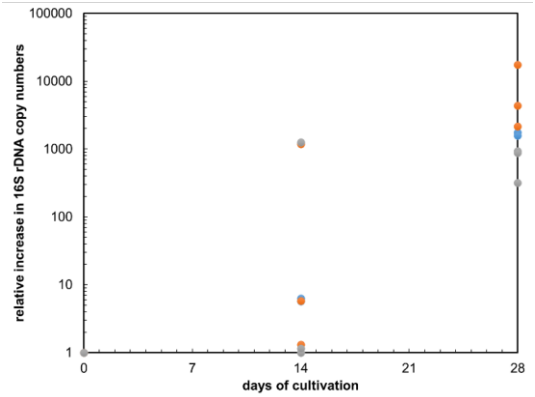

Figure 10.8 qPCR analysis of the 16S rDNA gene in anaerobically cultivated bentonite suspensions (IN blue, 0.5_y orange, 1.0_y grey)

NGS sequencing technique enabled describing the microbial composition in the suspensions. The results of NGS sequencing (see Figure 10.9) were consistent with the qPCR analyses. The low NGS signal was found for the studied samples with low 16S rDNA copy numbers and microbial abundance.

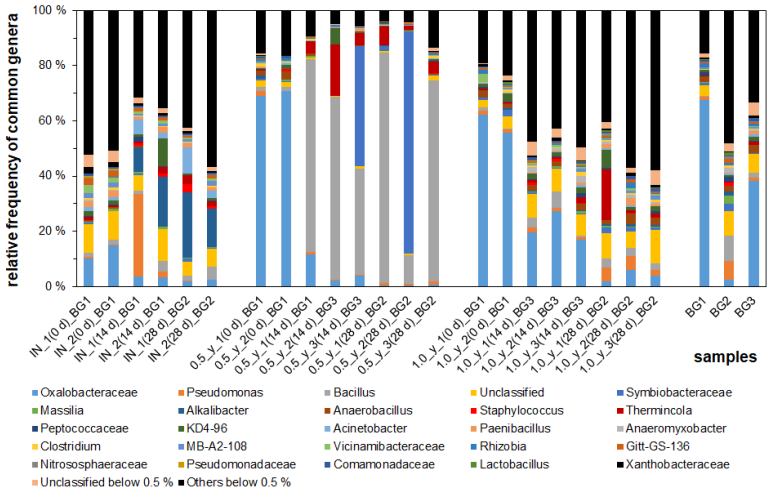

Figure 10.9 Relative abundance of detected microbial genera by NGS sequencing. The sample notation reflects the number from replicates, the cultivation time and background (BG) controls coextracted with each batch

Various facultative anaerobic nitrate-reducing (NRB) genera such as *Alkalibacter, Acinetobacter, Bacillus, Pseudomonas, Paenibacillus, Symbiobacterium* or *Massilia* or iron-reducing (IRB) genus *Thermincola* were detected in BCV_IN samples. All these genera are typical for Czech Mg/Ca bentonite [38]. Much lower genera diversity was found in the BCV_0.5_y samples. After 14 or 28 days of cultivation, the suspensions contained mostly the NRB genus *Bacillus* or the IRB genus *Thermincola*. In the samples 0.5_y_3(14 d)_BG3 and 0.5_y_2(28 d)_BG2, the presence of an unspecified bacterial clone from the family *Symbiobacteraceae* was detected. Sequencing of DNA from BCV_1.0_y samples

resulted in poor NGS results. Only sample 1.0_y_1(28 d)_BG2 showed an increased frequency of the thermophilic genus *Thermincola* compared with the background controls (BG) coextracted with the samples. This result indicates that although the relative increase in 16S rDNA copy numbers in the BCV_1.0_y samples cultivated for 28 days was detected, this increase did not result in sufficiently high absolute gene copy numbers for successful NGS analysis. Microbial composition of all zero-point samples was similar to the pattern detected in coextracted background controls (0 d) compared with BG1, 1.0_y_1,2,3(14 d)_BG3 compared with BG3 and 1.0_y_1,3(28 d)_BG2 compared with BG2, which reflects their very low DNA content.

10.4 Conclusion

The results of all analysis show that the thermal loading of a dry powder with a temperature of 150 °C causes a deterioration of the monitored parameters. The decrease of the cation exchange capacity correlates well with the decrease of specific surface area. Given that the mineralogical composition and illite/smectite ratio have not significantly changed, it can be presumed that these decreases are given by the changes within montmorillonite layer structure, probably collapsing of some of the montmorillonite interlayer spaces connected to the smectite dehydration. However, the results of cation exchange capacity and specific surface area of the wet samples, as well as the results of measuring the saturated hydraulic conductivity and especially the water retention curves of both dry and wet samples indicate that the changes are at least partially reversible. The impact of thermal loading on the bentonite composition was registered by aqueous leachates, TIC and TA-EGA mainly for carbonate phases, then for sulphates and fluorides. Thermal loading caused decrease in caesium distribution coefficients as well; it also resulted in a reduction of microbial survivability and thus affected possible future microbial activity in bentonite.

The results of all the analysis of the wet samples show little or none difference compared to the thermally unloaded bentonite and if so, the results were even better than in the unloaded bentonite. It can be presumed thus that the deterioration of the monitored parameters is given not by the temperature itself, but probably by the loss of the water content induced by the elevated temperature.

11. VTT

11.1 Introduction

The main objective of VTT's research is to characterize the effect of heat treatment of bentonite on its mechanical elastoplastic properties, more specifically compressibility (when the pressure component of the stress of the material changes) and shear behaviour (in isochoric conditions).

11.1.1 Material

The basic material is Wyoming Na-bentonite (with tradename BARA-KADE) powder as provided by the manufacturer.

11.2 Procedures

11.2.1 Sample preparation and test procedures

The developed sample preparation procedure introduces a fully controlled bentonite sample production method from powder to a final solid sample to be used in volumetric compression and triaxial shear experiments (Figure 11.3). The process starts with powder heat treatment and wetting to desired water content. In the experiments, three batches of bentonite powder were prepared. One was heat treated in an oven in 105 °C, the second in 150 °C and the third was reference batch, which was left untreated. The treated and untreated batches can be wetted into a wanted water content either by a water vapour equilibrium technique or mechanical mixing to liquid water. In the first one bentonite powder is placed inside a Sicco Star-Vitrum desiccator cabinet with a supersaturated saline solution on the bottom of the cabinet. The solution creates a specific relative humidity inside the closed environment and the bentonite sets into equilibrium with the atmosphere by absorbing or desorbing water. This method minimizes mechanical disturbances and dissolution of side minerals to the material but takes several months to complete. The alternative wetting method uses a stirrer to mix a fine water spray to the powder. The production volume of this method is limited but allows wetting of smaller powder sets very rapidly. The latter method was used in the experiments.

According to the original plan, the hydraulically actuated triaxial measurement system (GDS Instruments HLF 250 kN load frame with 32 MPa triaxial cell, Figure 11.1) was to be used to compact pre-samples and to perform isotropic compression on the material during compaction (step 3 in sample preparation). The used cell fluid is low viscosity silicon oil (Julabo H10 Thermal fluid) which allows also above 100 °C temperatures. The aim of the isotropic compression tests is to obtain data on the volumetric elastoplastic behaviour of bentonite. In order to separate the plastic and elastic deformations, the test are conducted cyclically such that the pressure is increased in steps, 2 MPa per minute finally up to 32 MPa, and the pressure is relaxed to zero between the steps. Pressure-volumetric data is collected throughout the compaction.

Commenté [LJ18]: tolerates?

Reliability issues combined to the worldwide supply chain disturbances followed from COVID-19, as well as simultaneously updating to the triaxial system to enable high temperature (also other updates), developing shear test procedures, and producing volumetrically compacted samples have meant that the device has been out of operation for volumetric compaction for prolonged periods. As mitigation action to this realised risk, it was decided to build a volumetric compaction cell that can be fully maintained by our own resources. This was performed successfully with a tight schedule, but has taken resources from the rest of the project work. The basic functioning of the system with respect to volumetric compaction is similar to the original one but it uses degassed water as the compression fluid in a 100 MPa tolerated pressure vessel. The water used for the compression is degassed by cavitation in a deaerator tank and vacuum is created inside the tank with a vacuum pump. Degassed operating water is transferred and stored inside another vacuum tank. The pressure vessel is supplied with operating water from the storage tank and cyclic compaction is executed with a FloxLab BTSP-series high pressure syringe pump.

Figure 11.1 The triaxial device (left) and the self-built alternative experimental system for isotropic compaction (right).

After compaction the pre-samples were machined to a fixed size and shape using a lathe. The final form of the samples is a 100 mm tall cylinder with a 50 mm diameter. The samples are stored in vacuum while waiting for further tests to prevent reactions with the surrounding atmosphere.

Cyclic isochoric shearing of the final samples is performed with the GDS Instruments triaxial cell at a constant sample pressure of 0-12 MPa. The aim of the shear tests is to obtain data on the shear elastoplastic behaviour of bentonite. In order to separate the plastic and elastic deformations, the shear stress is increased cyclically stepwise such that the shear stress is relaxed close to zero between the steps. The test cycles are performed relatively fast (in minutes) in order to avoid adsorbed water diffusion within the samples. Axial stress is applied to the sample with a piston and the pressure component of stress is kept constant by decreasing the cell pressure while the axial strain increases. Measuring the volumetric change is inaccurate, but if the pressure component of stress is constant, the sample volume should not change.

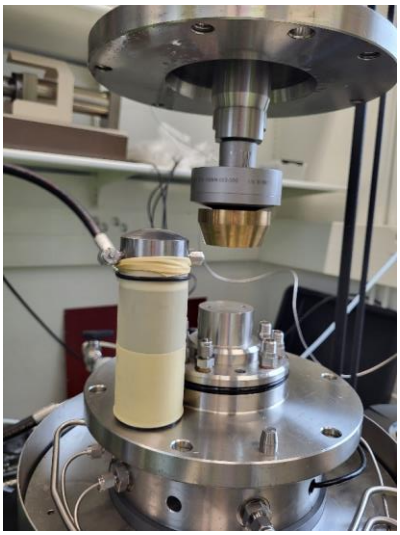

Figure 11.2 Setup for the isochoric shearing tests.

The volumetric and shear triaxial systems are calibrated with steel and PVC dummies to exclude the deformation of the equipment from the deformation of the sample. The calibration data is collected of similar test cycles as the actual experiments for both the isotropic compression and shear tests.

The sample preparation and experimental procedure is summarized to the following steps (see also Figure 11.3):

1. Heat treatment
    a. Batches of bentonite powder in oven in 105 °C and in 150 °C for six months.
    b. No heat treatment for reference samples.
2. Saturation to desired water content by
    a. Water vapour equilibrium: The powder is saturated to a desired water content by placing it to a desiccator cabinet with controlled relative humidity for suitably long period of time
        i. The method is used to
            1. minimise dissolution of side minerals (to prevent possible cation exchange)
            2. minimise mechanical disturbances (no mixing needed)
            3. allow wetting of larger batches at a time
    b. Mixing: The powder is mechanically mixed to liquid water to reach a wanted water content
        i. The method allows much faster wetting of the material but the volume is limited
        ii. The same water content is used for heat treated and reference samples
3. Compaction of pre-samples with isotropic pressure in with the volumetric compaction device or with the triaxial cell
    a. The powder is first de-aired with a vacuum pump.
    b. Volume deformation is measured while compaction.

   c. Cyclic compression to be able to differentiate between elastic and plastic deformations.
      i. The pressure steps are for example 0-2-0-4-0-8-0-16-0-32 MPa, but the exact steps vary by sample. The compaction rate is 2 MPa per minute with the triaxial cell.

4. Machining the pre-samples
   a. Machining the samples to correct shape and size for shearing experiments
   b. Sample size: 50 mm diameter and 100 mm height
5. Quality control
6. Shearing tests
   a. Cyclic loading/unloading to be able to differentiate between elastic and plastic deformation.
   b. With the triaxial device.

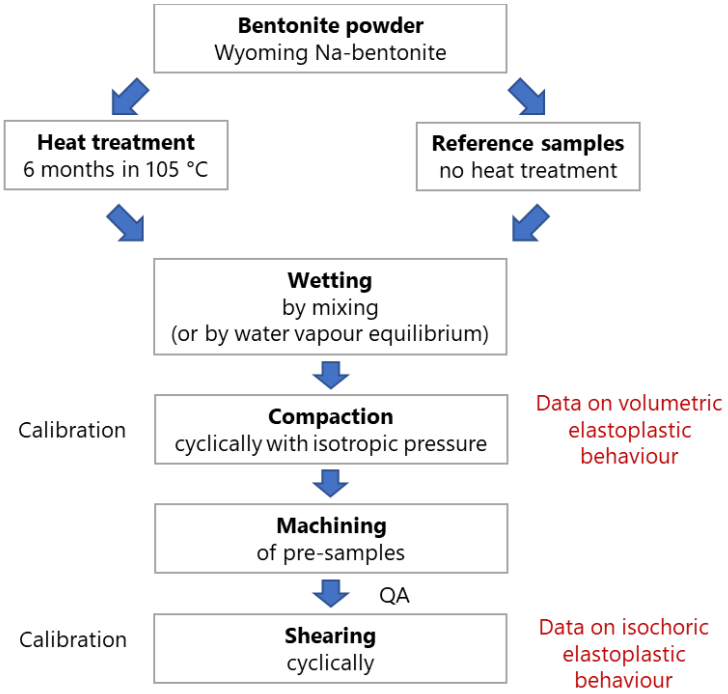

Figure 11.3 Experiment process flowchart.

11.2.2 Sample treatment and conditions

Two batches of BARA-KADE were heat treated for the experiments, one for 6 months in 105 ˚C and one for 6 months in 150 ˚C. Six samples of each and six reference samples without a heat treatment were wetted by mixing to a 17 w% water content which is the bentonite average installation moisture in the Posiva final disposal engineered barrier system. The moisture content of a wetting set was confirmed by drying a sample amount in 105 ˚C for 24 hours. Minor variation between wettings was observed due

to the wetting method used. The series of six samples each was chosen to get a comprehensive amount of comparable data from the cyclic isotropic compression and isochoric shearing tests.

The samples were compacted using the self-built volumetric compaction device to a dry density of 1600 kg/m^3, the dry density upper limit of the Posiva application accepted material. The wanted result was reached by cyclic compaction up to 12 MPa, including steps 0-2-4-8-10-11-12 MPa. The compaction system was calibrated with PVC dummy accordingly to exclude equipment deformation from the data. The measured sample water contents and compaction dry densitities of machined samples are presented in Table 11.1.

Table 11.1. Sample types (no heat treatment, or in oven at given temperature for 6 months), mass, water contents and dry densities of machined samples.

Sample type	Compacted pre-sample mass	Water content	Dry density
	(g)	(-)	(kg/m^3)
ref	615.0	0.174	1613
ref	618.5	0.178	1586
ref	607.5	0.174	1603
ref	629.4	0.168	1615
ref	607.9	0.176	1612
105 ˚C	618.9	0.164	1643
105 ˚C	633.9	0.164	1638
105 ˚C	624.6	0.164	1627
105 ˚C	633.9	0.167	1640
105 ˚C	630.2	0.164	1617
150 ˚C	617.9	0.169	1618
150 ˚C	633.1	0.169	1617
150 ˚C	629.2	0.169	1601
150 ˚C	622.2	0.165	1615
150 ˚C	629.0	0.165	1617

Commenté [LJ19]: Change all the “commas” to “periods” for decimal points in this table.

The triaxial shearing experiments are ongoing while writing this deliverable (October 2023).

11.3 Results

11.3.1 Volumetric compaction tests with the triaxial device

An example raw data from isotropic compaction of a reference (non-heat treated) sample with the triaxial cell is illustrated in Figure 11.4. The related calibration data using a steel dummy (with volume shift to zero at the maximum pressure of the cycle) is presented in Figure 11.5 and the final calibrated data in Figure 11.6.

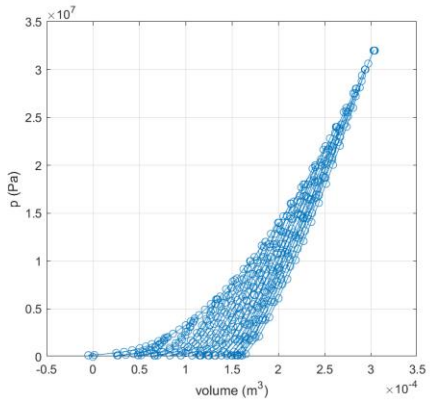

Figure 11.4 Raw data from isotropic compaction of a reference sample.

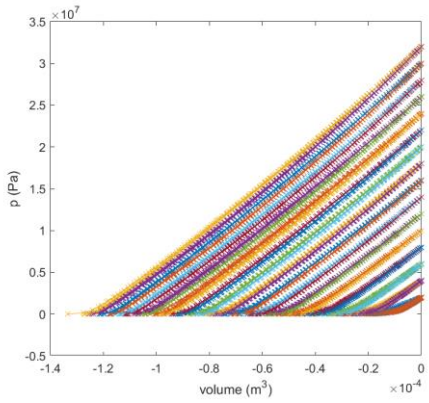

Figure 11.5 An example of collected calibration data from a number of calibration runs.

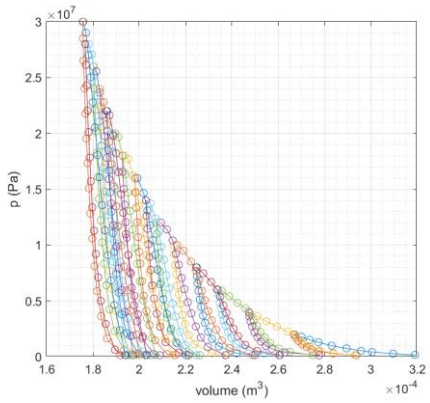

Figure 11.6 An example of final calibrated data of isotropic compaction of a reference sample.

11.3.2 Volumetric compaction of heat treated samples

The samples have been compacted cyclically as illustrated in Figure 11.7., where an example of measured raw data for a 105° C heat treated sample and using the volumetric compaction device is shown. The cell liquid volume increase, which equals to sample volume reduction, is on the x-axis in the graph. The calibration data with PVC dummy and a calibration model fit (cubic spline interpolation) for loading and unloading cycles are illustrated in Figures 11.8. and 11.9.

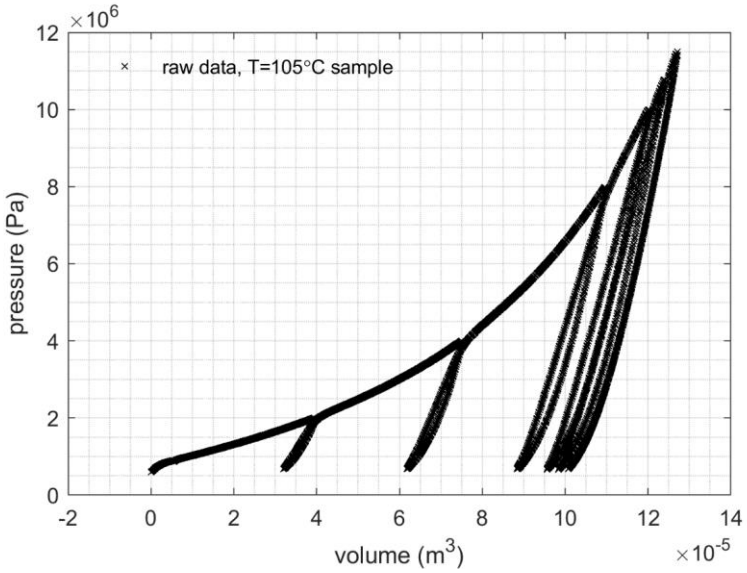

Figure 11.7 An example of measured raw data for a 105° C heat treated sample and using the volumetric compaction device. The cell liquid volume increase (which equals to sample volume reduction) is towards right.

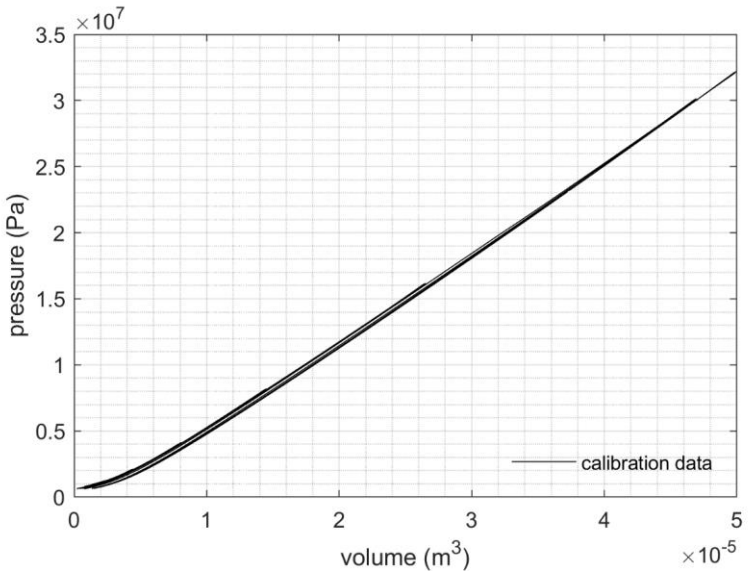

Figure 11.8 Calibration raw data with PVC dummy for the volumetric compaction device. The cell liquid volume increase (which equals to sample volume reduction) is towards right.

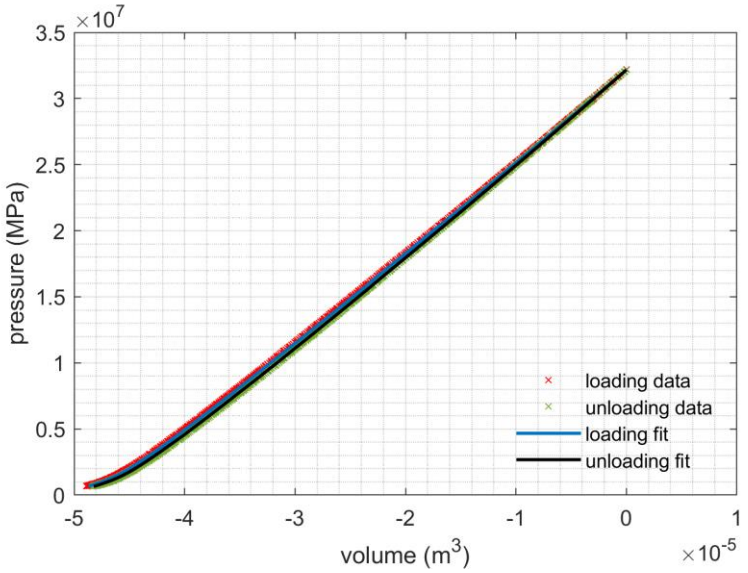

Figure 11.9 The cubic spline calibration functions have been fitted to the loading and unloading calibration data separately. The cell liquid volume increase (which equals to sample volume reduction) is towards right.

The equipment deformation has been reduced from the raw data using the calibration function and the loading and unloading cycles have been separated (see Figure 11.10. for an example). The sample volume change has been reduced from the sample initial volume as powder, which is calculated from the measured compacted sample volume by adding the total sample volume change to it (Figure 11.11.). The elastic deformation during loading, the virgin curve and the plastic deformation have also been separated.

Similarly treated data has been collected from all the samples (reference, heat treated at 105° C and 150° C) in Figure 11.12. It can be noticed that there is scatter in the data, but any of the batches cannot be distinguished from each other. Consequently, based on the experiments, it seems that the heat treatment as powder does not affect the volumetric compression properties of bentonite. The scatter in the data due to small variations in the water contents, the variations in powder composition and the measurement accuracy seems to have more effect on the results than the heat treatment.

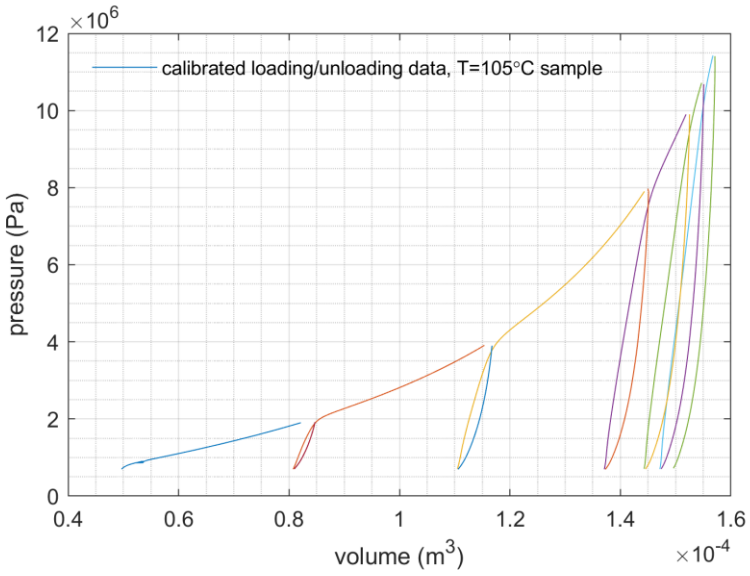

Figure 11.10 The loading and unloading stages have been separated from the calibrated data for the 105° C heat treated sample. The cell liquid volume increase is towards right.

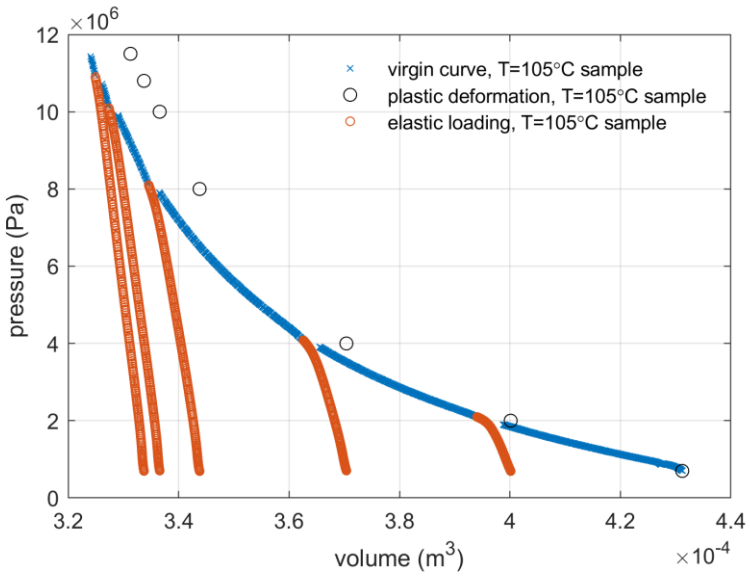

Figure 11.11 The 105° C heat treated sample volume versus compaction pressure during loading cycles. The sample volume changes have been reduced from the initial sample volume (sample volume after the compaction has been measured). The virgin curve and plastic deformation have been separated from the data.

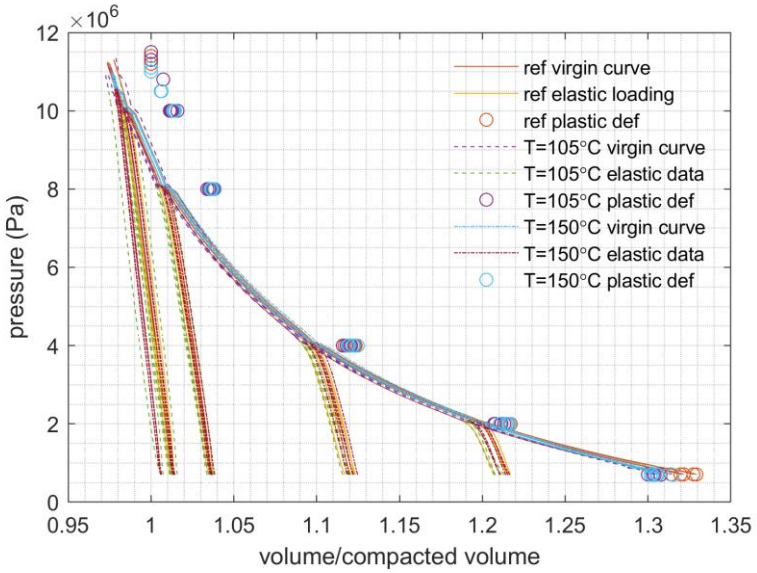

Figure 11.12 The volume versus compaction pressure during loading cycles for 5 reference samples, 5 samples heat treated in 105° C, and 5 samples heat treated in 150° C. The virgin curves and plastic deformations have been separated.

11.4 Conclusions

Sample preparation and experimental procedures for volumetric, isotropic compression and shear test for heat treated bentonite were successfully developed and set up. In addition, a completely new volumetric compaction device was designed, developed and built from components as a mitigation action for problems with the triaxial device, which was originally planned as the only device to be used in this work.

Volumetric compaction of heat treated, water content stabilized Wyoming Na bentonite powder in 105° C and in 150° C as well as unheated, water content stabilized reference material has been successfully performed. The results indicate that the effect of heat treatment as powder is less significant for the volumetric compressibility than small changes in water content or variation material as powder.

The original plan for conducting the experiments with the triaxial device only was hindered by reliability issues combined to the worldwide supply chain disturbances followed from COVID-19 as well as by the simultaneous updating the triaxial system to enable high temperatures (also other updates), developing shear test procedures and producing volumetrically compacted samples. Consequently, the triaxial device has been out of operation for volumetric compaction for prolonged periods. As a mitigation action of this realised risk, a separate volumetric compaction device was successfully built from components with a tight schedule to allow compacting the samples with a separate device, while concentrating on the shear tests and tests at high temperatures with the triaxial cell. The shear tests are on-going while writing this deliverable (October 2023).

12. Conclusions

Material from field and laboratory experiments were included in this Task and reported above. This indeed implied that there were significant differences in the spatial and time scales considered, but even among the laboratory tests there was a large variety of scales and actual conditions of treatment. For example, there were tests in which the bentonite was treated under thermo-hydraulic gradient (ABM and CIEMAT's cell tests) and others in which the bentonite was just heated without simultaneous hydration. Among the latter some were performed with dry bentonite and others with wet bentonite, either allowing evaporation during heating or not. These experimental conditions may have an effect on the changes observed and should be considered when assessing the results.

Compacted bentonite samples that were heated after water saturation in the Alternative buffer material experiment ABM5 were studied by SKB and BGR (KIT). The ABM-tests were conducted to be able to directly compare the performance of different bentonites and clays under repository conditions at the Äspö hard rock laboratory, Sweden. The ABM5 was heated during 2012-2017 at 50°C in the early years, and from 2016 the temperature was increased up to 250°C.

Results from the different analytical tecniques were not always concise, due to the fact that many mineralogical changes were close to the detection limit of the methods. Cl concentrations did not depend on material properties or temperature, and the Cl content was assumed to result from effects such as inflowing water. Most corrosion and migration of Fe into the blocks was observed in the upper parts of the test. Mg enrichment at the heater, as observed in most of the previous bentonite field experiments, was comparably low. The Mg rich 'Saponite' lost some of its Mg content, indicating some mobility of Mg within the clays. Carbonate dissolution and precipitation (redistribution) showed different patterns not correlating to clay type or the temperature. At the Fe-bentonite contact, there were observations where siderite formed at the expense of Ca(Mg)carbonates (proved by STA and LECO and sometimes XRD).

The gypsum redistribution resembled that which was found in the LOT test (increase in the center of the blocks), but this effect was much less pronounced in the ABM5 test. The most significant gypsum increase was found in the upper and lowermost blocks. The identified gypsum may possibly have been anhydrite in the experiment that may have hydrated during storage, as there are indications of moisture in the samples during the storage.

XRD showed no additional interstratification of smectites for any block in comparison with the reference materials. The neoformation of trioctahedral phases could be indicated only in block #7 (Ikosorb). In the only block with trioctahedral smectites as starting material, #17 ('Saponite'), no evidence for the presence of (additional) dioctahedral phases was observed.

Minor decrease in CEC in bulk samples was observed, and on the contrary, moderate increase in CEC of the clay fractions (< 2 µm). This is possibly due to aggregate formation in the bulk samples upon the high temperature drying, and the clay fractions were possibly activated by the ultra-sonic treatment during the sample preparation of the clay fractions.

No significant changes could be seen in swelling pressure and hydraulic conductivity. Compared to the references lower maximum deviator stress was seen in all materials during unconfined compression tests. When ABM5 field samples were compared to the references (after Ca-exchange and washing with DI -water to remove excess salt) a lower maximum deviator stress was seen in all materials. The exchange to Ca and washing process removed any effects due to cation exchange and/or salt accumulation.

The most dramatic impact from the high temperature was on the bentonites physical state as many blocks fractured and some even disintegrated during the experiment. This is perhaps the most unexpected observation at this point. None of the analyses performed could detect any specific high temperature reaction. The studies were published as Kaufhold et al. (2021) and Svensson et al. (2023).

XRD measurements on Na-Kunipia and Ca-Kunipia were performed at 25°C and 80°C by **BRGM (ANDRA)** ***for various relative humidity****. The results suggest that the temperature had little effect on the interlayer water retention capacity. The results also showed that, at low relative humidity, Ca-Kunipia more easily hydrated than Na-Kunipia.*

Water retention isotherms were measured on Na-Kunipia compacted at densities of 1.4, 1.5, 1.6 and 1.6 g/cm^3 at a temperature of 24°C. Depending on the vicinity to sample saturation, water hydrates different types of porosity, namely the intra-aggregate porosity at low relative humidity and the macroporosity at higher relative humidity. A temperature of 42°C was later applied on the same cells. A comparison between the isotherms at 42°C and 24°C will allow further conclusions.

Two sets of thermo-hydraulic tests were analysed by CIEMAT + UAM (CIEMAT). The tests consisted in heating a bentonite column through the base while water was injected on top for ~3 and ~10 years (including an initial only heating phase). In one set of tests (C3, C4, C5) the columns were 10 cm high and the heater was set at 110°C. Two of these tests were performed using MX-80 powder (saturated with saline and dilute water, C4 and C5 respectively) and the other one using Ibeco bentonite (C3). In the other set of TH tests (consisting just of test HEE-B) the height of the column was 50 cm and the heater was set at 140°C. It was saturated with saline water and MX-80 pellets were used.

In tests C3-C5 no significant montmorillonite structural modifications took place during operation. Octahedral Mg relatively increased near the heater, although globally the octahedral Mg content was lower in the treated MX-80 samples compared to the reference one and higher in the Ibeco treated samples than in the reference one. In all the samples from the cells the layer charge decreased with respect to the values of the reference samples.

In cell C3 with Ibeco bentonite, chlorite (2:1:1 sheet silicate) was detected at less than 1-2 mm from the heater. Abundant halite precipitation was observed in large pores (triggered by heating) at distances of less than 5 mm from the heater. The overall content of carbonates increased in the area at less than 4 cm from the heater. In the area at less than 2 cm from the heater calcite predominated over dolomite, in contrast with the rest of the cell, where dolomite was the predominant carbonate. This would match with the dissolution of dolomite in the contact with the heater and the incorporation of magnesium to the newly formed chlorite. The exchangeable magnesium content also increased above the initial value close to the heater.

In the MX-80 samples from tests C4 and C5, calcium sulphate (probably anhydrite) was detected in areas at less than 4 cm from the heater. Total consumption of oxygen seems to have occurred in both experiments, explaining the presence close to the heater of pyrite and oxides in different oxidation states in the case of C4. As a result of the hydration with saline water in cell C4, carbonates and sulphates precipitated at various locations, NaCl-spotted areas were observed close to the heater and corrosion occurred in the contact with the steel elements. None of these features were observed in cell C5, hydrated with glacial water. In this cell, close to the hydration surface calcium carbonates precipitated.

The changes in the pore water composition inferred from the aqueous extracts were affected by 1) the composition of the incoming water, 2) the dissolution of mineral species present in the initial bentonite as a result of the water content increase, 3) cation exchange processes.

The ions coming with the hydration water and those coming from the dissolution of minerals were transported by advection and accumulated in the lower half of the columns at the bottom, precipitating closer to the heater. The overall concentration of the ions in the samples increased significantly with respect to the initial one. The maxima in sulphate concentration were in all cells accompanied by increases in the soluble sodium and calcium contents, possibly indicating the precipitation of anhydrite at less than 4 cm from the heater in cells C4 and C5 and at 3 cm from the heater in cell C3 (in the latter case it was not possible to ascertain if the sulphate was gypsum or anhydrite). The precipitation of carbonates close to the heater in all cells was reflected in the decrease in bicarbonate content from the hydration surface towards the heater.

At the end of the HEE-B test all the samples continued to consist predominantly of a dioctahedral smectite, with no significant differences from the original with respect to the distribution of structural cations and layer charge. No evidence of mixed-layer formation was detected. Sodium continued to predominate in the exchangeable cation complex (according to the measurement of the basal spacing, thermogravimetry, and Cs displacement results), probably as a consequence of the hydration with a predominantly sodic solution. However, some contribution of divalent cations toward the hydration surface could be detected.

Despite the lack of montmorillonite alteration at the structural level, the drier samples, those that were submitted to temperatures >60°C, remarkably had a significant resistance to rehydration under room relative humidity conditions. However, this was not an irreversible process, as the samples hydrated normally when the relative humidity was high (97%) and expanded as expected when suspended in water.

Although hydration took place with a highly saline water – which seems to have inhibited the formation of colloids – the overall increase in water content allowed the dissolution of some species and the solubilised ions were transported toward the heater and precipitated at two distinct areas: sulphate, sodium, and calcium peaked at ~18 cm from the heater whereas chloride moved closer to the heater (accompanied by sodium and calcium), concentrating at 9 cm from it, coinciding with a vapour leak area. This leak started at some undetermined moment during the test through a sensor inlet. This experimental artefact seems to have conditioned the processes around it, such as the movement of solubilised ions. The liquid-water availability was probably affected also in the areas of temperatures higher than 60°C, which would limit the reactivity there. Nevertheless, evidence of precipitation of calcite and calcium sulphates and dissolution of cristobalite and quartz were observed in the areas where the temperature was higher than 100°C.

Around this sensor inlet the specific surface area of the bentonite was lowest, indicating aggregation of particles likely caused by shrinkage when water evaporated from bentonite whose water content was higher prior to the start of the leak. From this point towards the heater the bentonite was disaggregated, with specific surface areas smaller than the initial one.

It can be concluded that in any of the tests structural modifications of the bentonite were observed, but that dissolution and precipitation of species occurred and were conditioned by the kind of bentonite and hydration water. These processes were accompanied by modification of the exchangeable cation complexes. The use of pellets instead of compacted blocks does not seem to have been an additional source of uncertainty.

The effect of long-term thermal exposure (1 year at 150°C) on the hydromechanical properties of BCV bentonite was studied by CU (SÚRAO). The differences between the original BCV and the thermally treated bentonite were investigated by swelling pressure tests, constant load swelling tests, suction controlled swelling pressure tests and hydraulic conductivity measurements.

Hydraulic conductivity measurements showed slightly higher values for the thermally treated samples. Despite the higher hydraulic conductivity, the thermally loaded material exhibited a slower equilibration of swelling pressure. Different retention properties were also indicated from equilibration of the bentonite powder after thermal treatment, which resulted in water content of 7.5% at 43.2 % relative humidity compared to 10.7 % for the original BCV bentonite.

Constant load swelling tests showed no difference between the two materials. Swelling pressure tests also showed similar values for both materials. Thermally loaded samples compacted to higher dry densities showed slightly lower swelling pressures compared to untreated samples. However, suction controlled swelling pressure tests gave very similar results for both materials at all suction levels, with thermally treated samples even giving slightly higher maximum swelling pressures compared to water

saturated tests. Overall, the experiments investigating swelling properties provided no clear evidence of a reduction in the swelling capacity of BCV bentonite as a result of thermal treatment.

Hydro-mechanical properties of bentonite after exposure to elevated temperatures was studied by CTU (SÚRAO), as well as the potential evolution of these properties depending on the duration of the treatment.

Hydraulic conductivity, swelling pressure, liquid limit and swell index of dry treated and wet treated bentonite were tested. Based on the research carried out, the following conclusion can be drawn:

- Exposure to elevated temperatures had the most significant effect on the bentonite treated in the dry state.
- Behaviour of dry treated bentonite is consistent with respect to measured parameters.
- Hydraulic conductivity of dry treated bentonite is slightly higher, and it does not depend on the duration of heating. The change of hydraulic conductivity occurred in the first heating time step and remained stable thereafter.
- Swelling pressure of dry treated bentonite is less affected by heating than hydraulic conductivity. The swelling pressure is lower, but not significantly. No trend depending on duration of heating observed.
- The liquid limit and swell index of dry treated bentonite are lower. The decrease of both parameters is observed as a function of the heating time.
- In contrast to dry treated bentonite, wet treated bentonite shows slight improve of hydro-mechanical characteristics compared to untreated bentonite. Although the change is not significant, this finding is valuable with respect to behaviour of dry treated bentonite.

Thermal treatment of PBC bentonite was carried out at 150°C for 3, 6, 12 months and analysed using XRD and DTA/GA by KIPT (ChRDI). Results of XRD investigation of PBC bentonite before and after 150°C heating for period up to 12 months showed that no phase transformations occurred during thermo- treatment, the weight ratios of the phases remained. Permeability and swelling pressure were measured at room temperature for bentonite thermo-treated at 150°C for 6 and 12 months.

SIIEG NASU (ChRDI) concluded that further tests are needed in order to confirm the observations of the effect from thermal loading on the bentonite samples.

Thermal loading of a dry powder at 150 °C was studied by ÚJV (SÚRAO), that concluded that the monitored parameters deteriorated. The decrease of the cation exchange capacity correlates well with the decrease of specific surface area. Given that the mineralogical composition and illite/smectite ratio have not significantly changed, it can be presumed that these decreases are given by the changes within montmorillonite layer structure, probably collapsing of some of the montmorillonite interlayer spaces. However, the results of cation exchange capacity and specific surface area of the wet samples, as well as the results of measuring the saturated hydraulic conductivity and especially the water retention curves of both dry and wet samples indicate that the changes are at least partially reversible. The impact of thermal loading on the bentonite composition was registered by aqueous leachates and TA-EGA mainly for carbonate phases, then for sulphates and fluorides. Thermal loading caused decrease in caesium distribution coefficients as well; it also resulted in a reduction of microbial survivability and thus affected possible future microbial activity in bentonite.

The results of all the analysis of the wet samples show little or none difference compared to the thermally unloaded bentonite and if so, the results were even better than in the unloaded bentonite. It can be presumed thus that the deterioration of the monitored parameters is given not by the temperature itself, but probably by the loss of the water content induced by the elevated temperature.

Sample preparation and experimental procedures for volumetric, isotropic compression and shear test for heat treated bentonite were successfully developed by VTT and set up. In addition, a completely new volumetric compaction device was designed, developed and built from components as a mitigation action for problems with the triaxial device, which was originally planned as the only device to be used in this work. Volumetric compaction of heat treated, water content stabilized Wyoming Na bentonite powder in 105°C and in 150°C as well as unheated, water content stabilized reference material has been successfully performed. The results indicate that the effect of heat treatment as powder is less significant for the volumetric compressibility than small changes in water content or variation material as powder.

The original plan for conducting the experiments with the triaxial device only was hindered by reliability issues combined to the worldwide supply chain disturbances followed from COVID-19 as well as by the simultaneous updating the triaxial system to enable high temperatures (also other updates), developing shear test procedures and producing volumetrically compacted samples. Consequently, the triaxial device has been out of operation for volumetric compaction for prolonged periods. As a mitigation action of this realised risk, a separate volumetric compaction device was successfully built from components with a tight schedule to allow compacting the samples with a separate device, while concentrating on the shear tests and tests at high temperatures with the triaxial cell.

Overall conclusions:

1. No general significant transformation of montmorillonite was observed in the experiments.

2. In several cases the CEC of the bentonite was affected by the heating.

3. There are indications that dry heating of bentonite seems to affect the clay in other ways, than heating of water saturated bentonite.

4. Swelling pressure seemed mainly unaffected by thermal treatment, while hydraulic conductivity sometimes increased somewhat.

5. Unconfined compression test showed that a lower maximum deviator stress was seen in all materials compared to the references.

6. There were examples of (i) redistribution of sulphates, (ii) formation of carbonates, (iii) dissolution of quartz and cristobalite.

7. There were examples of compacted bentonite blocks that were physically disintegrated in parts of the experiments. The mechanism for this is not fully understood, and it is unclear if this could actually happen in a real repository as well at high temperatures.

8. The liquid limit and swell index of dry treated bentonite are lower. The decrease of both parameters is observed as a function of the heating time.

9. None of the analyses performed could detect any specific high temperature reaction.

10. During the test period the experiments did not alter the bentonite in a way that it lost its important properties as a buffer material.

References

Ammann L, Bergaya F, Lagaly G, 2005. Determination of the cation exchange capacity of clays with copper complexes revisited. Clay Minerals 40, 441–453.

ASTM standard D 5084-03. Standard Test Methods for Measurement of Hydraulic Conductivity of Saturated Porous Materials Using a Flexible Wall Permeameter

Borys Zlobenko, et al. (2023). "Test of the Thermal-Hydro-mechanical Behaviors of Cherkasy Bentonite as Buffer Material of HLW Repository", pp. 185-196, 2023, Systems, Decision and Control in Energy IV, Volume II. Nuclear and Environmental Safety, https://doi.org/10.1007/978-3-031-22500-0_12 (Springer Nature Switzerland AG)

Cases, J.M., Berend, I., Besson, G., Francois, M., Uriot, J.P., Thomas, F., Poirier, J.E., 1992. Mechanism of adsorption and desorption of water vapor by homoionic montmorillonite. The sodium-exchanged form. Langmuir 8, 2730–2739.

Červinka R. Vašíček R. et al. Kompletní charakterizace bentonitu BCV 2017 [Kniha]. - Prague : SÚRAO, 2018. - Technical report 419/2019.

ČSN EN ISO 17892-12: Determination of consistency limits [Kniha]. - 2018.

Dobrev D. Hančilová I., Hasal M., Hokr M., Kašpar V., Kouřil M., A. N. Mendoza Miranda, M. Zuna Test omezení koroze UOS využitím drenážní vrstvy v úložných vrtech, Technická zpráva číslo 291/2018, 118 str. [Kniha]. - [místo neznámé] : SÚRAO, 2018.

Eng, A., Nilsson, U., Svensson, D. (2007) Alternative Buffer Material – Installation report. Swedish Nuclear Fuel and Waste Management Co (SKB) Report, IPR-07-15.

Gaus, I., et al. (2014). The HE-E Experiment: Lay-out, Interpretation and THM Modelling. Nagra Arbeitsbericht Wettingen, NAGRA. NAB 14-53: 140.

Hausmannová L., Hanusová I. and Dohnálková M. Summary of the research of Czech bentonites for use in the deep geological repository – up to 2018 [Book]. - Prague : SÚRAO, 2018. - Technical report 309/2018/ENG.

IAEA-TECDOC-1718 "Characterization of Swelling Clays as Components of the Engineered Barrier System for Geological Repositories", IAEA, Vienna, ISBN 978-92-0-112410-4, http://www-pub.iaea.org/MTCD/publications/PDF/TE-1718_web.

ISO/TS 17892-5:200, GOST 12248 – 2010 Geotechnical investigation and testing - Laboratory testing of soil.

Karnland O, Olsson S, Nilsson U, 2006. Mineralogy and sealing properties of various bentonites and smectite-rich clay materials. SKB TR-06-30, Svensk Kärnbränslehantering AB.

Kaufhold, S., Dohrmann, R., Sandén, T., Sellin, P., and Svensson, D. (2013) Mineralogical investigations of the first package of the alternative buffer material test – I. Alteration of bentonites. Clay Minerals, 48, 199-213.

Kiviranta, L. and S. Kumpulainen (2011). Quality control and characterization of bentonite materials. Posiva Working Report Olkiluoto, Posiva. **2011-84:** 154.

Kiviranta, L., et al. (2018). Characterization of bentonite and clay materials 2012-2015. Posiva Working Report Olkiluoto. **2016-05:** 154.

Kozaki, T., Sato, Y., Nakajima, M., Kato, H., Sato, S., Ohashi, H., 1999. Effect of particle size on the diffusion behavior of some radionuclides in compacted bentonite. J. Nucl. Mater. 270, 265–272.

Kuligiewicz, A., Derkowski, A., Szczerba, M. et al. Revisiting the Infrared Spectrum of the Water—Smectite Interface. Clays Clay Miner. 63, 15–29 (2015) https://doi.org/10.1346/CCMN.2015.06301022.

Laufek F., Hanusová I., Svoboda J., Vašíček R., Najser J., Koubová M., Čurda M., Pticen F., Vaculíková L., 2021. Mineralogical, geochemical and geotechnical study of BCV bentonite – initial state and state after thermal treatment at 200°C. Minerals, 2021, 11, 871.

Leupin O.X (ed), Birgersson M, Karnland O, Korkeakoski P, Sellin P, Mäder U, Wersin P, 2014. Montmorillonite stability under near-field conditions. NAGRA TR14-12. Wettingen, 104 pp.

M.V. Villar, 2004. MX-80 Bentonite. Thermo-hydro-mechanical characterisation performed at CIEMAT in the context of the prototype project. Report CIEMAT/DIAE/54540/2/04. https://inis.iaea.org/collection/NCLCollectionStore/_Public/36/083/36083408.pdf".

Massat, Luc, Olivier Cuisinier, Isabelle Bihannic, Francis Claret, Manuel Pelletier, Farimah Masrouri, and Stéphane Gaboreau. 2016. "Swelling Pressure Development and Inter-Aggregate Porosity Evolution upon Hydration of a Compacted Swelling Clay." Applied Clay Science 124–125: 197–210. https://doi.org/10.1016/j.clay.2016.01.002.

Meier L P, Kahr G, 1999. Determination of the cation exchange capacity (CEC) of clay minerals using the complexes of copper(II) ion with triethylenetetramine and tetraethylenepentamine. Clays and Clay Minerals 47, 386–388.

Orsini, L., Rémy, J., 1976. The use of the chloride of cobaltihexamine for the simultaneous determination of the exchange capacity and exchangeable bases in soils. Sci. Sol 4, 269–275

Rukavičková L. Pačes T., Holeček J. Expertní odhad hydraulických a hydrochemických parametrů, DZZ 3.3 projektu „Výzkum procesů pole vzdálených interakcí HÚ vyhořelého jaderného paliva a vysoce aktivních odpadů". ČGS Praha, 77 str. [Kniha]. - Praha : ČGS, 2009.

Sandén, T., Nilsson, U., Andersson, L., Svensson, D., 2018. ABM45 experiment at Äspö Hard Rock Laboratory. Installation report. SKB report P-18-20.

Svensson D, Dueck A, Nilsson U, Olsson S, Sandén T, Lydmark S, Jägerwall S, Pedersen K, Hansen S, 2011. Alternative buffer material. Status of the ongoing laboratory investigation of reference materials and test package 1. SKB TR-11-06, Svensk Kärnbränslehantering AB.

Svensson P D, 2015. The bentonite barrier: swelling properties, redox chemistry and mineral evolution. PhD thesis. Lund University.

Svensson, D., Eriksson, P., Johannesson, L-E, Lundgren, C., Bladström, T., 2019. Development and testing of methods suitable for quality control of bentonite as KBS-3 buffer and backfill. SKB report TR-19-25.

Svensson, P. D., Hansen, S. (2013) Redox chemistry in two iron-bentonite field experiments at Äspö hard rock laboratory, Sweden: an XRD and Fe K-edge XANES study. Clays and Clay Minerals, 61, 566-579.

Svensson, D., Bladström, T., Sandén, T., Dueck, A., Nilsson, U., Jensen, V., 2023. Alternative Buffer Material (ABM) experiment - Investigations of test packages ABM2 and ABM5. SKB report TR-23-25.

Svoboda J. Vašíček R., et al. Interakční experiment – přípravné a podpůrné práce [Kniha]. - Prague : SÚRAO, 2019. - Technical report TZ385/2019. Brunauer, S., Emmett, P.H., Teller, E., 1938. Adsorption of gases in multimolecular layers. J. Am. Chem. Soc. 60, 309–319.

Tarasevich, Yu.I. (1988), p. 20. Structure and chemical properties of layered silicates surface, Nauk. dumka, Kyiv, UA, 248 p.

Valter, M. & Plötze, M. 2013. Characteristics of variably saturated granular bentonite after long-term storage at near-field relevant temperatures. Clay Minerals 48(2): 343-361.

Villar, M. V. (2005). MX-80 bentonite. Thermo-hydro-mechanical characterisation performed at CIEMAT in the context of the Prototype Project. Informes Técnicos CIEMAT. Madrid, CIEMAT. **1053:** 39.

Villar, M. V., et al. (2021). Project MINALBEN. Report on postmortem analyses of samples from cells running for 2.5 years (C3, C4 and C5). Technical Report CIEMAT. Madrid, CIEMAT. **Technical Report CIEMAT/DMA/2G219/1/21:** 86.

Villar, M. V., et al. (2006). Behaviour of MX-80 bentonite at unsaturated conditions and under thermo-hydraulic gradient. Work performed by CIEMAT in the context of the TBT project. Informes Técnicos CIEMAT Madrid, CIEMAT. **1081:** 45.

Zlobenko, B.P.; et al. (1995). "Studies of clays from deposits in Ukraine as barrier material for radioactive waste repositories", ISBN 0-7918-1219-7; 1995; p. 857-859.

G